

## University of Southampton Research Repository

Copyright © and Moral Rights for this thesis and, where applicable, any accompanying data are retained by the author and/or other copyright owners. A copy can be downloaded for personal, non-commercial research or study without prior permission or charge. This thesis and the accompanying data cannot be reproduced or quoted extensively without obtaining permission in writing from the copyright holder/s. The content of the thesis and accompanying research data (where applicable) must not be changed in any way or sold commercially in any format or medium without the formal permission of the copyright holder/s.

When referring to this thesis and any accompanying data, full bibliographic details must be given, e.g.

Thesis: Author (Year of Submission) "Full thesis title", University of Southampton, name of the University Faculty or School or Department, PhD Thesis, pagination.

Data: Author (Year) Title. URI [dataset]



**University of Southampton**

FACULTY OF MEDICINE

SCHOOL OF HUMAN DEVELOPMENT AND HEALTH

**Individual and Collective Mechanosensing of  
Extracellular Matrix Thickness in Skeletal Stem  
Cell Differentiation**

by

**M.Sc. María Luisa Hernández Miranda**

Thesis for the degree of Doctor of Philosophy

May 2023



## **Abstract**

The elastic modulus of growth substrates and/or extracellular matrix (ECM) affects many cell types' spreading, proliferation and differentiation, including bone marrow stromal cells (BMSCs). However, the substrate modulus and geometry determine the stiffness a cell senses, including material thickness and cell crowding. In this study, we hypothesised that these factors would impact the traction force applied by BMSCs to the ECM and their differentiation. Soft and stiff polyacrylamide (PAAm) hydrogel matrices of different thicknesses were fabricated by varying the monomer ratio and PAAm mixture volume. Hydrogel stiffness and thickness were measured by nanoindentation and confocal microscopy. Cells were plated on collagen type I coated hydrogels to evaluate the effect of hydrogel mechanical properties on cell spreading (cell area), focal adhesions formation (immunocytochemistry), actin fibre formation (actin staining), proliferation (PicoGreen), and osteogenic (ALPL activity) and adipogenic (Oil red O) differentiation. The effect of hydrogel stiffness and thickness and cell crowding on cellular forces during osteogenic and adipogenic differentiation was evaluated by quantifying hydrogel deformations by Stro-1<sup>+</sup> BMSCs at different seeding densities on soft, thin, and thick PAAm hydrogels after being incubated in basal, osteogenic and adipogenic media. 1 kPa (soft) hydrogels were thicker than 40 kPa (stiff) and exhibited the presence of wrinkles on the hydrogel surface, and the increase in the PAAm volume increased hydrogel thickness. The addition of fluorescent microbeads decreased the thickness of thick, soft, and stiff PAAm hydrogels and the elastic modulus of stiff, thin hydrogels. The elastic modulus of soft and stiff hydrogels increases on thinner hydrogels; ~19Pa (5 $\mu$ L) vs ~5Pa (50 $\mu$ L) for soft and ~200Pa (5 $\mu$ L) vs ~60Pa (50 $\mu$ L) for stiff hydrogels. BMSC on soft, thick hydrogels spread to a lesser extent than those on thin hydrogels with a mean cell area of  $2600 \pm 79$  and  $5600 \pm 990 \mu\text{m}^2$ , respectively and modified their morphology depending on the hydrogel mechanical properties. The hydrogel elasticity and thickness also influenced the formation of focal adhesions and actin fibres. ALPL activity, expression of osteogenic genes (*ALPL* and *RUNX2*) and Oil red O absorption showed that BMSCs differentiated into osteoblasts and adipocytes regardless of the hydrogel's elasticity and thickness. Stro-1<sup>+</sup> BMSCs highly deformed soft, thick, and soft, thin PAAm hydrogels but not stiff hydrogels. Hydrogel deformations decreased over time with the increase in cell crowding from ~14 pixels on day 0 to ~3 on week 7 on soft, thick hydrogels. These results were confirmed by evaluating the soft hydrogel deformations at different seeding densities for 24 hours in basal and osteogenic media; ~16 pixels (osteogenic) -21 pixels (basal) with cells at 1,000 cells/cm<sup>2</sup> and ~6 pixels (basal) -8 pixels (osteogenic) pixels at 20,000 cells/cm<sup>2</sup>. Additionally, results showed that at low seeding density BMSCs perceived differences in soft hydrogel thickness and caused more significant deformations. (basal: ~10 pixels; osteogenic: ~11 pixels) compared to cells at higher seeding density (basal: ~4 pixels; osteogenic: ~3 pixels) on soft, thick hydrogels on day 14. Further evaluations highlighted that osteogenic or adipogenic supplements modified hydrogel displacements, especially on soft, thick matrices; ~18 pixels in basal media and ~14 pixels in osteogenic media and ~12 pixels in basal media and ~6 pixels in adipogenic media on day 14. Stro-1<sup>+</sup> BMSCs mechanosense changes in substrate elasticity and thickness by modifying their morphology and slightly increasing their spreading. Despite cells detecting changes in hydrogel mechanical properties, no differences in osteogenic and adipogenic differentiation were encountered when modifying hydrogel elasticity and thickness. The quantification of hydrogel displacements suggests that cell mechanosensing is influenced by hydrogel elasticity and thickness, the increase in cell crowding and the differentiation state of stem cells. Indeed, cells perceive soft hydrogels as stiffer when the thickness is reduced and cell crowding increases, promoting osteogenic differentiation of Stro-1<sup>+</sup> BMSCs. This may suggest that by modifying the substrate thickness and controlling cell crowding, it would be possible to promote differentiation for tissue repair.



**Table of Contents**

<b>Table of Contents</b> .....	<b>i</b>
<b>Table of Tables</b> .....	<b>vii</b>
<b>Table of Figures</b> .....	<b>ix</b>
<b>List of Accompanying Materials</b> .....	<b>xvii</b>
<b>Research Thesis: Declaration of Authorship</b> .....	<b>xix</b>
<b>Contributors</b> .....	<b>xxi</b>
<b>Agradecimientos</b> .....	<b>xxiii</b>
<b>Acknowledgements</b> .....	<b>xxv</b>
<b>Definitions and Abbreviations</b> .....	<b>xxvii</b>
<b>Chapter 1 Introduction</b> .....	<b>1</b>
1.1 Mechanobiology and Physiology .....	2
1.2 Important concepts in Mechanobiology .....	2
1.3 Mechanobiology and tissue development.....	4
1.4 Role of stiffness in disease development.....	5
1.5 Mechanobiology and tissue engineering.....	6
1.6 Biomaterials mimicking the extracellular matrix .....	7
1.7 Extracellular matrix.....	10
1.8 ECM and stiffness sensing .....	12
1.9 Mechanosensing and mechanotransduction.....	13
1.9.1 Integrins.....	15
1.9.2 Focal adhesions .....	16
1.9.3 Actin cytoskeleton.....	17
1.9.4 Signalling pathways.....	18
1.10 Stem cells.....	20
1.11 Bone Marrow Stromal Cells .....	22
1.11.1 Bone Marrow Stromal Cells as a tool for bone recovery .....	23
1.11.2 Mechanobiology of skeletal stromal cells .....	24
1.11.3 SSCs osteogenic differentiation .....	25
1.12 Substrate stiffness and SSCs differentiation.....	25
1.13 Substrate mechanical properties to be controlled when evaluating stiffness sensing .....	28
1.13.1.1 Protein tethering and SSCs differentiation.....	28
1.13.1.2 Substrate thickness and stem cell differentiation .....	29
1.13.1.3 Cell density .....	31
1.14 Cell Micropatterning .....	33

1.15 Conclusion .....	34
1.16 Hypothesis .....	34
1.17 Aims.....	35
<b>Chapter 2 Methods .....</b>	<b>37</b>
2.1 Materials .....	38
2.1.1 Cells .....	38
2.1.2 Chemicals and materials .....	38
2.1.2.1 Fabrication, characterisation and micropatterning of polyacrylamide hydrogels .....	38
2.1.2.2 Cell culture.....	38
2.1.2.3 Cell dyes.....	39
2.1.2.4 Osteogenic differentiation .....	39
2.1.2.5 Adipogenic differentiation.....	39
2.1.2.6 DNA quantification .....	40
2.1.2.7 RNA isolation .....	40
2.1.2.8 RT-PCR.....	40
2.1.2.9 qPCR.....	40
2.2 Methods.....	41
2.2.1 Polyacrylamide hydrogels.....	41
2.2.1.1 Polyacrylamide hydrogels for traction force microscopy studies.....	42
2.2.1.2 PAAm hydrogels for thickness measurements .....	42
2.2.2 Thickness measurements.....	43
2.2.3 Stiffness measurements .....	43
2.2.4 Cell culture .....	44
2.2.5 Quantification of cell spreading area.....	44
2.2.6 Vinculin, actin, and nuclei staining.....	44
2.2.7 Osteogenic differentiation.....	45
2.2.7.1 ALPL staining.....	45
2.2.7.2 ALPL quantification .....	46
2.2.7.3 DNA quantification .....	46
2.2.8 Adipogenic differentiation .....	47
2.2.8.1 Oil Red O staining and quantification .....	47
2.2.9 <i>ALPL</i> , <i>RUNX2</i> expression quantification .....	47
2.2.9.1 RNA isolation .....	47
2.2.9.2 RNA measurements.....	48

2.2.9.3 Reverse Transcription PCR.....	48
2.2.9.4 Quantitative PCR .....	48
2.2.10 Quantification of cell traction forces by traction force microscopy .....	49
2.2.10.1 Time-lapse live cell Imaging .....	49
2.2.10.2 Substrate displacement tracking .....	49
2.2.11 Cell micropatterning.....	52
2.2.11.1 Preparation of acrylate-conjugated collagen.....	52
2.2.11.2 Collagen micropatterning on the glass slides by microcontact printing	
52	
2.2.11.3 Collagen inactivation .....	53
2.2.12 Statistical analysis .....	53
<b>Chapter 3 Polyacrylamide hydrogel characterisation.....</b>	<b>55</b>
3.1 Introduction .....	56
3.2 Aims .....	58
3.3 Results .....	59
3.3.1 Hydrogel morphology is affected by composition and volume.....	59
3.3.2 Thickness measurements of low and high elastic modulus PAAm hydrogels	60
3.3.3 Effect of the addition of fluorescent microbeads on the structure of PAAm	
hydrogel.....	61
3.3.4 Effect of the addition of fluorescent microbeads on PAAm hydrogel thickness	
61	
3.3.5 Effect of the supporting material and thickness on hydrogel elastic modulus	63
3.4 Discussion.....	66
<b>Chapter 4 Effect of stiffness and thickness on cell behaviour.....</b>	<b>71</b>
4.1 Introduction .....	72
4.2 Aims .....	74
4.3 Results .....	75
4.3.1 Effect of the increase in hydrogel elasticity on cell spreading.....	75
4.3.2 Effect of the increase in hydrogel elastic modulus on actin stress fibres .....	76
4.3.3 Effect of hydrogel elastic modulus on focal adhesions .....	77
4.3.4 Effect of seeding density on stiffness sensing.....	78
4.3.5 Effect of substrate thickness on cell spreading .....	80
4.3.6 Effect of substrate thickness on actin fibres .....	80
4.3.7 Effect of substrate thickness on focal adhesions.....	81
4.4 Discussion.....	84

<b>Chapter 5 Bone marrow stromal cells differentiation .....</b>	<b>89</b>
5.1 Introduction .....	90
5.2 Aims.....	92
5.3 Results.....	93
5.3.1 Effect of substrate stiffness on BMSCs osteogenic differentiation .....	93
5.3.2 Effect of substrate stiffness on BMSCs adipogenic differentiation .....	97
5.3.3 Effect of substrate thickness on BMSC osteogenic differentiation .....	101
5.4 Discussion .....	112
<b>Chapter 6 Cell traction forces and cell differentiation .....</b>	<b>117</b>
6.1 Introduction .....	118
6.2 Aims.....	120
6.3 Results.....	121
6.3.1 Structure of soft and stiff PAAm hydrogels .....	121
6.3.2 Soft and stiff hydrogel deformations by Stro-1 <sup>+</sup> BMSCs during cell spreading 122	
6.3.3 Effect of cell crowding on hydrogel deformations by Stro-1 <sup>+</sup> BMSCs .....	124
6.3.4 Effect of the seeding density on hydrogel deformations.....	128
6.3.5 Hydrogel deformations by Stro-1 <sup>+</sup> BMSCs at low seeding densities during osteogenic differentiation.....	130
6.3.6 BMSCs adipogenic and osteogenic differentiation and hydrogel deformations 140	
6.3.7 Cell micropatterning .....	144
6.3.8 Hydrogel deformations by single and groups of Stro-1 <sup>+</sup> BMSCs .....	149
6.4 Discussion .....	155
<b>Chapter 7 Discussion and future work .....</b>	<b>159</b>
7.1 Discussion .....	160
7.1.1 Achievements of the study .....	160
7.1.2 Discussion of the main findings and their context .....	163
7.1.2.1 Embryonic and tissue development .....	164
7.1.2.2 Tissue homeostasis and disease development .....	165
7.1.2.3 Tissue regeneration .....	165
7.1.2.4 Cancer development.....	166
7.2 Limitations of the study and suggestions for future work .....	167
7.3 Conclusions .....	170

<b>Appendix A</b>	<b>MATLAB Functions</b> .....	<b>171</b>
A.1	rrImageTrackGUI.m.....	171
A.2	processresults6v3.m .....	188
<b>List of References</b> .....		<b>193</b>



## Table of Tables

Table 1.1. Characteristics of natural and synthetic polymers forming hydrogels used as biomaterials.....	9
Table 1.2. Components, characteristics, and functions of the extracellular matrix.....	11
Table 3.1. Hydrogel thickness of PAAm hydrogels with and without fluorescent microbeads with different elasticity.....	63



## Table of Figures

Figure 1.1. Representation of Hooke's law.....	3
Figure 1.2. Representation of the extracellular and basement extracellular matrix components .....	11
Figure 1.3. Mechanical forces are sensed by cells.....	13
Figure 1.4. Cell morphology and cytoskeleton change on a substrate with increasing stiffness.....	13
Figure 1.5. Structures involved in the mechanosensing and mechanotransduction process. ....	15
Figure 1.6. Mechanical stimuli direct the cell fate of skeletal stem cells; loading and stiff materials lead to osteogenesis, while unloading and soft materials lead to adipogenesis.....	20
Figure 1.7. Substrate elasticity defines the protein and transcript profiles of SSCs under identical media conditions. ....	27
Figure 1.8. Stiffness sensing of cells on soft hydrogels with different thicknesses.....	30
Figure 2.1. Synthesis of polyacrylamide hydrogels.. ....	42
Figure 2.2. Sulfo-SANPAH and collagen type I attachment to the polyacrylamide hydrogels with different elastic modulus.. ....	42
Figure 2.3. The process to obtain the fluorescent intensity profiles of the polyacrylamide hydrogels to measure thickness by confocal microscopy.. ....	43
Figure 2.4. Grid and correlation graph for analysis.....	50
Figure 2.5. Tracking parameters in the MATLAB function.....	51
Figure 2.6. Images were obtained by running the second function in MATLAB.....	51
Figure 3.1. Hydrogel surface changes with hydrogel elastic modulus and thickness... ..	59
Figure 3.2. The number of wrinkles on the surface of soft polyacrylamide hydrogels decreases on thicker hydrogels.....	60
Figure 3.3. Soft PAAm hydrogels are thicker than their stiff counterparts when using high PAAm mixture volumes. ....	60
Figure 3.4. Wrinkles on soft PAAm hydrogels dictate microbead positioning. ....	61

Figure 3.5. PAAm hydrogels with low elastic modulus are thicker than high elastic modulus hydrogels on 25, 50 and 100 $\mu$ L PAAm samples with fluorescent microbeads.....	62
Figure 3.6. Adding fluorescent microbeads decreases the thickness of soft and stiff hydrogels with high PAAm volumes.....	62
Figure 3.7. The underlying material increases the effective stiffness of soft, thin PAAm hydrogels.....	64
Figure 3.8. Young's apparent modulus of stiff, thin hydrogels was higher than the corrected Young's modulus.....	64
Figure 3.9. The change in thickness influenced Young's modulus of stiff and soft PAAm hydrogels containing fluorescent microbeads.....	65
Figure 3.10. The Young modulus of stiff, thin PAAm but not soft hydrogels increased with the addition of fluorescent microbeads.....	65
Figure 4.1. Cell morphology of Stro-1 <sup>+</sup> BMSCs on PAAm hydrogels with different elastic modulus.....	75
Figure 4.2. The cell-spreading area of BMSCs increased with the hydrogel elastic modulus.....	76
Figure 4.3. Actin staining of Stro-1 <sup>+</sup> BMSCs on PAAm hydrogels with different elasticities.....	77
Figure 4.4. Nuclei, actin, and vinculin staining of Stro-1 <sup>+</sup> BMSCs on PAAm hydrogels with different stiffness.....	78
Figure 4.5. Phase-contrast images of BMSCs plated at 300, 500 and 1000 cells/cm <sup>2</sup> on PAAm hydrogels of different stiffness after 24hrs of incubation.....	79
Figure 4.6. The substrate elastic modulus increases the single-cell spreading of Stro-1 <sup>+</sup> BMSCs regardless of cell seeding density.....	79
Figure 4.7. Cell morphology of Stro-1 <sup>+</sup> BMSCs on soft PAAm hydrogels with different thicknesses.....	80
Figure 4.8. Cell-spreading area of Stro-1 <sup>+</sup> BMSCs slightly increased with the decrease in hydrogel thickness.....	80
Figure 4.9. Actin staining of Stro-1 <sup>+</sup> BMSCs on soft and stiff PAAm hydrogels with different thicknesses.....	81

Figure 4.10. Nuclei, actin, and vinculin staining of Stro-1 <sup>+</sup> BMSCs on soft PAAm hydrogels with different thicknesses.....	82
Figure 4.11. Nuclei, actin, and vinculin staining of Stro-1 <sup>+</sup> BMSCs on stiff PAAm hydrogels with different thicknesses.....	83
Figure 5.1. ALPL activity of unselected BMSCs increases under osteogenic conditions on TCP. BMSCs (M53) appear denser in the presence of osteogenic supplements.....	93
Figure 5.2. Stro-1 <sup>+</sup> BMSCs differentiate into osteoblasts on TCP. (Left) ALPL staining of selected Stro-1 <sup>+</sup> BMSCs from 2 patients (M53 and F97) on TCP in basal and osteogenic medium. ....	94
Figure 5.3. ALPL activity and DNA of selected BMSCs (M53) increase under osteogenic conditions.....	94
Figure 5.4. Stro-1 <sup>+</sup> BMSCs (F97) on 1, 40 PAAm hydrogels and TCP.....	95
Figure 5.5. Stro-1 <sup>+</sup> BMSCs (F97) differentiation was similar on soft and stiff matrices in basal and osteogenic conditions.. ....	96
Figure 5.6. Stro-1 <sup>+</sup> BMSCs (M53) equally differentiate on soft and stiff matrices.....	97
Figure 5.7. Stro-1 <sup>+</sup> BMSCs (M53) at different seeding densities in basal and adipogenic medium on TCP.. ....	98
Figure 5.8. Stro-1 <sup>+</sup> BMSCs (M53) differentiated into adipocytes on TCP regardless of the seeding density.. ....	98
Figure 5.9. Stro-1 <sup>+</sup> BMSCs (M53) differentiated into adipocytes on PAAm hydrogels. ....	99
Figure 5.10. Stro-1 <sup>+</sup> BMSCs (M53) differentiated into adipocytes on PAAm hydrogels regardless of the hydrogel elastic modulus.....	100
Figure 5.11. Adipogenic differentiation of Stro-1 <sup>+</sup> BMSCs (M53) increased on 1 kPa PAAm hydrogels and TCP.....	100
Figure 5.12. Stro-1 <sup>+</sup> BMSCs (M53) differentiated into adipocytes on PAAm hydrogels regardless of the hydrogel elastic modulus at high seeding density.....	101
Figure 5.13. Stro-1 <sup>+</sup> BMSCs (M53) DNA concentration increased on thin PAAm hydrogels. ....	102
Figure 5.14. The substrate thickness influenced Stro-1 <sup>+</sup> BMSCs (M53) DNA concentration and ALPL activity on soft and stiff PAAm hydrogels. ....	103

Figure 5.15. ALPL staining of Stro-1 <sup>+</sup> BMSCs (M53) on soft and stiff PAAm hydrogels with different thicknesses in basal and osteogenic medium. ....	104
Figure 5.16. The decrease in hydrogel thickness did not significantly influence the percentage of the stained area of Stro-1 <sup>+</sup> BMSCs (M53).....	105
Figure 5.17. Substrate thickness did not influence the DNA concentration of Stro-1 <sup>+</sup> BMSCs (F67).....	106
Figure 5.18 ALPL activity of Stro-1 <sup>+</sup> BMSCs (F67) did not change when varying the thickness of soft and stiff PAAm hydrogels. ....	107
Figure 5.19 The substrate mechanical properties did not significantly influence the RNA concentration of Stro-1 <sup>+</sup> BMSCs (F63).....	108
Figure 5.20 ALPL expression of Stro-1 <sup>+</sup> BMSCs (F63) increased on stiff PAAm hydrogels in osteogenic conditions.....	109
Figure 5.21 The substrate mechanical properties did not modify <i>RUNX2</i> expression of Stro-1 <sup>+</sup> BMSCs (F63).....	109
Figure 5.22 Substrate mechanical properties and osteogenic supplements modified Stro-1 <sup>+</sup> BMSCs (F67) morphology.. ....	110
Figure 5.23 The substrate mechanical properties did not significantly influence <i>ALPL</i> and <i>RUNX2</i> expression in Stro-1 <sup>+</sup> BMSCs (F67).....	111
Figure 6.1 Phase-contrast and fluorescent images of soft and stiff PAAm hydrogels with different thicknesses containing embedded fluorescent microbeads.....	121
Figure 6.2 Time-lapse imaging of the Stro-1 <sup>+</sup> BMSCs on soft, thick PAAm hydrogels with embedded fluorescent microbeads.....	123
Figure 6.3 Time-lapse imaging of the Stro-1 <sup>+</sup> BMSCs on stiff, thick PAAm hydrogels with embedded fluorescent microbeads.....	123
Figure 6.4 Hydrogel displacements by Stro-1 <sup>+</sup> BMSCs 1 h after seeding.....	124
Figure 6.5 Representative fluorescent images of Stro-1 <sup>+</sup> BMSCs on soft, stiff, thin, and thick PAAm hydrogels with embedded fluorescent microbeads on day 10..	125
Figure 6.6 Hydrogel displacements by Stro-1 <sup>+</sup> BMSCs after 10 days of incubation....	126
Figure 6.7 Phase-contrast and fluorescent images of Stro-1 <sup>+</sup> BMSCs on soft, thin and soft, thick PAAm hydrogels with embedded fluorescent microbeads in week 7 over 24 h.....	127

Figure 6.8 Hydrogel deformations remained stable over 24 h on week 7, regardless of their mechanical properties..	127
Figure 6.9 Displacements on soft, thick, and stiff, thick PAAm hydrogel decreased from day 0 to week 7..	128
Figure 6.10 Phase-contrast images of Stro-1 <sup>+</sup> BMSCs at different seeding densities on soft, thick PAAm hydrogels in basal and osteogenic media at the beginning and end of the time-lapse experiment..	129
Figure 6.11 Soft, thick hydrogel deformations decreased with the increase of the seeding density.....	130
Figure 6.12 Phase-contrast images of Stro-1 <sup>+</sup> BMSCs on soft, thin, and thick PAAm hydrogels in basal and osteogenic media at low seeding densities at 5 minutes and 20 hours on day 1.....	131
Figure 6.13 Soft, thick hydrogels were highly deformed; displacements increased in osteogenic conditions and were influenced by seeding density on day 1....	132
Figure 6.14 Stro-1 <sup>+</sup> BMSCs on soft, thin, and thick PAAm hydrogels at different seeding densities in basal and osteogenic conditions on day 7..	133
Figure 6.15 Stro-1 <sup>+</sup> BMSCs created greater deformations on soft, thick hydrogels at low seeding density and in osteogenic conditions on day 7..	134
Figure 6.16 Stro-1 <sup>+</sup> BMSCs at 1,000 and 5,000 cells/cm <sup>2</sup> on 1kPa PAAm hydrogels with different thicknesses in basal and osteogenic media on day 14..	135
Figure 6.17 Stro-1 <sup>+</sup> BMSCs at lower seeding densities produced greater deformations on soft, thick hydrogels in osteogenic medium on day 14.....	135
Figure 6.18 Stro-1 <sup>+</sup> BMSCs at 5,000 cells/cm <sup>2</sup> on soft, stiff, thin, and thick PAAm hydrogels in basal and osteogenic media on day 4..	137
Figure 6.19 Stro-1 <sup>+</sup> BMSCs at 5,000 cells/cm <sup>2</sup> produced the greatest deformations on soft, thick hydrogels in osteogenic media on day 4.....	137
Figure 6.20 Stro-1 <sup>+</sup> BMSCs on soft, stiff, thin, and thick PAAm hydrogels in basal and osteogenic conditions on day 7..	138
Figure 6.21 Stro-1 <sup>+</sup> BMSCs at 5,000 cells/cm <sup>2</sup> generated greater deformations in basal medium on soft PAAm hydrogels on day 7.....	139

## Table of Figures

Figure 6.22 Hydrogel deformations by Stro-1 <sup>+</sup> BMSCs at 1,000 cells/cm <sup>2</sup> during osteogenic differentiation on day 1 and day 7..	139
Figure 6.23 Hydrogel displacements by Stro-1 <sup>+</sup> BMSCs at 1,000 cells/cm <sup>2</sup> increased in the presence of osteogenic supplements on day 1 and day 7..	140
Figure 6.24 Morphology of Stro-1 <sup>+</sup> BMSCs on PAAm hydrogels of different elasticity and thickness during adipogenic differentiation on day 7..	141
Figure 6.25 Adding adipogenic supplements decreased hydrogel displacements by Stro-1 <sup>+</sup> BMSCs on day 7..	142
Figure 6.26 Stro-1 <sup>+</sup> BMSCs generated small deformations on soft, thick matrices in adipogenic media on day 14..	142
Figure 6.27 Stro-1 <sup>+</sup> BMSCs created smaller deformations on soft, thick matrices in adipogenic media on day 3..	143
Figure 6.28 Soft hydrogel displacements by Stro-1 <sup>+</sup> BMSCs decreased in the presence of adipogenic supplements on day 12..	143
Figure 6.29 Designs of the 3D printed PLA moulds to fabricate the PDMS stamps with and without patterns..	144
Figure 6.30. MG63 cells on stiff, flat, and patterned (collagen 0.1 mg/mL) PAAm hydrogels after 24h incubation in DMEM+10% FBS..	145
Figure 6.31. MG63 cells on stiff, flat, and patterned (collagen 1 mg/mL) PAAm hydrogels after 24h incubation in DMEM+10% FBS..	145
Figure 6.32. Stro-1 <sup>+</sup> BMSCs on the 5 mm collagen islands on the 40 kPa PAAm hydrogels..	146
Figure 6.33. Design of the 3D printed PLA mould to fabricate the PDMS stamps with 1 mm diameter circular patterns..	146
Figure 6.34. FBS increased cell attachment to the collagen islands after 24 h incubation in 0.1% BSA..	147
Figure 6.35 FBS increased cell attachment to the collagen islands after 24 h incubation in 0.1% BSA..	147
Figure 6.36 The direct addition of the collagen-acrylate solution to the treated slide disrupts the hydrogel surface...	149

Figure 6.37 Time-lapse imaging of Stro-1 <sup>+</sup> BMSCs on soft hydrogels of different thicknesses for 24 hours..	150
Figure 6.38 Stro-1 <sup>+</sup> BMSCs highly deformed soft hydrogels when arranged in groups (more than 3 cells) and not as single cells.....	151
Figure 6.39 Groups of Stro-1 <sup>+</sup> BMSCs on soft hydrogels of different thicknesses for 24 hours.....	151
Figure 6.40 Stro-1 <sup>+</sup> BMSCs created greater displacements on soft hydrogels when arranged in big rather than small groups..	152
Figure 6.41 4 kPa and 40 kPa hydrogels with wells of different sizes (10, 20 $\mu$ m)..	152
Figure 6.42 MG63 cells within wells of different diameters: 20, 50 and 100 $\mu$ m on 4 kPa and 40 kPa hydrogels after 4 hours of incubation.....	153
Figure 6.43 MG63 cells on 4 kPa and 40 kPa hydrogels with wells of different diameters: 20, 50 and 100 $\mu$ m after 48 hours of incubation..	153
Figure 6.44 MG63 cells at 1,000 cells/cm <sup>2</sup> on 4 kPa and 40 kPa hydrogels with wells of different diameters: 20, 50 and 100 $\mu$ m after 48 hours of incubation..	154



## List of Accompanying Materials

Supplementary Video 1a: 1kPa 25 $\mu$ L 1h BF.  
Supplementary Video 1b: 1kPa 25 $\mu$ L 1h Cy3.  
Supplementary Video 2a: 40 kPa 25 $\mu$ L A 1h BF.  
Supplementary Video 2b: 40 kPa 25 $\mu$ L 1h Cy3.  
Supplementary Video 3a: 1kPa 5 $\mu$ L 1 h BF.  
Supplementary Video 3b: 1kPa 5 $\mu$ L 1h Cy3.  
Supplementary Video 4a: 40 kPa 5 $\mu$ L 1h BF.  
Supplementary Video 4b: 40 kPa 5 $\mu$ L 1h Cy3.  
Supplementary Video 5a: 1kPa 25 $\mu$ L day 10 BF.  
Supplementary Video 5b: 1 kPa 5 $\mu$ L day 10 BF.  
Supplementary Video 6a: 1kPa 25 $\mu$ L day 10 Cy3.  
Supplementary Video 6b: 1 kPa 5 $\mu$ L day 10 Cy3.  
Supplementary Video 7a: 40kPa 25 $\mu$ L day 10 BF.  
Supplementary Video 7b: 40kPa 5 $\mu$ L day 10 BF.  
Supplementary Video 8a: 40kPa 25 $\mu$ L day 10 Cy3.  
Supplementary Video 8b: 40kPa 5 $\mu$ L day 10 Cy3.  
Supplementary Video 9a: 1kPa 25 $\mu$ L week 7 BF.  
Supplementary Video 9b: 1kPa 5 $\mu$ L week 7 BF.  
Supplementary Video 10a: 1kPa 25 $\mu$ L week 7 Cy3.  
Supplementary Video 10b: 1kPa 5 $\mu$ L week 7 Cy3.  
Supplementary Video 11a: Basal 1,000 cells BF.  
Supplementary Video 11b: Basal 5,000 cells BF.  
Supplementary Video 11c: Basal 10,000 cells BF.  
Supplementary Video 11d: Basal 20,000 cells BF.  
Supplementary Video 12a: Osteogenic 1,000 cells BF.  
Supplementary Video 12b: Osteogenic 5,000 cells BF.  
Supplementary Video 12c: Osteogenic 10,000 cells BF.  
Supplementary Video 12d: Osteogenic 20,000 cells BF.  
Supplementary Video 13a: Basal 1KPa 5 $\mu$ L 1,000 cells day 1 BF.  
Supplementary Video 13b: Osteogenic 1KPa 5 $\mu$ L 1,000 cells day 1 BF.  
Supplementary Video 14a: Basal 1KPa 5 $\mu$ L 5,000 cells day 1 BF.  
Supplementary Video 14b: Osteogenic 1KPa 5 $\mu$ L 5,000 cells day 1 BF.  
Supplementary Video 15a: Basal 1KPa 25 $\mu$ L 1,000 cells day 1 BF.  
Supplementary Video 15b: Osteogenic 1KPa 25 $\mu$ L 1,000 cells day 1 BF.  
Supplementary Video 16a: Basal 1KPa 25 $\mu$ L 5,000 cells day 1 BF.  
Supplementary Video 16b: Osteogenic 1KPa 25 $\mu$ L 5,000 cells day 1 BF.  
Supplementary Video 17a: Basal 1KPa 25 $\mu$ L 1,000 cells day 14 BF.  
Supplementary Video 17b: Osteogenic 1KPa 25 $\mu$ L 1,000 cells day 14 BF.  
Supplementary Video 18a: 40kPa micropatterned hydrogels with 100 $\mu$ m wells.



## Research Thesis: Declaration of Authorship

Print name: María Luisa Hernández Miranda

Title of thesis: Individual and Collective Mechanosensing of Extracellular Matrix Thickness in Skeletal Stem Cell Differentiation

I declare that this thesis and its work are my own and have been generated by me as the result of my original research.

I confirm that:

1. This work was done wholly or mainly while in candidature for a research degree at this University;
2. Where any part of this thesis has previously been submitted for a degree or any other qualification at this University or any other institution, this has been clearly stated;
3. Where I have consulted the published work of others, this is always clearly attributed;
4. Where I have quoted from the work of others, the source is always given. Except for such quotations, this thesis is entirely my work;
5. I have acknowledged all primary sources of help;
6. Where the thesis is based on work done by myself jointly with others, I have made clear exactly what was done by others and what I have contributed myself;
7. Parts of this work will be published as:

1. Hernandez-Miranda M, Xu D, Johnston DA, Browne M, Cook RB, Sengers BG<sup>2\*</sup>, Evans ND: Geometric constraint of mechanosensing in marrow stromal cell cultures prevents stiffness-induced differentiation. *Biophysical Journal*. *In progress*.

2. Xu D., Hernandez-Miranda M.L., Evans N., Sengers B., Browne M., Cook R. Depth profiling via nanoindentation for characterising the elastic modulus and hydraulic properties of thin hydrogel layers. *Acta biomaterialia*. *In progress*

Signature: Maria Luisa Hernandez Miranda.....Date: 22<sup>nd</sup> May 2023



## Contributors

### Section 3.3.1, 4.3.3, 4.3.7

Dr David Johnston performed confocal microscopy at the Biomedical Imaging Unit, University of Southampton.

### Section 3.3.5

Nanoindentation was performed and analysed by Dr Dichu Xu in the National Centre for Advanced Tribology at Southampton (nCATS), University of Southampton—research collaboration.

### Chapter 6

Dr Edward Sander and Dr Hoda Zarkoob, University of Iowa, USA, provided the main MATLAB code for measuring hydrogel displacements.

Dr Bram Sangers, University of Southampton, wrote and improved the MATLAB code for plotting displacements.



## Agradecimientos

Mami Tonchis, aunque ya no estes aquí físicamente para leer esto, quiero darte el reconocimiento que mereces. Quiero agradecerte todo el apoyo que siempre me diste; desde llevarme a la guardería para estar con más niños hasta pagarme los cursos de inglés. Siempre te preocupaste en que tuviera lo mejor y sin duda nada de lo que soy y tengo lo hubiera logrado sin tu ayuda. Gracias por enseñarme a ser una persona responsable, comprometida, resiliente e independiente. Fuiste y serás la mejor mamá del mundo y siempre voy a tenerte presente. Te amo.

Papi Vir, gracias por apoyarme, motivarme en todo momento y sobre todo darme alas para volar. Gracias porque siempre has trabajado muy duro, haciendo equipo con mi mamá para que nunca me faltara nada. Siempre has estado conmigo consintiéndome y cuidándome desde llevándome a ortopedia hasta al trabajar. Te agradezco por enseñarme a ser una persona responsable, trabajadora, empática y por creer en mí. Eres el mejor papá del mundo y espero que la vida me permita devolverte un poco de lo mucho que me has dado. Te amo.

Hermanita Carmen, muchas gracias por siempre apoyarme, ayudarme e impulsarme para cumplir mis metas y enseñarme a ser responsable y trabajadora. Siempre has sido mi modelo para seguir y estoy muy agradecida por todo el esfuerzo que has hecho para apoyarme. Te quiero muchísimo y deseo seguir compartiendo nuestros logros juntas.

Hermanita Mago, gracias por el apoyo y ayuda que siempre me has dado. Este logro también es gracias a ti y espero que podamos seguir compartiendo muchas más experiencias juntas. Te quiero mucho.

Roxanna y Juan, gracias por todos los momentos que hemos pasado juntos, por haberme brindado su amistad, ayuda y apoyo en los buenos y malos momentos. Esta experiencia del PhD no hubiera sido la misma sin su compañía. Los quiero mucho.

Nadia, Alan, Tania, Isabel, Jaz, Mari, Ismael y Ale, gracias porque a pesar de la distancia y los horarios, siempre han estado para escucharme, apoyarme, y aconsejarme en los buenos y en los malos momentos. Porque con sus palabras me impulsaron siempre a seguir adelante y eso es invaluable para mí. Los quiero mucho.

Norberto, muchas gracias por apoyarme y ayudarme a desarrollar las herramientas para adaptarme a los diferentes cambios y retos en esta etapa que ha sido llena de crecimiento y aprendizaje.

## Agradecimientos

Rosario, muchas gracias por darme apoyo y ayudarme a aprender ser más resiliente para sobrellevar los dos momentos más difíciles de mi vida para seguir adelante y lograr conseguir esta meta.

Héctor, muchas gracias por estar, apoyarme, motivarme y consentirme en esta etapa complicada de la escritura. Valoro mucho que me has escuchado en todo momento y has sido muy comprensivo conmigo. Te quiero.

Dianita, gracias por estar presente, incluso a lo lejos, motivándome y apoyándome siempre, sin ti la experiencia del PhD no hubiera sido la misma. TQM.

Daniela, gracias por esas platicas y ayuda que me ayudaron a seguir adelante. Encontré gran apoyo y motivación y eso lo agradezco infinitamente.

Irene, Gaby, gracias por esas lindas platicas, convivencias y apoyo, sin duda la experiencia del doctorado no hubiera sido la misma sin ustedes. Las quiero.

## Acknowledgements

I want to thank my sponsors and those who helped me during my PhD journey.

I am grateful for the sponsorship from the National Council of Science and Technology in Mexico (CONACyT) and the Faculty of Medicine at the University of Southampton.

Special thanks to my supervisor Nick Evans. Thanks for accepting me into your research group and supporting me since I applied to the university. I appreciate your help and support, especially during my difficult situations. Thanks also for challenging and guiding me always to do my best.

Thanks to my supervisor Bram Sengers for always supporting this project's development, providing feedback and helping me solve issues with MATLAB with a great disposition.

I am grateful for David Wilson's support. Thanks for always helping me and offering advice throughout this PhD journey.

Thanks to David Johnston for his great disposition to help me with the confocal microscope.

Thanks to my friend Aya for supporting me during these four years in and outside the lab. We have learned together and supported each other, having excellent memories.

Thanks to the B&J group, especially my colleagues Jon May, Anna, Yanghee and Julia, for listening to me and offering their help and support when I needed it.



## Definitions and Abbreviations

4-MU	fluorescent 4-Methylumbelliferone
A <sub>2</sub> P	ascorbate-2-Phosphate
AFM	atomic force microscopy
ALPL	alkaline phosphatase
APES	3-Aminopropyltriethoxysilane
APS	ammonium persulfate
<i>BMP2</i>	bone morphogenetic protein 2
BMPs	bone morphogenetic proteins
BMSCs	bone marrow stromal cells
BP-G	B-glycerophosphate
cDNA	complementary DNA
DAPI	4', 6-diamidino-2-phenylindole
DCDMS	dimethyldichlorosilane
DMEM	Dulbecco's modified Eagle's medium.
DNA	deoxyribonucleic acid
<i>E</i>	Young's modulus
ECM	extracellular matrix
EDTA	ethylenediaminetetraacetic acid
ESCs	embryonic stem cells
ETA	ethanolamine
FAK	focal adhesion kinase
FAs	focal adhesion
FBS	fetal bovine serum
HEPES	4-(2-hydroxyethyl)-1-piperazineethanesulfonic acid
IBMX	3-isobutyl-1-methylxanthine
iPS	induced pluripotent stem cells
ITS	Insulin-Transferrin-Selenium

## Definitions and Abbreviations

MAPK	mitogen association protein kinase
MUP	4-Methylumbelliferyl phosphate
NaOH	sodium Hydroxide
OCN	osteocalcin
OPN	osteopontin
PAAm	polyacrylamide
PBS	Phosphate-buffered saline
PCR	polymerase Chain Reaction
PDMS	polydimethylsiloxane
PEG	polyethene glycol
PFA	paraformaldehyde
qPCR	polymerase Chain Reaction
RhoA	rho kinase
RNA	ribonucleic acid
ROCK	RhoA-Rho-kinase
RT-PCR	Reverse Transcription Polymerase Chain Reaction
<i>RUNX2</i>	runt-related transcription factor 2
Sulfo-SANPAH	sulfosuccinimidyl 6-(4'-azido-2'-nitrophenylamino)hexanoate
SSCs	skeletal Stem Cells
TAZ	transcriptional coactivator with PDZ-binding motif
TCP	tissue culture polystyrene
TEMED	tetramethylethylenediamine
TFM	traction force microscopy
TGFb1	transforming growth factor-beta
TRIS	(hydroxymethyl)aminomethane
YAP	Yes-associated protein
.	minimum essential medium Eagle - ALPLha modification

# Chapter 1 Introduction

## 1.1 Mechanobiology and Physiology

Mechanical forces, such as gravity, tension, compression, and hydrostatic pressure, are essential in normal physiological processes such as breathing, blood flow, muscle contraction, tissue formation and patterning. Friedrich Pauwels highlighted in "A New Theory Concerning the Influence of Mechanical Stimuli the Differentiation of the Supporting Tissues" that mechanical stimuli such as hydrostatic pressure and tensile and compressive strains promote bone remodelling and cartilage (Pauwels, 1980). Meanwhile, Carter and co-workers proposed that cartilage formation, maturation and degeneration could be accelerated or inhibited by applying stress (Carter and Wong, 1988).

Besides tissue formation, these mechanical forces also form the different patterns we observe in nature. In "Chemical Basis of Morphogenesis", Alan Turing suggested that pattern formation depends on chemical, mechanical stimuli, and biology (Turing, 1953). During this process, independent cells produce the spots and stripes of mammals and fish, the pigmentation patterns of bird feathers, and the spiral growth of plant leaves and mollusc shells (Turing, 1953). Another "positional information" model supported the connexion between biomechanics and cell biology, stating that cells differentiate according to their position depending on the chemical and mechanical information they receive (Turing, 1953).

In addition to external forces, cells are exposed to internal forces exerted by neighbouring cells that continuously stretch and compress during development and growth. These forces determine the final volume occupied by a cell within a tissue; while osmotic pressure expands the cell, contractile forces within the cortex shrink it. Furthermore, the mechanical forces generated by the cells can influence crucial biological processes such as angiogenesis, metastasis, wound healing, and tissue formation through cell division, differentiation, mature cell function and migration changes. Because of this, cell mechanosensing and mechanobiology have been essential in tissue engineering to design materials that guide stem cells for tissue regeneration. (Wang *et al.*, 2008; Parekh *et al.*, 2011; Evans and Gentleman, 2014; Kular *et al.*, 2014; Heller and Fuchs, 2015; Jansen *et al.*, 2015; Tusan *et al.*, 2018).

Mechanobiology is an interdisciplinary field that studies the biological responses of cells to mechanical changes and the mechanisms by which this mechanical information is translated into cellular and molecular responses (Wang and Thampatty, 2006).

## 1.2 Important concepts in Mechanobiology

Once a force ( $F$ ) is applied to a material, it is transmitted through it and balanced by equal and opposite forces. Newton's third law explains this effect; for every action in nature, there is an equal and opposite reaction. As a result, the material will experience mechanical

stress and stress intensity ( $\sigma$ ) is expressed in force units per area (Pa). The extracellular matrix (ECM) stress propagation depends on its physical properties, such as porosity, rigidity, and cell density (Basu *et al.*, 2018; Jones and Ashby, 2019). The force applied to the hydrogel causes a deformation that can be measured and reflects the changes in length concerning the original state (strain). At specific stress, stiff materials experience less strain than soft materials. The relationship between stress and strain is determined by the elastic modulus or Young's modulus ( $E$ ), obtained by the initial slope of the stress-strain curve, and can be defined by Hooke's law. It highlights a linear relationship between stress and strain when strains are minor (for instance, in solids), but this can change, and the material can break (Jones and Ashby, 2019).

The property that describes how much a material resists deformation in response to the applied force is stiffness. In mechanobiology, this refers to the rigidity of the matrix sensed by the cells when applying forces, and the property described is the modulus (units of force/area). Applying mechanical stress and observing the resulting deformations makes it possible to measure a material stiffness; in this way, it is possible to assess the cell's mechanical properties by externally deforming them with a defined force and measuring the strain (Lange and Fabry, 2013; Evans and Gentleman, 2014; Caliaro *et al.*, 2016; Vining *et al.*, 2017; Venugopal *et al.*, 2018; Nehls *et al.*, 2019). Figure 1.1 summarises these essential concepts to understand mechanobiology.

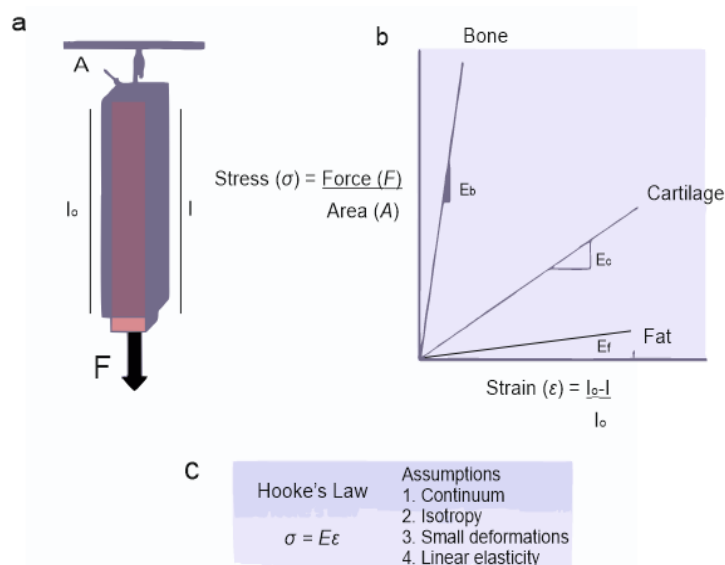


**Figure 1.1. Representation of Hooke's law.** (a) The mechanical properties of a material with the defined area ( $A$ ) can be obtained by applying force ( $F$ ) and measuring the change in length ( $l$ ) from an initial length ( $l_0$ ). (b) According to Hooke's law, if stress ( $\sigma$ ) is plotted as a function of strain ( $\epsilon$ ), the slope of the curve reflects Young's or elastic modulus ( $E$ ). Atomic Force Microscopy (AFM) is a method that can be used to measure this relation. Indeed, stiffer tissues (bone) have more significant  $E$  than softer tissues (cartilage and fat). (c) Assumptions that should be valid for calculating  $E$ . Many biomaterials used as cell substrates do not comply with these assumptions (Evans and Gentleman *et al.*, 2014).

The relation between stress and strain depends on the material's properties; elastic materials such as crosslinked hydrogels store the energy during deformation, and linearly elastic materials show a linear relationship between stress and strain. In contrast, viscoelastic materials dissipate energy and show a combination of solid and liquid properties with stress and/or strain changing as a function of time. Different tissues and organs, such as the breast, skin, muscle, liver, adipose tissues, coagulated bone marrow, and the brain, are the most viscoelastic tissues, where this property might be responsible for separating grey from white matter. In addition to cartilage, bone, tendons, ligaments, and cranial sutures, cells and ECM are also viscoelastic (Vining *et al.*, 2017; Chaudhuri *et al.*, 2020).

Skin and fat tissues can recover their shape after being compressed or pinched due to their viscoelastic behaviour; tendons can be broken abruptly or extended permanently. Therefore, viscoelasticity might also dictate disease progression, promoting tumour formation (breast cancer, gliomas, multiple sclerosis) and ageing (Chaudhuri *et al.*, 2020).

### **1.3 Mechanobiology and tissue development**

The ECM mechano-chemical cues control the patterns of self-organisation during development and dictate tissue behaviour (Shivashankar *et al.*, 2015). The ECM comprises fluids, solids, gases, and other cells and exerts external resistance that might be maintained, transmitted, or depleted (Vining *et al.*, 2017).

Intrinsic and extrinsic mechanical forces dictate embryonic growth, differentiation, and morphogenesis. For instance, fluid shear forces during development determine body asymmetry and dictate fetal haematopoiesis and cardiac tissue formation. Meanwhile, tensile forces support smooth muscle development in the lung, and stress, strain, and hydrostatic pressure promote ossification following bone collar formation (Vining *et al.*, 2017).

Besides mechanical forces, cell division contributes to patterning by directing the position of daughter cells and generating the necessary tension and adhesion for changes in cell shape and rearrangement. Then, cells use these mechanical anisotropies and contractile forces to control cell density and couple cell fate with position to promote tissue self-organisation and patterning through "cell sorting". It is influenced by chemotaxis, differences in cell attraction, repulsion, and cell migration rates. During this process, two or more cell populations with different fates and mechanical properties create boundaries to define structures and generate and maintain embryonic, adult, and diseased tissues (Lange and Fabry, 2013; Bellas and Chen, 2014; Heller and Fuchs, 2015; Wickström and Niessen, 2018; Nehls *et al.*, 2019).

Differences in ECM composition can also influence cell sorting by modifying the adhesion to its cellular populations. The presence or absence of cell-ECM contact may alter dynamic rearrangements and the viscoelastic interactions between cells. This prevents the formation of adhesions between cells and ECM, affecting cell polarisation and positioning. Then, adhesion receptors can recognise and mechanically respond to local changes in the microenvironment. During contractility, the energy released by the ligation of cadherins expands the interface. The mechanical balance of these forces throughout tissues determines the final morphology of cells and sorting. Overall, dynamic changes in the microenvironment that control adhesion, confinement, and contractility can cause substantial phenotypic and functional alterations in cell spreading, proliferation, stem cell differentiation and migration (Lange and Fabry, 2013; Heller and Fuchs, 2015; Wickström and Niessen, 2018).

Cell-cell contact predominates during early development, but later, progenitor cells begin to differentiate and deposit ECM where they adhere (Vining *et al.*, 2017). When cells migrate within the tissues, they must generate mechanical forces to overcome resisting stresses. Cell migration is not a random process; the cell employs a specialised structure (lamellipodium) to establish new adhesions to sense the surroundings for appropriate directions. Cell movements tend to follow the direction of the changes in stress. Along with the interactions with neighbouring cells, they contribute to the coordinated movements of cell colonies and sheets, maintaining tissue homeostasis (Lange and Fabry, 2013).

Due to the importance of the ECM properties in regulating tissue homeostasis, the ability of cells to sense and respond to chemical and mechanical information from the ECM is imperative for numerous biological processes (Ringer *et al.*, 2017). For example, ECM stiffness influences stem cell differentiation, cell migration and proliferation, which are crucial to understanding embryonic development, tissue regeneration and disease progress (Li *et al.*, 2017).

#### **1.4 Role of stiffness in disease development**

The ECM provides essential signals to regulate cell growth and apoptosis and maintain tissue architecture and polarity. Therefore, the dysregulation of the ECM components or the mechano-signalling process can lead to many pathological conditions (Handorf *et al.*, 2015; Venugopal *et al.*, 2018). The ECM functionality depends on its biochemical and mechanical properties, a set of genes that codify 274 ECM proteins and 753 ECM-associated proteins. It is estimated that alterations in 34% of the ECM glycoprotein, 31% of the proteoglycan and 61% of the collagen genes lead to genetic diseases (Lamandé and Bateman, 2020).

The absence or dysfunction of collagen and fibronectin due to genetic deletion is often embryonic lethal, while mutations in genes encoding ECM proteins, such as COL1A1, affect bone formation (Bonnans *et al.*, 2014). For instance, the decrease in bone mass in osteogenesis imperfecta is caused by mutations in the genes encoding the two chains of procollagen type I, COL1A1 and COL1A2 (Lamandé and Bateman, 2020). In contrast, an increase in collagen deposition and cross-linking increases ECM stiffness, alters tissue morphogenesis and contributes to the progression of different diseases, such as fibrosis, where fibrous and stiff tissue replaces the original ECM (Bonnans *et al.*, 2014; Handorf *et al.*, 2015; Jansen *et al.*, 2015).

Besides metalloproteinases, enzymatic degradation through heparanases and sulphatases can also control ECM integrity. Metalloproteinase activity is regulated but increases during repair or remodelling in normal conditions. For instance, high heart-specific metalloproteinase expression disrupts collagen, which might lead to different pathologies such as cardiopathy. Here, myofibroblasts respond to the increase in ECM stiffness by activating their actin cytoskeleton, causing a loss of contractility (Bonnans *et al.*, 2014; Gaetani *et al.*, 2020).

ECM also directs immune responses.  $\alpha 1\beta 1$  integrin, which binds collagen type I and IV, is expressed by peripheral CD8<sup>+</sup> T cells during influenza infection and mediates the specific memory of T cells after infection. Immune cell migration also depends on the density and orientation of the ECM fibres; In contrast, areas without fibronectin and collagen ease T cell motility, and dense ECM areas can limit immune response in cancer (Bonnans *et al.*, 2014).

The increase in ECM stiffness also stimulates tumour formation in breast cancer, while the failure in cell mechanosensing relates to muscular dystrophies or kidney defects (Wall *et al.*, 2018).

In conclusion, a better understanding of ECM mechanobiology facilitates the development of treatments for different diseases and tissue regeneration through tissue engineering (Mullen *et al.*, 2015).

## **1.5 Mechanobiology and tissue engineering**

One million non-union fractures occur annually in the United States, and nearly 5-10% of the fractures worldwide do not heal. Besides bone fractures, traumas, tumours, infections, and diseases might affect bone health. Because of the above, there is an increased demand for creating materials that promote bone regeneration (Carvalho *et al.*, 2021).

Tissue engineering develops different biomaterials that mimic the ECM by combining cells, scaffolds, and cell-growth stimuli to regenerate connective tissues and organs (Kim *et al.*, 2016).

The ECM provides positional and structural support of the surrounding tissue to the cells. It binds and regulates the availability and activation of growth factors; therefore, it acts as a signalling source and topographical cue (Wickström and Niessen, 2018). Indeed, the ECM dictates cell shape, cell mechanics, cell motility and, more importantly, the coordinated movement of the cells to specific locations, which is essential for tissue development (Kim *et al.*, 2016).

Synthetic niches formed by scaffolds help create tissues *in vitro* for repairing or replacing organs *in vivo* by promoting the homing of the host cells. For this, the material should have a specific shape that maintains tissue structure and integrity functionality by promoting new tissue formation and maturation (Chen and Liu, 2016).

Tissue engineering has been successfully applied to regenerate some tissues. For instance, a patient's trachea was regenerated with a decellularised cadaver trachea and the tympanic membrane of a child with decellularised porcine small intestine mucosa (Wang *et al.*, 2023). The materials used for tissue regeneration might come from different sources.

## 1.6 Biomaterials mimicking the extracellular matrix

Most tissues in the body are soft viscoelastic materials with variable stiffness, from 100 Pa for the brain to 100 kPa for cartilage. However, most *in vitro* cell research occurs on tissue culture polystyrene (TCP), which has a modulus of ~1 GPa and allows the adsorption of serum and secreted proteins (Syed *et al.*, 2015). Healthy mammary epithelial cells exhibit tumorigenic potential in conventional monolayer culture on TCP but form multicellular spherical structures resembling healthy acini when encapsulated in a 3D basement membrane-derived hydrogel (Syed *et al.*, 2015). Similarly, embryonic stem cells (ESCs) spontaneously differentiate within a few days on plastic but not on hydrogels; whereas lung fibroblasts growing on stiff substrates undergo myofibroblast differentiation and preserve that phenotype even when moved later to soft substrates (Caliari *et al.*, 2016). Therefore, the stiffness mismatch dramatically affects how the cells respond to their environment (Syed *et al.*, 2015). Because of this, materials used for regenerative medicine should mimic the mechanical properties of the tissues to promote repair (Evans and Gentleman, 2014).

Clinical trials based on skeletal stem cells (SSCs) suggest a limited host response when cells are implanted, as less than 5% of injected cells remain at the site after some days of transplantation. Hydrogels are biomaterials composed of water (90%–99% depending on the polymer concentration) with polymeric networks that hold the injected cells in the target

site, acting as mechanical barriers by increasing the viscosity of the injected solution. Hydrogels mimic the physicochemical properties of the stem cell niche; tailorable stiffness/softness, high water content, and high permeability for oxygen, nutrients, and metabolites support cell survival and tissue regeneration (Burdick, Mauck and Gerecht, 2016). Hydrogel topography, degradation, and adhesion also influence the differentiation of stem cells, support the recruitment of endogenous cells and angiogenesis for tissue repair, and modify the inflammatory response to protect injected cells, stimulating cell function *in vivo* (Christensen *et al.*, 2016; Lee *et al.*, 2016).

Because of their tuneable mechanical and biochemical properties, hydrogels have been used for different biomedical applications such as contact lenses in ophthalmology, absorbable sealants in general surgery, fillers for scars correction, anti-adhesive coatings on meshes for abdominal wall and hernia repair, for repairing acute (e.g. traumatic injuries, stroke) or chronic (e.g. Parkinsonism, multiple sclerosis) neural damage and support cell growth in soft tissues such as the skin and bladder neck (Hunt *et al.*, 2014).

Physical or chemical cross-linking methods facilitate hydrogel polymerisation. Physical cross-linking consists of weak interactions between polymer networks that quickly relax. It occurs by changes in pH, temperature, and other physical stimuli. In contrast, chemical cross-linking forms covalent bonds between different polymer chains (Michael-type addition or Schiff base reactions) that are deformation-resistant. Endogenous or exogenous enzymes allow hydrogel formation *in situ* (enzyme-initiated cross-linking) mainly by transglutaminases activity, whereas ionic cross-linking occurs when a hydrophilic and ionisable polymer cross-links with a soluble di- or trivalent ion of opposite charge (Hunt *et al.*, 2014; Lee *et al.*, 2016).

Different synthetic or natural polymers can constitute hydrogels. Natural polymers include collagen, chitosan, gelatine, fibrin, alginate, hyaluronic acid, agarose, chondroitin sulphate, dextran, Matrigel, or silk. Meanwhile, synthetic hydrogels can be a form of polyethylene glycol (PEG), polydimethylsiloxane (PDMS) or polyacrylamide (PAAm) (Zhao *et al.*, 2014; Mullen *et al.*, 2015; Syed *et al.*, 2015; Caliaro *et al.*, 2016; Lee *et al.*, 2016). Using synthetic or non-mammalian ECM-derived polymers helps to decouple the hydrogel mechanical properties from cell adhesion; however, they exhibit a limited capacity to mimic 3D organisation and be remodelled by cells (Vining *et al.*, 2017).

**Table 1.1. Characteristics of natural and synthetic polymers forming hydrogels used as biomaterials** (Nakamura *et al.*, 2010; Pawar and Edgar, 2012; Rouillard *et al.*, 2011; Evans *et al.*, 2009; Zao *et al.*, 2013; Christensen *et al.*, 2016).

Polymer	Nature	Monomers	Characteristics
<b>Chitosan</b>	Natural	Glucosamine and N-acetylglucosamine	Linear polysaccharide Non-toxic Stable Biodegradable Sterilisable
<b>Alginate</b>	Natural	(1_4)-linked b-D-mannuronic acid (M) and a-Lguluronic acid (G)	Hydrophilic unbranched polysaccharide From brown seaweed and bacteria
<b>Hyaluronic acid</b>	Natural	D-glucuronic acid and N-acetylglucosamine	Non-sulfated linear glycosaminoglycan Ubiquitous in cells and serum
<b>Polyethylene glycol (PEG)</b>	Synthetic		High biocompatibility Lack of toxicity Ease of processing
<b>Polydimethylsiloxane (PDMS)</b>	Synthetic		Hydrophobic Requires proteins for cell attachment
<b>PVA</b>	Synthetic		Hydrophilic Used for injectable hydrogels Requires proteins for cell attachment
<b>Polyacrylamide (PAAm)</b>	Synthetic		Non-degradable Non-toxic With water-exchanging abilities

Polyacrylamide hydrogels have been widely used *in vitro* and *in vivo* to evaluate the effect of substrate stiffness on cell behaviour and, consequently, tissue formation. For example, soft hydrogels reduce cell spreading and increase cell motility, whereas cells on stiff materials generate larger traction forces, create more stable focal adhesions and form more defined fibres (Disher *et al.*, 2005; Christensen *et al.*, 2016).

PAAm hydrogel fabrication initiates by combining acrylamide (monomer) and bis-acrylamide (crosslinker) in the presence of ammonium persulfate (APS) and tetramethylethylenediamine (TEMED). APS is a source of free radicals, while TEMED is a catalyst to initiate redox radical polymerisation of the PAAm. PAAm hydrogels are typically fabricated on coverslips functionalised with aminosilanes, and once polymerised, a bifunctional crosslinker such as sulfo-SANPAH promotes protein conjugation and cell attachment (Caliari *et al.*, 2016). Signalling molecules such as bone morphogenetic proteins (BMPs), transforming growth factor-beta 1 (TGFb1) or neurotrophic factors are

often attached to hydrogels to drive osteogenic, chondrogenic, or neurogenic differentiation (Lee *et al.*, 2016).

PAAm and PDMS help study the effect of ECM stiffness on cell behaviour and quantify cell traction forces by traction force microscopy (TFM), described further in Section 2.2.1.1. Cell traction forces and consequent substrate deformations can be studied by quantifying the substrate displacements of fluorescent beads embedded in the PAAm hydrogels or micropatterned PDMS. Studies using these materials indicate that adherent cell continuously perceives their microenvironment and generate forces depending on substrate stiffness; cells pull harder on stiff materials compared to their behaviour on soft hydrogels. (Li *et al.*, 2017).

Biomaterials frequently used as scaffolds for stem cells need to mimic the ECM physicochemical, biochemical, and mechanical properties to provide an appropriate and specialised microenvironment (stem cell niche) composed of soluble factors and membrane components that control stem cell self-renewal and differentiation to regenerate tissues (Kolios and Moodley, 2013; Zhao *et al.*, 2014).

## 1.7 Extracellular matrix

Tissue engineering combines stem cells and biomaterials by establishing an appropriate microenvironment to promote tissue regeneration. Recently, the mechanical properties of the extracellular matrix (ECM) have acquired more interest in tissue engineering as they dictate cellular behaviour and stem cell differentiation.

The ECM is a three-dimensional, non-cellular structure that binds and maintains cells together, supporting tissue integrity and elasticity. It is present in all tissues, and every organ has an ECM with a particular composition and topographical characteristics generated in the early embryonic stages. The ECM biochemical and mechanical properties vary from one tissue to another (from lung, bone to skin tissues), within the same tissue (renal cortex versus renal medulla) and depending on the normal or cancerous state. This structure is essential for life as it participates in cell proliferation, migration, and differentiation (Frantz *et al.*, 2010; Bonnans *et al.*, 2014; Kular *et al.*, 2014; Janson and Putnam, 2015).

Two main types of ECM differ in their location and composition: the interstitial connective tissue matrix, which surrounds cells and provides structural support for tissues, and the basement membrane, which is a specialised form of ECM that separates the epithelium from the surrounding stroma (Bonnans *et al.*, 2014).

Nearly 300 proteins forming the core matrisome, including collagen, proteoglycans, and glycoproteins, comprise the ECM in mammals (Bonnans *et al.*, 2014). Table 2 summarises, and Figure 1.2 represents the ECM components.

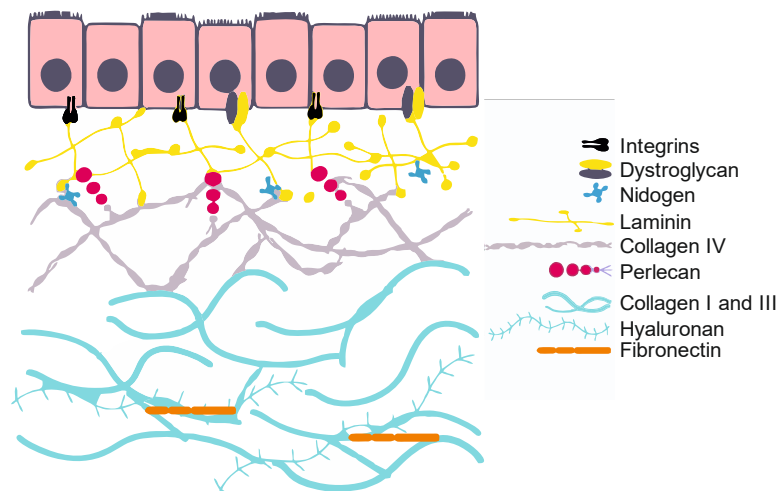


**Figure 1.2. Representation of the extracellular and basement extracellular matrix components-** adapted from Husell *et al.*, 2018.

**Table 1.2. Components, characteristics, and functions of the extracellular matrix** (Bonnans *et al.*, 2014).

Component	Characteristic	Classification or examples	Functions
<b>Collagens</b>	Predominant and primary structural proteins of the ECM	<ul style="list-style-type: none"> <li>Fibrillar (collagens I–III, V and XI)</li> <li>Non-fibrillar forms.</li> </ul>	<ul style="list-style-type: none"> <li>Provide tensile strength to connective tissues that are required to resist different mechanical stresses like tension, shear, and pressure.</li> <li>Limit tissues distensibility</li> </ul>
<b>Proteoglycans</b>	Core proteins with attached glycosaminoglycan (GAG) side chains found among collagen fibrils	<ul style="list-style-type: none"> <li>Aggrecan</li> <li>Versican</li> <li>Perlecan</li> <li>Decorin</li> </ul>	<ul style="list-style-type: none"> <li>Fill the extracellular interstitial space</li> <li>Confer hydration functions by sequestering water within the tissue</li> <li>Bind many growth factors</li> </ul>
<b>Glycoproteins</b>	Role in ECM assembly	<ul style="list-style-type: none"> <li>Laminins</li> <li>Elastin</li> <li>Fibronectins</li> <li>Thrombospondins</li> <li>Tenascins</li> <li>Nidogen</li> </ul>	<ul style="list-style-type: none"> <li>Participates in the ECM and cell interaction by acting as ligands for cell surface receptors such as integrins.</li> <li>Reservoir of growth factors</li> <li>Elastin helps to recover from continuous stretching</li> </ul>
<b>ECM-associated proteins</b>	Important for cell modelling	<ul style="list-style-type: none"> <li>Cytokines</li> <li>Mucins</li> <li>Secreted C-type lectins</li> <li>Galectins</li> <li>Semaphorins</li> <li>Plexins</li> <li>ECM-enzymes</li> </ul>	<ul style="list-style-type: none"> <li>Growth factors</li> <li>Involved in cross-linking</li> </ul>

ECM components such as collagen, elastin, laminin, perlecan and other proteins and proteoglycans compose tissues. For example, elastin in two different forms can be circulating in blood plasma and delivered to the target site during wound healing or as a cellular protein synthesised by fibroblasts. Meanwhile, various cell types express fibronectin, which directs the interstitial ECM organisation and regulates cell attachment (Frantz *et al.*, 2010; Kular *et al.*, 2014).

ECM plays an essential role in cell communication as cells sense the changes in their biochemical and mechanical properties, which influence cell behaviour and tissue homeostasis. Then, the materials used for tissue regeneration must mimic the ECM properties as it was aimed in this PhD project by coating polyacrylamide hydrogels of the desired elastic modulus with collagen type I.

## 1.8 ECM and stiffness sensing

ECM stiffness might cause changes in cell organisation, which influences cellular processes such as migration, proliferation, and differentiation that dictate tissue development and cancer progression. Because of its impact on cellular behaviour, stiffness is one of the most studied ECM mechanical properties (Engler *et al.*, 2006; Parekh *et al.*, 2011; Mathieu and Lobo, 2012).

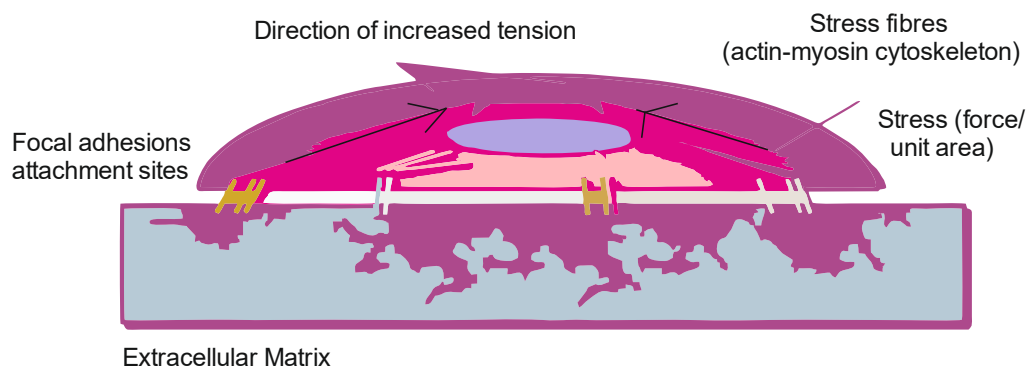
Natural ECMs are viscoelastic, displaying viscous liquid and solid elastic properties, and their mechanical response depends on time. Then, the ECM structure is susceptible to deformation (determined by  $E$ ) due to cell-applied forces. Still, cells can also experience changes in their specific elasticity, which can be measured in individual cells by AFM indentation experiments as a function of cell area (Nehls *et al.*, 2019).

Most ECM components show a higher elastic modulus than cells; for instance, brain tissue has an elastic modulus of around 1 kPa as it consists predominantly of cells and has only a relatively small ECM (Janson and Putman, 2015).

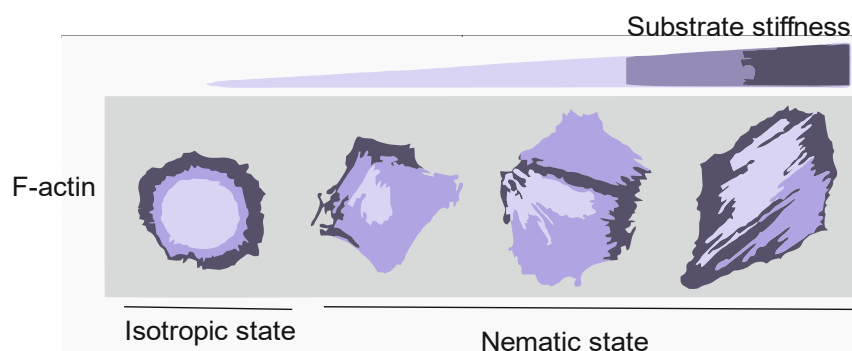
Cells sense the substrate elasticity by exerting traction forces at the anchorage points (focal adhesions) and sensing their displacement as a function of the applied force. If the substrate is stiff, it may not move or be deformed; therefore, all the generated tension will remain within the cell and promote cell spreading. In contrast, a soft substrate can be easily deformed, which causes cells to generate much less internal tension within the cytoskeleton and less polymerisation in stress fibres which provokes cells to appear round and small (Gupta *et al.*, 2016).

Figure 1.3 exemplifies the components that participate in ECM stiffness sensing, such as focal adhesions and the actin cytoskeleton, where tension and stress increase. Figure 1.4

illustrates the changes in the actin cytoskeleton from an isotropic to a nematic state (where the cytoskeleton is randomly arranged but in the same direction) with increased substrate stiffness.



**Figure 1.3. Mechanical forces are sensed by cells.** A cell interacts with the stiff ECM through the integrins at the focal adhesions, which simultaneously interact with the actin cytoskeleton. They pull the matrix and sense its resistance to deformation, which increases tension within the cell—adapted from Wells, 2008.



**Figure 1.4. Cell morphology and cytoskeleton change on a substrate with increasing stiffness.** The cell is in the isotropic state before interacting with the substrate. It will remain the same on a soft substrate after applying force and deforming it, which generates slight tension within its cytoskeleton and less actin polymerisation, which maintains its round shape. On a stiffer substrate, the cell applies force. Still, it cannot deform the substrate, which generates cell tension and promotes fibre polymerisation and, consequently, cell spreading—adapted from Gupta *et al.*, 2016.

The ECM is outstanding for cells to sense the mechanical properties of the surroundings (mechanosensing), which activates specific biochemical pathways (mechanotransduction) that lead to different biological responses, such as differentiation (Parekh *et al.*, 2011).

## 1.9 Mechanosensing and mechanotransduction

Cells exert force on the materials they adhere to and sense the resulting displacement in a process known as mechanosensing (Adamopoulos *et al.*, 2016). Static and dynamic mechanical stress continuously influences all tissues, which respond by two mechanisms: transmission or transduction. Indeed, the transmission of these mechanical forces all over the cell produces changes in the cytoskeleton and other organelles and activates biochemical signals through mechanotransduction (Iolascon *et al.*, 2013).

The mechanisms by which cells identify and process this mechanical information into chemical signals depend on its nature and the structures involved (ion channels, G-protein coupled receptors, integrins and protein kinases). For instance, plasma membrane tension changes are translated by mechanosensitive ion channels, whereas intercellular stresses are detected by cadherin-based adherents' junctions or other cellular proteins or organelles (Rustad *et al.*, 2013; Janson and Putman, 2015; Doyle and Yamada, 2016; Ringer *et al.*, 2017). In the bone, the osteocyte is the mechanosensor that transforms mechanical information (shear stress and stretch, modifications in extracellular pressure and strains) into biochemical signals, directing osteogenesis; osteocytes detect microcracks and promote bone remodelling (Iolascon *et al.*, 2013).

The mechanotransduction processes that identify and translate changes in ECM stiffness initiate when cells adhere to the ECM proteins (laminins, collagens, fibronectin, vitronectin and osteopontin) through the arginine, glycine, and aspartic acid amino acid sequence RGD in integrins. Integrins cluster together and associate with various intracellular proteins to form a focal complex that grows and matures into a focal adhesion (FAs). FAs form a physical bridge to interchange mechanical information between the ECM and the cell. The adhesion strength and the mechanical feedback cells decrease with larger anchored collagen fibres. Cell traction forces generated through these interactions modify the cytoskeletal tension on actin, myosin II, and microtubules. This leads to changes in cell shape and the activation of the associated signalling cascades that regulate gene expression and alters cell migration, proliferation, and differentiation (Parekh *et al.*, 2011; Trappmann *et al.*, 2012; Lee *et al.*, 2013; Shin *et al.*, 2013; Janson and Putnam, 2015; Lee *et al.*, 2015). Figure 1.5 illustrates the structures participating in the mechanosensing and the mechanotransduction processes.

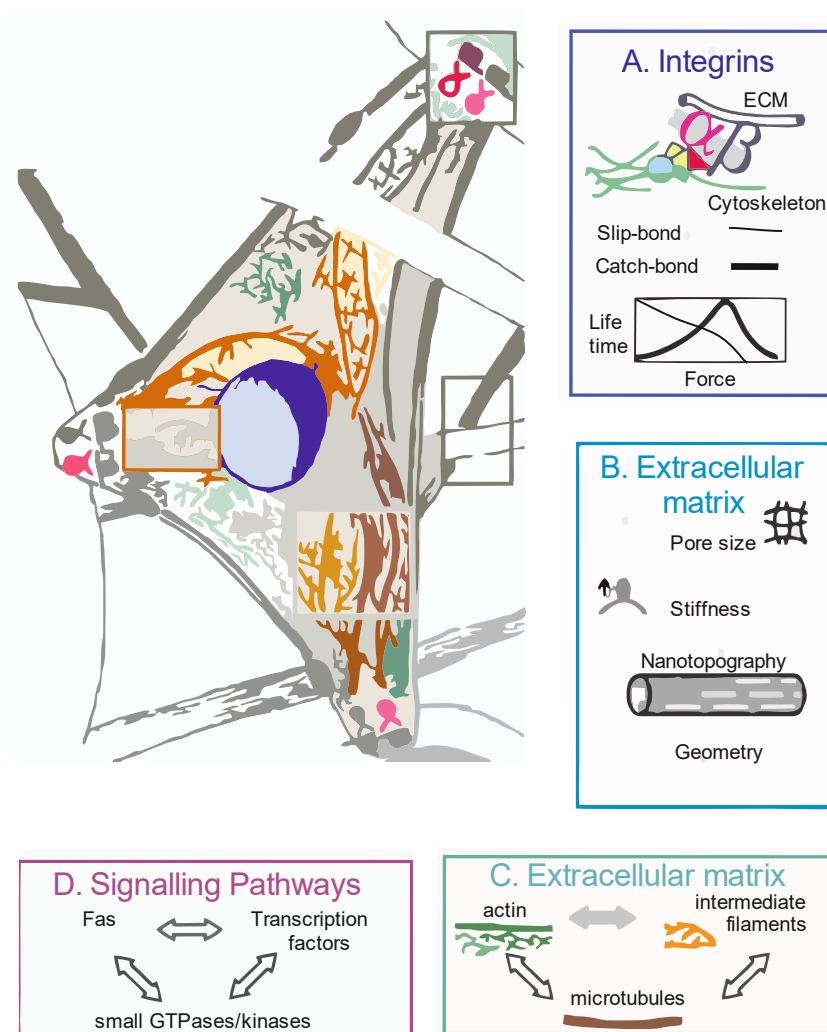


**Figure 1.5. Structures involved in the mechanosensing and mechanotransduction process.** (a) An  $\alpha$  and  $\beta$  subunit of the integrins with other molecules form the slip-bond (lifetime decreases with force) and catch-bond (lifetime increases gradually with force). (b) The ECM stiffness defines its geometry (pore size and nano topography). (c) Actin fibres, intermediate filaments and microtubules conform to the ECM's actin cytoskeleton. (d) FAs and transcription factors activate different signalling pathways, directing cell behaviour- adapted from Janson and Putnam, 2015.

Besides the above structures, the plasma membrane translates mechanical tension and activates ion channels. Multiple membrane proteins such as connexins forming Gap junctions, support intracellular communication and ATP, cAMP, calcium (essential to maintain cell binding as it induces conformational changes in cadherins), and inositol phosphate trafficking, directing mechanotransduction (Hao *et al.*, 2015).

### 1.9.1 Integrins

Integrins are heterodimers of  $\alpha$  and  $\beta$  subunits that bind to the ECM, and ALP-alpha-2 integrin expression rises with increasing stiffness (Mathieu and Lobo, 2012). The integrin cytoplasmic tails start recruiting actin-binding proteins inside the cell, such as talin and vinculin. After the cell receives mechanical information from the outside, the integrin tails

undergo conformational changes that facilitate talin binding and promote active conformation. After activation, the cytoplasmic domain of integrins binds to the actin and stimulates the formation of new adhesions (Rustad *et al.*, 2013; Salvi *et al.*, 2018). These changes influence cytoskeletal re-organisation, gene expression, cell proliferation, and adhesion, which are especially crucial for osteogenesis. For instance, when cells are cultured on glass with no ECM and then exposed to an osteogenic differentiation medium, cytoskeletal changes can be detected in the first 24 h. In contrast, changes in SSCs plated on fibronectin-coated materials occur after 72 h as they deposit their own ECM. Therefore, osteogenic differentiation requires binding integrins to the ECM (Mathieu and Lobo, 2012).

Because of the above, integrins operate as mechanosensors and mechanotransducers communicating the actin cytoskeleton and the ECM through dynamic interactions on soft ECM or focal adhesions on stiffer matrices (Kular *et al.*, 2014; Lee *et al.*, 2015).

Integrins are also crucial for cell-ECM adhesion, maintaining stem and progenitor cell pools in germline and adult epidermal niches, and influencing cell proliferation, differentiation, and self-renewal by activating FAK and PI3K signalling pathways (Hao *et al.*, 2015; Vining *et al.*, 2017).

## **1.9.2 Focal adhesions**

Adhesion proteins such as talin, vinculin, and p130cas form focal adhesions. These structures show dynamic movement compared to actin, integrins and signalling molecules. The cells receive mechanical strain through focal adhesions, and as a result, they increase or limit ECM production, modify their cytoskeleton, and reorder the forces they apply (Rustad *et al.*, 2013; Kular *et al.*, 2014; Lee *et al.*, 2015; Doyle and Yamada, 2016).

FAs consist of different vertical layers; an outer layer where integrin receptors link to the ECM, an intermediate layer where chemical and mechanical signals are processed, and an inner layer dominated by the actomyosin cytoskeleton (Ringer *et al.*, 2017).

Focal adhesion kinase (FAK) is the major component of focal adhesions, which activates with changes in nano topography and substrate elasticity and activates RhoA (Rustad *et al.*, 2013; Janson and Putnam, 2015).

Once the new FAs, which are force-independent, are formed, they mature into force-dependent focal adhesions. Changes in cell spreading, local curvature, actin organisation, and cellular geometry determine the number of focal adhesions. Then, if there is a proper binding with the actin cytoskeleton, FAs are transformed into fibrillary adhesions (Oakes *et al.*, 2014; Doyle and Yamada, 2016).

Focal adhesions influence cell migration by modifying the traction forces generated by the cells. Cells spread to a greater extent on stiff substrates, forming more focal adhesions or points of interaction with the ECM, which diminishes cell speed migration. In contrast, cells on soft substrates are more agile as they establish less interaction with the ECM by forming fewer focal adhesions, which promotes migration (Lange and Fabry, 2013).

Differences in focal adhesion size, strength, and composition affect actin contractility. It interacts with RhoA, a small GTPase whose activation increases non-muscle myosin II-dependent actin contractility by stimulating the formation of stress fibres and focal adhesions (Janson and Putnam, 2015). Hence, focal adhesions regulate actin movement by integrating the contractile force with integrins (Doyle and Yamada, 2016).

### 1.9.3 Actin cytoskeleton

The actin cytoskeleton is the primary cellular force machine crucial in cell mechanosensing and mechanotransduction. It is characteristic of each cell type, and it directs different cellular responses (Shin *et al.*, 2013):

- Pushing (protrusive) forces through coordinated polymerisation of multiple actin filaments organised into branched or parallel bunches.
- Pulling (contractile) forces via sliding of bipolar filaments of myosin II along actin filaments
- Resistance (shaping) forces by forming cross-linked membrane-associated filament arrays

These generated forces are crucial for cell migration, extracellular communication, cell shape, and synthesis of membrane organelles (Svitkina, 2018).

Actin is an essential component of the cytoskeleton that also includes stress fibres that are non-muscle contractile structures and terminate on focal adhesions, forming a potent network that transduces mechanical forces (Hao *et al.*, 2015).

Tension within the cytoskeleton is influenced by substrate elasticity and cell shape. For instance, the cytoskeletal tension increases in cells in shapes, adopting an osteogenic profile, while those in a plastic state undergo adipogenesis (Lee *et al.*, 2015).

Microtubules and actin microfilaments organised into different arrays by complementary proteins constitute the actin cytoskeleton. Actin filaments within the stress fibres show variable lengths and continuous distribution with overlapping filaments. Such overlaps allow stress fibres to be stretched to twice their original length by external force without forming gaps in actin distribution because actin is the main component of the cytoskeleton, and its synthesis and elongation are widely regulated (Kular *et al.*, 2014; Svitkina, 2018).

Most non-muscle cells are abundant in actin and myosin and generate significant contractile forces. When a cell attaches to the ECM, these contractile forces cause internal stress called cytoskeletal pre-stress that stiffens the adherent cells and is perceived by neighbouring cells (Lange and Fabry, 2013).

Myosin II is crucial in ECM stiffness sensing and cell differentiation into neurons, myoblasts, osteoblasts, brain, muscle, or bone cells. This occurs as the interactions between the cytoskeletal proteins and integrins activate signalling pathways that regulate gene expression and cell behaviour (Mathieu and Lobo, 2012; Lange and Fabry, 2013; Hao *et al.*, 2015).

#### 1.9.4 Signalling pathways

Cell mechanosensing can be divided into two types: integrin-mediated mechanosensing and non-integrin mechanosensing. The latter is based on TRP channels, specifically TRPV4, a calcium channel activated when mechanical force is applied to integrins. The former is based on integrins (mainly integrin class  $\beta 1$ ) binding to ECM proteins such as collagen, fibronectin, or laminin. Depending on the origin of the signalling (external matrix or focal adhesions) to the cytoplasmic integrin, integrin signalling works bi-directionally, “outside-in” (ECM properties such rigidity, force, and geometry direct integrins response) or “inside out” (integrins response directed by cytokines and chemokines) (Angelini *et al.*, 2020). Indeed, ECM components such as integrins, cytoskeletal and signalling proteins of the FAs, actin cytoskeleton, the Rho family small GTPases, and downstream effectors (Rho-associated protein kinase; ROCK; that direct the assembly of these components) are crucial in cell mechanosensing (Humphrey *et al.*, 2014).

Mechanical homeostasis is maintained by controlling the assembly and disassembly of focal adhesions and cytoskeleton contractility, which modify focal adhesion ligand affinity (Vining *et al.*, 2017).

FAK (focal adhesion kinase) is the initial component of the focal adhesions participating in cell mechanosensing. External tension and the binding of ECM ligands through integrins activate it. For example, cellular strain and stiff substrates increase the force experienced at the FAs and promote FAK phosphorylation (Vining *et al.*, 2017; Tapia *et al.*, 2020). FAK differential activation induces downstream signalling through the MAPK cascade, specifically, the extracellular-related kinase (ERK), which transmits the mechanical information from the ECM to the nucleus and plays an essential role in normal and pathologic development (Rustad *et al.*, 2013; Janson and Putnam, 2015). Indeed, mechanical stretching activates ERK, enters the nucleus and up-regulates the expression of different transcription factors such as TFS, AP1, AP2, SSRE, CREB, c-fos, c-myc, STAT,

and JNK, and activates nuclear binding proteins (nuclear factor kB (NF-kB) for phosphorylation (Wang and Thampatty, 2006; Wall *et al.*, 2018).

Changes in ECM nano topography and stiffness prompt MAPK activity by modifying the upstream RhoA-Rho-kinase (ROCK) pathway, which influences the transcription factor *RUNX2*, leading to stem cell osteogenic differentiation and matrix mineralisation (Janson and Putnam, 2015).

RhoA (member A of the Ras homolog gene family) is a small GTPase protein from the Rho family. It is predominantly localised in the plasmatic membrane, cytoplasm, cell-cell contacts, and cell projections. It directs different cellular activities such as cell growth, the regulation of the cytoskeleton, actin fibres formation and actomyosin contractility (Deng *et al.*, 2019).

ROCK (Rho-associated protein kinase) is a downstream effector of RhoA with two isoforms: ROCK1 and ROCK2. ROCK proteins mediate actin depolymerisation and actomyosin contraction and promote the phosphorylation of myosin. Cell growth, differentiation, and migration are highly regulated by the Rho/ROCK signalling pathway (Deng *et al.*, 2019). The activation of the mechanotransduction pathways RhoA and MAPK activates other downstream mechanotransduction pathways components such as MAL (a G-actin-binding coactivator of serum response factor (SRF)), Yes-associated protein (YAP), and transcriptional coactivator with PDZ-binding motif (TAZ)) (Vining *et al.*, 2017).

YAP and TAZ are mechanosensitive transcription factors, differentially expressed in the nucleus, and essential for growth and organ size coordination. YAP and TAZ remain in the cytosol when they are phosphorylated and are degraded by the proteasome when suffering dephosphorylation. Yap and b-catenin enter the nucleus when external forces are applied, promoting cell cycle re-entry. On stiff materials, the knockdown of YAP/TAZ promotes adipogenic differentiation, while its depletion prevents osteogenic differentiation. Therefore, YAP/TAZ plays a vital role in mechanosensing and cell differentiation (Bellas and Chen, 2014; Janson and Putnam, 2015; Wickström and Niessen, 2018).

Wnt/b catenin and Oct 3/4 are other key developmental pathways that also respond to the mechanical properties of the ECM and influence cell fate decisions (Wickström and Niessen, 2018). Wnt signalling promotes Rho signalling activation by decreasing E-cadherin-based cell adhesion, and changes in ECM stiffness and structure modify b-catenin, determining cell-cell contact (Heller and Fuchs, 2015; Wickström and Niessen, 2018).

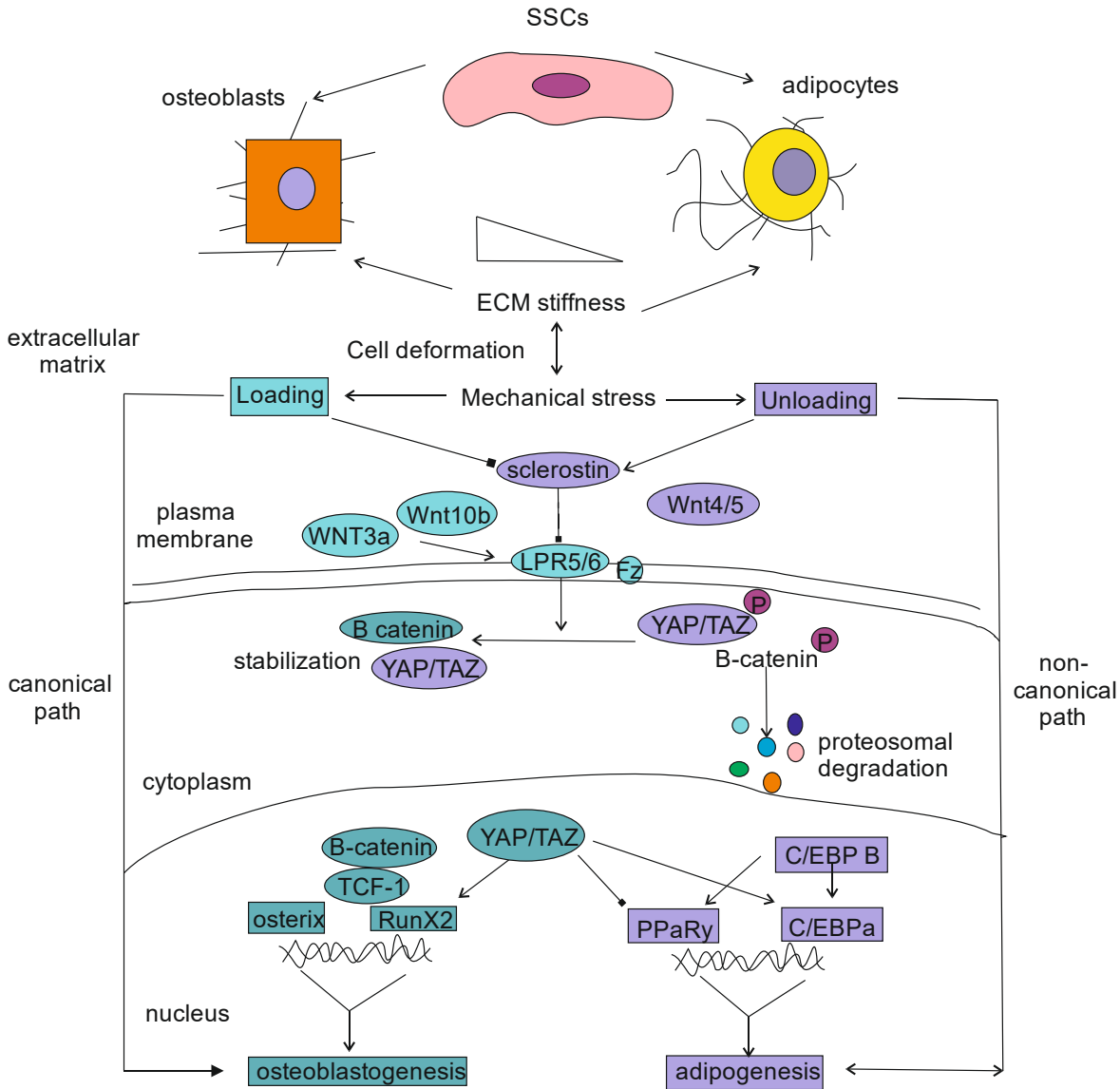


**Figure 1.6. Mechanical stimuli direct the cell fate of skeletal stem cells; loading and stiff materials lead to osteogenesis, while unloading and soft materials lead to adipogenesis.** The Wnt pathway and its interaction with the YAP/TAZ complex are crucial to determining MSC fate. The interplay between activation of Wnt- $\beta$ /catenin signalling and YAP/TAZ cytoplasmic or nuclear translocation leads to the transcriptional regulation of these cell lineages. EBP: enhancer-binding protein; ECM: extracellular matrix; LRP: Low-density lipoprotein receptor-related protein; MSC: mesenchymal stem cell; PPAR $\gamma$ : peroxisome proliferator-activated receptor; TAP: transcriptional coactivator with PDZ-binding motif; TCF1: T-cell factor 1 (TCF1); YAP: yes-associated protein, Adapted from Benayahu *et al.*, 2018.

### 1.10 Stem cells

Stem cells are non-differentiated cells found in embryonic, fetal, and adult stages that play an essential role in organ regeneration and are crucial for treating different health conditions such as diabetes mellitus, heart failure, and nervous disorders (Barreca *et al.*, 2020). Spinal cord injuries, heart failure, retinal degeneration, diabetes type I, Parkinson’s and Alzheimer’s diseases are other disorders treated with stem cell therapies as cells can improve effectiveness in drug testing (Zakrzewskiet *et al.*, 2019).

Self-renewal (high proliferation), clonality (emerge from a single cell), and potency (differentiate into specific cell types) are essential characteristics to define skeletal stem cells. Plastic-adherent cells differentiate into osteoblasts, adipocytes and chondroblasts (Ho-Shui-Ling *et al.*, 2018).

Depending on their differentiation potential, stem cells divide into (Kolios and Moodley, 2013; Dulak *et al.*, 2015; Zakrzewski *et al.*, 2019; Barreca *et al.*, 2020):

- Totipotent stem cells: Differentiate into cells of all lineages.
- Oligopotent stem cells: Differentiate into different cell types, such as myeloid stem cell that divides into white but not red cells.
- Pluripotent stem cells: Cells specialise in all cells, such as embryonic stem cells (ESC) and induced pluripotent stem cells (iPS). Pluripotent stem cells differentiate into cells of all three lineages: ectoderm, mesoderm, and endoderm facilitating blastocyst formation and tumour formation.
- Adult stem cells: Stem cells with multipotent (hematopoietic, neuronal, intestinal, and skeletal stem cells) or unipotent potential (satellite and epidermal stem cells). These cells stimulate tissue repair by secreting molecules with anti-apoptotic, angiogenic, immunomodulatory and chemoattractant characteristics. The most well-known multipotent cells live in the bone marrow, adipose tissue, bone, umbilical cord blood peripheral blood. Therefore, adult stem cells can regenerate the haematopoietic and nervous systems, whereas skeletal stem cells (SSCs) regenerate bone, cartilage, stroma, and marrow adipocytes (Bianco and Robey, 2015). SSCs are advantageous as they do not express histocompatibility molecules and do not lead to graft rejection after transplantation, promoting angiogenesis and tissue regeneration. In contrast, unipotent cells only differentiate into one cell type, such as keratinocytes or skeletal muscle.

SSCs secrete different components, such as extracellular vesicles that contain mRNAs, regulatory mRNAs and bioactive proteins that promote angiogenesis and tissue regeneration and inhibit fibrosis, apoptosis, and inflammation by influencing proliferation, migration, and gene expression (Luby *et al.*, 2019; Lukomska *et al.*, 2019).

The tissue components dictate the host cell populations, the availability of soluble factors, and SSCs' behaviour, viability, and differentiation potential (Zheng *et al.*, 2019). The ECM's mechanical and biochemical properties control SSCs by regulating cell signalling, gene expression, proliferation, migration, and differentiation (Kolios and Moodley, 2013). Because of this and their multipotent capacity, SSCs are widely used to regenerate tissues through biomaterials with similar mechanical properties to the target tissue. SSCs isolated from the bone marrow (BMSCs) are widely used for multipotency.

## 1.11 Bone Marrow Stromal Cells

The postnatal bone marrow comprises two central systems rooted in distinct lineages: the hematopoietic tissue and the associated supporting stroma with a subpopulation of stromal cells with multipotent capacity as stem cells. Thus, the bone marrow is the only organ in which two separate and distinct stem cells and dependent tissue systems coexist and functionally collaborate (Bianco *et al.*, 2001; Fitzsimmons *et al.*, 2018).

BMSCs are non-hematopoietic and multipotent stem cells that reside in the bone marrow and were discovered in 1968 through the work of Friedenstein and his co-workers. They defined them as adherent, clonogenic, non-phagocytic, and fibroblastic cells. These cells can be isolated from the bone marrow stroma of the postnatal organism after the ECM breakdown, where the stroma and hematopoietic cells converge into a single-cell suspension. At low seeding density, BMSCs rapidly adhere and can be easily separated from the non-adherent hematopoietic cells by repeated washing (Bianco *et al.*, 2001).

BMSCs are essential in tissue regeneration, and biochemical (chemokines, cytokines, and growth factors) and mechanical factors (shear stress, vascular stretching, and ECM stiffness) influence the transit of these cells from their niche to the target tissues. The delivery of BMSCs to target sites depends on different factors such as (Fu *et al.*, 2019):

- Osteopontin (OPN): O-glycosyl phosphate protein produced after heart, kidney, lung, or bone inflammation or injury, which increases  $\beta$ 1-integrin expression. The addition of OPN reduces the actin cytoskeleton activity, which promotes migration.
- Growth factors: A type of polypeptides such as basic fibroblast growth factor (bFGF), vascular endothelial growth factor (VEGF), hepatocyte growth factor (HGF), insulin-like growth factor-1 (IGF-1), platelet-derived growth factor (PDGF), and transforming growth factor -1 (TGF-1) are widely used in tissue repair as they regulate migration, proliferation, differentiation, and ECM production.
- TGF- $\beta$ 1: Increases during injuries for promoting tissue repair by promoting the migration and engraftment of cells through the N-cadherin, PI3K/Akt, ERK1/2, FAK, and p38 signal pathways.

BMSCs only differentiate into skeletal cell types at specific developmental phases or anatomic locations, such as osteoblasts for bone, chondrocytes for cartilage and adipocytes for bone marrow stroma. However, it has been claimed that BMSCs differentiate into skeletal, smooth, and cardiac muscles (Bianco *et al.*, 2001; Bianco *et al.*, 2008).

Individual colony-forming fibroblastic units possess different cell morphology, proliferation rates, and ability to form multilayer or nodular structures. For instance, osteoblastic, chondrogenic, and adipogenic phenotypes are variable between different cell strains and

within a cell strain as a function of time in culture. Within the bone marrow, lineages do not switch phenotype at a late stage of differentiation; however, some reversible capacity is maintained until the late stages. This plasticity is essential for cells to adapt to different tissues that reside next to each other during organ growth. It differentiates it from the hematopoietic system, in which the commitment of precursor cells is generally progressive and irreversible (Bianco-Robbey, 2000; Bianco *et al.*, 2001).

### 1.11.1 Bone Marrow Stromal Cells as a tool for bone recovery

Progenitor, inflammatory, endothelial, and hematopoietic cells direct bone fracture healing. It begins with an inflammatory phase, the formation of a hematoma, recruitment of progenitor cells, callus formation and maturation and remodelling of the body callus. The process leads to bone healing, but different health problems such as diabetes, injuries, tumour treatments or infections might delay fracture repairs, increasing worldwide orthopaedic sales to nearly 5.5-7 billion dollars (Ho-Shui-Ling *et al.*, 2018; Luby *et al.*, 2019).

Bone grafting is a valuable strategy for improving slow bone healing; however, autografts might lead to morbidity at the damaged site, and allografts are associated with poor healing. Because of these drawbacks, different alternatives for long-term treatment have been developed, such as bone graft substitutes. These structures need to mimic the mechanical properties of the natural tissues and can be used alone, combined with molecules or cells, or composed only by cells (Ho-Shui-Ling *et al.*, 2018).

Bones are subject to consistent mechanical stress and stimulation, whereas their native osteoblasts and progenitor cells experiment interstitial pressure and shear stress. As a result, new studies focus on the effect of mechanical properties on stem cells to mimic *in vivo* conditions (Luby *et al.*, 2019).

Bone graft substitutes require progenitor cells, stimulatory factors, and the biomaterial template. Typical progenitor cells are BMSCs, adipose-derived mesenchymal cells and periosteum-derived stem cells. The process consists of the chondrogenic and/or osteogenic differentiation, encapsulation and plating of the material that might contain stimulatory molecules. Then, the construct is cultured in the lab before the implantation. The required number of cells for a 4 cm bone fracture is approximately 600 million (Ho-Shui-Ling *et al.*, 2018), and the regenerative potential of transplanted MSCs highly depends on the microenvironment of donors and recipients, oxygen conditions, biomechanics of the bone site and the presence of bone factors (Ho-Shui-Ling *et al.*, 2018; Zheng *et al.*, 2019).

BMSCs are crucial in regenerative medicine, and several laboratories have developed monoclonal antibodies to identify markers for sorting stromal cell preparations. The most important is the Stro-1, which is highly expressed in clonogenic stromal cells (Stro-1<sup>+</sup> bright)

(Bianco *et al.*, 2001). Stro-1 enriches CFU-F more than 1000-fold in the bone marrow, which helps to identify stromal and osteogenic progenitors (Murphy *et al.*, 2013).

Because of their osteogenic potential, BMSCs have been widely harnessed to reconstruct skeletal defects through scaffolds that overcome bone defects' size and shape limits to be repaired. For this, transplanted BMSCs must be in the appropriate skeletal and extravascular environment, be competent for engraftment, produce high levels of differentiated progeny, and cause the desired biological effect in preclinical models (Bianco-Robbey, 2000; Parekh *et al.*, 2011). The scaffold should mimic ECM biochemical and mechanical properties so cells adapt to the microenvironment and differentiate into osteoblasts (Lee *et al.*, 2015).

### 1.11.2 Mechanobiology of skeletal stromal cells

Many bone regeneration studies focus on the effects of ECM stiffness on SSCs (Kular *et al.*, 2014). The tensional integrity or tensegrity theory can explain the mechanotransduction processes in SSCs. SSCs sense the ECM rigidity by applying contractile forces against it through adhesion complexes, the actin cytoskeleton, and integrins (Hao *et al.*, 2015).

The combination of two different chains ( $\alpha$  and  $\beta$ ) of integrins defines the receptors of the cell surface (VCAM, ICAM), which promotes the recognition and binding to the ECM proteins. For example, during osteogenic differentiation, cells up-regulate integrin  $\alpha 5$ ,  $\alpha 5\beta 1$  and  $\alpha v\beta 3$ , which promotes the formation of focal adhesions, the generation of traction forces and differentiation of MSC plated on deformable biomaterials (Lee *et al.*, 2015; Ringer *et al.*, 2017).

Actin is the primary and stiffest filamentous component of the cytoskeleton in SSCs that varies depending on the differentiation pathway. A highly developed cytoskeleton is an effective mechanosensor in osteogenic cells (Olson and Nordheim, 2010; Mullen *et al.*, 2015), whereas an immature and soft cytoskeletal architecture is present in SSCs (Chaudhuri *et al.*, 2020; Shin *et al.*, 2013). Indeed, Kim *et al.*, 2012 confirmed that SSCs reduced their Young's modulus after being incubated for 21 days in an adipogenic medium, implying that adipocytes do not have a very dense cytoskeleton. In contrast, Mathieu and Lobo, 2012 reported that spherical and spread osteoblasts had an elastic modulus of 2 kPa and 5.8, respectively, higher than adipocytes.

The previous examples illustrate that changes in ECM modify SSCs morphology and, therefore, might affect gene expression (Bianco-Robbey, 2000). Changes in ECM stiffness direct BMSCs' differentiation into specific tissue lines when ECM reaches the stiffness of the native tissues (Leong *et al.*, 2010), which is outstanding for tissue regeneration (Parekh *et al.*, 2011).

### 1.11.3 SSCs osteogenic differentiation

SSCs differentiation depends on the mediation of cell proliferation, mineralisation, and matrix development, which at the same time are regulated by different signalling pathways (Hao *et al.*, 2015) directed by different genes whose activity is enhanced at different stages of direct osteogenic differentiation. That is alkaline phosphatase (*ALPL*) and *RUNX2* (early osteogenic markers), bone sialoprotein (*BSP*), osteopontin (*OPN*) (late osteogenic markers), and osteocalcin (*OCN*) (very late osteogenic marker). They promote calcium phosphatase mineral deposition and osteocalcin production. Osteogenic differentiation can also be promoted by increasing the expression of osteogenic factors such as osteopontin, bone sialoprotein, osteocalcin, collagen 1A1, TGF- $\beta$ 1, BMP-2, BMP-4, and BMP-7 and VEGFA (Parekh *et al.*, 2011; Zhao *et al.*, 2014; Hao *et al.*, 2015; Lee *et al.*, 2015).

*ALPL* is a membrane-bound enzyme that has four isoenzymes. TSAP (tissue-specific alkaline phosphatases) are intestinal alkaline phosphatase, placental alkaline phosphatase, and germ cell alkaline expressed by embryonic and carcinoma cells. The fourth isoenzyme is tissue non-specific alkaline phosphatase (TNAP) in bone, liver, and kidney and is associated with germ layers, while TSAPs are expressed with increasing differentiation. The activity within the developing skeleton is associated with the expression of TNAP in chondrocytes and osteoblasts (Stefkova *et al.*, 2015).

Cell fate might also depend on the ECM mechanical cues (Hao *et al.*, 2015). Compression forces and hydrostatic pressure induce chondrogenic differentiation, while tensile forces influence migration as they lead the spatial rearrangement of SSCs to form knob-like three-dimensional structures. (Hao *et al.*, 2015).

### 1.12 Substrate stiffness and SSCs differentiation

Cells sense the ECM elasticity by pulling against it. The generated mechanical information is transmitted to the cells through focal adhesions and translated into signals depending on the force the cell should exert to deform the ECM. (Engler *et al.*, 2006, Wells, 2008).

Adult stem cells continuously migrate away from their niche to attach and differentiate within various tissue microenvironments. ECM stiffness highly influences this process by directing cell adhesion, proliferation, migration, and the expression of the focal adhesion components such as filamin, talin, FAK and NMM  $\alpha$  actin (Engler *et al.*, 2006; Wells, 2008; Wang *et al.*, 2012; Janson and Putnam, 2016).

Focal adhesions help SSCs sense the microenvironment through actin-myosin contractions, which increases cell tension. They also participate in different signalling pathways and stabilise integrin-binding that defines cell shape and influences cell

differentiation (Engler *et al.*, 2006; Wells, 2008; Steward and Kelly, 2015). Osteoblasts form more focal adhesions than SSCs as they hold more ERM proteins (ezrin, radixin, moesin family). When lacking, mRNA expression for osteogenic markers (including *ALPL*) decreases. FAK and  $\alpha$ 2 integrin is also crucial in osteogenic differentiation as their inhibition decreases osteogenesis in SSCs (Mathieu and Lobo, 2012).

The relationship between ECM stiffness and differentiation is regulated by YAP/TAZ signalling (Vining *et al.*, 2017). YAP and TAZ regulate gene expression in the nucleus and promote cell growth by directly binding to factors such as TEAD, T-box 5 (TBX5), and ErbB4 and p73. In the cytoplasm, YAP/TAZ is confined by interacting with proteins that form the  $\beta$ -catenin destruction complex, limiting the transcription of *RUNX2* and promoting adipogenic differentiation (Benayahu *et al.*, 2019).

Substrate elasticity also directs the osteogenic fate of SSCs through the ROCK and ERK pathways (Hao *et al.*, 2015).

Another crucial component in SSCs osteogenic differentiation mediated by the increase in mechanical strain is Wnt/ $\beta$ -catenin. Wnt binds to lipoprotein receptor-related protein 5/6 (LRP5/6) co-receptors, leading to  $\beta$ -catenin nuclei translocation and the expression of osteogenic genes. Mechanical strain also inhibits SSCs adipogenic differentiation by suppressing C/EBP $\alpha$  and PPAR $\gamma$ . PPAR $\gamma$  can bind to the *RUNX2* promoter, preventing the bond to the OSE2 osteocalcin promoter and suppressing Wnt signalling by promoting  $\beta$ -catenin degradation (Benayahu *et al.*, 2019).

The ECM elastic constant  $E$  defines the ECM resistance to deformation that the cell perceives, which determines SSCs differentiation. SSCs on soft materials that mimic the brain elasticity (0.1-1 kPa) exhibit branched morphology and highly express neurogenic markers such as nestin and  $\beta$ -tubulin. Intermediate stiff materials mimicking muscle elasticity (8-17 kPa) promote spindle-shaped cells and the expression of 6-fold more myogenic factors. Instead, stiffer materials (25-40 kPa) enhance the polygonal morphology of SSCs, which is like osteoblasts and increases the expression of osteocalcin and the early transcriptional factor CBF $\alpha$ 1. Figure 1.7 exemplifies the detection of neurogenic, myogenic, and osteogenic markers in SSCs on hydrogels with different elastic modulus (Engler *et al.*, 2006).

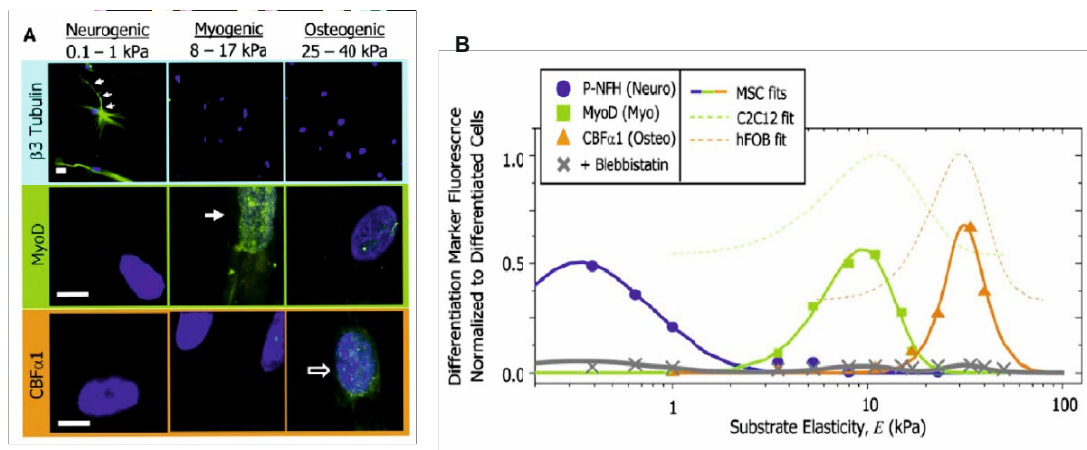


**Figure 1.7. Substrate elasticity defines the protein and transcript profiles of SSCs under identical media conditions.** (a) The neuronal cytoskeletal marker  $\beta 3$  tubulin is expressed in branches of SSCs on soft hydrogels. The muscle transcription factor is upregulated and localised in the nuclei in SSCs on relatively stiff hydrogels. The osteoblast transcription factor CBF $\alpha$ 1 is only expressed on stiff hydrogels. (b) The fluorescent intensities of differentiation markers depend on substrate elasticity- adapted from Engler *et al.*, 2006.

Parekh *et al.*, 2011 reported that cells on soft hydrogels (250 Pa), like the modulus of bone marrow, show a non-proliferative state while osteogenic differentiation increases on stiffer hydrogels (7.5 kPa) and much more on rigid glass surfaces with an increase in a mineral deposition. Similarly, Mullen *et al.*, 2015 showed high levels of ALPL activity in cells cultured on stiff hydrogels but lower levels on soft hydrogels. Mathieu and Lobo, 2012 highlighted that SSCs exposed to osteogenic media for 10 days significantly increased cell stiffness from 2 kPa to 3.2 kPa, and actin and focal adhesions arrangement were more related to osteoblast than SSCs.

Besides the increase in ALPL activity, stiff substrates enhance the expression of other osteogenic markers. Indeed, changes in substrate elasticity influence the RhoA-Rho kinase (ROCK) pathway upstream of changes in the MAPK cascade that influence the transcription runt-related transcription factor 2 (RUNX2), osteopontin (OPN), osteocalcin (OCN) and bone morphogenetic protein 2 (BMP2) (Janson and Putnam, 2016; Liu *et al.*, 2018; Sun *et al.*, 2018).

In summary, ECM stiffness is crucial in cell fate and depends on additional factors rather than the intrinsic elastic modulus. The ECM organisation is essential as the cellular mechanical forces pass through the structure. For instance, when sensing overlapping fibres, cells might perceive the ECM as stiffer than the actual stiffness. Indeed, the ECM geometry might influence cell behaviour through changes in cell shape and the actin cytoskeleton (Trappmann *et al.*, 2012; Doyle and Yamada, 2016; Basu *et al.*, 2018).

### 1.13 Substrate mechanical properties to be controlled when evaluating stiffness sensing

ECM stiffness sensing and cell behaviour in 3D microenvironments depend on ECM topography, ligand density, fibre alignment, ECM pore size, and intra- and extra-fibril cross-linking. Therefore, tissue engineering should consider substrate geometry when designing biomaterials as they might influence stem cell differentiation and tissue regeneration. To exemplify, human epidermal stem cells on porous substrates are round and detach after a period, while cells on compact substrates spread and remain undifferentiated (Engler *et al.*, 2006; Parekh *et al.*, 2011; Trappmann *et al.*, 2012; Kular *et al.*, 2014; Lee *et al.*, 2016).

Substrate geometry also influences cell migration in 3D microenvironments by modifying pore size. Tiny pores can limit nuclei translocation, which influences contractile forces; however, cells in 2D environments show lamellipodial-driven migration that does not depend on nuclei translocation. Cell migration is also affected by the substrate elastic behaviour; for example, nonlinear elastic hydrogels enable fibroblast communication via long-distance contractile forces (showing lamellipodia-based migration), while linear elastic hydrogels support pressure-based lobopodia migration (Doyle and Yamada, 2016).

The grade of porosity of polyacrylamide hydrogels influences cell differentiation in SSCs more than the intrinsic elastic modulus by defining collagen attachment to the biomaterial (Janson and Putnam, 2015).

#### 1.13.1.1 Protein tethering and SSCs differentiation

Non-specific protein adsorption might also direct cell response through topographic cues. It is possible that substrates with nanotopographic features of different sizes differentially absorb ECM proteins from serum, bind different integrin receptors, activate different signalling pathways, and subsequently favour distinct cell responses (Janson and Putnam, 2015). For example, SSCs' osteogenic potential increases with collagen I and vitronectin through ERK signalling (Hao *et al.*, 2015).

The identity of the attached protein also affects how the integrins apply force on the matrix, form focal adhesions and transmit the mechanical and biochemical cues from the ECM to the nuclei. For instance, cells express the protein Zyxin and  $\beta 1$  integrin on collagen hydrogels, while fibrin favours the expression of vinculin and Paxilin. Also, cells growing on fibronectin or collagen hydrogels highly expressed *RUNX2* as elastic modulus rise, while SSCs cultured on laminin did not differentiate even when the stiffness increased (Lee *et al.*, 2013; Lee *et al.*, 2015; Doyle and Yamada, 2016).

Protein identity might also promote other differentiation pathways besides osteogenic differentiation. SSCs differentiate into adipocytes on fibronectin and express neurogenic

markers on collagen matrices, while cell differentiation did not change on laminin matrices. Nevertheless, combining different adhesion ligands on soft hydrogels can favour specific differentiation lines. Cells on laminin-coated hydrogels expressed neurogenic and adipogenic markers and underwent adipogenic differentiation on fibronectin-coated hydrogels; however, any combination containing collagen promoted the expression of neurogenic markers (Lee *et al.*, 2015).

In addition to the protein identity, protein length is crucial for mechanosensing. For example, when increasing collagen fibre length, the strength of adhesion and the mechanical response from the cells decreases (Trappmann *et al.*, 2012).

Besides protein tethering, local fibre stiffness is crucial as cells perceive individual collagen fibres as stiffer than the overall gel stiffness. Fibre stiffness depends on whether tension is generated parallel (stiff) or perpendicular (soft) to a particular fibre. For instance, fibres that reach the bottom of the substrate will transfer most of the force; as a result, cells on thin hydrogels will spread more (Mullen *et al.*, 2015; Doyle and Yamada, 2016).

Altogether, these spatial differences in geometry affect collective cell mechanosensing as cells are actively interacting with each other within tissues (Tusan *et al.*, 2018), so substrate thickness and cell crowding should also be considered when studying stiffness sensing in SSCs.

#### **1.13.1.2 Substrate thickness and stem cell differentiation**

As previously mentioned, ECM thickness plays a meaningful role *in vivo* as cells are not entirely isolated or form a uniform monolayer (except for epithelial cells) but are continuously interacting within various tissue levels and often remain connected through the ECM (Leong *et al.*, 2010; Venugopal *et al.*, 2018).

Cells pull the ECM and respond based on the mechanical information they receive from this action. Cells on stiff materials cannot deform them when they apply force, increasing their internal tension and spreading. Instead, cells deform soft materials; therefore, no tension is generated inside the cell and cells do not spread and remain round. However, cell behaviour in soft hydrogels might vary when hydrogel thickness changes. The distance the cell can feel is smaller on thick hydrogels than the thickness of the hydrogels. In contrast, on thin hydrogels, the cell might be able to perceive the complete depth of the hydrogel and even the supporting material beneath it (Evans and Gentleman, 2014). This underlying material significantly influences how the cell perceives the effective stiffness of a soft hydrogel. Then, depth sensing needs to be considered when designing devices or implants for tissue regeneration, as the stiffness perceived by the cells might dictate cell behaviour. The effective shear stiffness (the stiffness that the cell experiences) increases on soft, thin

hydrogels because of the closeness of the support below it. So that if the cell perceives the hydrogel as stiffer, the forces required to exert such strains on the hydrogel become too high for the cell, creating tension within its cytoskeleton and promoting cell spreading (Figure 1.8). Thus, SSCs seeded on soft polyacrylamide surfaces that generally do not promote cell-spreading increase their area on thin hydrogels (Evans and Gentleman, 2014; Mullen *et al.*, 2015). Tusan *et al.*, 2018 reported that single cells remained rounded on soft (2 KPa) hydrogels above a "critical thickness" but began to spread progressively more as the hydrogel thickness decreased.

The increase in cell spreading by the reduction in hydrogel thickness is also explained as thin substrates transmit contractile forces throughout the entire hydrogel, enabling the cell to sense global and not only local (at point of contact) mechanical information (Leong *et al.*, 2010; Mullen *et al.*, 2015).

Proteins tethered to the hydrogels might also define the effect of substrate thickness on cell behaviour. Cells on thin collagen hydrogels that are highly cross-linked do not perceive them as stiffer but do on hydrogels with low collagen concentration and spread more (Mullen *et al.*, 2015).

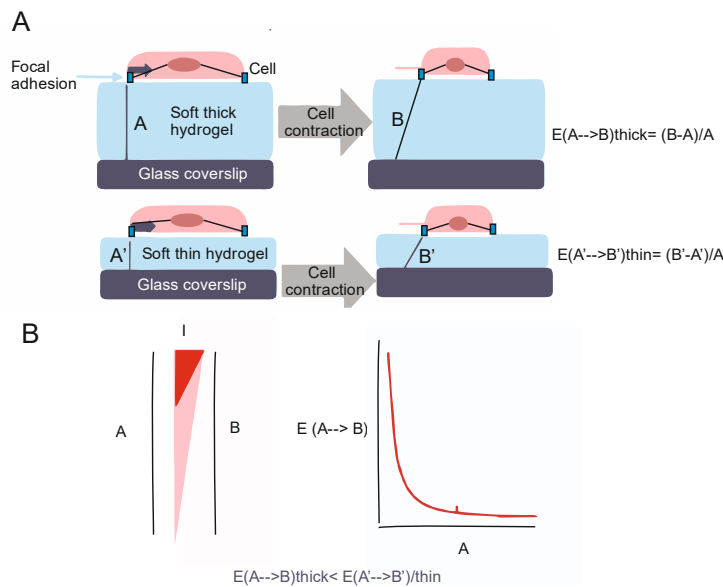


**Figure 1.8. Stiffness sensing of cells on soft hydrogels with different thicknesses. (a)** The image illustrates the differences in the force a cell should exert to contract the same distance on a soft thick (up) and soft, thin (below) hydrogel. The cell adheres to a **soft, thick hydrogel**, forms a focal adhesion, and applies a contractile force on the hydrogel (top left). Then, the hydrogel deforms at a distance (top right), and the strain progression from  $(E(A-B)_{\text{thick}})$  is given by  $(B-A)/A$ . **On a soft, thin hydrogel**, the cell also attaches to the hydrogel and forms focal adhesions, but it needs to apply more force to deform from  $(E(A'-B')_{\text{thin}})$  given by  $(B'-A')/A'$ . Then, the cell generates force within the cytoskeleton and spreads, which does not occur on soft, thick hydrogels. **(b)** The graph represents the force or strains the cell needs to apply to deform the hydrogel a distance  $l$  and increases with decreasing hydrogel depth. On the one hand, A indicates the initial state, while B indicates the imaginary hypotenuse after the cell contraction and consequent deformation of the soft, thick hydrogel. On the other hand, A' is the initial condition when cells interact with the hydrogel and progress to B' after the cell contraction and small deformation of the soft, thin hydrogel (Evans and Gentleman, 2014).

Studying thickness sensing is vital as *in vivo* cells are not isolated; they generally interact with other cells by forming colonies or layers, which influences cell mechanosensing. Cells exert more force when forming colonies than single cells, so groups of cells deform hydrogels to a higher degree and can feel greater distances in the hydrogel (Evans and Gentleman, 2014). Tusan *et al.*, 2018 indicated that colonies contract hydrogels. However, the contraction grade depends on hydrogel thickness as the contraction is constrained on thin hydrogels by the proximity of the underlying material.

Then, ECM geometry and cell density might also influence cell forces and differentiation by determining cell-cell interaction, cell spreading and shape, which activates specific signalling pathways (Bellas and Chen, 2014).

### **1.13.1.3 Cell density**

Cells at high confluence sense the stiffness of the surrounding cells, whereas cells at low seeding densities only sense the actual substrate stiffness (Wells, 2008). Cell density is one of the best-recognised regulators of cell proliferation and differentiation. It arrests cell growth, promotes cell flattening and controls cell spreading by modulating Rac and Rho GTPase signalling (Mathieu and Lobo, 2012; Bellas and Chen, 2014).

BMSCs differentiate into adipocytes when plated at a low seeding density on a soft substrate or high density on stiff substrates (Mao *et al.*, 2016; Nehls *et al.*, 2019). McBeath *et al.*, 2004 showed that in adipogenic media, cells seeded at low density did not undergo adipogenic differentiation but did at high density. In contrast, low density on stiff substrates favours osteogenesis in BMSCs detected by high ALPL activity (McBeath *et al.*, 2004; Venugopal *et al.*, 2018). SSCs also spread and exhibit higher osteogenic potential at low seeding density than cells plated at a high density. Even if the cell culture was overcrowded after 48h, cells exhibited increased osteogenic potential (Mathieu and Lobo, 2012).

Cell crowding simultaneously dictates cell-cell contact, spreading and shape, directing cell differentiation.

#### **1.13.1.3.1 Cell spreading**

The mechanical performance of the cell is regulated by the spreading area alone, where cell curvatures regulate the distribution of traction forces on the substrate. Interestingly, cells with the same spreading area cause the same mechanical output (Oakes *et al.*, 2014). The increase in cell area raises RhoA/Rock activity, myosin phosphorylation, traction forces and osteogenesis, while RhoA stimulates adipogenic differentiation (Bellas and Chen, 2014). Therefore, cell spreading can indicate the differentiation stage of SSCs (Mullen *et al.*, 2015).

Because of the importance of spreading cell area in cell differentiation, restricting it might stimulate one fate lineage over the other regardless of stiffness or ligand composition. For instance, an upturn in cell spreading enables the extension of dendritic processes required for neurogenic gene expression in adherent SSCs, promoting neuronal differentiation on soft hydrogels (Lee *et al.*, 2013).

Besides stiffness, ECM viscoelasticity impacts cell spreading, explained by the motor-clutch model that considers the dissipative process within the cells and the ECM. Here, the myosin motors pull the actomyosin networks to the nucleus at the cell's leading edge, which causes retrograde actin flow. Adhesion molecules resist this by linking or separating from the actin bundles and ECM. The retrograde flow causes the polymerisation of actin fibres and pushes the membrane forward, promoting cell spreading (Chaudhuri *et al.*, 2020).

#### **1.13.1.3.2 Cell shape**

Cell density and differentiation direct the expression of specific proteins that modify the overall cell shape and contractility. At the same time, several studies highlight those changes in cell shape can alter differentiation in pre-committed lineages. (McBeath *et al.*, 2004; Bellas and Chen, 2014; Wickström and Niessen, 2018). Round cells with compact morphology express higher adipogenesis markers, cells that spread and extend dendrite-like processes on soft hydrogels show elevated neurogenesis markers (Lee *et al.*, 2013), whereas hMSC on stiff hydrogels in osteogenic conditions exhibit cuboidal and elongated forms and linear, stretched assembly of actin filaments (Zhao *et al.*, 2014)

Cell shape determines cell fate through the regulation of the actin cytoskeleton. It controls the interrelation between focal adhesions, traction stress, and differentiation of a single SSCs (Lee *et al.*, 2015). Cell patterning has been widely used to control cell spreading, shape, and early differentiation. SSCs plated on micropatterns that allowed them to spread expressed more RhoA than those with restricted areas. As mentioned earlier, RhoA is responsible for the actin organisation and the adhesion arrangements that occur in spreading cells more like osteoblasts than SSCs that are less spread. Therefore, the performance of SSCs cell shape, osteogenic potential, and actin cytoskeleton are interrelated (Mathieu and Lobo, 2012).

Lee *et al.*, 2015 analysed traction stress exerted by circular and star-shaped SSCs on hydrogels of two different stiffness (10 and 30 kPa) using three different ECM proteins (fibronectin, laminin, and collagen). They identified that SSCs show classical actin patterns in circles but pentagonally organised regions of actin stress fibres and higher expression of osteogenic and myogenic markers in star shapes. Integrins and focal adhesions mediate the effect of cell shape changes on the cytoskeletal re-organisation; therefore, star-shaped cells expressed more integrins regardless of hydrogel stiffness. Besides this, MSC

produced higher tension forces in star geometries, which were enhanced on a fibronectin matrix. In contrast, more minor circular features favoured adipogenic differentiation, while 4-branched stars and ovals promoted neurogenic outcomes. The finding that cell shape controls differentiation is essential, as previous reports have only demonstrated adipogenesis on hydrogels in the presence of adipogenic supplements (Lee *et al.*, 2013).

#### 1.14 Cell Micropatterning

To evaluate the effects of single parameters that are often coupled, such as cell crowding, cell spreading area, and the number of focal adhesions, it is necessary to control cell shape by micropatterned surfaces that consequently influence shape-induced differentiation (Trappmann *et al.*, 2012; Lee *et al.*, 2013; Oakes *et al.*, 2014). Several techniques, including nanoimprint lithography, capillary force lithography, ultraviolet-assisted lithography, photolithography, and micromachining, can produce surfaces with defined physical topographical features (lines, gratings, holes, pillars) and chemical, topographical features (islands of printed or adsorbed ECM proteins) such as micropatterning (Janson and Putnam, 2015).

Micropatterning requires collagen attachment to enhance cell adhesion and forces the cells to occupy only the desired area of the hydrogel (Nehls *et al.*, 2019). Nevertheless, the impact of the ECM coating on cell behaviour is not crucial in micropatterned hydrogels (Trappmann *et al.*, 2012).

The micropatterning technique has been used to evaluate osteogenic differentiation in SSCs. McBeath *et al.*, 2004 showed that adipogenesis occurs on small islands; meanwhile, large islands promote osteogenic differentiation. Similarly, Parekh *et al.*, 2011 reported that small protein islands promoted adipogenic differentiation in BMSCs, although osteogenic supplements were also present in the media. Meanwhile, Lee *et al.*, 2013 showed an increase in adipogenic markers in SSCs on small islands but also a mixture of cells expressing adipogenic (p-par  $\gamma$ , in patterned cells) and neurogenic (beta3 tubulin in spread cells) markers on unpatterned soft hydrogels. In addition to the size of the island, its geometry is also crucial.

McBeath *et al.*, 2004 identified cell shape as a critical regulator in SSCs commitment that provokes changes in several structures and the activation of different regulatory signals, specifically RhoA activity on ROCK-mediated cytoskeletal tension. Mathieu and Lobo, 2012 found that micropatterned squares promoted more adipogenic differentiation than rectangles. Focal adhesion distribution also changes between shapes as vinculin location changes in flower and star-patterned cells. Cells on both patterns became equally osteogenic after disrupting microtubules (nocodazole). However, disrupting the actin

cytoskeleton (cytochalasin) and Rho-kinase (Y-27632) stimulated the nonosteogenic phenotype.

Besides differentiation, micropatterning influences cell proliferation in hydrogels. Mao *et al.*, 2016 patterned fibronectin islands on PAAm hydrogels, showing that BMSCs proliferation increased on unpatterned substrates with high stiffness while micropatterns decreased cell proliferation on hydrogels with the same elastic modulus.

For all the above, micropatterning helps to control the effect of cell density, cell shape and cell spreading in differentiation. Nonetheless, it also provides a strategy to decouple other factors that dictate substrate stiffness sensing apart from the intrinsic substrate elastic modulus.

Cells can sense the 3D microenvironment by applying dynamic 3D forces on the matrix during locomotion. For instance, SSCs' osteogenic differentiation on 2-D alginate polymers is promoted at 11-30kPa, while cells remain spherical in 3-D cultures regardless of substrate stiffness (Hao *et al.*, 2015).

## **1.15 Conclusion**

To summarise, the mechanical properties of the ECM and their interaction with the SSCs are crucial for cellular and tissue functionality. Therefore, the possibility of regenerating tissues based on stem cell strategies will depend on how much the biomaterial mimics the elastic modulus but also the thickness of the specific ECM to support cell adaptation, viability, and differentiation.

The effect of ECM stiffness on SSCs behaviour has been widely studied; however, there is still much to know about the impact of ECM thickness on cell differentiation. Then, this PhD project focused on studying how the elastic modulus and thickness of the ECM influence SSCs' behaviour—particularly studying the interrelation between the mechanical forces exerted by the cells (depending on the ECM mechanical properties and cell crowding) in cell differentiation and vice versa.

## **1.16 Hypothesis**

Bone marrow stromal cells differentiate to the osteogenic lineage to a greater degree and produce greater cell traction forces as the thickness of soft materials decreases, which is crucial during collective cell mechanosensing and adaptation to the tissue microenvironment during bone regeneration.

### 1.17 Aims

- To evaluate if the changes in acrylamide/bisacrylamide ratio and polyacrylamide mixture volume modify the surface, elastic modulus, and thickness of PAAm hydrogels.
- To test if adding fluorescent microbeads to the PAAm hydrogels modifies the hydrogel's elasticity and thickness.
- To confirm that bone marrow stromal cells sense changes in elastic modulus and thickness and differentiate into osteoblasts as shear stiffness increases.
- To confirm that BMSCs generate more significant deformations on soft, thick PAAm hydrogels.
- To evaluate the effect of cell crowding and cell differentiation on cell traction forces.



## **Chapter 2 Methods**

## 2.1 Materials

### 2.1.1 Cells

MG63 human osteosarcoma cell line was acquired from Sigma (St. Louis, USA), and SSCs were thawed from the Bone & Joint group cell bank. SSCs were previously isolated from human bone marrow samples obtained from the Spire Southampton Hospital and Southampton General Hospital (Janeczek *et al.*, 2016).

### 2.1.2 Chemicals and materials

#### 2.1.2.1 Fabrication, characterisation and micropatterning of polyacrylamide hydrogels

Reagent	Supplier	Catalogue
Glass coverslips (13- and 25-mm diameter)	VWR international	631-1577P, 631-1584P
Sodium Hydroxide (NaOH)	Sigma-Aldrich	221465
3-Aminopropyltriethoxysilane (APES)	Sigma-Aldrich	440140
Glutaraldehyde	Sigma-Aldrich	340855
Phosphate-buffered saline (PBS)	Sigma-Aldrich	P4417
Acrylamide	Sigma-Aldrich	A4058
Bisacrylamide	Sigma-Aldrich	M1533
FluoSpheres, 0.5 µm diameter, Ex/Em= (580/605)	ThermoFisher Scientific	F8813
Allylamine	Sigma-Aldrich	145831
Ammonium persulfate (APS)	Sigma-Aldrich	A6761
N, N,N', N'-tetramethylethane-1,2-diamine (TEMED)	Sigma-Aldrich	110732
Dimethyldichlorosilane (DCDMS)	Sigma-Aldrich	440272
Sulfosuccinimidyl6-(4'-azido-2'-nitrophenylamino) hexanoate (Sulfo-SANPAH)	Sigma-Aldrich	803332
4-(2-hydroxyethyl)-1-piperazineethanesulfonic acid (HEPES)	Sigma-Aldrich	H4034
Collagen type I	CellSystems Biotechnologie Vertrieb GmbH	5005
Ethanolamine (ETA)	Sigma-Aldrich	E9508
Acrylate-PEG2K-NHS	Sigma-Aldrich	JKA5021
Microstructured PAAm hydrogels	4Dcell	G-CM-6

#### 2.1.2.2 Cell culture

Reagent	Supplier	Catalogue
Dulbecco's modified Eagle's medium (DMEM)	Sigma-Aldrich	D6429
Streptomycin and Penicillin	Sigma Aldrich	P4333-100ML
Minimum essential medium Eagle – Alpha modification (α-MEM)	Sigma Aldrich	M0644-10L
Fetal bovine serum (FBS)	Sigma Aldrich	F7524-500ML
Phosphate-buffered saline (PBS)	Sigma-Aldrich	P4417-100TAB
Trypsin-EDTA (Ethylenediaminetetraacetic acid)	Sigma-Aldrich	T9285-100ML

### 2.1.2.3 Cell dyes

Reagent	Supplier	Catalogue
4', 6-diamidino-2-phenylindole (DAPI)	ThermoFisher Scientific	D1306
CellTracker™ Red CMTPX Dye	ThermoFisher Scientific	C34552
Fluorescein phalloidin	Fisher Scientific	F432
Vinculin rabbit anti-Human, Mouse, polyclonal antibody (Primary antibody)	Fisher Scientific	PA529688
Goat anti-Rabbit IgG (H+L) Highly Cross-Adsorbed Secondary Antibody, Alexa Fluor Plus 594 (Secondary antibody)	ThermoFisher Scientific	A32740
Vibrant™ TM DiD-Labeling solution	ThermoFisher Scientific	V22887
Vibrant™ TM DiI-Labeling solution	ThermoFisher Scientific	V22888
Paraformaldehyde (PFA)	ThermoFisher Scientific	J61899.AK

### 2.1.2.4 Osteogenic differentiation

Reagent	Supplier	Catalogue
Minimum Essential Medium Eagle – Alpha modification ( $\alpha$ -MEM)	Lonza	BE12-169F
Fetal bovine serum (FBS)	Gibco, Life sciences	26140079
Trypsin-EDTA	Lonza	CC-5012
Ascorbic acid 2-Phosphate (A2P)	Sigma Aldrich	A8960
$\beta$ -glycerophosphate (BP-G)	Sigma Aldrich	G9422
Dexamethasone	Sigma Aldrich	D4902
Fast violet LB salt and 1-Naftol	Sigma Aldrich	F3381
Igepal CA-630	Sigma Aldrich	I8896
Phosphatase substrate	Sigma Aldrich	P4744

### 2.1.2.5 Adipogenic differentiation

Reagent	Supplier	Catalogue
Minimum essential medium Eagle – Eagle modification ( $\alpha$ -MEM)	Lonza	M4655
Fetal Bovine Serum (FBS)	Gibco, Life sciences	F7524
Trypsin-EDTA	Lonza	T9285
Dexamethasone	Sigma Aldrich	D4902
ITS (Insulin-Transferrin-Selenium) solution	Sigma Aldrich	I3146
Rosiglitazone	Sigma Aldrich	R2408
Paraformaldehyde (PFA)	ThermoFisher Scientific	J61899.AK
Isopropanol	Sigma Aldrich	34863
Oil Red O	Sigma Aldrich	O0625

**2.1.2.6 DNA quantification**

Reagent	Supplier	Catalogue
Pico Green.	Invitrogen.	P11495
DNA stock.		
TRIS (hydroxymethyl)aminomethane)/EDTA (Ethanalamine) buffer.	Sigma Aldrich	93283

**2.1.2.7 RNA isolation**

Reagent	Supplier	Catalogue
ReliaPrep™ Minicolumns	Promega	A207B
Elution tubes	Promega	Z200C
Collection tubes	Promega	A130A
BL Buffer	Promega	Z103B
DNase I	Promega	Z358A
MnCl <sub>2</sub> , 0.09M	Promega	Z318A
Yellow Core Buffer	Promega	Z317A
RNA Wash Solution	Promega	Z309E
1-Thioglycerol	Promega	A208B
Nuclease-Free Water	Promega	P119E
100% Isopropanol	Sigma Aldrich	34863
95% Ethanol	Sigma Aldrich	493511

**2.1.2.8 RT-PCR**

Reagent	Supplier	Catalogue
ReliaPrep™ Minicolumns	Fisher Scientific	N8080234
200µl PCR reaction tubes	Fisher Scientific	15645367
10x PCR Buffer II (500mM KCL, 100mM Tris/HCL pH8.3)	Applied Biosystems	4379878
25 mM Magnesium chloride	Fisher Scientific	10690471
DeoxyNTPs mixture (2.5nM each dNTP)		
Random Hexamer (50uM)	Fisher Scientific	N8080127
RNase Inhibitor (20 U/ul)	Fisher Scientific	N8080119
MultiScribe Reverse Transcriptase (50 U/ul)	Fisher Scientific	4311235
Thermal Cycler Verity	Applied Biosystems	A48141
TE (Tris-EDTA) Buffer: prepared from 100x concentrate with ultra-pure water	Sigma Aldrich	T9285

**2.1.2.9 qPCR**

Reagent	Supplier	Catalogue
96-well PCR plate and adhesive film	Eppendorf	0030129504
cDNA samples		
primers ( <i>ALP</i> , <i>RUNX2</i> , <i>ACTB</i> ) at 5 µM dilution		

## 2.2 Methods

### 2.2.1 Polyacrylamide hydrogels

Polyacrylamide (PAAm) hydrogels were prepared using the Pelham and Wang protocol (Pelham and Wang, 1997). Firstly, the glass coverslips used as a rigid support for the hydrogels (13 mm or 25 mm diameter) (VWR International, Leicestershire, UK) were cleaned with tissue paper and functionalised with 250 or 500  $\mu\text{L}$  0.1 M NaOH (Sigma-Aldrich, Gillingham, UK), on a plate heater at 80° for 20 min. Next, coverslips were washed with distilled water and dried to add 120 or 250  $\mu\text{L}$  of 100% (v/v) 3-Aminopropyltriethoxysilane (APES) to incubate at room temperature for 5 min (Sigma-Aldrich) and rinsed with distilled water. Secondly, dried coverslips were immersed for 30 minutes in 0.5% (v/v) glutaraldehyde (Sigma-Aldrich) in phosphate-buffered saline (PBS) (Sigma-Aldrich). Hydrogels with different elastic moduli were prepared by varying the concentration of acrylamide-bisacrylamide. 12.5% (v/v) acrylamide, 1.5% (v/v) bisacrylamide and 85% (v/v) PBS for 1 kPa hydrogels and 20% (v/v) acrylamide, 24% (v/v) bisacrylamide and 55% (v/v) PBS for 40 kPa hydrogels. The mixture was degassed for 15 minutes under a vacuum. Thirdly, 1  $\mu\text{L}$  of N, N, N', N'-tetramethylethane-1,2-diamine (TEMED) and 10  $\mu\text{L}$  of 10% (w/v) ammonium persulfate (APS) (Sigma-Aldrich) was added to the mixture and vortexed to initiate the polymerisation. Specific mixture volumes (depending on the desired thickness; Chapter 3) were situated between a pre-treated coverslip and glass. Once the hydrogels polymerised, they were placed in PBS for 10 minutes, separated from the glass slide, placed on well plates with PBS and washed overnight at 4°. Hydrogels were washed 3 times with new PBS and covered with sulfosuccinimidyl 6(4-azido-2-nitrophenyl-amino) hexanoate (sulfo-SANPAH) (Thermo Fisher Scientific, Loughborough, UK) 0.5 mg/mL in 4-(2-hydroxyethyl)-1-piperazineethanesulfonic acid (HEPES) and exposed to UV light (Chromato-vue TM-20, UVP transilluminator, 240 V) for 20 minutes. Later, the hydrogels were washed 3 times with HEPES 50 mM pH 8.5, and 0.1 mg/mL collagen solution type I (Sigma Aldrich) was added to cover the hydrogels before incubating overnight at 4°. Lastly, the PBS was removed, and the PAAm hydrogels were accessible.

Figure 2.1 represents hydrogel polymerisation; the concentration of acrylamide/bisacrylamide defines hydrogel's geometry (porosity and swelling). Figure 2.2 illustrates collagen I attachment to the PAAm networks through the Sulfo-SANPAH molecules depending on the hydrogel stiffness. Stiff (40 kPa) hydrogels allow the attachment of more Sulfo-SANPAH molecules, and more collagens adhere compared to the soft (1 kPa) hydrogels where Sulfo-SANPAH encounters fewer sites to attach, which reduces collagen attachment.

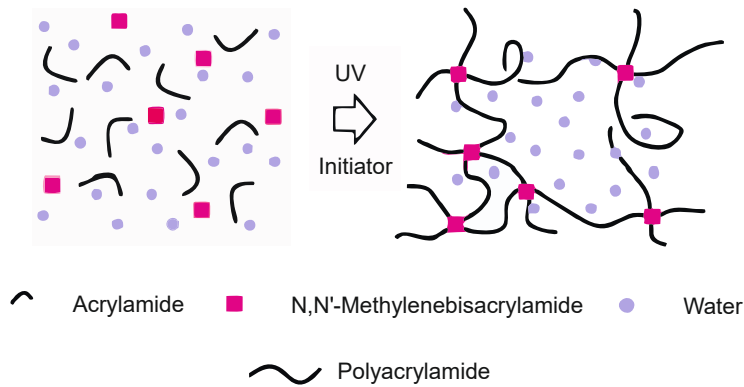


**Figure 2.1. Synthesis of polyacrylamide hydrogels.** The mixture comprises acrylamide (monomer), N, N'-Methylenebisacrylamide (crosslinker), and water molecules. UV light directs free radical polymerisation. Acrylamide links with the polymer chains forming a polymer network that is not perfect. —adapted from Yang *et al.*, 2019.

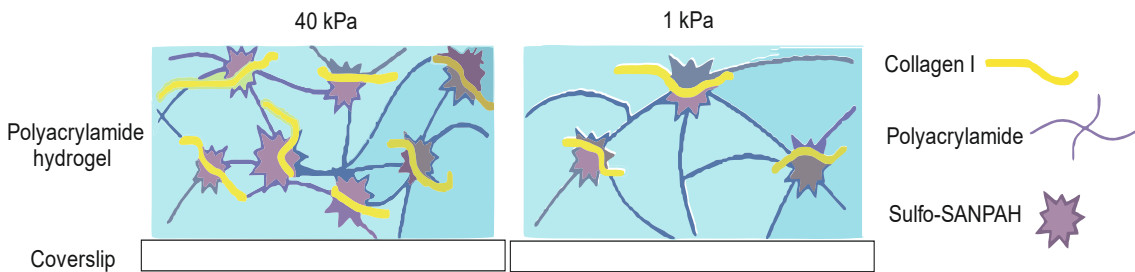


**Figure 2.2. Sulfo-SANPAH and collagen type I attachment to the polyacrylamide hydrogels with different elastic modulus.** The acrylamide and bisacrylamide concentration defines the hydrogel's elastic modulus and the pore size within the PAAm network. The network within the stiff hydrogel (40 kPa) is more compact than in the soft hydrogel (1 kPa), which promotes the attachments of more Sulfo-SANPAH molecules and collagen-scheme designed for this thesis.

### 2.2.1.1 Polyacrylamide hydrogels for traction force microscopy studies

Before polymerisation, 10 $\mu$ L of fluorospheres (ThermoFisher Scientific) of 0.5  $\mu$ m diameter were added to the PAAm mixture to track hydrogel displacements by BMSCs. Except for this modification and a sonication step for 20 min in a water bath, the rest of the process is detailed in Section 2.2.1.

### 2.2.1.2 PAAm hydrogels for thickness measurements

Firstly, allylamine (Sigma-Aldrich) was added to the acrylamide-bis-acrylamide mixture before polymerisation at 0.196% v/v. It does not modify the intrinsic elastic modulus but adds the primary amine groups that facilitate the fluorescent labelling of the hydrogel (Muresan, 2019). Once the PAAm hydrogels polymerised, Alexa Flour 568 (Thermo Fisher Scientific) 1 mg/mL was added (1:50) and incubated at room temperature for 3 h before washing 3 times with PBS 1X.

## 2.2.2 Thickness measurements

Hydrogel thickness was measured with a confocal microscope (Leica TCS SP5, Leica, Cambridge, UK). Soft and stiff PAAm hydrogels of different thicknesses (3 samples per condition) on 13 mm glass coverslips were placed upside-down on a thin glass slide and hydrated with 1x PBS. Hydrogels were imaged at 20X magnification and 2  $\mu\text{m}$  or 10  $\mu\text{m}$  z-stacks from top to bottom by Dr David Johnston at the Biomedical Imaging Unit, University of Southampton. The fluorescent intensity profiles were obtained and analysed using the Leica Software (LAS X Core Offline version 1.1.0.12420). Firstly, each file was uploaded individually (Figure 2.3a); then, channel 1 was used to save the XZ and XY images, as illustrated in Figure 2.3b. Figure 2.3c represents the rectangle across the image that was drawn before using the determine "FWHM" tool and the "show half maxima" option and defining the threshold (20) and width (1) represented in Figure 2.3d. Then the intensity profile for each hydrogel was obtained, and the measurements were obtained (Figure 2.3e). The images were manually used to quantify the number of wrinkles on the hydrogel surface.

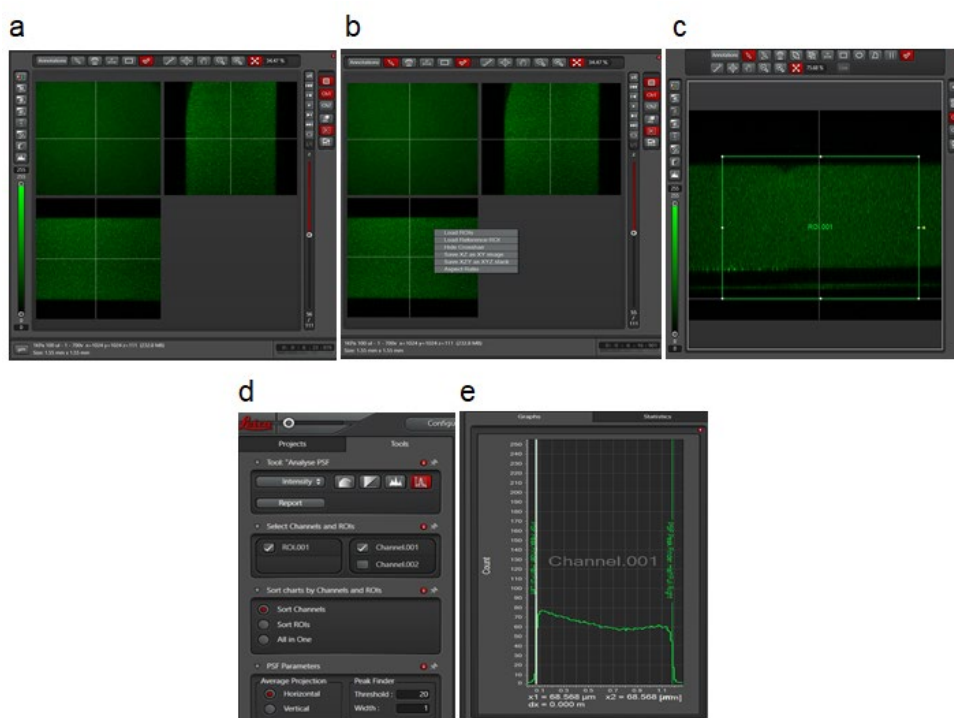


**Figure 2.3.** The process to obtain the fluorescent intensity profiles of the polyacrylamide hydrogels to measure thickness by confocal microscopy. (a) Files uploaded on the Leica software. (b) Image saving in XY and XZ. (c) Rectangle to measure intensity. (d) Parameters for the analysis: Threshold:20, Width:1. (e) Example of the intensity profile.

## 2.2.3 Stiffness measurements

Soft and stiff PAAm hydrogels with different thicknesses were fabricated as described in Section 2.1.2.1, and stiffness measurements were carried out by Dr Dichu Xu (Mechanical engineering department, University of Southampton) as part of a collaboration. The detailed

procedure is described in the protocol of Xu *et al.*, 2023 (in progress) and the NanoTest Vantage system (MicroMaterials Ltd., Wrexham). In brief, the samples immersed in PBS solution were tested using a spherical diamond tip (500  $\mu\text{m}$ ). Nanoindentation was carried out in load control to various maximum loads (10  $\mu\text{N}$  to 850  $\mu\text{N}$ , minimum load step: 2  $\mu\text{N}$ ) to obtain the indentation modulus ( $E_r$ ) vs depth ( $\delta$ ) profile. The indentation depth/hydrogel thickness ratios ( $\delta/h$ ) varied between 0.01 and 0.5, with the indents spaced apart by 250  $\mu\text{m}$ . The maximum load was applied for 120 s at rates of 1  $\mu\text{N/s}$  for loading and 5  $\mu\text{N/s}$  for unloading at ( $20 \pm 1^\circ\text{C}$ ).

#### **2.2.4 Cell culture**

SSCs selected for antigen Stro-1<sup>+</sup> (passage 1-5) previously isolated from human bone marrow samples were grown in  $\alpha$ -MEM media with 10% v/v Fetal Bovine Serum (FBS), 1% Penicillin/Streptomycin in 75 or 175  $\text{cm}^2$  flasks. Media was changed every two days until 80% confluence was achieved. Subsequently, cells were trypsinised and incubated for 5 min at 37° before adding complete media and centrifuging for 5 min at 200 g. Later, the supernatant was discarded, and the new cell suspension was split into new flasks or seeded on the PAAm hydrogels with different stiffness and/or thickness.

MG63 cells (variable passage number) were thawed and transferred to a new plastic tube where DMEM with 10% FBS and 1% Penicillin/Streptomycin was added. The cell suspension was centrifuged for 5 min at 200 g to remove DMSO. The supernatant was removed, new DMEM media was added, and cells were suspended and seeded on flasks or PAAm hydrogels.

#### **2.2.5 Quantification of cell spreading area**

Stro-1<sup>+</sup> BMSCs were plated on PAAm hydrogels and TCP (tissue culture plastic: Polystyrene) and incubated for 24 hours at 37°C under a Nikon Ti inverted microscope. Five microscopic fields of each soft, stiff hydrogel of different thicknesses ( $n=3$ ) were imaged in the brightfield channel at 10X magnification. The pictures were analysed using the FIJI software by uploading the images, setting the scale, and drawing around the cell periphery using the wand (tracing) tool. The cell area was measured using the analyse menu. It is worth mentioning that the number of cells varied depending on the hydrogel elastic modulus and thickness.

#### **2.2.6 Vinculin, actin, and nuclei staining**

Vinculin was stained to identify focal adhesions of Stro-1<sup>+</sup> BMSCs by immunocytochemistry. Firstly, cells were fixed in 4% (w/v) paraformaldehyde (PFA) for 20 minutes at room

temperature, rinsed with PBS 1X and permeabilised with 0.5 % (v/v) Triton, X-100 in PBS for 30 minutes at the same temperature. After washing 3 times with PBS 1X, cells were incubated in 0.1% (w/v) BSA in PBS at 4° for 2 hours. Next, cells were incubated with the primary vinculin rabbit anti-Human, Mouse, polyclonal antibody (ThermoFisher Scientific) at 2 µg/mL (final concentration) in 0.1% (w/v) BSA in PBS overnight at room temperature. Cells were washed with 0.1% BSA in PBS 3 times and incubated with the Goat anti-Rabbit IgG (H+L) Highly Cross-Adsorbed Secondary Antibody, Alexa Fluor Plus 594 at 10 µg/mL (final concentration) for 1 hour at room temperature. Secondly, F-actin (FITC) (ThermoFisher Scientific) was added (1:1000) to stain actin fibres and incubated for 30 minutes at room temperature (foil covered) and finally rinsed 3 times with PBS 1X. Thirdly, cells were stained with DAPI (1:1000) for 5 min at room temperature to stain nuclei and finally rinsed with PBS twice. Cells were imaged using a Nikon Ti inverted microscope and Leica confocal microscope with the Alexa 568, eGFP (535/50), and DAPI (460/60) filters and merged in the FIJI programme.

## **2.2.7 Osteogenic differentiation**

Cells were seeded at 5,000 cells/cm<sup>2</sup> on PAAm hydrogels and TCP. After 24 h, new  $\alpha$ -MEM media with (osteogenic media) or without (basal media) ascorbate [280 µM], beta glycerophosphate [5 mM] and dexamethasone [10 nM] were added. In both cases, media was changed every two days for 7 days, and the DNA and ALPL activity was quantified on day 7 or 14.

The ALPL activity was evaluated using ALPL staining and biochemical quantification.

### **2.2.7.1 ALPL staining**

Basal and osteogenic media was removed from the cells growing for 7 or 14 days on TCP or PAAm hydrogels and washed twice with 2 mL PBS 1X. After PBS was aspirated, 1 mL ethanol (95%) was added to each well, and the plate was incubated for 10 minutes at 4°C. Ethanol was carefully aspirated, and the plate was washed twice with 2 mL PBS before leaving it to dry for 20 minutes at room temperature. After that, 0.0036 g fast violet (Sigma Aldrich) was dissolved in a solution containing 600 µL  $\alpha$ -naphthol and 14.4 mL distilled water, forming a yellow solution that was added to the cells. Next, the plate was incubated for 1 hour at 37°C before removing the solution, and the wells were rinsed with 1 mL Milli-Q water. Finally, pictures were taken in the following 2-3 days using the Zeiss microscope (Axiovision software).

### **2.2.7.2 ALPL quantification**

#### **2.2.7.2.1 Colorimetric method**

Cells were grown on 24 well plates on hydrogels and TCP to quantify DNA and ALPL activity. Basal and osteogenic media were removed from the plates before 500  $\mu$ L cell Lytic (Sigma-Aldrich) was added to each well and incubated on an orbital shaker for 15 minutes at room temperature. Later, the suspension was recovered and transferred into 1.5 mL tubes and centrifuged for 15 minutes at 4° at 80 g. Finally, 450  $\mu$ L of the cell suspension was recovered and transferred to new tubes, frozen at -80° until their use.

For the ALPL analysis, the assay buffer for the standards was first prepared by mixing 5 mL of 1.5 M alkaline buffer solution (Sigma Aldrich), 10 mL distilled water and 30  $\mu$ L Igepal CA-630. Secondly, the ALPL substrate was obtained by mixing 0.04 g phosphatase substrate (Sigma Aldrich) (cover foiled), 10 mL alkaline buffer solution (1.5 M) (Sigma Aldrich) and 20 mL distilled water. Later, p-nitrophenol standards at different concentrations were prepared to construct the standard curve. For the assay, 100  $\mu$ L standards, 20  $\mu$ L of cell lysate and 80  $\mu$ L substrate were added in triplicates to a 96 transparent well plate. Additionally, 100  $\mu$ L NaOH 1M was added to each background control. After that, the well plate was incubated at 37° for 60 min or until samples acquired a yellow colour, and the reaction was finished with 100  $\mu$ L NaOH. The absorbance was quantified in a Glomax reader at 405nm.

#### **2.2.7.2.2 Fluorometric method**

Firstly, the ALPL assay buffer and stop solution were placed at room temperature, the ALPL enzyme solution was reconstituted with assay buffer, and the MUP (4-Methylumbelliferyl phosphate) standards were prepared following the manufacturer's protocol (Abcam®) by varying the volume of the standard and assay buffer. The dilutions of the standards accounted for the standard wells. The reaction wells contained the samples, whereas the backgrounds included the ALPL assay buffer and stop solution. The MUP reaction mix was prepared using the MUP (5 mM) substrate and assay buffer. Then, this mixture was added to the sample and background wells and ALPL enzyme was added only to the standard wells. The ALPL enzyme converts the MUP substrate into an equal amount of fluorescent 4-Methylumbelliferone (4-MU). Later, the well plate was cover-foiled and incubated for 30 min at room temperature. Finally, the reaction was stopped by adding a stop solution to all wells (except backgrounds). The plate was placed in a microreader and measured at 360/440 nm.

### **2.2.7.3 DNA quantification**

The same cell supernatant used to measure the ALPL activity was employed to measure the DNA concentration by the PicoGreen Assay, as it was necessary to normalise the data.

Firstly, DNA standards were prepared at different concentrations (0-1000  $\mu$ M) using Tris/EDTA (TE) buffer 1X and DNA stock (10 mg/mL). Cell samples were prepared by resuspending the cell pellets in 100 $\mu$ L assay buffer before homogenising and centrifuging the cells and collecting the supernatant. Next, the PicoGreen solution (dilution 1:200) was prepared, and the foil was covered. Secondly, 100  $\mu$ L standards, 10  $\mu$ L cell samples, 90  $\mu$ L TE, and 100  $\mu$ L Pico Green (1:200) were added in duplicates in a 96 black well plate. Finally, the fluorescent measurements were obtained in a Glomax reader (emission filter: 500-550 and excitation filter: blue 475 nm).

## **2.2.8 Adipogenic differentiation**

Stro-1<sup>+</sup> BMSCs were plated at different seeding densities (3,750-30,000 cells/cm<sup>2</sup>) on plastic or PAAm hydrogels during 14 days in basal  $\alpha$ -MEM and supplemented media with dexamethasone [100 nM], IBMX [0.5 mM], ITS solution [3  $\mu$ g/mL] and rosiglitazone [1  $\mu$ M]. Basal and adipogenic media were changed every 3 days, and cells were stained with Oil Red O, followed by absorbance quantification after 14 days of incubation.

### **2.2.8.1 Oil Red O staining and quantification**

Firstly, the oil red O stock solution (saturated) was prepared by mixing 1g of oil red O in 100 mL 99% isopropanol. The working solution was prepared in distilled water (3:2), filtered through a Whatman filter paper for 2 hours, and used 20 min after preparation. Secondly, the solution was ready to be used after filtering again through a 0.22  $\mu$ m filter.

Cells were first fixed with PFA and rinsed with 60% isopropanol. 1 mL of the oil red O working solution was added to each well and left to stain for 15 minutes. Later, wells were rinsed 3 times with dH<sub>2</sub>O, and 1 mL of PBS for each well was added to visualise the cells under the microscope. For oil red O quantification, 1 mL of 100% isopropanol was added to each well, and the absorbance was measured at 510 nm in a spectrophotometer.

## **2.2.9 ALPL, RUNX2 expression quantification**

### **2.2.9.1 RNA isolation**

The Promega ReliaPrep RNA Cell Miniprep extraction kit was used to extract RNA from the Stro-1<sup>+</sup> cell samples. In brief, cells were transferred into a 1.5mL tube, centrifuged for 4 min at 270 RCF, washed with PBS and newly centrifuged. Lysis buffer BL-TG was added to each sample, and cells were resuspended. Later, molecular-grade isopropanol was added to each sample, mixed, and transferred into minicolumns (placed in collection tubes), centrifuged at 12,000 x g for 30 seg at 25°. The collection tubes were emptied, and RNA wash solution was added into the minicolumns and newly centrifuged. DNase I solution

(DNase I,  $\text{MnCl}_2$  0.09M and Yellow Core Buffer) was added into the minicolumns before emptying the collection tubes and incubated for 15 min at room temperature. Next, RNA wash solution was added to the minicolumns and centrifuged before discarding the collection tube. A new volume of RNA wash solution was added to the minicolumns before centrifugation, and the collection tube was discarded. The minicolumns were transferred into elution tubes, and 30 $\mu\text{L}$  nuclease-free water was added and centrifuged to recover the RNA samples.

### **2.2.9.2 RNA measurements**

The nanodrop instrument was cleaned before 1  $\mu\text{L}$  of nuclease-free water was placed on it. Nuclease-free water was used to blank the instrument, and the RNA samples were measured by a spectrophotometric method at 260 and 280 nm to determine the concentration (ng/ $\mu\text{L}$ ). Purification was assessed at 260/280 and 260/230 ratios. After its usage, the instrument was cleaned again with 1  $\mu\text{L}$  of nuclease-free water and dried with paper.

### **2.2.9.3 Reverse Transcription PCR**

Reverse transcription PCR was carried out to produce cDNA from the RNA samples used for quantitative PCR. Initially, the RT reaction mix was prepared by mixing 10X PCR buffer II, 25 mM Magnesium chloride, deoxyNTPs mixture (2.5nM each dNTP), random hexamer (50  $\mu\text{M}$ ), RNase inhibitor (50 U/ $\mu\text{L}$ ) and multiscribe reverse transcriptase. The mixture was divided into 200  $\mu\text{L}$  tubes, the RNA samples at 150 ng/ $\mu\text{L}$  and RNase-free water was added to complete 20 $\mu\text{L}$ . Finally, the tubes were placed in the cycler, and the program (25° for 10 min, 37° for 30 min, 95° for 5 min, and 4° finalisation) was initialised. cDNA samples were stored at -20° until their usage.

### **2.2.9.4 Quantitative PCR**

The expression of housekeeping (*GAPDH* and *HBB*) and osteogenic genes (*RUNX2* and *ALPL*) was quantified in a thermal cycler (ThermoFisher Scientific). For this, the master mix for each gene was prepared by mixing GoTaq® SYBR Green, forward and reverse primer and nuclease-free H<sub>2</sub>O. The mixture designated for each gene was divided into 200  $\mu\text{L}$  tubes, and cDNA samples were carefully added to the 96-well PCR plate and covered with adhesive film. The cycle was run for about 2 h 25 min after selecting SYBR Green as a reagent and assigning targets and samples (Livak and Schmittgen, 2001).

#### **2.2.9.4.1 Calculation of the *ALPL* and *RUNX2* relative expression**

Firstly, the *ALP* or *RUNX2* Ct values from the triplicates of each condition were averaged.  $\Delta\text{Ct}$  was calculated by subtracting the average Ct of the housekeeping gene *ACTB* from the

average Ct of *ALPL* or *RUNX2* genes (correspondingly). Then,  $\Delta\Delta\text{Ct}$  values were obtained by subtracting the geometric mean of the  $\Delta\text{Ct}$  in basal media of the housekeeping gene *ACTB* from the  $\Delta\text{Ct}$  of the *ALPL* or *RUNX2* genes (correspondingly). Later, the  $2^{-(\Delta\Delta\text{Ct})}$  were calculated in each hydrogel triplicate (at each condition) and averaged only for basal conditions. Finally, the relative expression values were obtained by dividing  $2^{-(\Delta\Delta\text{Ct})}$  in osteogenic conditions divided by the average  $2^{-(\Delta\Delta\text{Ct})}$  basal. Indeed, the relative expression in basal media corresponds to 1, whereas the osteogenic genes exhibited greater values.

## **2.2.10 Quantification of cell traction forces by traction force microscopy**

### **2.2.10.1 Time-lapse live cell imaging**

For all the experiments, Stro-1<sup>+</sup> cells were plated on soft and stiff polyacrylamide hydrogels with different thicknesses containing fluorescent microbeads and incubated in  $\alpha$ -MEM with 10% FBS and 1% pen/strep at 37° for 24 h. Before the experiment, cells were washed with PBS, and the media was changed. Later, the well-plate was placed on a Nikon Eclipse Ti Microscope equipped with an environment chamber set at 37° and 5% CO<sub>2</sub>. Cells were localised, and coordinates were saved once the focus and brightness were adjusted. Phase-contrast and fluorescent images of fluorosphere-labelled hydrogels with cells growing on their surfaces were taken at 10X magnification with a time interval of 5 min between 12 and 24 hours. An ND2 file was obtained after each time-lapse experiment.

### **2.2.10.2 Substrate displacement tracking**

A custom MATLAB (The Math Works R2017a, Natick, MA) algorithm was used to track hydrogel displacements based on the set of time-lapse images. (Zarkoob *et al.*, 2015). Spatial cross-correlation was used to determine relative displacements between subsequent image pairs. Relative displacements between image pairs were then summed cumulatively to yield the total displacements to the first reference image at any given time.

The phase-contrast and fluorescent images from the ND2 file were extracted with the FIJI programme. The function was tested, and the maximum number of images that could be analysed was 80; therefore, the images corresponding to each hour were selected, renamed, and placed in different folders for each well.

A MATLAB-specialised function (`rrlImageTrackGUI.m`) was opened, and the fluorescent images were uploaded using the load image button. Secondly, a grid of 10 columns x 8 rows were drawn, and it determined the number of nodes where displacements were analysed in the selected fluorescent pictures. The grid size can vary; however, the same size should be used to analyse all the hydrogel samples. A large grid might include background noise if few cells are seen but include more information with high cell crowding

cultures. Later, the specify guide button was used to establish a guide (near the grid corners and where no cells were found) to verify the image correlation between images p01 and p02. Figure 2.4 exemplifies the grid size (left) and the image correlation plot (right).

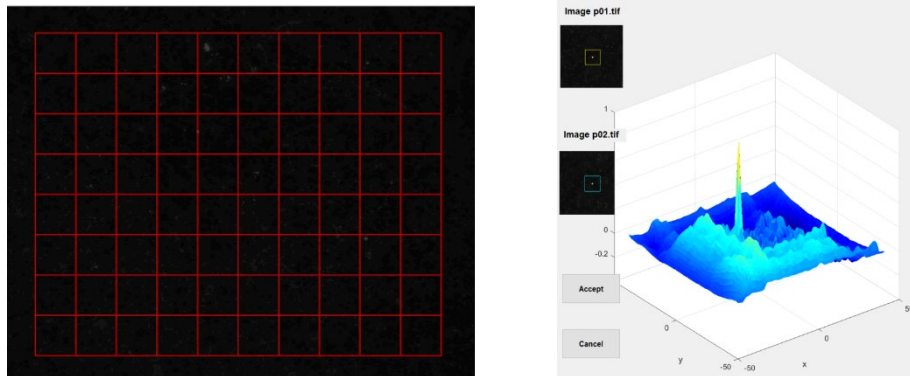


**Figure 2.4. Grid and correlation graph for analysis.** (Left) Example of the grid drawn on the first image (p01). The image uploading and the grid are obtained using the function in MATLAB. (Right) Graph showing the correlation surface when comparing images at the guide node.

This MATLAB function includes different tracking parameters: smoothness, smooth grid, kernel size, subpixel size and maxMove; the last three of them and the guide node were modified to check any differences in the displacement quantification. Figure 2.5. shows that the choice of guide node did not significantly modify hydrogel displacements, and max move increased the displacements values. Greater kernel size (the area around each node used for correlation as visualised by the coloured squares indicated in Figure 2.4b) decreased displacements values as it considers the average displacement of a greater area, lowering the resolution. The subpixel size did not modify displacements with a kernel size of 31. To sum up, except for using maxMov=15, all parameters were kept the same as default; guide: variable, kernel size=31 and subpixel size=9.

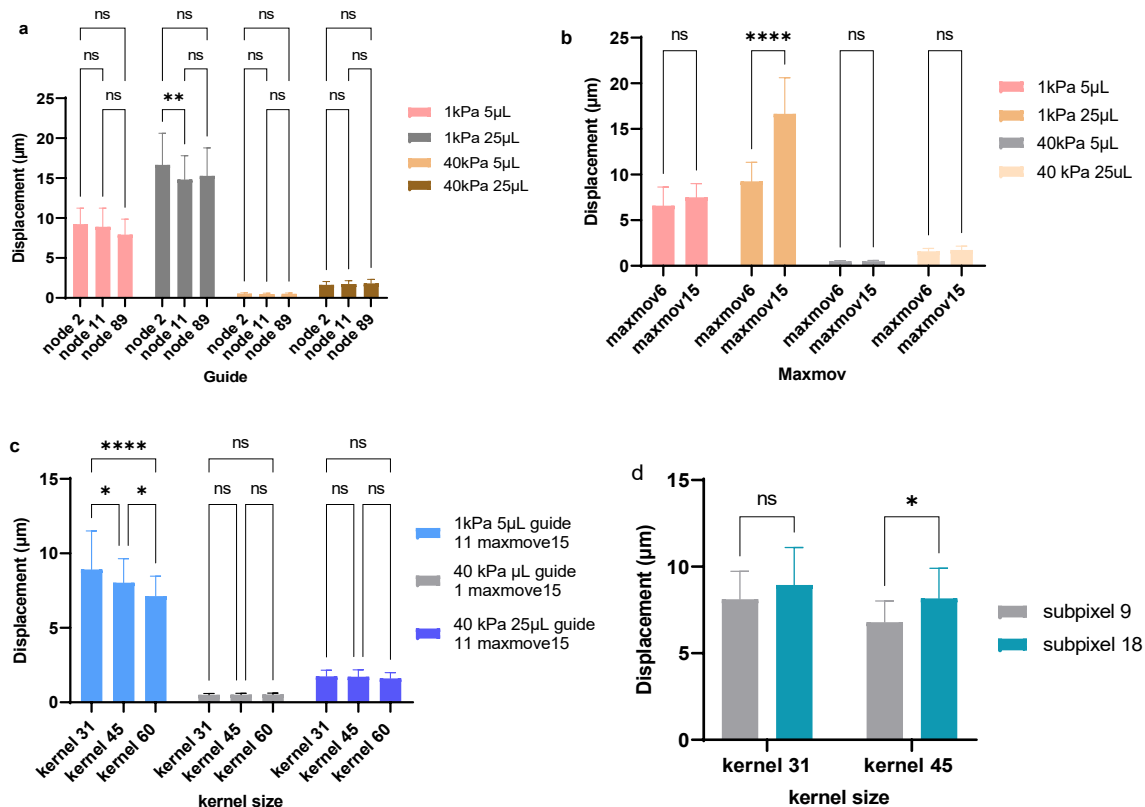


**Figure 2.5. Tracking parameters in the MATLAB function.** (a) The guide node does not significantly influence displacement quantification. (b) Greater maxMove increases hydrogel displacements. (c) Smaller kernel size increased displacements values. (d) Subpixel size did not modify hydrogel displacements with a kernel size=31.

After running the first function, various DAT format files were generated by clicking the perform tracking button. The second function (*processresults6v3.m*) was used to calculate the total displacements as a function of time by summing the change of displacements between images (backgrounds). The fluorescent images (Figure 2.6 left) are helpful for visually verifying the displacements, while the phase contrast images (Figure 2.6 right) also show the cells.

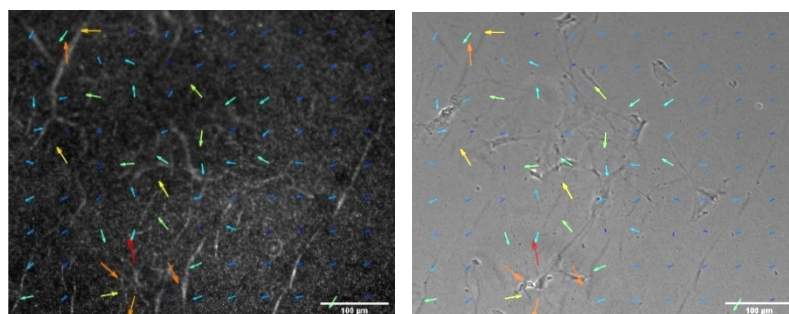


**Figure 2.6. Images were obtained by running the second function in MATLAB.** (Left) Fluorescent image of the beads embedded in the PAAm hydrogels with arrows showing the displacements from images p01 to p25. (Right) Phase-contrast image of BMSCs and arrows indicating hydrogel deformations. Scale factor=3 (arrow size).

It is important to note that the *processresults6v3.m* function was modified to remove the background movement (the product of using the microscope's motorised stage to capture time-lapse images of multiple wells). This was detected as the vectors in the phase contrast and fluorescent images were directed in the same direction. The movement of the image was corrected by subtracting the displacement of a reference node located in an area without any cell-induced displacements. The selection of the reference node where no cells were seen was crucial. The scale factor was defined for visualisation purposes; it extended the arrow size but did not affect the displacement quantification.

The functions used for the analysis and videos showing hydrogel deformations by Stro-1<sup>+</sup> are included in the appendices.

The average 90<sup>th</sup> percentiles of the hydrogel's displacements at the 99 nodes in the 3 hydrogel replicates was plotted over time in GraphPad prism. Significant differences were determined by plotting the average of the 90<sup>th</sup> percentiles of the hydrogel's displacements after 8 hours of incubation.

### **2.2.11 Cell micropatterning**

Dr Chaenyung Cha from the School of Materials, Science and Engineering, Ulsan National Institute of Science and Technology, kindly provided the micropatterning method.

#### **2.2.11.1 Preparation of acrylate-conjugated collagen**

Collagen type I (Sigma Aldrich) (0.1-3.0 mg/mL) was incubated for 4 hours with acrylate-PEG-NHS (5 mg/1 mL collagen) (Sigma Aldrich) in a roller at 4°.

#### **2.2.11.2 Collagen micropatterning on the glass slides by microcontact printing**

The collagen solution (0.1, 1 or 3 mg/mL) was placed on the PDMS stamps and incubated at 37° for 2 hours. Later, the excess of the collagen-acrylate-PEG solution was removed with the micropipette to avoid the formation of any specific pattern. Then, the PDMS stamps were placed on the glass slides, gently pressed, and incubated for 1 hour at 37°. After the incubation, PDMS stamps were removed, and the polyacrylamide mixture was placed on top of the glass slide. After PAAm polymerisation, coverslips were removed from the glass slides, placed in 6 well plates, covered with PBS and stored at 4°.

To note, for studying the hydrogel deformations by groups of cells, collagen was attached by placing 1 µL of collagen-acrylate-PEG solution on the glass slides. After 1 hour of incubation at 37°, the PAAm mixture was placed on the slides and sandwiched with glass coverslips until hydrogel polymerisation. Coverslips were detached from the glass slides, glued to the well plates before adding PBS, and stored at 4°.

### 2.2.11.3 Collagen inactivation

PBS was removed from the well plate, and PAAm hydrogels were rinsed 3 times with PBS 1X. After removing the PBS, hydrogels were washed with 1% v/v ethanolamine in PBS (2 ml/well) for 30 min at room temperature to inactivate the reactive groups of the Sulfo-SANPAH or acrylate-PEG collagen. Then, hydrogels were washed twice with PBS 1X (2 mL/well) and stored at 4°C until used.

### 2.2.12 Statistical analysis

Data were analysed using the Two-way ANOVA method with Turkey's post hoc correction for multiple comparisons and the T-test for comparing two groups.

- Hydrogel thickness and elastic modulus were measured on 3 hydrogels (n=3) of each elasticity and thickness ( $p < 0.0001$ ).
- Cell spreading area was measured by imaging 5 microscopic fields of each hydrogel triplicate (n=3) of each elasticity and thickness. The number of cells attached to each hydrogel varied due to their mechanical properties. The measurements of the cell spreading area of the 5 fields were averaged, and the plotted mean and standard deviation were obtained from each hydrogel triplicate.
- ALPL activity and *ALPL* and *RUNX2* expression was quantified in cells on 3 hydrogels triplicates (n=3) of each elasticity and thickness ( $p < 0.05$ ) in different experiments. ALPL activity was normalised to DNA content, and *ALPL* and *RUNX2* expression was normalised to the expression of the housekeeping gene *ACTB*.
- Hydrogel displacements by cells were quantified on each condition's hydrogel triplicates (n=3). 90<sup>th</sup> Percentiles were calculated on the 99 nodes (locations for analysis) on each hydrogel ( $p < 0.0001$ ).



## **Chapter 3 Polyacrylamide hydrogel characterisation**

### 3.1 Introduction

The main aim of this thesis was to study the effect of ECM stiffness and thickness on stem cell behaviour (refer to Sections 1.12 and 1.13 in Chapter 1) to evaluate whether changes in these mechanical properties might promote BMSCs osteogenic differentiation for bone regeneration. For this, PAAm hydrogels were used to mimic the mechanical properties of the ECM, and this chapter aimed to characterise these materials.

Polyacrylamide hydrogels are elastic polymer networks embedded in aqueous solutions (Ahmed, 2015). Their rigidity or elastic modulus can be easily modified by varying the acrylamide and bisacrylamide ratio and their thickness using different volumes of the polyacrylamide mixture. Hydrogels thicker than 5  $\mu\text{m}$  can be fabricated by sandwiching the polyacrylamide mixture sample between the hydrophobic slide and the hydrophilic coverslips. In contrast, thinner hydrogels are fabricated with an activated solution with polystyrene beads of different diameters (Maloney *et al.*, 2008).

Dembo and Wang, 1999 measured the PAAm hydrogel elastic modulus by covering its surface with a glass coverslip and applying compressive forces with small weights on the upper glass (Dembo and Wang 1999). Ten years later, Boudou *et al.* measured Young's moduli of PAAm hydrogels by the micropipette aspiration technique. More recently, atomic force microscopy (AFM) has been used for the same purpose. Here, the hydrogel is indented by a sharp or spherical tip probe with a specific trigger force and speed. The generated force-distance curve is saved and transformed into a force-indentation depth graph, and Young's modulus is calculated by fitting the Hertz model against the curve (Lee *et al.*, 2019).

Substrate stiffness depends on the intrinsic elastic modulus and geometry (Boudou *et al.*, 2009). Indeed, elasticity, structure and thickness might vary between soft and stiff materials. Soft hydrogels are more prone to swelling than stiff hydrogels by absorbing more water molecules, altering the hydrogel structure and thickness. Therefore, differences in stem cell behaviour on matrices with different elasticity might also be related to differences in hydrogel thickness.

Initial studies based on PAAm hydrogels measured their thickness by focusing their top and bottom with the microscope and subtracting the difference (Dembo and Wang, 1999). However, a more accurate method based on confocal microscopy uses z-stack fluorescence images (Buxboim *et al.*, 2010) that, at the same time, provide information about the structure of the hydrogel.

Thin PAAm hydrogels ( $\sim 10\text{-}500\ \mu\text{m}$ ) attached to glass coverslips are valuable tools in tissue regeneration for evaluating cell behaviour (Saha *et al.*, 2010) as they mimic the mechanical

and biochemical properties of the ECM and promote protein and cell attachment (Caliari-Burdick, 2016). Also, the produced cellular forces can be (indirectly) evaluated by tracking the displacements of the fiducial markers embedded within the hydrogels during/after deformations (Schwarz *et al.*, 2015).

On soft, thin materials, the effective substrate modulus that cells sense is greater than the intrinsic elastic modulus because of the interference of the underlying support, promoting cell spreading (Leong *et al.*, 2010). Tusan *et al.*, 2018 reported that osteosarcoma cells *in vitro* could sense hydrogel thickness changes by increasing their spreading area on thinner materials. *In vivo*, differences in substrate stiffness and thickness within tissues are also encountered. Chondrocytes are immersed in a 25kPa gelatinous thin matrix immersed in a stiffer collagenous matrix, whereas osteoblast cells adhere to a very thin osteoid matrix on top of the calcified bone (Buxboim *et al.*, 2010).

Because of the importance of these mechanical properties on cell behaviour, this chapter aims to evaluate the differences in Young's modulus, hydrogel structure and thickness, comparing soft and stiff hydrogels (before and after adding fluorescent microbeads used for tracking hydrogel deformations). These studies are essential before evaluating the behaviour of BMSC cultured on these materials.

Stiffness measurements are different at the nanoscale, microscale, and macroscale, which needs to be considered for tissue engineering (Guimarães *et al.*, 2020).

The ECM consists of organised lamellae of collagen fibrils that are wavy elastic fibres composed of collagen molecules accommodated in all orientations (Chen *et al.*, 2018). Packaging the small-diameter collagen fibrils with hierarchical organisation dictates tissue shape and functionality (Zhou *et al.*, 2017). For instance, collagen fibrils fill structures and adapt to their peripheral environment. Their distribution defines the corneal biomechanical and curvature functions, and damage in the microstructure leads to pathological corneal changes (Zhou *et al.*, 2017). Engineered corneal tissues with collagen fibrils with the same diameter represent a novel biomaterial for corneal blindness (Zhou *et al.*, 2017).

Cell responses depend on how the matrix is presented to the cells. Changes in collagen fibrils modify the phenotype of vascular muscle cells and fibroblasts, increase the stiffness of fibrils, and promote cell spreading and proliferation (McDaniel *et al.*, 2007).

Besides the stiffness of collagen fibrils, the mechanical properties of single cells, determined by the cytoskeleton, define cell proliferation, differentiation, migration, and adhesion and might lead to cell malfunction and disease progression (Quan and Kim, 2016). The mechanical properties of cells change in cancer and ageing. Cancer cells are softer than their normal counterparts, facilitating migration and their mechanical properties are

considered early cancer biomarkers (Quan and Kim, 2016). Whereas fibroblasts from older donors were softer than those from younger patients due to decreased actin contents (Quan and Kim, 2016).

Cells exhibit a characteristic stiffness due to their interaction with the surrounding microenvironment and biological and/or genetic status (Guimarães *et al.*, 2020). Overall, cells are soft (0.1-10 kPa), which hardly varies with cell type; however, different cellular components, such as the cytoskeletal fibres, show high elastic moduli (Guimarães *et al.*, 2020). Cell stiffness varies with cell area; more giant cells exhibit higher stiffness even being part of the same cell layer (Nehls *et al.*, 2019).

Micropipette aspiration, AFM, optical tweezers, and magnetic tweezers are different approaches to measuring cell mechanical properties (Quan and Kim, 2016).

Tissue engineering must consider the stiffness of the native biological tissue as well as the implications of this stiffness for the behaviour of resident cells (Guimarães *et al.*, 2020).

Cells sense tissue stiffness when adhering to the matrix proteins and apply tension (Wells, 2013). The brain is a very soft tissue with an elastic modulus of 100 Pa, the liver with 400-600 Pa, and muscle and bones at  $10^4$  and  $10^6$  Pa (Wells, 2013).

Fibrotic organs are stiffer due to the increase in the extracellular matrix, specifically fibrillar collagens. However, only the increase in the matrix does not increase the stiffness of fibrotic tissues; stiffness and ECM quantity are not linearly related. An increase in collagen and elastin cross-linking increases the elastic modulus in liver fibrosis, and the mechanical properties of the injured liver change significantly after injury, before ECM deposition (Wells, 2013).

On stretching, the collagen molecules align and become an extremely stiff network, which modifies Young's modulus of the tissue (Guimarães *et al.*, 2020).

## 3.2 Aims

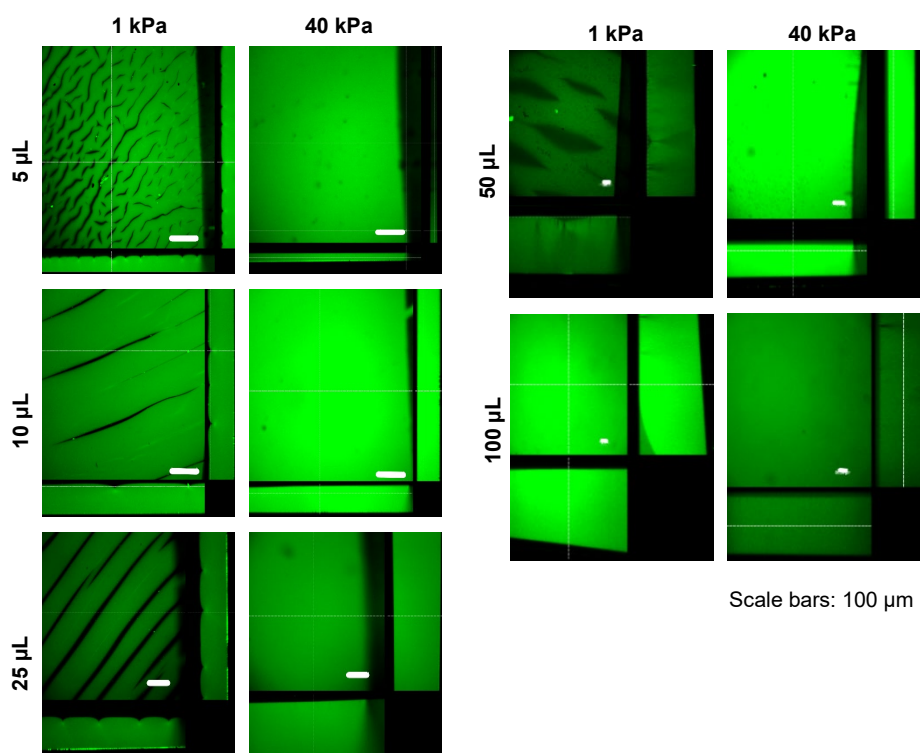
- To evaluate if changes in the acrylamide/bisacrylamide ratio and thickness modify the structure and surface of PAAm hydrogels assessed by confocal microscopy.
- To measure the thickness and Young modulus of PAAm hydrogels with different stiffness and thickness by confocal microscopy and nanoindentation, respectively.
- To determine if the addition of fluorescent microbeads modifies the stiffness and thickness of the PAAm hydrogel.

### 3.3 Results

#### 3.3.1 Hydrogel morphology is affected by composition and volume.

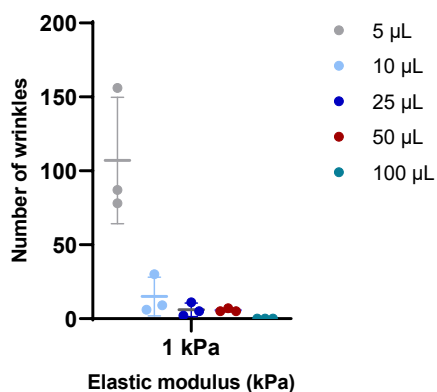
Collagen-coated polyacrylamide hydrogels were used to evaluate the effects of the changes in the ECM mechanical properties on cell behaviour. First, these materials were characterised by identifying structure, thickness, and elastic modulus changes with increasing monomer concentration, PAAm volume, and fluorescent microbeads.

PAAm hydrogels were fabricated by varying the monomer and cross-linker concentrations according to information in the literature to generate either 1 or 40 kPa stiffness hydrogels (see Section 2.2.1 for hydrogel composition). The hydrogel thickness was modified by varying the volume of the PAAm mixture using 5, 10, 25, 50 and 100  $\mu\text{L}$ . After polymerisation, hydrogels were stained with Alexa Fluor 488, coated with collagen type I, and imaged by Dr David Johnston at the Biomedical Imaging Unit at the University of Southampton. Figure 3.1 shows representative images of PAAm hydrogels with low and high elastic modulus fabricated with different volumes of polyacrylamide mixture. The surface of soft hydrogels exhibits features like wrinkles that vary in number and length with different hydrogel thicknesses. However, the surface of stiff PAAm hydrogels remains intact with no patterns.



**Figure 3.1. Hydrogel surface changes with hydrogel elastic modulus and thickness.** Representative images of soft and stiff PAAm hydrogels with different thicknesses stained with Alexa Fluor 488. Pictures were taken with a Leica SP8 confocal microscope ( $n=3$ ). Soft polyacrylamide hydrogels showed surface wrinkles, which varied with the hydrogel thickness. Stiff hydrogels did not display any surface features.

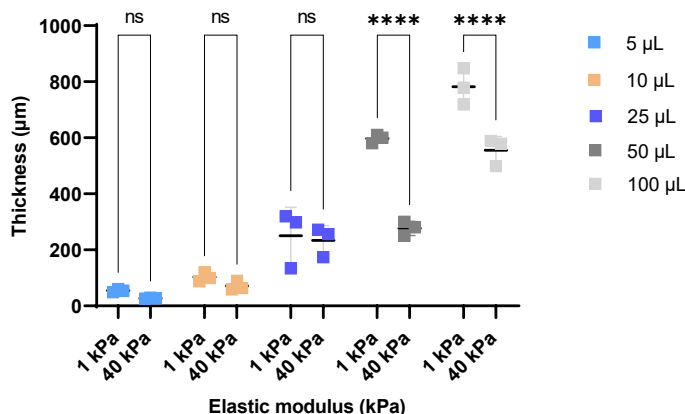
The number of wrinkles on the surfaces of soft hydrogels with different thicknesses decreases on thicker hydrogels and is plotted in Figure 3.2. This factor might be necessary when evaluating cell behaviour on soft hydrogels.



**Figure 3.2. The number of wrinkles on the surface of soft polyacrylamide hydrogels decreases on thicker hydrogels.** Each point represents the number of wrinkles on each hydrogel triplicate (n=3) counted manually. The error bars represent the standard deviation.

The soft and stiff PAAm hydrogels with different thicknesses, shown in Figure 3.1, were used to quantify the thickness of the hydrogel by a confocal microscope. The results are plotted in Figure 3.3. The plot graph shows that soft hydrogels are significantly thicker than stiff hydrogels when made with 50  $\mu\text{L}$  and 100  $\mu\text{L}$  acrylamide/bisacrylamide, which might impact cell mechanosensing but not with apparent with smaller volumes.

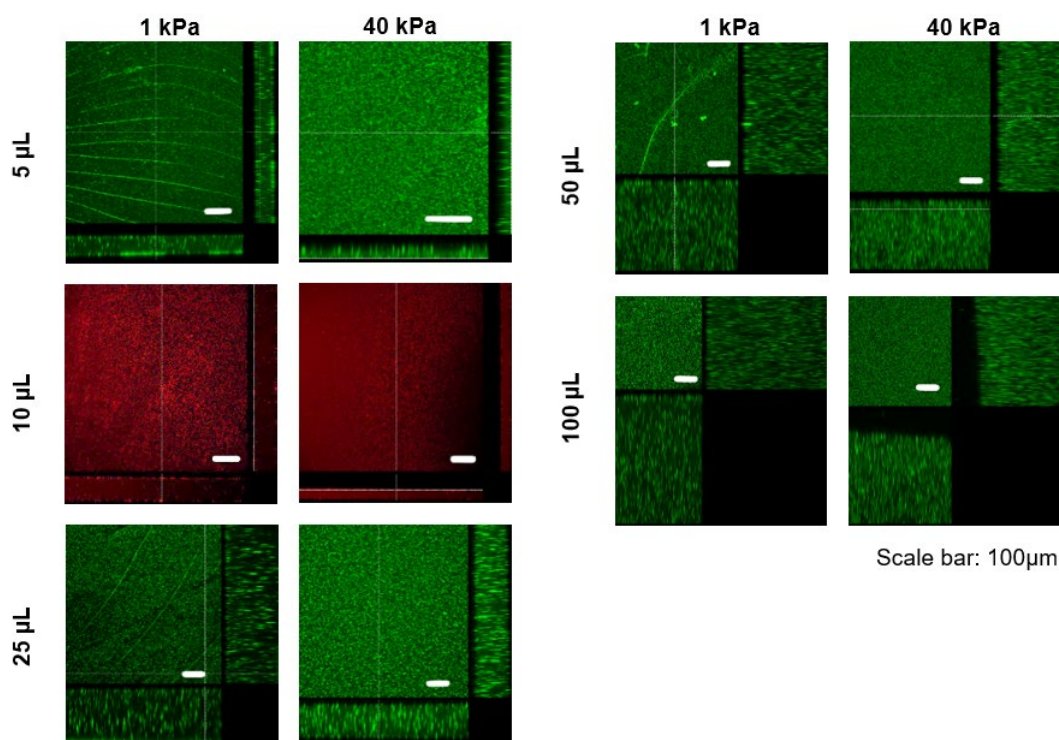
### 3.3.2 Thickness measurements of low and high elastic modulus PAAm hydrogels



**Figure 3.3. Soft PAAm hydrogels are thicker than their stiff counterparts when using high PAAm mixture volumes.** The thickness of soft and stiff PAAm hydrogels was measured by confocal microscopy. Hydrogel thickness increases with the PAAm mixture volume, and soft hydrogels are thicker than stiff hydrogels when using 50 and 100  $\mu\text{L}$ . The two-way ANOVA method was used to analyse significant differences (n=3). \*\*\*\*=  $p < 0.0001$ .

### 3.3.3 Effect of the addition of fluorescent microbeads on the structure of PAAm hydrogel

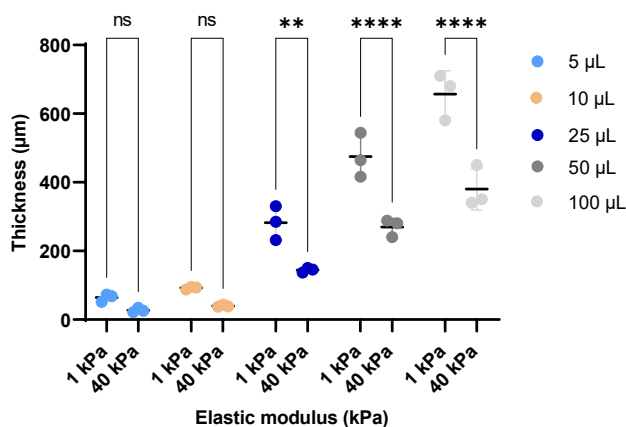
To enable PAAm hydrogels for displacement microscopy (Chapter 6), fiduciary fluorescent microbeads must be embedded in the hydrogels so that cell-induced hydrogel displacements can be measured using optical microscopy. Experiments aimed to identify if adding fluorescent microbeads before polymerisation would impact the substrate thickness. The images presented in Figure 3.4 denote that those fluorescent microbeads are equally distributed on stiff hydrogels while aligned within the wrinkles on the surface of soft hydrogels.



**Figure 3.4. Wrinkles on soft PAAm hydrogels dictate microbead positioning.** Representative confocal images of 1 kPa and 40 kPa PAAm hydrogels with different thicknesses containing 0.5  $\mu\text{m}$  fluorescent microbeads were stained with Alexa Fluor 488. Fluorescent microbeads aligned, forming patterns on the surface of soft PAAm hydrogels and were equally distributed on stiff hydrogels.

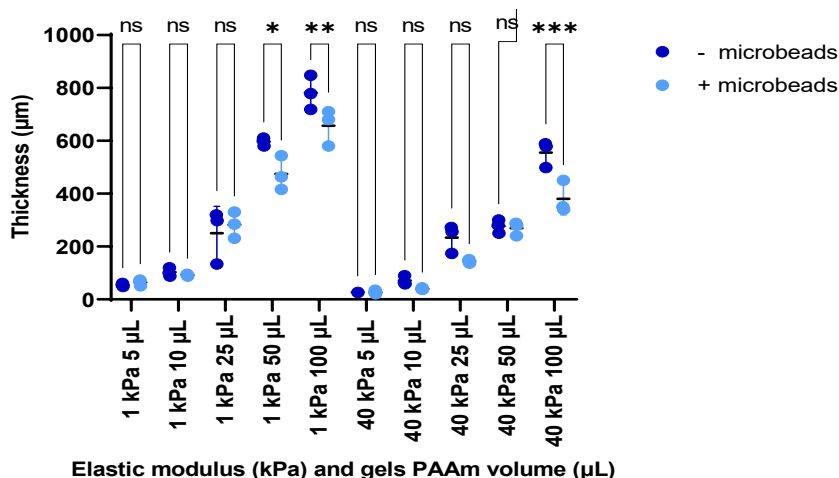
### 3.3.4 Effect of the addition of fluorescent microbeads on PAAm hydrogel thickness

Figure 3.5 compares the thickness of soft and stiff PAAm hydrogels with embedded microbeads. Like hydrogels without microbeads, soft hydrogels with microbeads are thicker than their stiff counterparts when using 25  $\mu\text{L}$ , 50  $\mu\text{L}$  and 100  $\mu\text{L}$ .



**Figure 3.5. PAAm hydrogels with low elastic modulus are thicker than high elastic modulus hydrogels on 25, 50 and 100 µL PAAm samples with fluorescent microbeads.** The thickness of soft and stiff PAAM hydrogels was measured by confocal microscopy. Hydrogel thickness increases with the PAAm mixture volume, and soft hydrogels are thicker than stiff hydrogels when using a higher PAAm volume than 25 µL. \*\*\*\*= $p < 0.0001$ .

Figure 3.6 shows that hydrogel thickness decreases with the addition of fluorescent microbeads on the thickest (100 µL) soft and stiff hydrogels and the soft gels (50 µL). This might impact traction force microscopy studies when evaluating forces exerted by the cells using those PAAm volumes.



**Figure 3.6. Adding fluorescent microbeads decreases the thickness of soft and stiff hydrogels with high PAAm volumes.** The thickness of soft and stiff PAAm hydrogels was measured by confocal microscopy. The addition of fluorescent microbeads decreases hydrogel thickness with 100 µL on 1 and 40 kPa hydrogels and 50 µL on 1 kPa hydrogels. Dots represent the hydrogel thickness of each hydrogel triplicate and line the standard deviation. Significant differences were calculated by the 2-way ANOVA method, \*\*\*\*= $p = < 0.0001$ .

Table 3.1 summarises the hydrogel thickness measurement of soft and stiff PAAm hydrogels with and without fluorescent microbeads for further reference. The following chapters will indicate hydrogel thickness as PAAm mixture volume.

**Table 3.1. Hydrogel thickness of PAAm hydrogels with and without fluorescent microbeads with different elasticity.** The data represent the average hydrogel thickness of three triplicates at each condition.

	(-) Microbeads ( $\mu\text{m}$ )			(+) Microbeads ( $\mu\text{m}$ )		
<b>1 kPa 5 <math>\mu\text{L}</math></b>	60.44	54.18	48.97	72.88	68.59	51.45
<b>1 kPa 10 <math>\mu\text{L}</math></b>	99.97	87.97	119.96	94.85	87.93	93.86
<b>1 kPa 25 <math>\mu\text{L}</math></b>	297.91	133.96	319.9	231.51	284.9	330.41
<b>1 kPa 50 <math>\mu\text{L}</math></b>	610.05	600.05	580.05	544.1	416.08	464.08
<b>1 kPa 100 <math>\mu\text{L}</math></b>	778.35	718.47	848.2	580.05	710.06	680.06
<b>40 kPa 5 <math>\mu\text{L}</math></b>	26.05	27.09	29.18	25.72	21.44	34.3
<b>40 kPa 10 <math>\mu\text{L}</math></b>	63.98	58.98	89.97	37.54	38.53	43.47
<b>40 kPa 25 <math>\mu\text{L}</math></b>	271.92	255.92	173.95	137.31	150.19	145.89
<b>40 kPa 50 <math>\mu\text{L}</math></b>	300.03	280.02	250.02	240.04	288.05	280.05
<b>40 kPa 100 <math>\mu\text{L}</math></b>	588.75	498.94	578.77	350.03	340.03	450.04

### 3.3.5 Effect of the supporting material and thickness on hydrogel elastic modulus

New soft and stiff PAAm hydrogels with and without microbeads were fabricated to measure Young's elastic modulus. The PAAm hydrogels were created as previously described, except they were not stained with Alexa Fluor 488. Dr Dichu Xu conducted the measurements in a research collaboration at the National Centre for Advanced Tribology at Southampton (nCATS) at the University of Southampton (Xu *et al.*).

The measurements were obtained with a NanoTest Vantage system (see Section 2.2.3 in Chapter 2). In brief, soft and stiff hydrogel duplicates were immersed in PBS at each thickness and tested using a 500  $\mu\text{m}$  spherical diamond tip. The Young's modulus was carried out in load control from 10  $\mu\text{N}$  to 850  $\mu\text{N}$ ; 2  $\mu\text{N}$  with the minimum load step for 120 s with an indentation depth/hydrogel thickness ratio from 0.01 to 0.5 and indents separated by 250  $\mu\text{m}$ .

Dr Dichu Xu kindly provided the raw and corrected data extracted from the system. The corrected data are obtained after introducing a correction factor in the Hertzian model to consider the effect of the decrease in elastic modulus with increased hydrogel thickness. Figure 3.7 compares soft hydrogels' original (left) and corrected (right) reduced modulus with different thicknesses. No differences between the original and corrected modulus were identified on hydrogels except on the 5  $\mu\text{L}$  samples. The supporting material might increase the effective stiffness reflected in Young's modulus values. Although all hydrogels had the

same acrylamide/bisacrylamide ratio, thinner hydrogels are stiffer than their thicker counterparts.

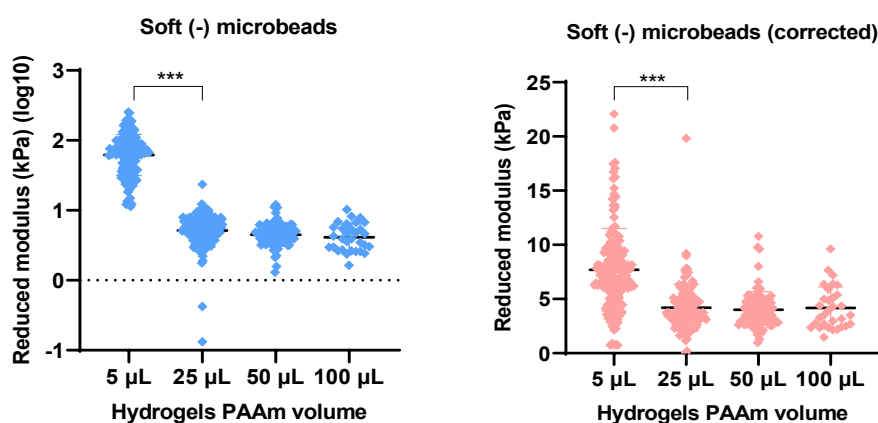


**Figure 3.7. The underlying material increases the effective stiffness of soft, thin PAAm hydrogels.** Young's modulus was measured by nanoindentation of two hydrogel duplicates. Significant differences were calculated by the Two-way ANOVA method. \*\*\*\*= $p < 0.0001$ . The corrected values consider the relation between the increase in thickness and the decrease in the hydrogel elastic modulus.

Stiff hydrogels were also measured, and the original (left) and corrected (right) reduced modulus were plotted in Figure 3.8. The original Young's stiff, thin hydrogels modulus was higher than their thicker counterparts. However, when removing the effect of the glass coverslip, the corrected Young's modulus of stiff, thin hydrogels was similar to thick hydrogels. This implies that the elastic modulus of stiff PAAm hydrogels also increases with the decreased thickness.

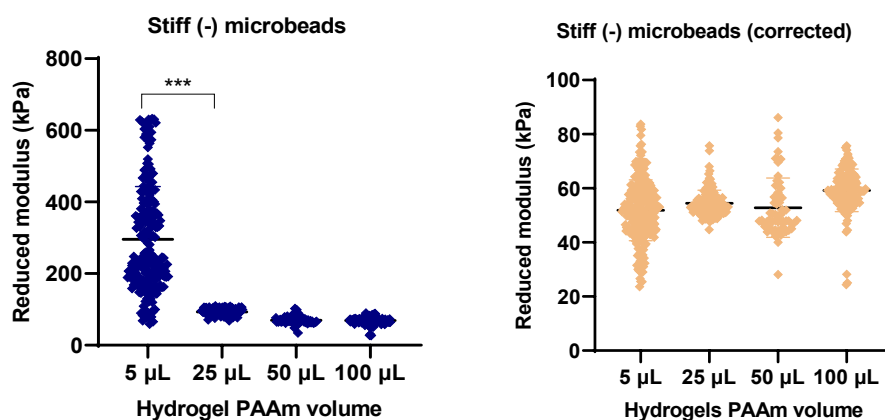


**Figure 3.8. Young's apparent modulus of stiff, thin hydrogels was higher than the corrected Young's modulus.** Stiff, thin hydrogels showed higher Young's modulus than stiff, thick hydrogels. The Young's modulus was measured by nanoindentation of two hydrogel duplicates ( $n=2$ ). Data were analysed using the Two-way ANOVA method. \*\*\*\*= $p < 0.0001$ .

Additionally, more PAAm hydrogels containing fluorescent microbeads were fabricated, and the reduced Young's modulus was measured using the previously described method in section 2.2.3. The data provided by Dr Dichu Xu were plotted in Figure 3.9. The graph

outlines that a change in thickness alters the reduced modulus of soft and stiff hydrogels containing fluorescent microbeads. Reduced values are also reported here instead of Young's modulus, as Poisson's ratio of the hydrogels was unknown. This information is essential to calculate the Hertz model equation's elastic load response for soft materials. If substrates exhibit a linear elastic response, no adhesion occurs between the contacting surfaces (indenter and substrate sample. The sample counts as an infinite half-space, meaning substrates are much thicker than the indenter radius or contact depth. As this cannot be assumed for very thin substrates, the Hertzian model was modified by adding a correction factor to the equation that considers the level of the geometrical confinement (Xu *et al.*).

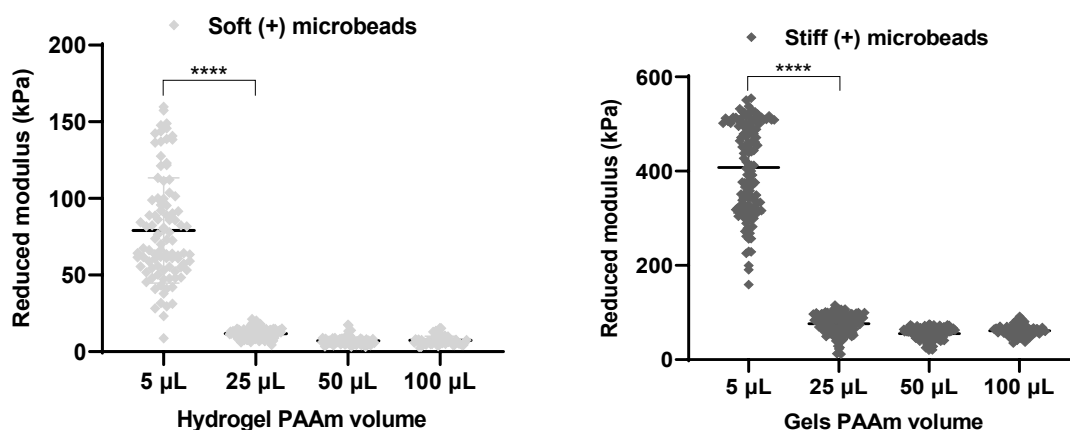


**Figure 3.9. The change in thickness influenced Young's modulus of stiff and soft PAAm hydrogels containing fluorescent microbeads.** The reduced modulus was measured by nanoindentation of two hydrogel duplicates ( $n=2$ ). Statistical analysis by the Two-way ANOVA method. \*\*\*\*= $p<0.0001$ .

Figure 3.10 illustrates that adding fluorescent microbeads did not alter the reduced elastic modulus of soft (left) PAAm hydrogels but increased on the thinnest stiff (right) counterparts.

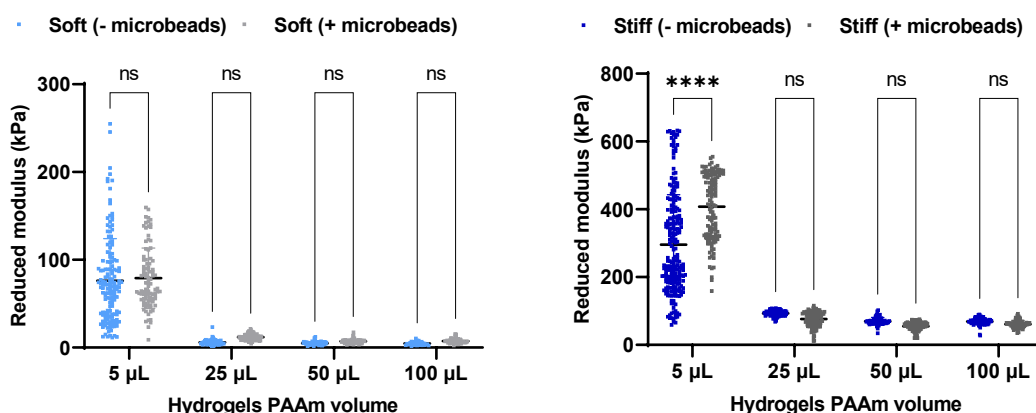


**Figure 3.10. The Young modulus of stiff, thin PAAm but not soft hydrogels increased with the addition of fluorescent microbeads.** The reduced modulus was measured by nanoindentation of two hydrogel duplicates. Statistical analysis by the Two-way ANOVA method. \*\*\*\*= $p<0.0001$ .

### 3.4 Discussion

The general aim of this chapter was to define the mechanical characteristics of PAAm hydrogels that were to be used for mechanotransduction studies. The main findings were:

- The acrylamide/bisacrylamide ratio and PAAm volume influence the presence and number of wrinkles on the hydrogel surface and thickness.
- Soft elastic modulus hydrogels are thicker than their higher elastic modulus counterparts, and the thickness increases in both cases with increased PAAm volume.
- Fluorescent microbeads can be aligned within wrinkles on the surface of soft PAAm hydrogels but homogeneously distributed on stiff hydrogels. Their addition reduces the thickness of the thickest PAAm hydrogel.
- The stiffness of the PAAm hydrogels decreases with increased thickness.

The first goal was to investigate any structural difference between soft and stiff PAAm hydrogels with different thicknesses. The surface of all soft hydrogels exhibited wrinkles varying in length and number, while stiff hydrogels showed flat surfaces (Figure 3.1). This agrees with previous reports highlighting that during hydrogel fabrication, wrinkles may appear on the surface of hydrogels with low elastic modulus during immersion in the aqueous media due to the difference in osmotic pressure, which causes swelling in the hydrogels. (Saha *et al.*, 2010). Wrinkles might also be due to non-uniform swelling, causing changes in the structure of the surface and elasticity that might also impact cell behaviour (Subramani *et al.*, 2020).

Lee *et al.*, 1994 modified Harris's methodology to avoid wrinkle formation by attaching the edges of the gel to a rigid vessel. However, problems arise controlling the osmotic pressure difference between hydrogels and the aqueous media outside. Wrinkle formation has also been reported in other materials, such as silicon substrates; Burton and Taylor, 1997 reported that surface wrinkles are usually larger than cells and randomly allocated (Dembo-Wang, 1999).

In this chapter, experiments showed that the number of wrinkles and their length on soft hydrogels varied with hydrogel thickness (Figure 3.2). A possible explanation is that thin hydrogels only expand at the surface due to tethering to the glass coverslip. In contrast, thick hydrogels freely expand as the supporting material is away from the surface, reducing the number of wrinkles (Saha *et al.*, 2010).

Hydrogel measurements showed that 50  $\mu$ L and 100  $\mu$ L soft hydrogels were thicker than their stiff counterparts (Figure 3.3). Because the ratio of acrylamide/bisacrylamide is lower on soft hydrogels than on stiff hydrogels, larger pores are found on the low elastic modulus

hydrogels that might hold more water molecules than the smaller pores formed on the high elastic modulus hydrogels.

Previous studies found hydrolysis increased hydrogel swelling, suggesting greater pores on low elastic modulus hydrogels absorb more water molecules (Zhou and Jin, 2020). Therefore, the swelling might also explain why the thickness of soft hydrogels increases as it increases the spatial heterogeneity of the PAAm hydrogels (Subramani *et al.*, 2020). For example, Protick *et al.*, 2022 showed that the swelling ratio of PAAm hydrogels decreased with the increase in stiffness; ~900% for soft hydrogels, ~675% for intermediate hydrogels and ~350% for stiff hydrogels. Accordingly, the pore size measured by electron microscopy decreased on high elastic modulus hydrogels; 9,000-11,000  $\mu\text{m}^2$  in soft hydrogels and 1,000  $\mu\text{m}^2$  in stiff hydrogels. These differences in the hydrogels can also be translated *in vivo*; the migration of cancer cells might be limited in ECM with tiny pores (Chaudhuri *et al.*, 2020). The pore size might also determine collagen crosslinking, attachment, and cell adhesion behaviour.

The impact of fluorescent microbeads on hydrogel thickness and structure was also evaluated. The confocal pictures showed that the fluorescent microbeads aligned within the wrinkles of the soft hydrogels but were equally distributed through the surface of the stiff hydrogels (Figure 3.4). As mentioned, wrinkle formation is explained by unconstrained hydrogel freely swelling in all directions, but this expansion is limited when hydrogels are attached to underlying support (Saha *et al.*, 2010). Hence, thin hydrogels exhibited more wrinkles because the surface is closer to the underlying material than thick hydrogels, where the hydrogels may expand over a wider area, reducing the number of wrinkles (Buxboim *et al.*, 2010). In this way, if the soft hydrogels are being folded during their fabrication, the embedded fluorescent microbeads might be pushed and accumulated, forming lines or patterns on the surface of the hydrogel. This is important to consider when evaluating hydrogel deformations through displacement microscopy. Initially, wrinkles formation might impact cell mechanosensing, the magnitude of the traction forces applied by the cells, and the consequent cell behaviour. Also, the accumulation of fluorescent microbeads within the wrinkles might facilitate quantifying and observing hydrogel displacements during time-lapse imaging.

It was also found that thick PAAm hydrogels containing fluorescent microbeads were thinner than hydrogels without beads, regardless of the hydrogel stiffness (Figure 3.6). This may be due to fluorescent microbeads influencing the osmotic pressure of hydrogels, which impedes water inflow into the hydrogels, reducing swelling and decreasing thickness. The cross-linking between the fluorescent microbeads and the polyacrylamide matrix can be dismissed as the carboxy terminated beads require an amine-reactive NHS ester to bind to

the acrylamide and bisacrylamide monomers by previous incubation with EDC/NHS (Mann and Leckband, 2010).

Knowing the exact mechanical properties of the substrates is vital in mechanobiology studies. Thus, the reduced modulus of the PAAm hydrogels was measured to detect the effect of hydrogel thickness on hydrogel stiffness by nanoindentation. This technique combines the application of small loads, the measurements of the generated displacements and the evaluation of the contact area between the nanoindenter and the sample. One factor cannot quickly determine the traction forces generated by the cells and the displacements on the hydrogel. They depend on the mechanical properties of the hydrogel, the forces generated by neighbouring cells, and all the components participating in cell mechanosensing, such as integrins, cadherins and the actin cytoskeleton.

Reduced Young's modulus data depend on the measuring conditions, such as the indentation speed (Perez-Calixto *et al.*, 2021). Feng *et al.*, 2013 measured the effective modulus of collagen hydrogels by atomic force microscopy; silicon nitride cantilevers with a pyramidal tip descended at a specific velocity. The force-distance data were analysed based on the Hertz model considering a Poisson ratio  $<0.5$  for compressible materials such as PAAm hydrogels attached to rigid supports that might generate a confinement region under the nanoindenter that might overshadow the actual hydrogel elastic modulus. Nevertheless, the method used here in this chapter and the inclusion of the correction factor in the Hertz model removes the effect of the increase in hydrostatic pressure under the indenter due to the confinement, which allows for obtaining more accurate measurements of the actual rigidity of the hydrogels (Xu *et al.*, 2022). Then, the method used here showed improvements by considering the effect of the geometrical confinement on the hydrogel stiffness and permeability and by controlling the speed and load.

The measurements provided by Dr Dichu Xu outlined that the corrected modulus of soft PAAm hydrogels was smaller than the initially reduced modulus (Figure 3.7), which implies that the underlying substrate increased the apparent stiffness of the hydrogel, especially on very thin matrices. These results are consistent with Leong *et al.*, 2011 where Young's moduli of 249 Pa and 750 Pa hydrogels were reduced on thicker hydrogels. This relates to the results previously reported by Tusan *et al.*, 2018 and Buxboim *et al.*, 2010 showing the increase in single cell spreading area of MG63 cells and SSCs, respectively, on thin PAAm hydrogels due to the increase in the stiffness sensed by the cells. This supports the hypothesis that changes in hydrogel thickness might influence cell spreading, proliferation, and differentiation as cells might perceive the effective stiffness of a hydrogel differently.

To summarise, hydrogel thickness and elastic modulus changed when varying the acrylamide/bisacrylamide ratio and polyacrylamide mixture volumes, and these changes might influence cell behaviour. However, another factor that might be considered is the

closeness of the hydrogel surface and cells to the glass support due to the increase in effective stiffness. If the cells were on the polyacrylamide hydrogel without an underlying material, cells would perceive the actual elastic modulus of the hydrogels.

Because many variables (hydrogel thickness, elastic modulus, collagen crosslinking and attachment, wrinkles formation and the distribution of fluorescent microbeads) are involved in the system, all of them should be considered when evaluating the effect of the mechanical properties on cell behaviour.



## **Chapter 4 Effect of stiffness and thickness on cell behaviour**

## 4.1 Introduction

The results in Chapter 3 demonstrated that soft hydrogels are thicker than their stiff counterparts and exhibit wrinkles on the surface that vary in length and number with the hydrogel thickness. Also, the nanoindentation data showed reduced modulus increases on thinner matrices. Likely, these variations encountered on the PAAm hydrogels with different stiffness and thickness might impact cell mechanosensing and, consequently, cell behaviour.

Mechanobiology is a field that studies how the mechanical properties of the ECM, especially stiffness, influence cell behaviour (Evans-Gentleman, 2014). PAAm hydrogels have been widely used in this field. Their mechanical properties can be easily modified to mimic the ECM microenvironment to evaluate how cells sense and translate the ECM mechanical information into biological signals.

Cells likely sense the mechanical properties of the hydrogel by pulling against it and detecting its deformation for a given force, which depends on its stiffness; cells easily deform soft but not stiff hydrogel (Tusan *et al.*, 2018). The first step in cell mechanosensing, or mechano-presentation, occurs between focal adhesions (formed by integrin receptor complexes and other proteins) on the cell surface and ECM proteins (fibronectin, vitronectin, collagens, laminins, VCAM or ICAM) through the FAs' outer layer. Mechanical forces activate the talin protein, facilitating vinculin attachment and its conformational change to form FAs. The inner layer of the FAs (constituted by docking proteins such as the FAK and vinculin) connects to the actin cytoskeleton. The tension within the cytoskeleton determines the propagation of the extracellular and cell traction forces, which dictate cell behaviour. This structure provides mechanical support to the cells, regulates motility, shape and tension equilibrium, and its disruption might lead to the modification of gene expression and the alteration of biological responses. Hence, this structure is essential in cell mechanosensing and mechanotransduction (Hao *et al.*, 2015; Chen *et al.*, 2017; Ringer *et al.*, 2017; Martino *et al.*, 2018).

Tensile forces or stiff substrates increase the actin filament length and promote myosin binding, forming actin stress fibres. The increased ratio of F-actin to G-actin and the formation of actin stress fibres promote YAP nuclear mobilisation (Hippo signalling pathway), promoting the transcription of genes involved in cell proliferation and differentiation (Ohashi *et al.*, 2017). Thus, evaluating the components participating as mechanosensors is important for understanding mechanobiology.

As previously mentioned, ECM stiffness is a crucial factor influencing mechanical cell responses. It depends on the ECM intrinsic elastic modulus (Young's modulus) and

geometry, including topography, thickness, and cell crowding (Evans-Gentleman, 2014; Venugopal *et al.*, 2018).

The effect of ECM elasticity on cell behaviour has been widely studied by mimicking its mechanical properties using collagen-coated PAAm hydrogels. Engler *et al.*, 2006 described that the elasticity of the PAAm hydrogels directed SSCs cell spreading and differentiation. SSCs spread on stiff substrates and show branches on soft matrices. This relates to their phenotypic profile as cells differentiated into neurons on 0.1-1 kPa hydrogels, myoblasts on 8-17 kPa and osteoblasts on 25-40 kPa hydrogels. Nevertheless, less attention has been paid to the effect of substrate geometry on cell behaviour.

Some studies support that cells can sense the difference in substrate thickness. For instance, Buxboim *et al.*, 2010 and Kuo *et al.*, 2012 showed that SSCs sense the underlying support on very thin hydrogels between 10-20  $\mu\text{m}$ . Similarly, Mullen *et al.*, 2015 highlighted that MC3T3 cells increased their cell spreading area on soft hydrogels with reduced thickness. Then, the substrate thickness might also impact cell behaviour.

A cell might only be able to sense a small fraction of a thick hydrogel but a more significant portion of a thin one, even the rigid underlying support. Nanoindentation data in Chapter 3 show that the reduced modulus increased on thin PAAm hydrogels. Hence, cells might easily deform a soft, thick hydrogel but need more force to deform a soft, thin hydrogel as the support underneath increases the effective stiffness cells sense, increasing cell spreading (Leong *et al.*, 2010) (Refer to Figure 1.7 in Section 1.14, Chapter 1 for a detailed explanation of the effect of substrate thickness on cell spreading).

Evaluating the effect of ECM stiffness on cell spreading is essential as it is the first point of contact between the cell and the ECM. Also, the cell area is essential as it influences RhoA and ROCK activity and determines the distribution of the cell-generated traction forces, which in turn influences cell fate through changes in transcript profiles and gene expression (Bianco-Robbey, 2000; Engler *et al.*, 2006; Bellas and Chen, 2014; Oakes *et al.*, 2014; Mao *et al.*, 2016). To exemplify, round cells relate to adipogenic differentiation, while cuboidal forms correlate to osteogenic differentiation (Lee *et al.*, 2013; Zhao *et al.*, 2014).

Moreover, evaluating the effect of substrate thickness on cell spreading provides information about the "critical thickness" or the depth at which substrate thickness does not influence cellular mechanical responses (Maloney *et al.*, 2008). For example, Tusan *et al.*, 2018 found that MG63 cells increased their cell spreading area on thin hydrogels (20  $\mu\text{m}$ ) compared to thick hydrogels (200  $\mu\text{m}$ ).

Besides hydrogel intrinsic elastic modulus and thickness, cell crowding might also influence stiffness sensing; Sen *et al.*, 2009 suggested that cells on PAAm hydrogels could sense their neighbour cells approximately 40  $\mu\text{m}$  away.

Because of the above, this chapter aimed to test the hypothesis that BMSCs sense changes in hydrogel elastic modulus and thickness by modifying cell spreading, FAs and actin stress fibres.

## 4.2 Aims

- To test if changes in the substrate intrinsic elastic modulus modify the cell morphology, spreading area, focal adhesions, and actin fibres of BMSCs.
- To evaluate if cell morphology, cell spreading area, focal adhesions, and actin fibres of BMSCs changed with the decrease in substrate thickness.

## 4.3 Results

### 4.3.1 Effect of the increase in hydrogel elasticity on cell spreading

The first experiment tested the hypothesis that cell spreading in Stro-1<sup>+</sup> BMSCs increases due to hydrogel stiffness. Firstly, cells were defrosted and cultured until reaching 80% confluence. Later, cells were trypsinised, plated at 1,000 cells/cm<sup>2</sup> and incubated for 24 h in  $\alpha$ -MEM/ FBS on PAAm hydrogels with different elasticities (0.5, 1, 2, 10, 20 and 40 kPa) and TCP. The cells from 5 fields of each hydrogel triplicate were imaged with a Nikon Eclipse Ti inverted microscope, and representative images are included in Figure 4.1. Cells spread more on stiffer materials (10-40 kPa), while cells on soft hydrogels (0.5-2 kPa) appeared small with long branches.

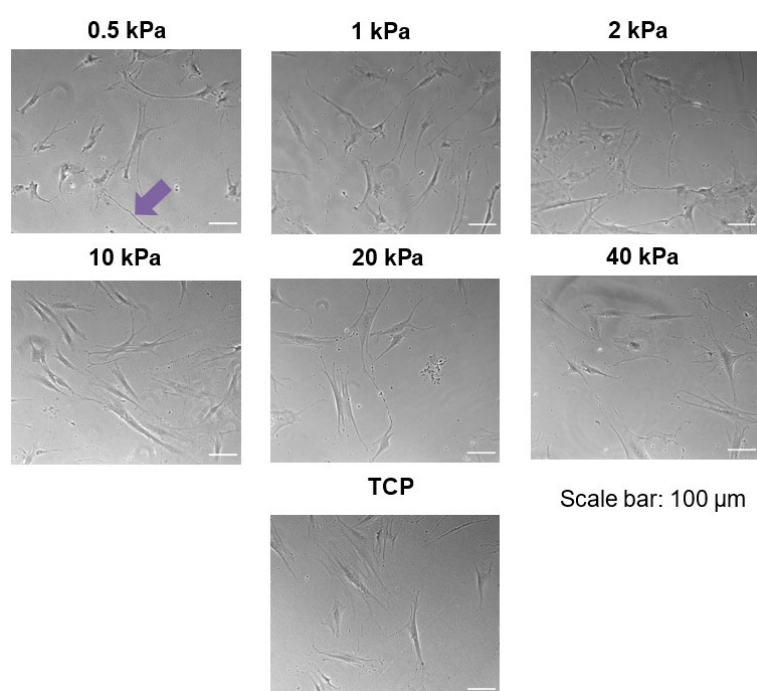


**Figure 4.1. Cell morphology of Stro-1<sup>+</sup> BMSCs on PAAm hydrogels with different elastic modulus.** The purple arrow illustrates a small cell with long branches on soft materials. 5 images per hydrogel triplicate at each elastic modulus were taken under a Nikon Eclipse Ti inverted microscope. The cell perimeter was drawn on the cells found in the 15 images per condition to quantify cell area.

The Fiji programme calculated the cell area after manually drawing around the cells (Refer to Section 2.2.5 in Chapter 2 for detailed methodology). All cells from 5 microscopic fields from each hydrogel triplicate ( $n=3$ ) at each stiffness (0.5, 1, 2, 10, 20 and 40 kPa) were quantified. The mean cell spreading area of cells on hydrogels at different elasticities increased on 0.5-2 kPa (0.5 kPa:  $5694 \pm 3212 \mu\text{m}^2$ ; 1 kPa:  $6963 \pm 4114 \mu\text{m}^2$ ; 2 kPa:  $7383 \pm 4454 \mu\text{m}^2$ ) hydrogels but remained constant on 10-40 kPa (10 kPa:  $8057 \pm 5357 \mu\text{m}^2$ ; 20 kPa:  $8837 \pm 5336 \mu\text{m}^2$ ; 40 kPa:  $8025 \pm 4459 \mu\text{m}^2$ ) PAAm hydrogels.

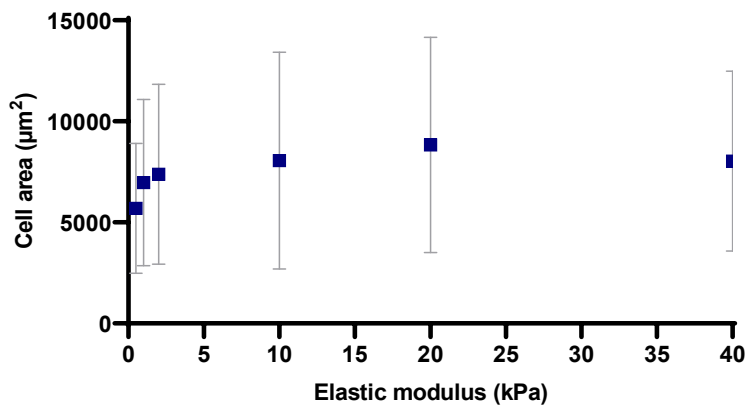


**Figure 4.2. The cell-spreading area of BMSCs increased with the hydrogel elastic modulus.** The mean cell spreading area increased on stiffer hydrogels, reaching a plateau on 10-40 kPa hydrogels. Cells from 5 microscopic fields of each hydrogel triplicate ( $n=3$ ) with different elastic moduli were imaged, and the cell area was quantified in FIJI after manually drawing the cell perimeter. 83 cells on 0.5 kPa, 84 cells on 1 kPa, 86 cells on 2 kPa, 85 cells on 10 kPa, 58 cells on 20 kPa and 51 cells on 40 kPa. Squares represent the mean single-cell spreading area, and the error bars show the standard deviation.

### 4.3.2 Effect of the increase in hydrogel elastic modulus on actin stress fibres

Actin stress fibres are essential structures in cell mechanosensing. For this reason, the second experiment aimed to identify any qualitative changes in these structures when increasing the hydrogel elastic modulus. Cells from the previous experiment were fixed with PFA, permeabilised with Triton, and stained with fluorescein-labelled phalloidin and DAPI for actin and nuclei staining. Figure 4.3 compares the morphology and actin fibres of Stro-1<sup>+</sup> BMSCs on PAAm substrates with different elasticities. It illustrates that the actin stress fibres of cells on the softest hydrogels (0.5 and 1 kPa) are condensed, while thin and defined fibres are presented on stiffer PAAm hydrogels (2-40 kPa and TCP).

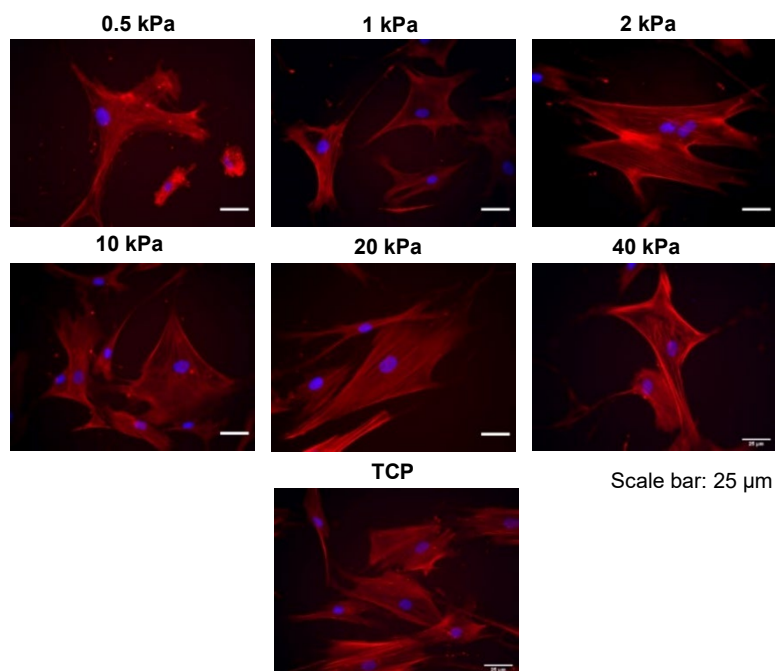


**Figure 4.3. Actin staining of Stro-1<sup>+</sup> BMSCs on PAAm hydrogels with different elasticities.** Clear actin stress fibres were seen on stiff materials, and nuclei did not show changes. BMSCs were fixed with PFA, stained with DAPI for nuclei and fluorescein phalloidin for actin and imaged under a Nikon Eclipse Ti inverted microscope.

### 4.3.3 Effect of hydrogel elastic modulus on focal adhesions

Besides the actin cytoskeleton, focal adhesions are crucial structures in cell mechanosensing. These structures transmit the mechanical information from the ECM to the cell. Various proteins, such as talin and vinculin, constitute them. Here, the changes in focal adhesions of BMSCs by increased hydrogel elasticity were evaluated through vinculin staining. BMSCs were plated at 1,000 cells/cm<sup>2</sup> and incubated for 7 days in  $\alpha$ -MEM media at 37°C. Immunocytochemistry was carried out for vinculin staining (refer to Section 2.2.6 in Chapter 2 for a detailed explanation) after fixing the cells with PFA and permeabilising with Triton. Later, actin and nuclei were visualised with fluorescein phalloidin and DAPI. Stro-1<sup>+</sup> BMSCs were imaged, and Figure 4.4 shows representative images showing the vinculin staining with Alexa Fluor 594 and the merged images showing nuclei, actin and vinculin staining on soft (0.5 and 1 kPa) and stiff (40 kPa) hydrogels. It denotes that the fluorescent intensity for vinculin is greater on the stiffest hydrogels (40 kPa). In contrast, cells on softer matrices are not equally stained, and the fluorescent intensity is lower than those on stiff matrices, suggesting FAs might be more stable when cells grow on stiff than on soft materials. No apparent differences in actin fibres of BMSCs were seen when modifying the hydrogel elastic modulus on these samples.

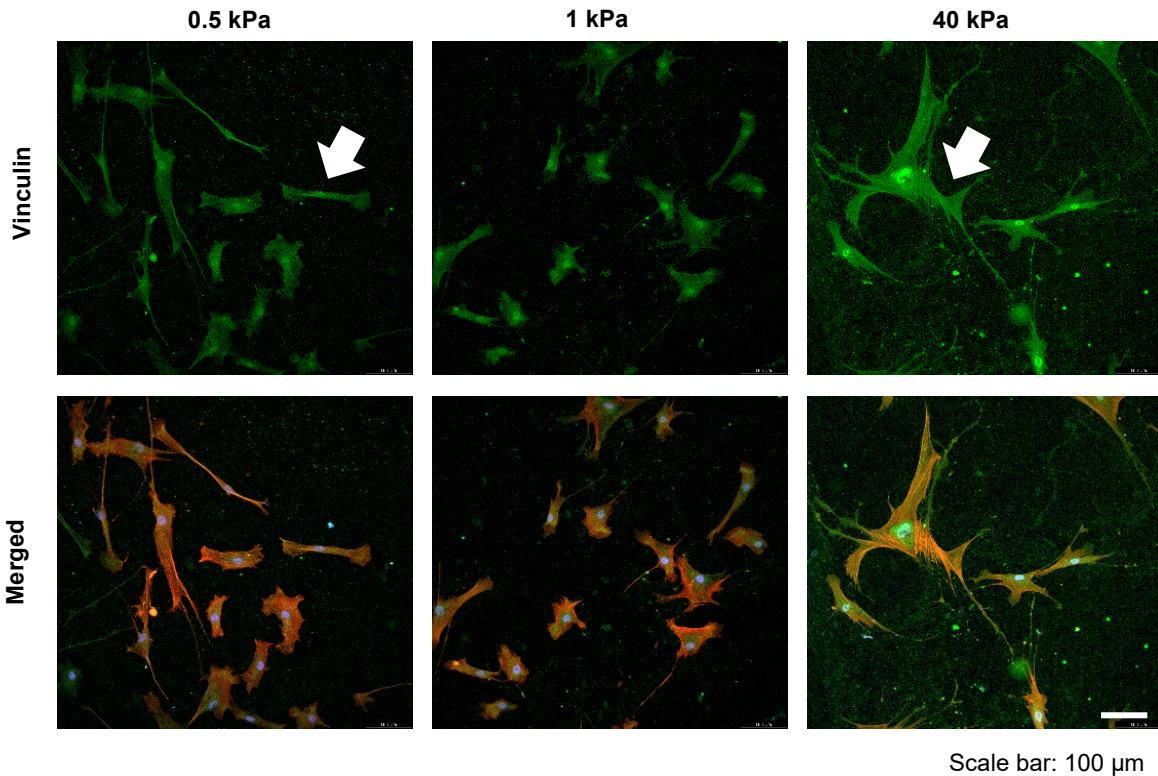


**Figure 4.4. Nuclei, actin, and vinculin staining of Stro-1<sup>+</sup> BMSCs on PAAm hydrogels with different stiffness.** Vinculin (green) staining with Alexa Fluor 594 and merged images showing nuclei (blue) with DAPI, actin (red) with fluorescein phalloidin, and vinculin (green) staining with Alexa Fluor 594. The intensity of the vinculin staining was greater on stiff materials compared to the soft counterparts (indicated with white arrows). No apparent differences in actin or nuclei were appreciated. Pictures of each hydrogel (n=3) were taken with a Leica confocal microscope SP8 by Dr David Johnston at the BIU, University of Southampton.

#### 4.3.4 Effect of seeding density on stiffness sensing

Cell crowding influences stiffness sensing in SSCs; therefore, the effect of the intrinsic elastic modulus on the single-cell spreading area of Stro-1<sup>+</sup> BMSCs at different seeding densities were evaluated, Stro-1<sup>+</sup> BMSCs cells were plated at three densities: 300, 500, and 1000 cells/cm<sup>2</sup> on PAAm hydrogels of different stiffness (0.5 kPa to 10 kPa) in  $\alpha$ -MEM complete media for 24h. Unlike Figure 4.1, where cells on 0.5 kPa hydrogels appear short with long branches, cells on the hydrogels with the same elastic modulus in Figure 4.5 are rounder than those on stiffer materials such as the 10 kPa hydrogels, which occupy a larger area. Round cells might have died due to the toxicity of the hydrogel batch. In addition, with higher seeding densities (500 and 1000 cells/cm<sup>2</sup>), cells formed colonies on stiffer hydrogels (5 and 10 kPa) while remaining isolated on softer matrices. The cell area of the cells was quantified in FIJI by manually drawing the cell perimeter and using the threshold tool.

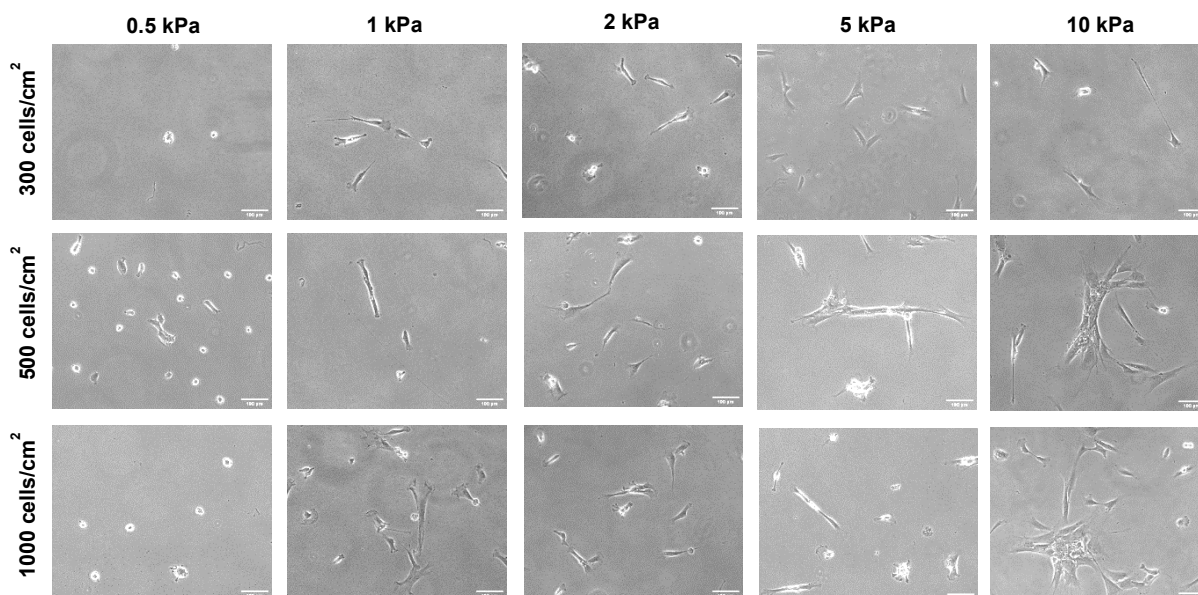


**Figure 4.5. Phase-contrast images of BMSCs plated at 300, 500 and 1000 cells/cm<sup>2</sup> on PAAm hydrogels of different stiffness after 24hrs of incubation.** Cells are round on 0.5 kPa hydrogels at all seeding densities, while a higher elastic modulus promotes spread morphologies. Cells from 5 microscopic fields of each hydrogel triplicate were imaged under a Nikon Eclipse Ti inverted microscope at 10X.

Results plotted in Figure 4.6 demonstrate increased cell area when the substrate elastic modulus increases. However, the single-cell spreading area was not different when varying seeding densities (300-1000 cells/cm<sup>2</sup>).

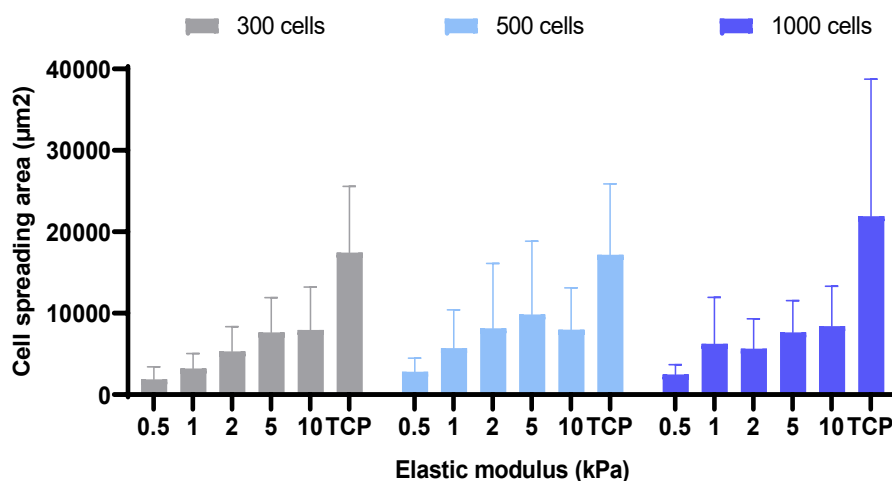


**Figure 4.6. The substrate elastic modulus increases the single-cell spreading of Stro-1<sup>+</sup> BMSCs regardless of cell seeding density.** The FIJI programme measured the cell-spreading area. The cell number varied with hydrogel's conditions and seeding density: 0.5 kPa: 9, 31 and 18 cells; 1 kPa: 12, 8 and 19 cells; 2 kPa: 16, 15 and 20 cells; 5 kPa: 11, 15 and 17 cells; 10 kPa: 10, 6 and 8 cells; TCP: 4, 4 and 3 cells (n=1).

After confirming that Stro-1<sup>+</sup> BMSCs sense changes in hydrogel elastic modulus, the following aim was to evaluate the capacity of these cells to perceive changes in hydrogel thickness on soft matrices.

### 4.3.5 Effect of substrate thickness on cell spreading

First, to evaluate the effect of hydrogel thickness on cell spreading area, 1,000 cells/cm<sup>2</sup> were plated on soft hydrogels (1 kPa) fabricated with different PAAm mixture volumes (5, 25, 50 and 100  $\mu$ L). Figure 4.7 illustrates that more cells are presented on the thinnest than thicker hydrogels. Cells on thin hydrogels showed different sizes, while short cells exhibited long filopodia on thick hydrogels. Pictures were used to quantify cell area and mean spreading area measurements slightly but not significantly decreased with the increase in hydrogel thickness; 5  $\mu$ L: 5920  $\pm$  3664  $\mu$ m; 25  $\mu$ L: 5611  $\pm$  3039  $\mu$ m; 50  $\mu$ L: 5215  $\pm$  2900  $\mu$ m; 100  $\mu$ L: 4829  $\pm$  3108  $\mu$ m (Figure 4.8).

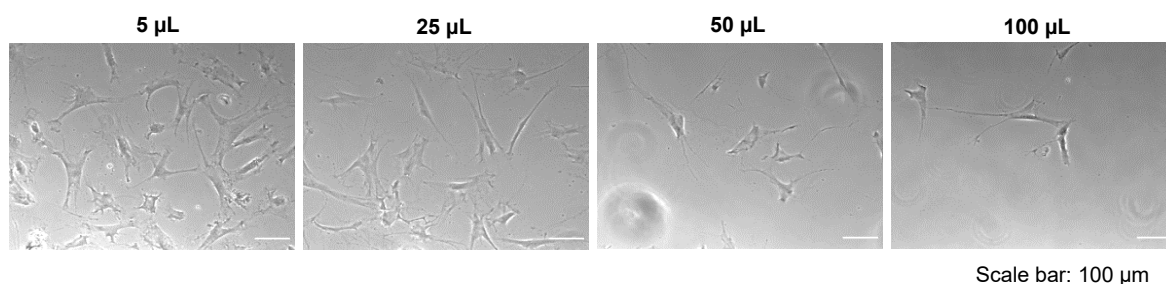


**Figure 4.7. Cell morphology of Stro-1<sup>+</sup> BMSCs on soft PAAm hydrogels with different thicknesses.** The number of cells attached decreased on thicker PAAm hydrogels. Cells with spreading morphologies and different sizes are seen on soft, thin (5  $\mu$ L) hydrogels, whereas shorter cells with long filopodia are seen on thick hydrogels (50 and 100  $\mu$ L). 5 images were obtained from each hydrogel triplicate at each thickness. 140 cells on 5  $\mu$ L hydrogels, 96 cells on 25  $\mu$ L hydrogels, 94 cells on 50  $\mu$ L hydrogels and 60 cells on 100  $\mu$ L hydrogels were imaged in the brightfield channel at 10X magnification with a Nikon Eclipse Ti inverted microscope.

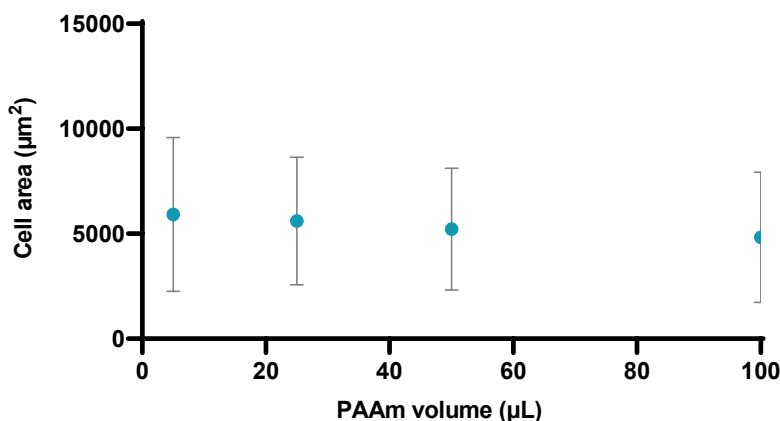


**Figure 4.8. Cell-spreading area of Stro-1<sup>+</sup> BMSCs slightly increased with the decrease in hydrogel thickness.** The cell area was quantified in FIJI after manually drawing the cell perimeter. The number of cells in hydrogels with different thicknesses varied: 5  $\mu$ L: 140 cells; 25  $\mu$ L: 96 cells; 50  $\mu$ L: 94 cells; 100  $\mu$ L: 60 cells. Dots and bars represent the mean and standard deviation of the spreading area of cells from 5 fields (n=3).

### 4.3.6 Effect of substrate thickness on actin fibres

The following experiment compared the actin cytoskeleton fibres of Stro-1<sup>+</sup> BMSCs on soft and stiff hydrogels with different thicknesses. First, cells were plated at 1,000 cells/cm<sup>2</sup> and incubated for 24 hours. Fixed and permeabilised cells were stained with DAPI and phalloidin

and imaged with a Nikon Eclipse Ti inverted microscope. Figure 4.9 shows that actin stress fibres of cells on soft PAAm hydrogels are not clearly distinguished but are defined on the soft, thinnest (5  $\mu\text{L}$ ) and stiff hydrogels regardless of thickness.

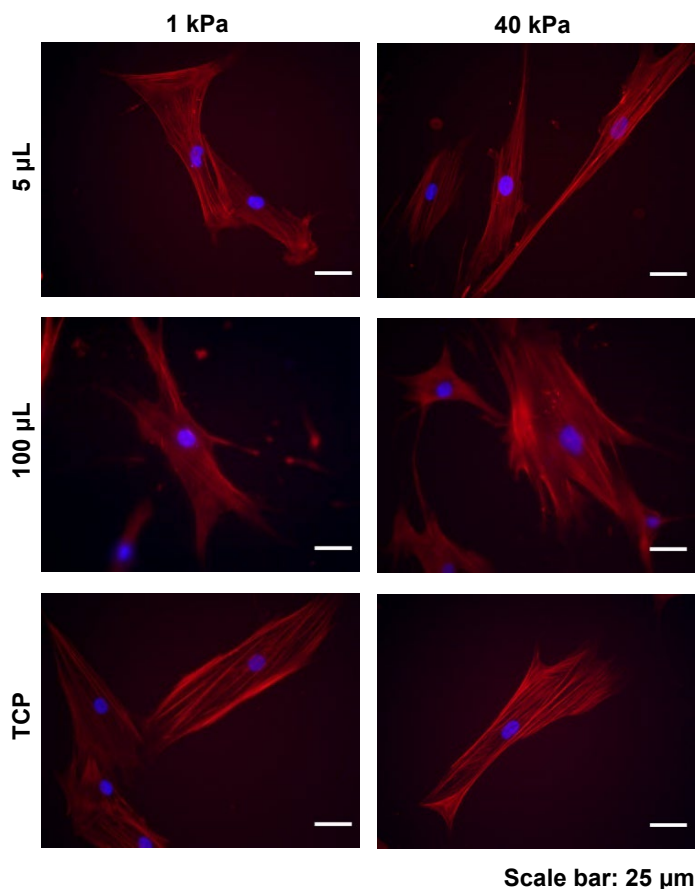


**Figure 4.9. Actin staining of Stro-1<sup>+</sup> BMSCs on soft and stiff PAAm hydrogels with different thicknesses.** Actin stress fibres of Stro-1<sup>+</sup> BMSCs on soft hydrogels are unclear, except on the thinnest hydrogels (5  $\mu\text{L}$ ). On stiff hydrogels, cells show clear actin stress fibres regardless of hydrogel thicknesses, like TCP.

#### 4.3.7 Effect of substrate thickness on focal adhesions

Changes in focal adhesions of Stro-1<sup>+</sup> BMSCs when modifying hydrogel thicknesses were also evaluated. Stro-1<sup>+</sup> BMSCs were incubated for 24 hours in  $\alpha$ -MEM media, and vinculin, actin, and nuclei were stained. Representative images in Figure 4.10 show no apparent differences in nuclei morphology and actin organisation in cells when varying hydrogel thicknesses. However, it was clear that the signal of Alexa Fluor 594 for vinculin staining was more evident in cells growing on soft, thin than on soft, thick hydrogels. This might suggest that focal adhesions are more stable on soft, thin gels than soft, thick hydrogels.

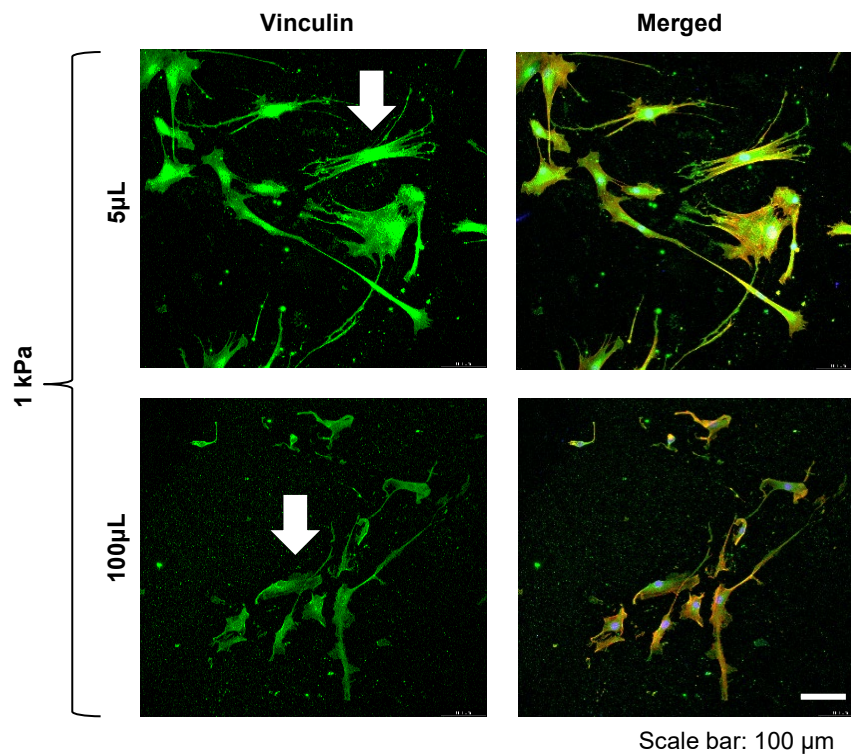


**Figure 4.10. Nuclei, actin, and vinculin staining of Stro-1<sup>+</sup> BMSCs on soft PAAM hydrogels with different thicknesses.** Vinculin (green) staining with Alexa Fluor 594 and merged images, including nuclei (blue), actin (red), and vinculin (green) staining. Cells exhibited greater vinculin staining intensity on thin hydrogels than on thick materials (indicated with white arrows). Three pictures of each hydrogel triplicate at each thickness were taken with a Leica confocal microscope SP8. by Dr David Johnston at the BIU, University of Southampton.

The differences in vinculin staining in cells growing on stiff PAAM hydrogels with different thicknesses are presented in Figure 4.11. More cells grew on stiff, thin hydrogels than on stiff, thick hydrogels, and actin fibres are similar when varying hydrogel thickness. Nevertheless, cell morphology differs as cells are spread on stiff, thin hydrogels and thin, thick hydrogels. Focal adhesions are also more evident on stiff, thin hydrogels than on thick hydrogels, suggesting they might be more stable on thin hydrogels.

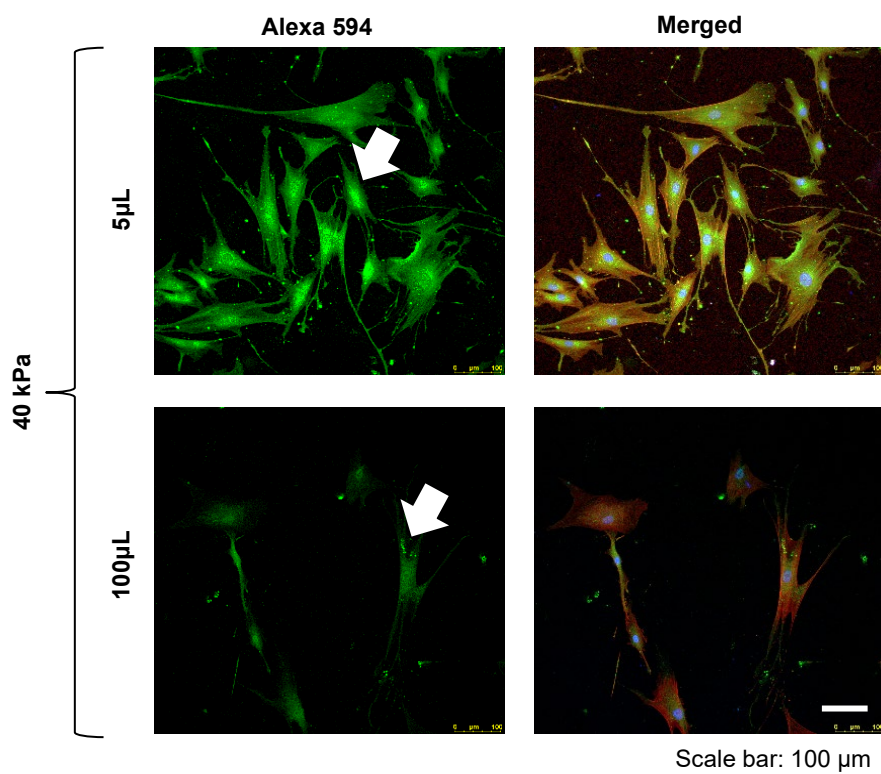


**Figure 4.11. Nuclei, actin, and vinculin staining of Stro-1<sup>+</sup> BMSCs on stiff PAAm hydrogels with different thicknesses.** Vinculin (green) staining with Alexa Fluor 594 and merged images showing nuclei (blue), actin (red), and vinculin (green) staining at each thickness (n=3). Higher intensity of vinculin staining was seen in cells on thin than thick hydrogels (indicated with white arrows). Three pictures of each hydrogel triplicate at each thickness were taken with a Leica confocal microscope SP8 by Dr David Johnston at the BIU, University of Southampton.

## 4.4 Discussion

AFM results in Chapter 3 showed that the elastic modulus increased on soft, thin hydrogels (Figure 3.7), and BMSCs are known to be mechanosensitive. Therefore, this chapter aimed to test if BMSCs sense the changes in substrate elastic modulus and thickness and respond by modifying their cell spreading area, FAs signal intensity and actin stress fibre arrangements.

The main findings in this chapter were:

- Cells perceive the changes in substrate elastic modulus by slightly modifying their spreading area (regardless of the cell density), showing more stable focal adhesions and defined actin fibres on stiffer materials.
- Cells detect changes in hydrogel thickness by slightly modifying their spreading area, acquiring different morphologies and the intensity of FAs and actin stress fibre depending on hydrogel thickness.

These findings suggest that hydrogel elasticity and thickness also influence BMSCs differentiation, which is outstanding in tissue regeneration as cells must adapt appropriately to the microenvironment and differentiate into the required specific cell type.

Evaluating cell spreading is vital because it is the first point of contact between cells and the substrate (Li *et al.*, 2014). The results in this Chapter demonstrated that the BMSCs spreading area was slightly smaller on 1 kPa hydrogels ( $6963 \pm 4114 \mu\text{m}^2$ ) than on 40 kPa ( $8025 \pm 4460 \mu\text{m}^2$ ) (Figure 4.2); this indicates that BMSCs can sense changes in the substrate's elastic modulus. Sun *et al.*, 2018 reported that BMSCs morphology and spreading depend on substrate stiffness. Tusan *et al.*, 2018 confirmed that MG63 cells increased their size on stiff PAAm hydrogels while remaining round on soft counterparts. The relation between substrates' stiffness and cell spreading area has been widely described; cells on soft materials create small forces and slight tension within the cytoskeleton, appearing small. In contrast, cells on stiff materials generate higher forces that promote the formation of rigid, stiff, and contractile stress fibres, which promote cell spreading (Leong *et al.*, 2010). This also correlates with the results of the third experiment, where BMSCs exhibited clear and defined actin stress fibres on hydrogels with high elastic modulus. In contrast, undefined fibres were seen on soft hydrogels (Figure 4.3).

In addition to the actin stress fibres, FAs are crucial in cell mechanosensing. According to section 4.3.3, vinculin was mainly localised near the nucleus on the softest hydrogels, close to the nuclei and cell ends on 1 kPa hydrogels, near the nuclei and throughout the cells on stiff PAAm hydrogels. This correlates with Zhou *et al.* 2017 findings suggesting that the localisation of FAs depends on the substrate's stiffness and that vinculin occupied a greater

area on stiff PDMS substrates than soft PDMS samples. This chapter also showed that the intensity of vinculin staining increases on hydrogels with a high elastic modulus (Figure 4.4), suggesting more stable focal adhesions forming on stiff than soft matrices. This agrees with Zhou *et al.*, 2019, highlighting the higher intensity of vinculin in chondrocytes on stiff PDMS compared to soft counterparts. Quantitative data would have been valuable in obtaining more information about substrate elasticity and FAs. For example, Fusco *et al.*, 2017 quantified the FA length on PDMS substrates, reporting more significant FAs areas and longer lifetimes on stiff substrates.

Although the cell spreading area of BMSCs was similar between soft and stiff PAAm hydrogels, cell morphology differed when varying hydrogel elasticities. Spread cells with different appearances were observed on 40k kPa hydrogels, and thin cells with noticeable long extensions were seen on 1 kPa, as reported by Engler *et al.*, 2006. In contrast, plenty of short cells with branches of different lengths were observed on 0.5 kPa hydrogels (Figure 4.1). Evaluating changes in cell morphology is crucial as it dictates cell shape, which modifies the activity of Rho family GTPases via a RhoA-ROCK pathway through changes in the internal cytoskeletal tension. This influences cell migration, apoptosis, proliferation and, most importantly, differentiation (Tee *et al.*, 2011, Mao *et al.*, 2016; Bao *et al.*, 2019). Indeed, McBeath *et al.*, 2004 found that hMSCs decreased ALPL activity and increased lipid production when exposed to an inhibitor of ROCK (Y-27632) against myosin-generated cytoskeletal tension. These results suggest that cell-shape-mediated commitment involves actomyosin contractility (McBeath *et al.*, 2004).

Besides the increase in the acrylamide/bisacrylamide ratio, the forces generated by the surrounding cells can also influence cell spreading. Then, evaluating the effect of cell crowding on BMSCs cell spreading might influence how cells perceive the hydrogel's mechanical properties and behaviour. The results showed that cells perceived the rise in hydrogel elastic modulus and increased their spreading area in response, regardless of the seeding density (Figure 4.6). Despite Venugopal *et al.*, 2018 reported an increase in the apparent stiffness by the rise in seeding density due to cellular traction; it may be possible that in the experiment presented here, cells were far enough away not to perceive each other and continued distinguishing the actual substrate stiffness (Figure 4.5).

Cells form stable focal adhesions that bind integrins to the actin cytoskeleton on more rigid substrates, promoting its polymerisation at the membrane periphery and forming an organised cytoskeleton. This might explain the changes in cell morphology (Figure 4.1) and the increase in cell spreading (Figure 4.2) found in this chapter. In contrast, cells on soft substrates can deform the matrix, form less defined fibres and appear rounder (Wells, 2008; Li *et al.*, 2014).

After evaluating the effect of the increase in hydrogel elastic modulus, the influence of hydrogel thickness on cell spreading, FAs and actin stress fibres were also considered. SSCs plated on soft polyacrylamide surfaces that generally do not promote cell spreading increase their area on thin hydrogels (Evans-Gentleman, 2014; Mullen *et al.*, 2015). For instance, Buxboim *et al.*, 2010 stated that SSCs are mechanosensitive as spreading and changes in substrate thickness influence the actin cytoskeleton. Similarly, Leong *et al.*, 2010 found that BMSCs can spread more and differentiate into osteoblasts on thin collagen hydrogels (130  $\mu\text{m}$ ) but could not sense and express osteogenic markers on thick hydrogels (1140  $\mu\text{m}$ ). A decrease of 1.5-fold in cell area on thick (1400  $\mu\text{m}$ ) hydrogels was also reported by Leong *et al.*, 2010. The results in Section 4.3.5 revealed that BMSCs exhibited a greater cell area on soft, thin ( $4842 \pm 3039 \mu\text{m}^2$ ) than on soft, thick hydrogels ( $1783 \pm 1265 \mu\text{m}^2$ ) and with no significant difference between stiff, thin ( $4913 \pm 3213 \mu\text{m}^2$ ) and stiff, thick ( $3233 \pm 1564 \mu\text{m}^2$ ) hydrogels. These changes highlighted that the cell senses changes in hydrogel thickness.

The small changes in cell spreading area with the change in hydrogel thickness (Figure 4.8) might be explained as the cells might only be able to sense the underlying support on the thinnest hydrogel. Plenty of spread cells with different sizes were appreciated on the soft 5  $\mu\text{L}$  hydrogels ( $\sim 54 \mu\text{m}$ ), cell numbers slightly decreased, and spread cells appeared with similar sizes on 25  $\mu\text{L}$  gels ( $\sim 251 \mu\text{m}$ ). In contrast, the cell number dramatically decreased at 50  $\mu\text{L}$  ( $\sim 597 \mu\text{m}$ ) and 100  $\mu\text{L}$  ( $\sim 782 \mu\text{m}$ ), where short cells with long filopodia were observed (Figure 4.7). These results suggest that hydrogel's thickness modifies BMSCs behaviour. Only a few studies have evaluated the spreading and morphology of cells on soft PAAm hydrogels with different thicknesses; for example, Buxboim *et al.*, 2010 (SSCs) and Tusan *et al.*, 2018 (osteosarcoma cells) showed round cells on soft hydrogels while elongated cells were observed on stiff matrices.

Variations in actin fibres of BMSCs when varying hydrogel thicknesses were also evaluated (Figure 4.9). Cells on high elastic modulus hydrogels exhibited clear actin stress fibres regardless of hydrogel thickness. Nevertheless, actin fibres in BMSCs on soft hydrogels appeared condensed on soft, thick hydrogels, while cells presented clear stress fibres on the thinnest hydrogels. Similarly, Leong *et al.*, 2010 stated that SSCs presented thick groups of aligned microfilaments on plastic, thin microfilaments on thin hydrogels and much thinner bundles on soft, thick collagen hydrogels. Implying that changes in the hydrogel elasticity might lead to changes in the actin cytoskeleton, morphology consequently, and potentially cell differentiation.

As previously mentioned, focal adhesions are crucial in cell mechanosensing, so these structures' changes were evaluated when modifying hydrogel thickness. Unlike the small changes in FAs of BMSCs when modifying hydrogel stiffness, thickness variations changed

FAs' signal intensity. Cells on soft, thin hydrogels showed an evident increase in vinculin signal throughout the cells but not on thicker hydrogels (Figure 4.10). Changes were also observed on stiff, thin hydrogels where BMSCs exhibited high fluorescent signal intensity in the central area of the cells but not on stiff, thick hydrogels (Figure 4.10). This finding is remarkable and contradicts Lin *et al.* 2010 reports, where hydrogel thickness did not affect focal adhesions of fibroblasts.

To sum up, hydrogel elastic modulus and mainly thickness influenced cell spreading, focal adhesion's location and actin fibres appearance, which may influence BMSCs differentiation.



## **Chapter 5 Bone marrow stromal cells differentiation**

## 5.1 Introduction

ECM mechanics (elastic modulus, geometry, and topography) have been reported to influence focal adhesion formation, cell shape, spreading, proliferation, migration, and differentiation (Engler *et al.*, 2006; Evans-Gentleman, 2014; Bao *et al.*, 2019). Hence, mimicking the ECM mechanical properties of the tissue of interest when designing biomaterials is a promising strategy to promote tissue regeneration.

SSCs are an essential source of stem and progenitor cells with multipotency. They quickly adapt and migrate into injured tissues, differentiate into the required cells, and secrete chemokines, cytokines, growth factors, vesicles, and ECM crucial in tissue repair and regeneration (Fu *et al.*, 2019; Novoseletskaya *et al.*, 2020). SSCs are also crucial in bone formation and remodelling; osteoblasts come from SSCs and promote bone resorption through osteoclasts activation (Yen *et al.*, 2020). SSCs isolated from the bone marrow (BMSCs) are frequently used for bone repair.

BMSCs are heterogeneous cell populations that intrinsically contain stem cells, and the Stro-1 antigen is one of the most recognised markers for their selection. Depending on the tissue source, it has different expression levels and is present in less than 10% of BMSCs. Stro-1<sup>+</sup> BMSCs are multipotent stem cells with *in vivo* quiescence, undifferentiated phenotype, and high multipotency that easily migrate and engraft in different tissues, support haematopoiesis, proliferation, and angiogenesis (Feng *et al.*, 2013; Fitter *et al.*, 2017).

The results in the previous chapter demonstrated that Stro-1<sup>+</sup> BMSCs sense and respond to changes in hydrogel stiffness and thickness; thus, this chapter aims to evaluate their effect on Stro-1<sup>+</sup> BMSCs differentiation.

The relation between ECM stiffness and stem cell differentiation has been widely studied. Changes in the ECM elastic modulus promote stem cell differentiation into specific tissue lines when ECM reaches the stiffness of the native tissues (Leong *et al.*, 2010). For instance, SSCs differentiate into adipocytes or neurons on soft substrates (~0.5-1 kPa) and osteoblasts on stiff matrices (~25-40 kPa) (Liu *et al.*, 2019; Sun *et al.*, 2018; Bao *et al.*, 2019).

Besides the biochemical cues and the substrate elasticity, cell seeding density regulates SSCs lineage commitment and proliferation (Xue *et al.*, 2013). Mullen *et al.*, 2013 reported that low seeding densities promote the osteogenic differentiation of SSCs and matrix mineralisation, whereas high seeding densities lead to adipogenic differentiation. In contrast, Ye *et al.*, 2015 found that adipogenic and osteogenic differentiation was promoted on stiff substrates at high seeding densities. Interestingly, Xue *et al.*, 2013 stated that the

expression of the osteogenic genes *ALPL*, *COL1A1* and *RUNX2* was higher on stiff compared to soft substrates at a low seeding density. However, there was no significant difference in the expression of osteogenic genes on soft and stiff PAAm hydrogels at high seeding density. They also highlighted that cell proliferation is influenced by cell density; at high seeding densities (20,000 cells/cm<sup>2</sup>), SSCs increased the percentages in the G0/G1 phases on soft and stiff compared to cells plated at low seeding density.

Cells *in vivo* continuously interact with others at different tissue levels, and mechanosensing is outstanding for maintaining their functionality. Varying the substrate thickness has been suggested as a strategy for varying the local stiffness of the cell microenvironment. As mentioned in previous chapters, cells perceive soft, thin hydrogels as stiffer than soft, thick matrices due to the proximity of the underlying support. In contrast, the forces cannot propagate across thick materials, and cells perceive the substrate stiffness. Indeed, SSCs on 0.5 mm PAAm hydrogels spread as cells plated on 34 kPa hydrogels, whereas SSCs on 2 mm hydrogels exhibit similar behaviour to cells plated on 1 kPa hydrogels (Naqvi and McNamara, 2020). In this way, the grade of deformations relies on the substrate's mechanical properties, making thin materials more difficult to deform than thick counterparts.

The increase in matrix stiffness leads to osteogenic differentiation and the consequent increase in expression of the genes encoding different transcription factors, such as *RUNX2*, *SP7*, Smad proteins, and  $\beta$ catenin. Initially, cells proliferate, TGF- $\beta$ 1, fibronectin, collagen and osteopontin expression increase. Later, cells differentiate and the expression of both *ALPL* and collagen increases, followed by ECM mineralisation and osteocalcin expression. In contrast, soft matrices promote SSCs adipogenic differentiation with the consequent increase of PPAR $\gamma$  and C/EBP $\alpha$  (El-Rashidy *et al.*, 2021).

*ALPL* is an early osteogenic marker expressed during calcification; *RUNX2* is a transcription factor highly related to osteoblasts differentiation and upregulated after three days; osteocalcin (OCN) is a bone protein secreted by osteoblasts, which increases on day 30, and OPN is a glycoprotein found in the bone ECM (Yen *et al.* 2020).

Engler *et al.*, 2006 reported that stiff substrates promote SSCs' osteogenic differentiation, whereas soft materials lead to adipogenic differentiation. This chapter first aims to confirm the multipotent capacity of the BMSCs to differentiate into osteoblasts and adipocytes on TCP and PAAm hydrogels with different elastic moduli. The substrate thickness was also modified to test if soft, thin hydrogels would promote osteogenic differentiation due to increased apparent stiffness. Cell fate was evaluated by quantifying ALPL activity and oil red O accumulation. Additionally, *ALPL* and *RUNX2* expression was quantified to assess the expression of osteogenic genes in cells growing on soft and stiff hydrogels with different thicknesses.

## 5.2 Aims

- To test if the modulation in substrate elastic modulus alters BMSCs' osteogenic and adipogenic differentiation by assessing ALPL activity, *ALPL* and *RUNX2* expression and lipid accumulation.
- To test if the decrease in substrate thickness increases the expression of the osteogenic markers *ALPL* and *RUNX2*.

### 5.3 Results

#### 5.3.1 Effect of substrate stiffness on BMSCs osteogenic differentiation

Results in the previous chapter confirmed that changes in substrate mechanical properties modify cell morphology, cell spreading area, actin fibres and FAs, intimately related to different cellular processes such as stem cell differentiation. This chapter aimed to determine the effect of substrate elasticity and thickness on Stro-1<sup>+</sup> BMSCs differentiation.

Firstly, unselected BMSCs (M53) were plated at 10,000 cells/cm<sup>2</sup> on TCP and incubated for 7 days in basal and osteogenic medium at 37°C. After incubation, cells were stained with fast violet (Sigma-Aldrich) to detect ALPL activity. Figure 5.1 shows qualitatively that the ALPL activity of BMSCs increased under osteogenic conditions on TCP.

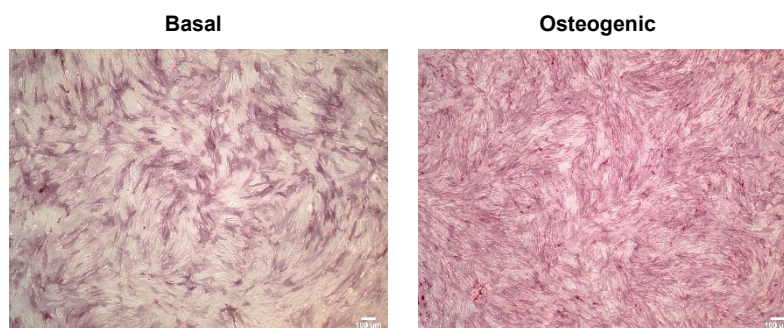


**Figure 5.1. ALPL activity of unselected BMSCs increases under osteogenic conditions on TCP.** BMSCs (M53) appear denser in the presence of osteogenic supplements. Cells were plated on TCP, incubated in basal and osteogenic medium at 37°C for 7 days, and fixed and stained with fast violet. Cells were imaged with an Olympus microscope at 5X.

Next, Stro-1<sup>+</sup> BMSCs previously isolated in the research group were grown at 10,000 cells/cm<sup>2</sup> on TCP in basal and osteogenic medium for 7 days and stained for ALPL with fast violet. Figure 5.2 (left) illustrates that Stro-1<sup>+</sup> BMSCs from 2 different clinical samples displayed higher ALPL activity in osteogenic than in the basal medium on TCP. The stained cell area from 5 microscopic fields on each hydrogel triplicate was quantified using the FIJI programme (see Section 2.2.7.1 in Chapter 2 for a detailed explanation). The results were plotted and represented in Figure 5.2 (right). ALPL was significantly higher in osteogenic medium than in basal medium, which means that Stro-1<sup>+</sup> BMSCs can differentiate into osteoblasts on TCP.

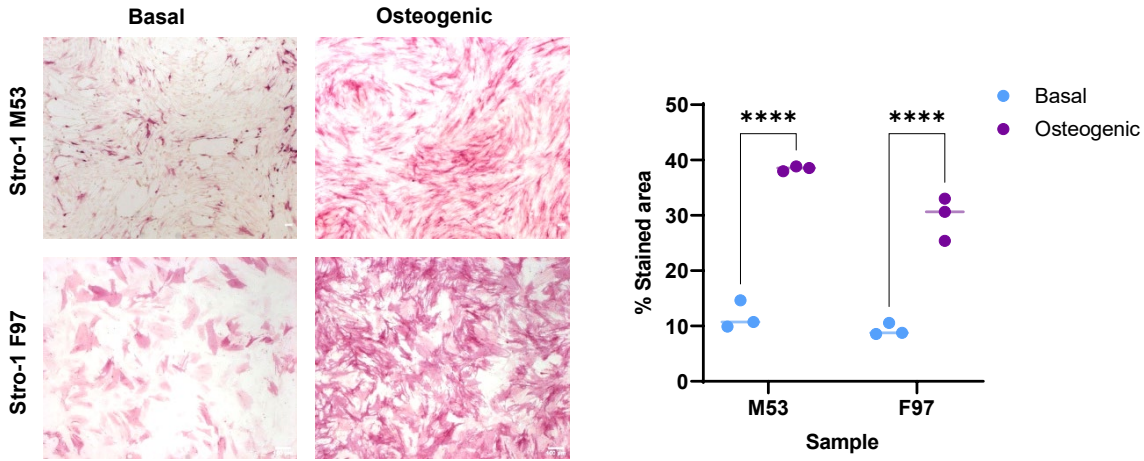


**Figure 5.2. Stro-1<sup>+</sup> BMSCs differentiate into osteoblasts on TCP.** (Left) ALPL staining of selected Stro-1<sup>+</sup> BMSCs from 2 patients (M53 and F97) on TCP in basal and osteogenic medium. (Right) The percentage of stained area in Stro-1<sup>+</sup> BMSCs significantly increased under osteogenic conditions (M53: 11.8 ± 2.5 μm<sup>2</sup> vs 38.5 ± 0.4 μm<sup>2</sup>, \*\*\*\*p<0.0001; M53: F97: 9.2 ± 1.1 μm<sup>2</sup> vs 29.7 ± 3.9 μm<sup>2</sup>, \*\*\*\*p<0.0001). Dots represent the mean stained area of the individual repeats, and lines are the standard deviation of the independent repeats. Data were analysed using the 2-way ANOVA method after imaging (n=3).

In the following experiment, ALPL activity and DNA concentration were quantified in Stro-1<sup>+</sup> BMSCs (M53) suspensions of cells growing for 7 days on TCP using a spectrophotometric (see Section 2.2.7.2.1) and fluorometric (see Section 2.2.7.3) method. Figure 5.3 shows that ALPL activity and DNA concentration increases when osteogenic supplements are added to the selected population's medium.

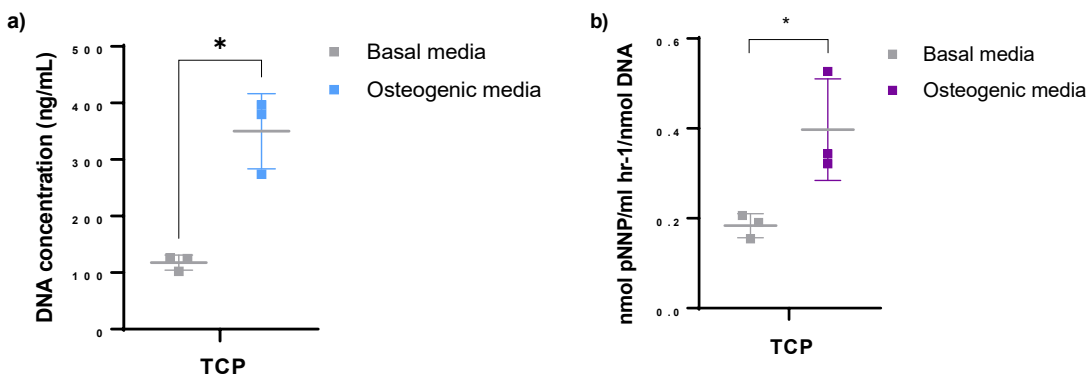


**Figure 5.3. ALPL activity and DNA of selected BMSCs (M53) increase under osteogenic conditions.** Absorbance and fluorescent measurements were obtained and interpolated to calculate the corresponding DNA concentration (a) and ALPL activity (b) DNA concentration analysed by a paired t-test (n=3): 117.8 ± 13.2 ng/mL vs 350.095 ± 66.5 ng/mL, \*p<0.05. Normalised ALPL activity data were analysed by a paired t-test (n=3): 0.184 ± 0.02 nmol pNMP/ml hr-1/nmol DNA vs 0.40 ± 0.11 nmol pNMP/ml hr-1/nmol DNA.

Once it was confirmed that Stro-1<sup>+</sup> BMSCs differentiated into osteoblasts on TCP, the following aim was to evaluate the ALPL activity and DNA concentration of Stro-1<sup>+</sup> BMSCs on soft (1 kPa) and stiff (40 kPa) PAAm hydrogels.

Cells from sample F97 were plated at 10,000 cells/cm<sup>2</sup> on collagen-coated PAAm hydrogels and TCP under basal and osteogenic conditions, and DNA concentration and ALPL activity were quantified on day 7. Figure 5.4 compares the morphology of Stro-1<sup>+</sup> BMSCs on 1, 40 kPa PAAm hydrogels and TCP in basal and osteogenic  $\alpha$ -MEM medium on day 1 and day 7. On day 1, cells on 40 kPa hydrogels and TCP in basal medium appeared elongated, whereas cell morphology varied on 1 kPa hydrogels and cell crowding increased in osteogenic media. On day 7, cell crowding increased, especially in the osteogenic medium. Thin cells randomly allocated were observed on TCP; 40 kPa hydrogels hold fewer and thicker cells, while cells with irregular morphologies were seen on soft hydrogels.

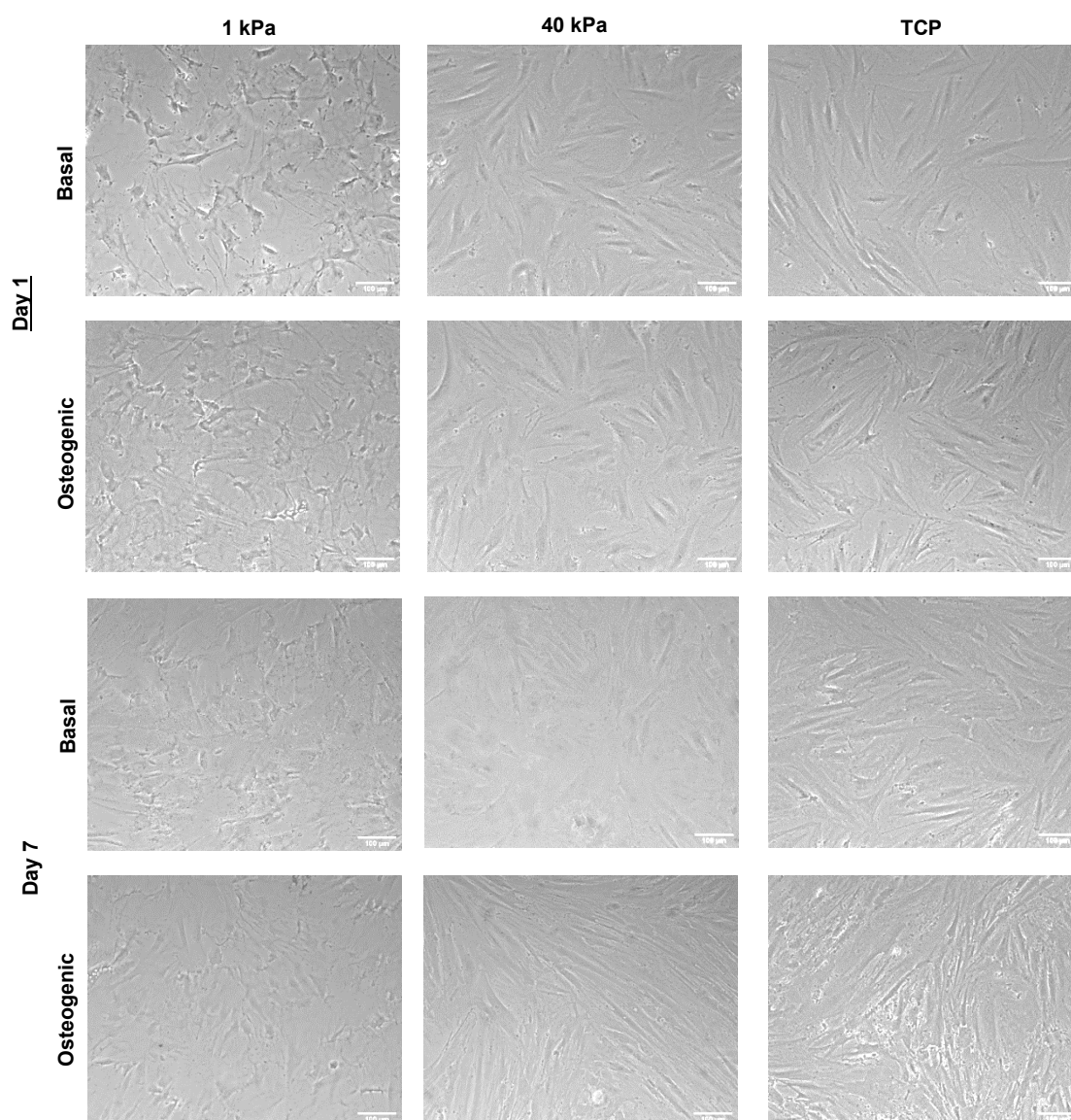


**Figure 5.4. Stro-1<sup>+</sup> BMSCs (F97) on 1, 40 PAAm hydrogels and TCP.** Cells showed a defined morphology on TCP and 40 kPa hydrogels, while cell morphology was irregular on 1 kPa hydrogels, where osteogenic supplements increased cell crowding on day 1. At the end of the incubation period, cells appeared thinner on TCP in osteogenic medium than in basal medium. Elongated cells were seen on 40 kPa hydrogels, while irregular cells were seen on 1 kPa hydrogels. Stro-1<sup>+</sup> BMSCs were imaged using a Nikon Eclipse Ti microscope (n=3) at 10X after incubating for 7 days.

After evaluating Stro-1<sup>+</sup> cell morphology on PAAm hydrogels in basal and osteogenic medium, cell suspensions were obtained to quantify DNA concentration and ALPL activity in the following experiment. Figure 5.5 (a) shows similar DNA concentrations in cells on soft and stiff PAAm hydrogels regardless of the presence of osteogenic supplements but increased on TCP under osteogenic conditions. Figure 5.5 (b) denotes that ALPL activity remained similar, disregarding the substrate's elasticity or media conditions.

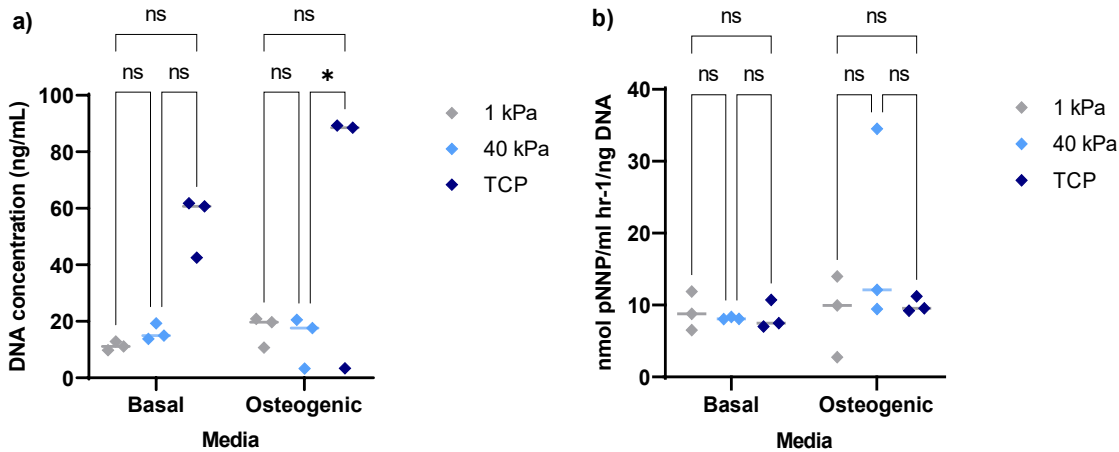


**Figure 5.5. Stro-1<sup>+</sup> BMSCs (F97) differentiation was similar on soft and stiff matrices in basal and osteogenic conditions.** (a) DNA concentration in cells on hydrogels with different elasticities was not significantly different regardless of media conditions ( $ns = p > 0.05$ ; Basal:  $11.3 \pm 1.5$  ng/mL (1 kPa) vs  $16.0 \pm 2.9$  ng/mL (40 kPa), osteogenic:  $17.1 \pm 5.5$  ng/mL (1 kPa) vs  $13.8 \pm 9.2$  ng/mL (40 kPa)) but significantly increased on TCP in osteogenic medium ( $55 \pm 10.8$  ng/mL (basal) vs  $60.4 \pm 49.3$  ng/mL (osteogenic)). (b) ALPL activity of BMSCs on hydrogels and TCP did not exhibit any significant difference in basal and osteogenic medium ( $ns = p > 0.05$ ; Basal:  $9 \pm 2.7$  nmol pNPP/ml hr-1/ng DNA (1 kPa) vs  $8.2 \pm 0.2$  nmol pNPP/ml hr-1/ng DNA (40 kPa); Osteogenic:  $8.9 \pm 5.7$  nmol pNPP/ml hr-1/ng DNA (1 kPa) vs  $18.7 \pm 13.8$  nmol pNPP/ml hr-1/ng DNA (40 kPa)). Diamonds represent the mean and SD of DNA concentration, ALPL activity, and data analysed by the 2-way ANOVA method ( $n=3$ ).

Because there was no increase in ALPL activity in osteogenic on TCP compared to basal media, the experiment was repeated by increasing the seeding density to 13,000 cells/cm<sup>2</sup> and using a different sample (M53). DNA concentration and ALPL activity were quantified using a fluorescent and colourimetric method on day 7. The graph in Figure 5.6 (a) shows small but not significantly higher DNA concentrations in Stro-1<sup>+</sup> BMSCs in osteogenic compared to basal medium in all substrates but no significant differences between soft and stiff PAAm hydrogels regardless of the medium conditions. Figure 5.6 (b) showed zero ALPL activity on PAAm hydrogels but moderate ALPL activity on TCP in basal conditions. ALPL activity was raised in osteogenic media on hydrogels but was significantly higher on TCP without any significant difference. Previous reports stated that osteogenic differentiation is enhanced on stiff materials but not soft matrices. This suggests that cells differentiate into osteoblasts regardless of substrate stiffness.

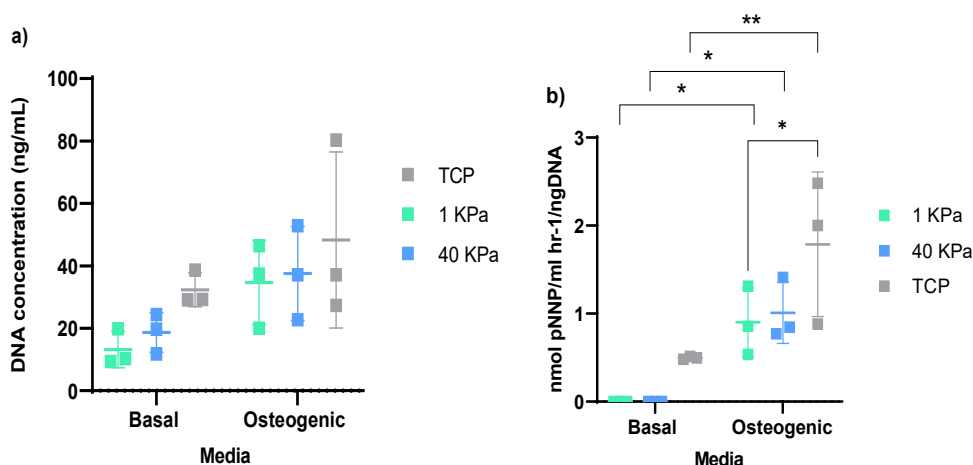
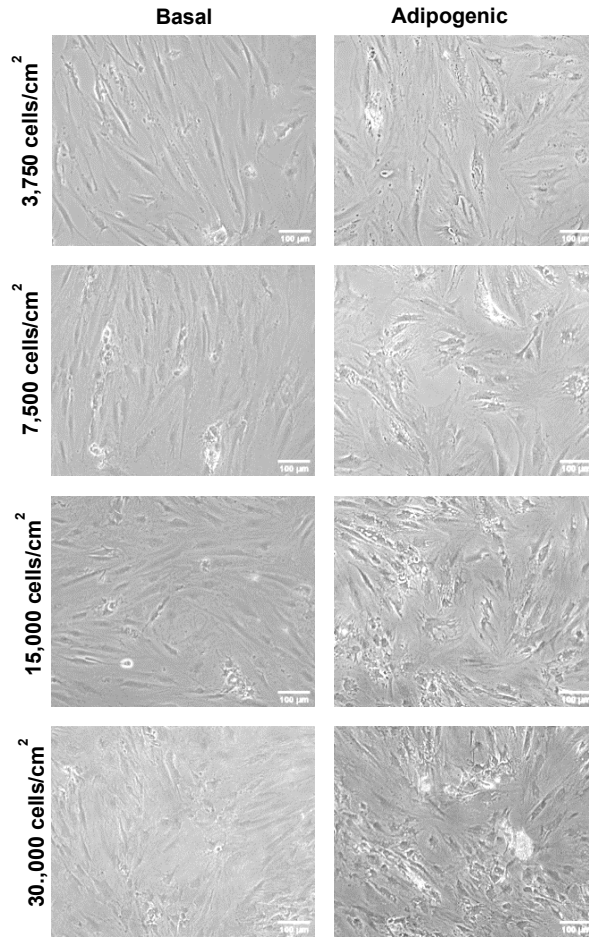


**Figure 5.6. Stro-1<sup>+</sup> BMSCs (M53) equally differentiate on soft and stiff matrices.** (a) No significant difference ( $ns = p > 0.05$ ) was detected in DNA concentration of Stro-1<sup>+</sup> BMSCs between soft and stiff hydrogels regardless of medium conditions (Basal:  $13.17 \pm 5.8$  ng/mL (1 kPa) vs  $18.7 \pm 6.4$  ng/mL (40 kPa), Osteogenic:  $34.6 \pm 13.5$  ng/mL (1 kPa) vs  $37.6 \pm 15.0$  ng/mL (40 kPa)) but increased on TCP in osteogenic medium  $32.3 \pm 5.4$  ng/mL (basal) vs  $48.3 \pm 28.3.4$  ng/mL (osteogenic). (b) ALPL activity of BMSCs remains zero on hydrogels in basal medium but significantly increased in osteogenic medium (1kPa:  $0.901 \pm 0.4$  ng/mL; 40 kPa:  $1.01 \pm 0.3$  ng/mL, TCP:  $1.787 \pm 0.8$  ng/mL;  $p < 0.05$ ) but no significant difference was identified between gels with different elasticity ( $ns = p > 0.05$ ;  $0.9 \pm 0.4$  nmol pNNP/ml hr-1/ng DNA (1 kPa) vs  $1.01 \pm 0.3$  nmol pNNP/ml hr-1/ng DNA (40 kPa)). Squares represent the mean and SD of DNA concentration and ALPL activity, and a significant difference was obtained by the two-way ANOVA method ( $n=3$ ).

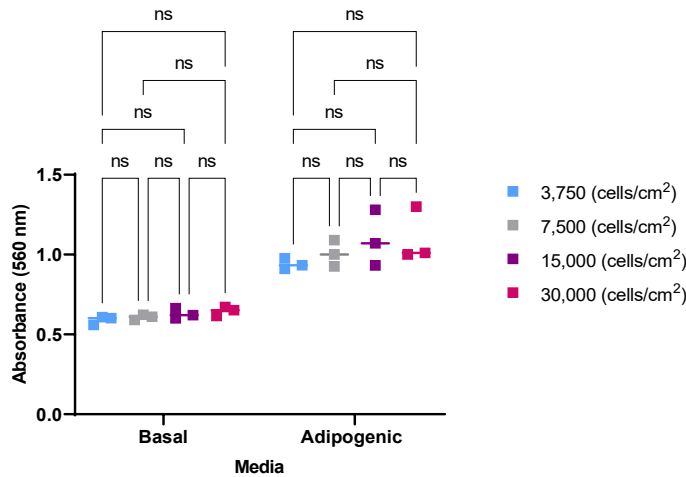
### 5.3.2 Effect of substrate stiffness on BMSCs adipogenic differentiation

Their self-renewal, clonality and potency characterise stem cells. Thus, the following experiment aimed to evaluate the adipogenic differentiation potential of Stro-1<sup>+</sup> BMSCs (M53) on TCP. Firstly, cells were plated at 3,750, 7,500, 15,000 and 30,000 cells/cm<sup>2</sup> in  $\alpha$ -MEM medium (basal and adipogenic) on TCP at 37°C for 14 days (refer to Section 2.2.8.1 in Chapter 2 for detailed methodology). Figure 5.7 illustrates that BMSCs acquired an elongated morphology in the basal medium at all seeding densities, with an evident increase in cell crowding when increasing seeding density. Cell density increased with seeding density in adipogenic medium but was reduced compared to the corresponding basal counterparts at each seeding density. Lipid accumulation was seen on cells at the highest seeding density (30,000 cells/cm<sup>2</sup>) on day 7.

Cells were stained with red oil O, and the absorbance was quantified at 560 nm after releasing the dye from the cells with isopropanol (refer to Section 2.2.8.1 in Chapter 2 for a complete description). Figure 5.8 denotes that BMSCs retained and released more red oil O under adipogenic conditions. BMSCs differentiated into adipocytes on TCP regardless of the seeding density.

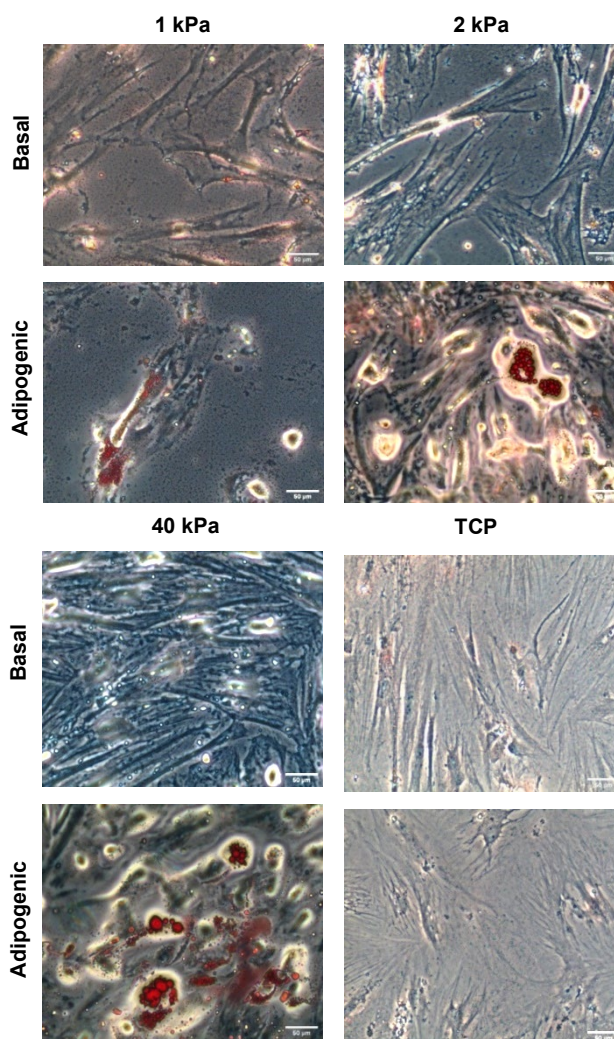


**Figure 5.7. Stro-1<sup>+</sup> BMSCs (M53) at different seeding densities in basal and adipogenic medium on TCP.** Cells plated at different seeding densities on TCP in basal and adipogenic media were imaged on day 7 using a Nikon Eclipse Ti inverted microscope.



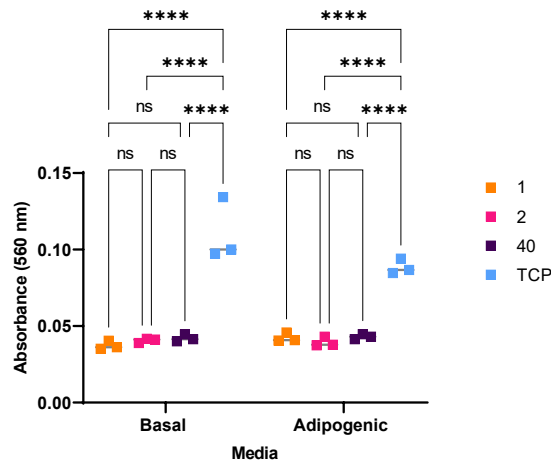
**Figure 5.8. Stro-1<sup>+</sup> BMSCs (M53) differentiated into adipocytes on TCP regardless of the seeding density.** Cells were stained with oil red O, which was released and quantified. ns= $p > 0.05$ ; basal:  $0.6 \pm 0.03$  (3,750 cells/cm<sup>2</sup>),  $0.6 \pm 0.01$  (7,500 cells/cm<sup>2</sup>),  $0.6 \pm 0.03$  (15,000 cells/cm<sup>2</sup>),  $0.6 \pm 0.02$  (30,000 cells/cm<sup>2</sup>); osteogenic:  $0.9 \pm 0.03$  (3,750 cells/cm<sup>2</sup>),  $1.0 \pm 0.08$  (7,500 cells/cm<sup>2</sup>),  $1.1 \pm 0.17$  (15,000 cells/cm<sup>2</sup>),  $1.1 \pm 0.17$  (30,000 cells/cm<sup>2</sup>). Data was not normalised to the number of cells or DNA content. Squares represent the mean and SD of the triplicates (n=3) at each seeding density, and a significant difference was calculated using the two-way ANOVA method.

After confirming that Stro-1<sup>+</sup> BMSCs (M53) differentiated into adipocytes on TCP, the next aim was to evaluate the effect of substrate elasticity on adipogenic differentiation. Stro-1<sup>+</sup> BMSCs (M53) were plated at 4,000 cells on 1, 2, and 40 kPa PAAm hydrogels and TCP, incubated at 37°C and stained with oil red O on day 14. Figure 5.9 shows elongated cells in basal conditions regardless of the substrate's stiffness, but cell crowding increased on stiffer hydrogels. BMSCs exhibited lipid and oil red O accumulation in adipogenic medium on PAAm hydrogels but not on TCP, implying that cells differentiated into adipocytes on hydrogels at all stiffness but not on TCP.



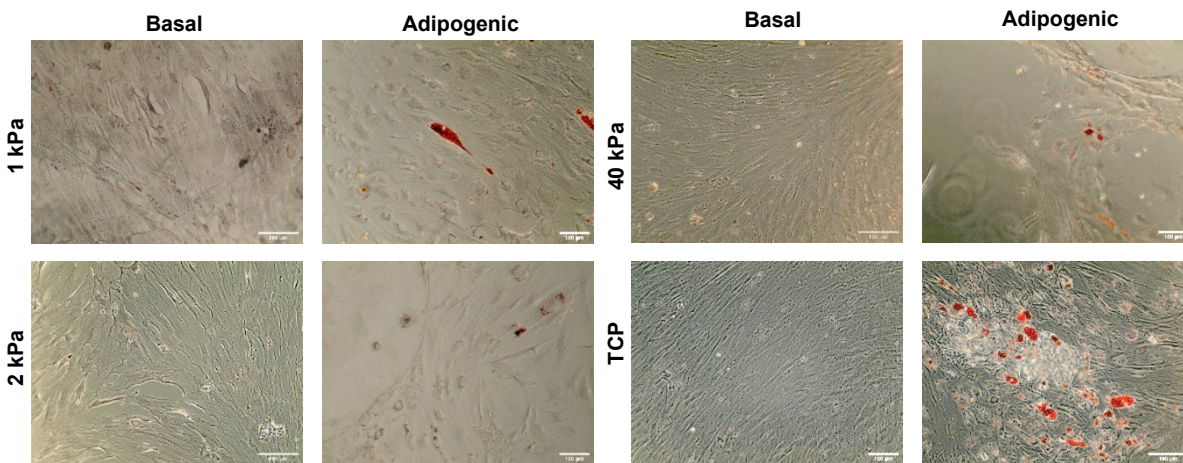
**Figure 5.9. Stro-1<sup>+</sup> BMSCs (M53) differentiated into adipocytes on PAAm hydrogels.** Elongated cells were observed in basal conditions, and cell crowding was evident on 40kPa and TCP. Cells accumulated lipids in adipogenic conditions on 1,2 and 40 kPa PAAm hydrogels but not on TCP. Cells were imaged on day 14 using a Zeiss microscope after oil red O staining.

Figure 5.10 shows no significant difference in the absorbance measurements of oil red O released by BMSCs on PAAm hydrogels with different stiffness.



**Figure 5.10. Stro-1<sup>+</sup> BMSCs (M53) differentiated into adipocytes on PAAm hydrogels regardless of the hydrogel elastic modulus.** Statistical differences between hydrogels were calculated by the two-way ANOVA method. No significant difference in oil red O absorption was identified when comparing cells on hydrogels with different elasticities disregarding the medium conditions (ns= p>0.05; Basal: 0.037 ± 0.003 (1 kPa), 0.041 ± 0.001 (2 kPa), 0.042 ± 0.002 (40 kPa); adipogenic: 0.042 ± 0.003 (1 kPa), 0.039 ± 0.003 (2 kPa), 0.043 ± 0.002 (40 kPa)). Squares represent the mean and SD of the hydrogel’s triplicates at each elastic modulus and TCP.

The previous experiment showed no oil red O absorbance increase with cells at 4,000 cells/cm<sup>2</sup> on 1 and 2 kPa PAAm hydrogels. Hence, the effect of substrate stiffness in Stro-1<sup>+</sup> BMSCs (M53) adipogenic differentiation was evaluated with a higher seeding density (20,000 cells/cm<sup>2</sup>) following the same procedure. Figure 5.11 denotes lipid and oil red O accumulation in BMSCs on 1 kPa hydrogels and TCP, while higher cell crowding was evident in basal compared to adipogenic conditions.



**Figure 5.11. Adipogenic differentiation of Stro-1<sup>+</sup> BMSCs (M53) increased on 1 kPa PAAm hydrogels and TCP.** Cell crowding was evident in basal medium, while lipid accumulation was seen on 1 kPa hydrogels and TCP in adipogenic conditions. Cells were imaged on day 14 using a Zeiss microscope at 5X.

Figure 5.12 shows a slight but insignificant increase in oil red O absorbance on 1kPa hydrogels and TCP in basal and adipogenic medium.

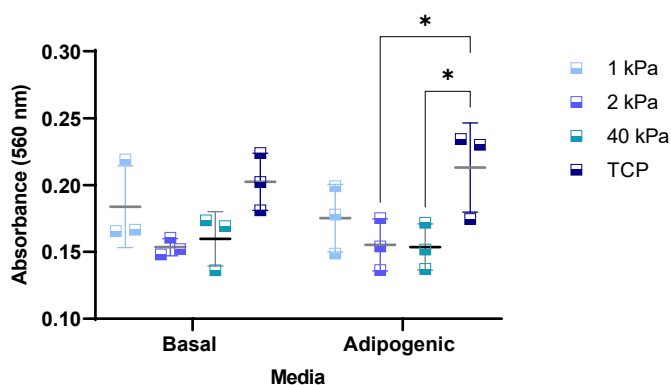


**Figure 5.12. Stro-1<sup>+</sup> BMSCs (M53) differentiated into adipocytes on PAAm hydrogels regardless of the hydrogel elastic modulus at high seeding density.** Oil red O was released and measured by a spectrophotometric method. No significant differences were encountered in cells on hydrogels with different elasticities. ns=  $p > 0.05$ ; Basal:  $0.18 \pm 0.03$  (1 kPa),  $0.15 \pm 0.006$  (2 kPa),  $0.160 \pm 0.020$  (40 kPa); adipogenic:  $0.17 \pm 0.025$  (1 kPa),  $0.15 \pm 0.019$  (2 kPa),  $0.154 \pm 0.017$  (40 kPa). Squares represent the mean and SD of the triplicates of hydrogels at different stiffness, and a significant difference was calculated by the 2-way ANOVA method.

Preliminary results suggest that substrate elastic modulus might not influence BMSC osteogenic and adipogenic differentiation. However, further standardisation might be necessary to evaluate osteogenic and adipogenic differentiation and draw conclusions due to red oil O staining and quantification variability.

The substrate stiffness also depends on the substrate thickness. Thus, the following experiments aimed to evaluate the effect of substrate thickness on Stro-1<sup>+</sup> BMSCs differentiation.

### 5.3.3 Effect of substrate thickness on BMSC osteogenic differentiation

The following experiment assessed the effect of substrate thickness on Stro-1<sup>+</sup> BMSCs DNA concentration. For this, Stro-1<sup>+</sup> BMSCs (M53) were plated at 5,000 cells/cm<sup>2</sup> on soft and stiff hydrogels with different thicknesses (3, 5, 10 and 25  $\mu$ L) PAAm hydrogels and the fluorescence was measured to calculate DNA concentration. Figure 5.13 shows that the decrease in substrate thickness increases BMSCs DNA concentration regardless of the hydrogel elastic modulus.

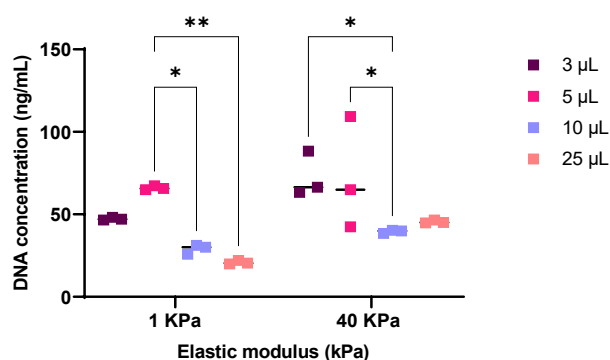


**Figure 5.13. Stro-1<sup>+</sup> BMSCs (M53) DNA concentration increased on thin PAAm hydrogels.** Cell suspensions were obtained, and DNA concentration was measured using a fluorometric method. DNA concentration varied with the thickness of the hydrogel. Significant differences were found when comparing soft 5  $\mu\text{L}$  and 10  $\mu\text{L}$  ( $*p < 0.05$ ;  $66 \pm 1.2 \text{ ng/mL}$  vs  $29 \pm 2.8 \text{ ng/mL}$ ), soft 5  $\mu\text{L}$  and 25  $\mu\text{L}$  ( $**p < 0.05$ ;  $66 \pm 1.2 \text{ ng/mL}$  vs  $20.8 \pm 1.1 \text{ ng/mL}$ ), stiff 3  $\mu\text{L}$  and 10  $\mu\text{L}$  ( $*p < 0.05$ ;  $72.7 \pm 13.5 \text{ ng/mL}$  vs  $39.5 \pm 1.01 \text{ ng/mL}$ ) and stiff 5  $\mu\text{L}$  and 10  $\mu\text{L}$  ( $*p < 0.05$ ;  $72.7 \pm 34.04 \text{ ng/mL}$  vs  $39.5 \pm 1.01 \text{ ng/mL}$ ). Squares represent the mean and SD of the hydrogel's triplicates at the different thicknesses, and a significant difference was calculated by the 2-way ANOVA method.

The following experiment assessed the effect of hydrogel thickness on BMSCs DNA concentration and ALPL activity. Stro-1<sup>+</sup> BMSCs (M53) were plated at 5,000 cells/cm<sup>2</sup> on 1 and 40 kPa PAAm hydrogels of different thicknesses (5, 25, and 100  $\mu\text{L}$ ). Cell suspensions were obtained on day 7 to measure DNA concentration and ALPL activity. Figure 5.14 (a) outlines that DNA concentration varied with no clear trend as in the previous experiment, where DNA increased on thinner substrates. Indeed, DNA concentration in cells on soft 5  $\mu\text{L}$  hydrogels was higher than 25  $\mu\text{L}$  hydrogels but lower than 100  $\mu\text{L}$  hydrogels. In comparison, higher DNA concentration was quantified in cells on stiff 5  $\mu\text{L}$  hydrogels than on 25 and 100  $\mu\text{L}$  counterparts. Figure 5.14 (b) highlights that ALPL activity varied with no specific trend. The highest ALPL activity was detected in cells on soft, thin (5  $\mu\text{L}$ ) and stiff, thick 25  $\mu\text{L}$  PAAm hydrogels. Normalised data in Figure 5.14 (c) show the highest ALPL activity on soft, stiff thick (25  $\mu\text{L}$ ) hydrogels.

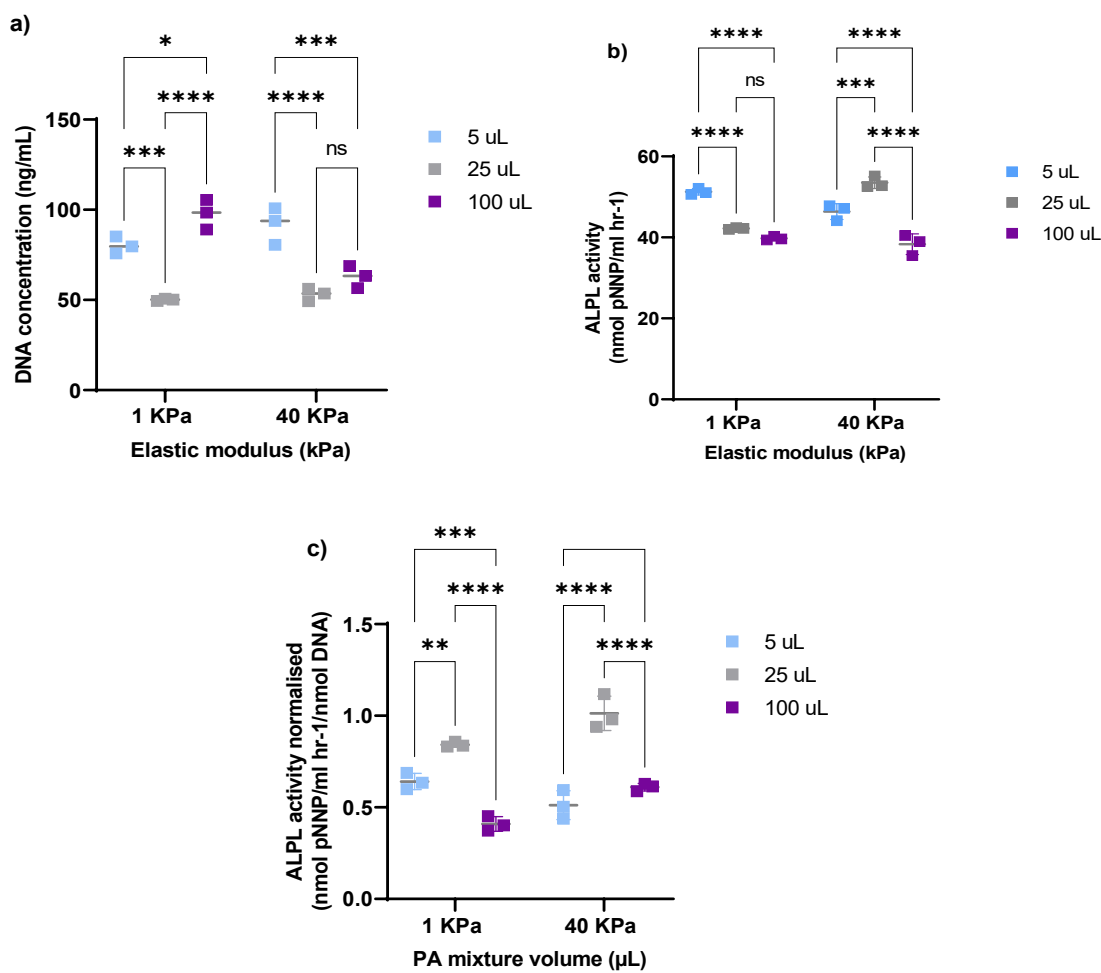


**Figure 5.14. The substrate thickness influenced Stro-1<sup>+</sup> BMSCs (M53) DNA concentration and ALPL activity on soft and stiff PAAm hydrogels. (a)** DNA concentration increased on soft and stiff hydrogels at 5  $\mu$ L compared to 25  $\mu$ L. Soft hydrogels: \* $p=0.0153$  ( $80.2 \pm 4.7$  ng/mL (5  $\mu$ L) vs  $97.7 \pm 8.2$  ng/mL (100  $\mu$ L)), \*\*\*\* $p<0.0001$  ( $50.1 \pm 0.7$  ng/mL (25  $\mu$ L) vs  $97.7 \pm 8.2$  ng/mL (100  $\mu$ L)). **(b)** ALPL activity varied with hydrogel thickness. Soft gels: \*\*\*\* $p<0.0001$  ( $51.2 \pm 0.8$  ng/mL (5  $\mu$ L) vs  $39.7 \pm 0.4$  ng/mL (100  $\mu$ L)),  $p=0.1503$  ( $42.2 \pm 0.2$  ng/mL (25  $\mu$ L) vs  $39.7 \pm 0.4$  ng/mL (100  $\mu$ L)). **(c)** Normalised ALPL activity to DNA content varied with hydrogel thicknesses. Soft gels: \*\* $p=0.0008$  ( $0.641 \pm 0.04$  nmol pNNP/ml hr-1/nmol DNA (5  $\mu$ L) vs  $0.40 \pm 0.04$  nmol pNNP/ml hr-1/nmol DNA (100  $\mu$ L)), \*\*\*\* $p<0.0001$  ( $0.84 \pm 0.01$  nmol pNNP/ml hr-1/nmol DNA (25  $\mu$ L) vs  $0.40 \pm 0.04$  nmol pNNP/ml hr-1/nmol DNA (100  $\mu$ L)). Squares represent the mean DNA concentration, or ALPL activity and SD of the cells on the hydrogel triplicates at each condition. Significant differences were calculated by the two-way ANOVA method ( $n=3$ ).

Later, the ALPL activity of Stro-1<sup>+</sup> BMSCs on soft and stiff PAAm hydrogels with different thicknesses was evaluated by quantifying the ALPL-stained area (see Section 2.2.7.1 for detailed methodology). Cells plated on hydrogels were incubated in basal and osteogenic mediums. ALPL staining was carried out on day 7; representative images are shown in Figure 5.15. These data indicate a slight increase in ALPL staining in cells on stiff, thick (25  $\mu$ L) PAAm hydrogels in basal medium. In contrast, similar ALPL activity was detected in osteogenic media regardless of the substrate's mechanical properties but increased on TCP compared to basal conditions.

The percentage of the stained area was quantified using the FIJI programme, and data were plotted in Figure 5.16. ALPL activity slightly decreased in basal medium with the increased thickness in soft hydrogels. In contrast, a significant increase was detected in stiff thin hydrogels compared to their thicker counterparts. Nevertheless, the percentage of the stained area on soft hydrogels under osteogenic conditions was slightly similar and decreased but not significantly with the increase in hydrogel thickness.

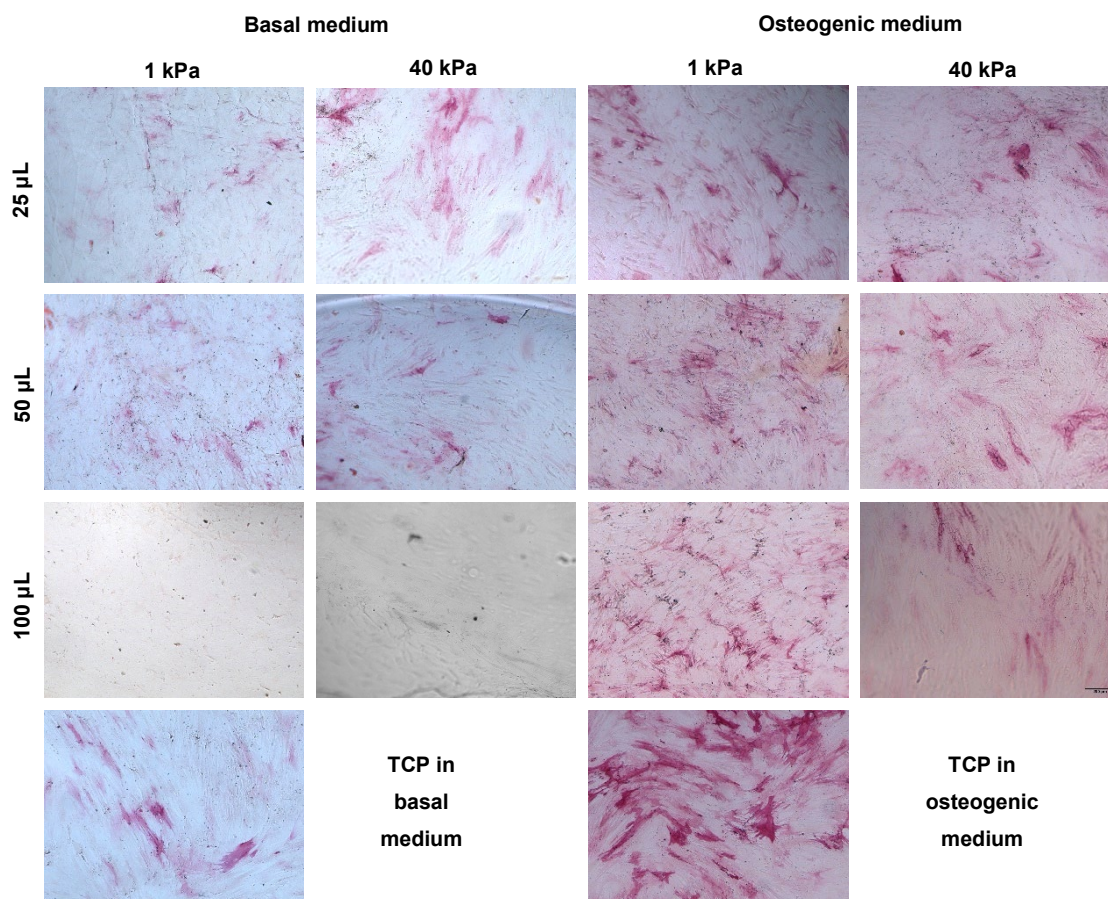


**Figure 5.15. ALPL staining of Stro-1<sup>+</sup> BMSCs (M53) on soft and stiff PAAm hydrogels with different thicknesses in basal and osteogenic medium.** ALPL staining was slightly higher on soft and stiff 25 µL hydrogels in basal and osteogenic medium but similar on soft hydrogels regardless of their thickness in basal and osteogenic medium. ALPL staining was more evident in osteogenic supplements than in basal medium on TCP. Cells were imaged under a Zeiss microscope at 5X. Scale bar: 200 µm.

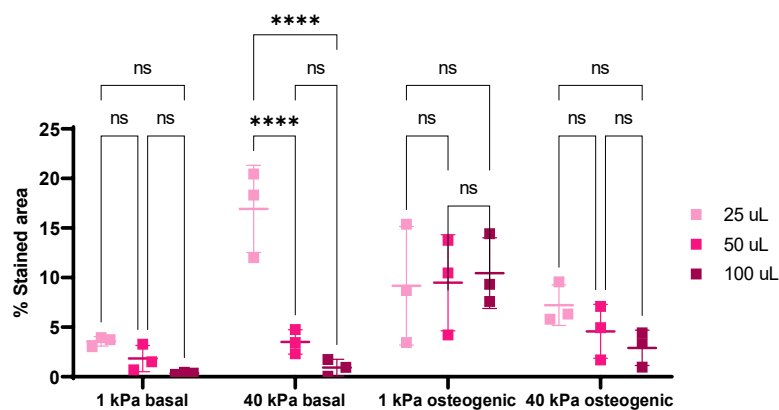


**Figure 5.16. The decrease in hydrogel thickness did not significantly influence the percentage of the stained area of Stro-1<sup>+</sup> BMSCs (M53).** The per cent of stained area decreased on soft, thicker hydrogels in basal medium but with no significant difference ( $ns > 0.05$ ). At the same time, the changes in the thickness of stiff gels significantly modified the per cent of the stained area ( $****p < 0.001$ :  $16.929 \pm 4.4\%$  (25  $\mu$ L) vs  $3.5 \pm 1.2\%$  (50  $\mu$ L),  $****p < 0.001$ :  $16.929 \pm 4.4\%$  (25  $\mu$ L) vs  $0.9 \pm 0.8\%$  (100  $\mu$ L)). The percentage of the stained area was similar on soft hydrogels with varied thicknesses with no significant difference ( $ns > 0.05$ ). In contrast, it slightly decreased on stiff thicker hydrogels in osteogenic medium with no statistical difference ( $ns > 0.05$ ). Pictures from five microscopic fields from each hydrogel's triplicate were analysed in the FIJI programme to quantify the percentage of the stained area ( $n=3$ ). Squares represent the mean percentage of the stained area and standard deviation. Significant differences were analysed by the 2-way ANOVA method.

Another method was carried out to define any significant difference in ALPL activity between soft and stiff PAAm hydrogels with different thicknesses, as the previous experiments showed variations. Here, the ALPL activity was quantified by a fluorometric (refer to Section 2.2.7.2.2 in Chapter 2) instead of a colourimetric method for more accuracy. In the experiment, Stro-1<sup>+</sup> BMSCs (F67) were plated at 10,000 cells/cm<sup>2</sup> on soft and stiff PAAm hydrogels with different thicknesses (5  $\mu$ L, 50  $\mu$ L, 100  $\mu$ L) in basal and osteogenic medium at 37 °C. Cell suspensions were obtained on day 14, and the DNA concentration and ALPL activity were measured by a fluorometric method. Figure 5.17 denotes DNA concentration in basal (a) and osteogenic medium (b) on soft and stiff hydrogels with different thicknesses. DNA concentration increased under osteogenic conditions. In basal  $\alpha$ -MEM medium, DNA concentration decreased on thicker hydrogels, while cells exhibited the highest DNA concentration on the thickest stiff hydrogels. In osteogenic medium, DNA concentration increases with the hydrogel's thickness on soft materials, while it varies on stiff hydrogels. DNA concentration increased in osteogenic supplements on TCP (c).

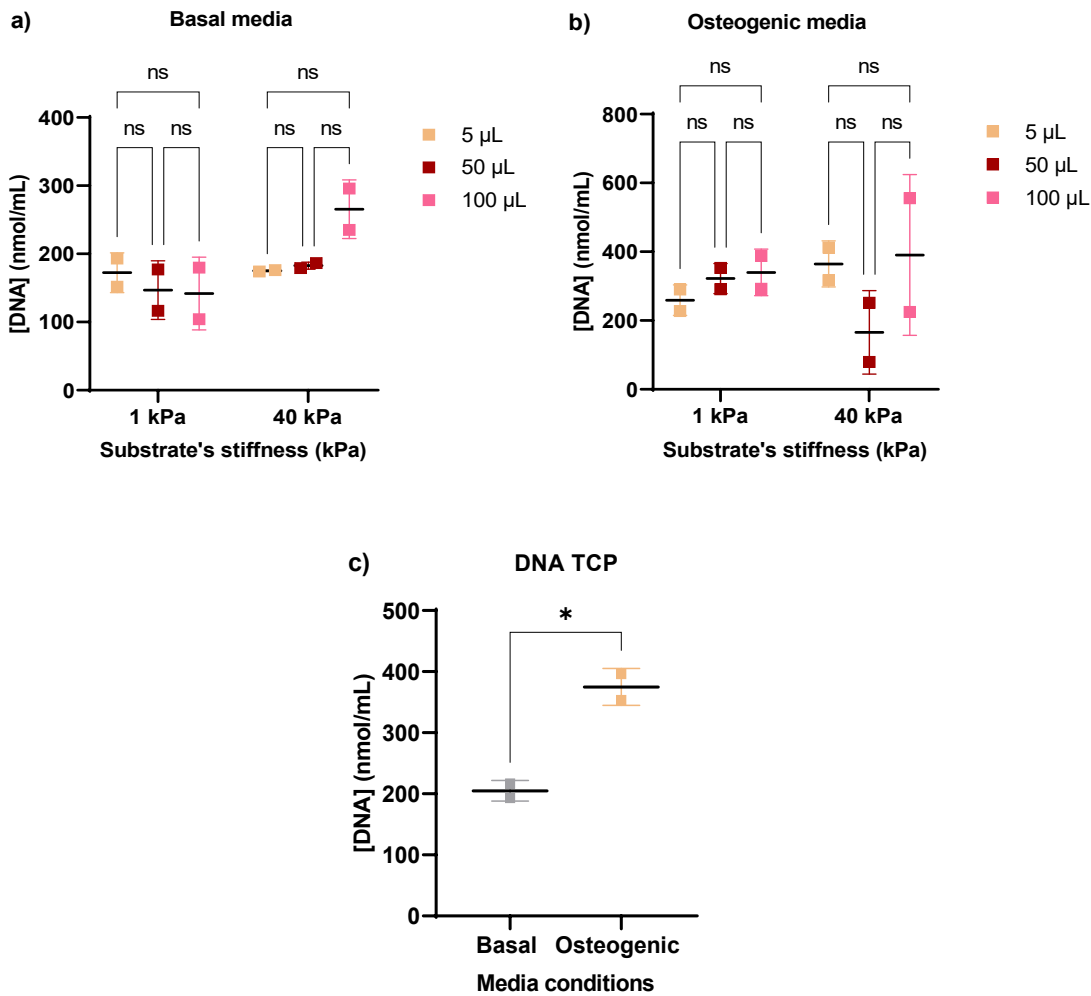


**Figure 5.17. Substrate thickness did not influence the DNA concentration of Stro-1<sup>+</sup> BMSCs (F67).** (a) Cells exhibited a slight decrease in DNA concentration on soft, thick hydrogels and a slight increase on stiff, thick counterparts but with no significant difference in both cases (ns>0.05) in basal media. (b) DNA concentration increased on the soft, thickest hydrogels (100 μL), while minor DNA concentration was registered on the stiff (50 μL), non-statistically different in osteogenic media. (c) Osteogenic supplements statistically increased the DNA concentration of BMSCs on TCP (\*p<0.05). Squares represent the media and SD of the DNA concentration, and data were analysed using the 2-way ANOVA method and t-test (n=2).

Figure 5.18 shows the ALPL activity of cells on soft and stiff hydrogels with different thicknesses in basal (a), osteogenic (b) and TCP (c). ALPL activity was lower in basal medium on the soft, thickest hydrogel but increased on stiff, thick hydrogels (with no significant difference). ALPL activity upturned in osteogenic medium, with a rise in the soft and a drop in the stiff, thickest hydrogels, which is non-significant. The enzymatic activity was also elevated in the presence of osteogenic supplements on TCP.

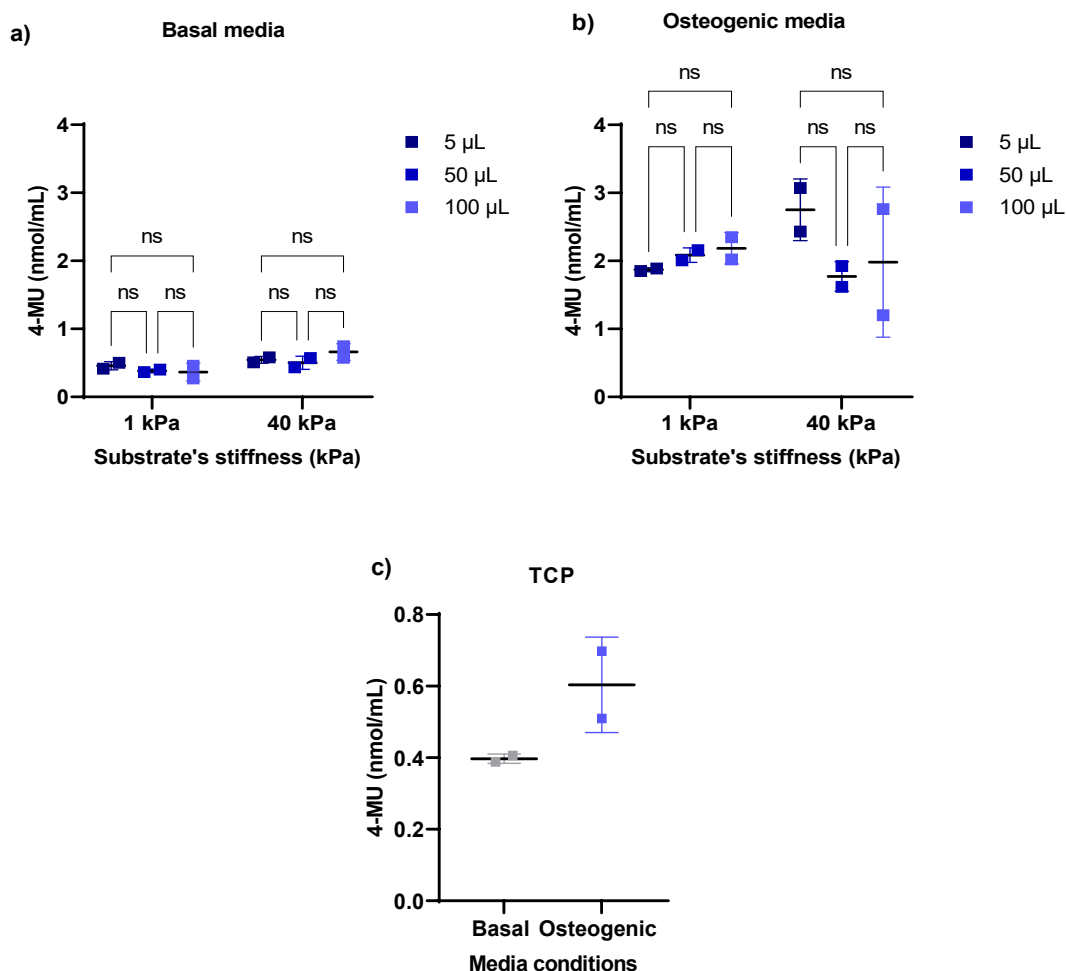


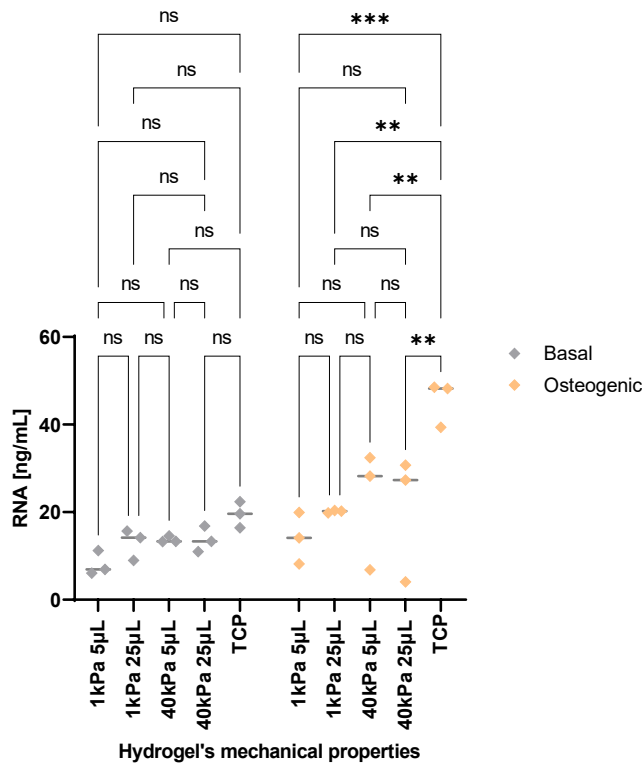
**Figure 5.18** ALPL activity of Stro-1<sup>+</sup> BMSCs (F67) did not change when varying the thickness of soft and stiff PAAm hydrogels. (a) ALPL activity slightly declined on soft and uplifted stiff, thicker hydrogels in basal media (ns=  $p > 0.05$ ). (b) Cells exhibited a rise in soft and a decrease in stiff thicker hydrogels (ns= $p > 0.05$ ). (c) ALPL activity in BMSCs significantly increased on TCP in osteogenic conditions. Squares represent the mean and SD of the ALPL activity, and data were analysed using the two-way ANOVA method and t-test ( $n=2$ ).

To summarise, the results from the previous experiments showed that the DNA concentration and ALPL activity of Stro-1<sup>+</sup> BMSCs on soft and stiff PAAm hydrogels did not significantly vary when modifying hydrogel thicknesses.

ECM mechanical properties influence the transcription of genes involved in cell differentiation. Thus, the following experiments aimed to evaluate how changes in hydrogel thickness might influence the expression of the osteogenic genes *ALPL* and *RUNX2* in Stro-1<sup>+</sup> BMSCs.

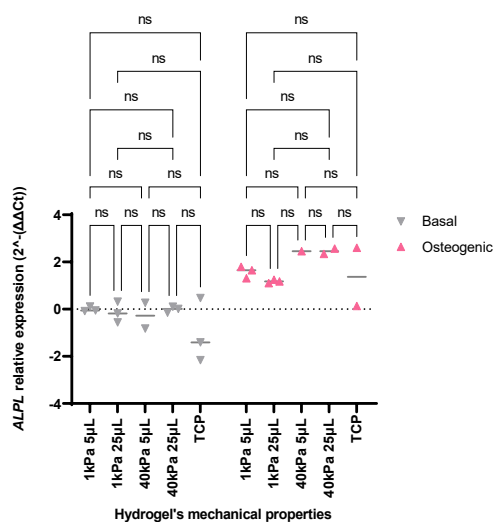
First, Stro-1<sup>+</sup> BMSCs (sample F63) were plated at 5,000 cells/cm<sup>2</sup> on 1 and 40 kPa PAAm hydrogels with different thicknesses (referred to as thin (5 μL) and thick (25 μL) onwards) and TCP in the basal and osteogenic  $\alpha$ -MEM medium at 37°C for 7 days. After incubation, cell suspensions were obtained to isolate and quantify RNA based on the manufacturer's protocol (refer to Section 2.2.9.1 in Chapter 2 for detailed methodology).

Figure 5.19 shows that osteogenic supplements increased RNA concentration while lower RNA measurements were obtained from cells in basal medium. Without osteogenic supplements, RNA concentration was slightly lower in cells on soft, thin hydrogels, but there was no significant difference when comparing soft, stiff, thin, and thick hydrogels. However, RNA concentration was slightly but not significantly higher on stiff than soft hydrogels disregarding hydrogels hydrogel in the osteogenic medium. Moreover, the RNA concentration of cells on TCP was higher when osteogenic supplements were added to the media.



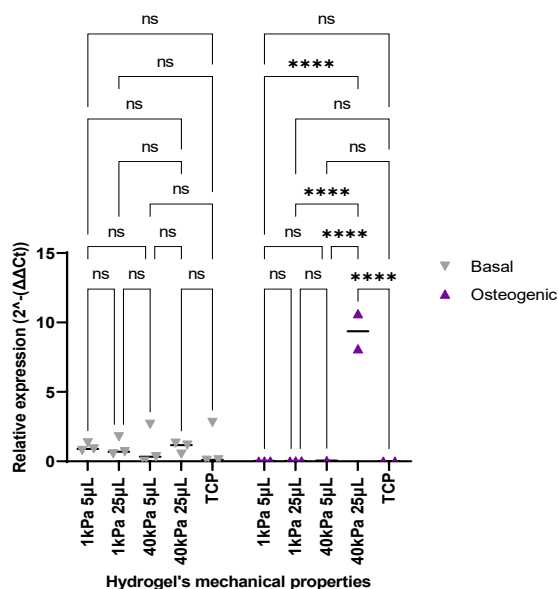
**Figure 5.19 The substrate mechanical properties did not significantly influence the RNA concentration of Stro-1<sup>+</sup> BMSCs (F63).** RNA concentration in basal medium remained similar on soft and stiff hydrogels except on soft and thin (ns= p>0.05). In osteogenic medium, RNA content was slightly higher on stiff hydrogels than on the soft counterparts, where cells on thin hydrogels exhibited lower RNA concentration than on thick hydrogels (ns= p>0.05). Diamonds represent the mean RNA concentration and SD obtained from the cells on the hydrogels (n=3), and data is analysed by the 2-way ANOVA method.

cDNA was obtained from the RNA samples at 50ng/mL through RT-PCR, and ALPL and RUNX2 gene expression was quantified by qPCR (see Sections 2.2.9.3, 2.2.9.4 and 2.2.9.4.1 for a detailed explanation of methodology and calculations). Figure 5.20 indicates that ALPL expression levels accounted for zero in basal medium regardless of the substrate’s mechanical properties, slightly increased on soft PAAm hydrogels and considerably on stiff hydrogels in osteogenic conditions.



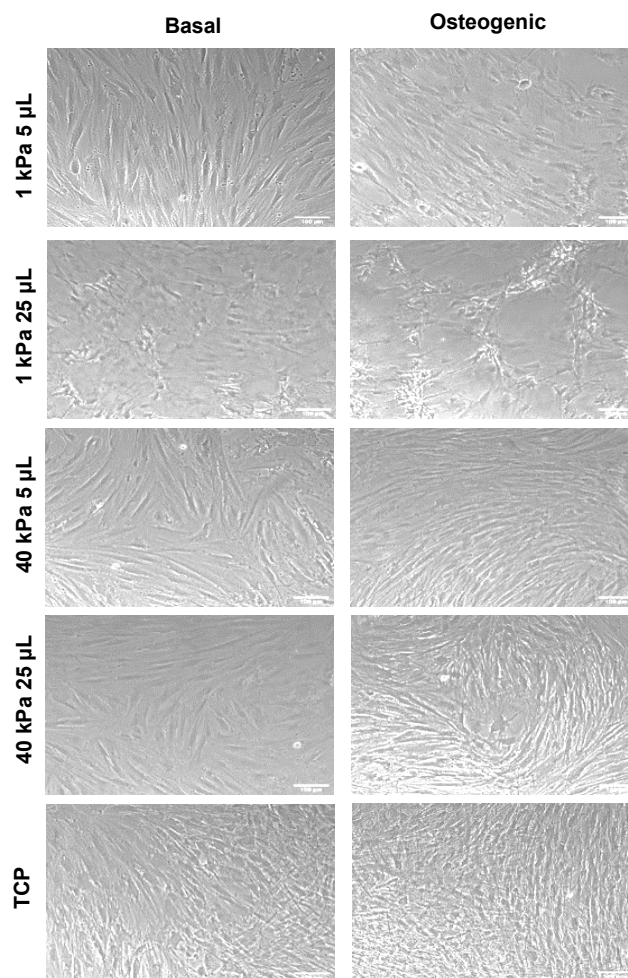
**Figure 5.20** *ALPL* expression of Stro-1<sup>+</sup> BMSCs (F63) increased on stiff PAAm hydrogels in osteogenic conditions. Cells did not express *ALPL* in basal medium regardless of the hydrogel mechanical properties (ns= p>0.05); stiff hydrogels promoted *ALPL* expression under osteogenic conditions regardless of the thickness of the hydrogel. A slight increase was seen in soft, thin, compared to soft, thick hydrogels. Triangles represent the mean *ALPL* expression and SD in BMSCs on each condition's soft and stiff hydrogel triplicates. A significant difference was calculated by the two-way ANOVA method.

Figure 5.21 compares the *RUNX2* expression of Stro-1<sup>+</sup> BMSCs on soft, stiff, thin, and thick PAAm hydrogels. It denotes that *RUNX2* expression in basal medium was low and not influenced by hydrogel stiffness. In contrast, it accounted for zero under osteogenic conditions except on stiff, thick hydrogels, where a noticeable upturn was presented.



**Figure 5.21** The substrate mechanical properties did not modify *RUNX2* expression of Stro-1<sup>+</sup> BMSCs (F63). *RUNX2* expression was low in basal medium with no significant difference when modifying hydrogel elastic modulus and thickness (ns= p>0.05). *RUNX2* expression was zero on soft (thin and thick) and stiff (thin) hydrogels but not on stiff, thick PAAm hydrogels in osteogenic medium. Triangles represent the mean *RUNX2* expression levels and SD in BMSCs on each condition's soft and stiff hydrogel triplicates. A significant difference was calculated by the two-way ANOVA method.

Because of the low expression levels of *ALPL* and *RUNX2* in Stro-1<sup>+</sup> BMSCs, a higher RNA concentration was used in the following experiments. Cells isolated from sample F67 were plated at 5,000 cells/cm<sup>2</sup> on the hydrogels and incubated at 37 °C in basal and osteogenic medium for 7 days. Figure 5.22 compares the cell morphology of Stro-1<sup>+</sup> BMSCs on soft and stiff (thin and thick) PAAm hydrogels. It illustrates that hydrogel's mechanical properties and medium conditions changed cell morphology, crowding, and alignment. Under basal conditions, cell crowding was evident on TCP, and elongated cells accommodated in all directions were observed on stiff hydrogels regardless of the thickness of the hydrogel. Meanwhile, elongated and aligned cells were observed on soft, thin hydrogels, and the cell periphery was challenging to define on soft, thick hydrogels. The increment in cell crowding on TCP in osteogenic medium was noticeable, where cells were perpendicularly aligned. Thin cells on stiff hydrogels, short cells on soft, thin hydrogels and intertwined cells were appreciated in some areas of the soft, thick hydrogels.



**Figure 5.22 Substrate mechanical properties and osteogenic supplements modified Stro-1<sup>+</sup> BMSCs (F67) morphology.** Elongated cells were seen on soft, thin hydrogels in basal and osteogenic medium; irregular cells on soft, thick hydrogels in basal medium and forming networks in osteogenic medium. Stiff hydrogels hold elongated cells regardless of the substrate's thickness in basal medium, but thinner cells were appreciated under osteogenic medium. Cell crowding was evident on TCP in basal medium and was higher in osteogenic media. Cells were imaged on day 7 using a Nikon Eclipse Ti inverted microscope at 10X magnification.

After cell imaging, no significant differences in RNA concentration in Stro-1<sup>+</sup> BMSCs were encountered when modifying the hydrogel mechanical properties. RNA concentration slightly increased on soft and stiff, thin hydrogels compared to soft and stiff, thick hydrogels in osteogenic medium. However, it increased in basal conditions compared to the previous experiment (data not shown).

Figure 5.23 outlines the *ALPL* (a) and *RUNX2* (b) gene expression in Stro-1<sup>+</sup> BMSCs (F67) on PAAm hydrogels and TCP. The graph plots show low *ALPL* expression on all hydrogels regardless of their mechanical properties in basal medium. At the same time, it was slightly higher on stiff, thick hydrogels in osteogenic media, with no significant differences in all cases. *RUNX2* expression highly varied in basal media and on stiff, thick hydrogels in osteogenic conditions.

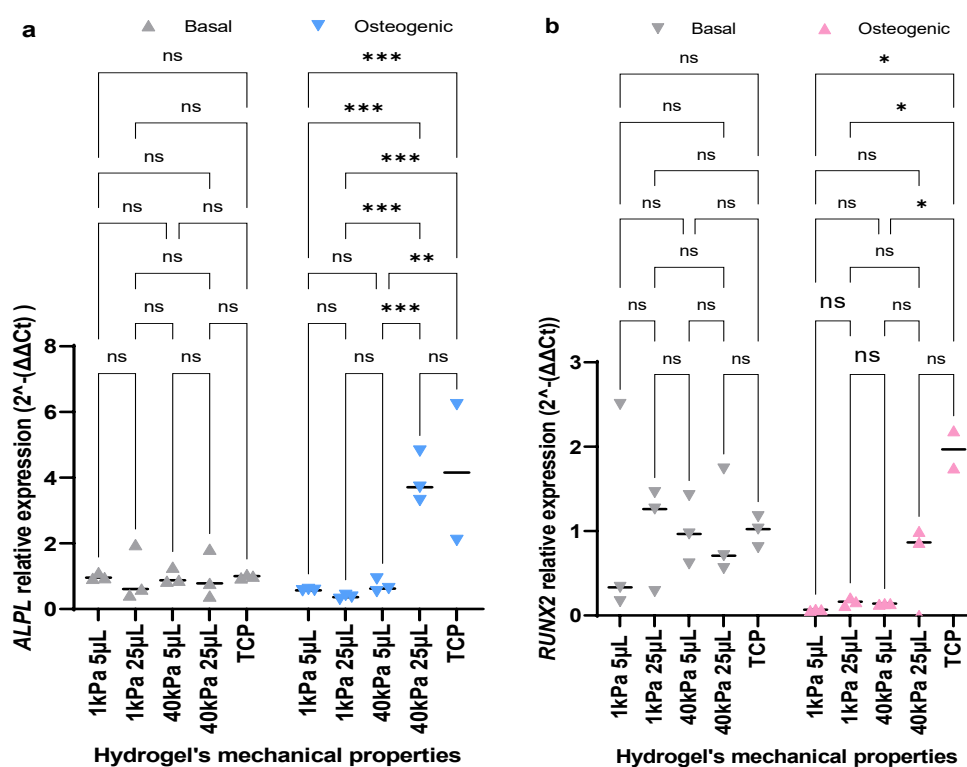


**Figure 5.23** The substrate mechanical properties did not significantly influence *ALPL* and *RUNX2* expression in Stro-1<sup>+</sup> BMSCs (F67). (a) *ALPL* expression remained low in basal medium regardless of the substrate's mechanical properties, while levels increased in osteogenic medium on stiff, thick hydrogels. (b) *RUNX2* expression varied in basal medium and increased on stiff, thick hydrogels in the osteogenic medium. Triangles represent the mean *ALPL* and *RUNX2* expression in BMSCs and SD on the gels at each condition (n=3), and a significant difference was calculated by the two-way ANOVA method.

To summarise, hydrogel elastic modulus and thickness did not significantly influence the expression of the osteogenic genes *ALP* and *RUNX2* in Stro-1<sup>+</sup> BMSCs. However, cells exhibited high *ALPL* and *RUNX2* expression on stiff, thick hydrogels and TCP. Also, cells exhibited no changes in ALP activity when modifying hydrogel's mechanical properties.

## 5.4 Discussion

Changes in ECM stiffness influence the differentiation potential of SSCs, which is crucial in tissue regeneration (Sun *et al.*, 2018). Therefore, this chapter aimed to define the effect of the substrate elastic modulus and thickness on BMSCs differentiation, finding:

- Stro-1<sup>+</sup> BMSCs differentiated into osteoblasts and adipocytes on TCP and PAAm hydrogels regardless of substrate elasticity.
- Changes in substrate thickness influenced Stro-1<sup>+</sup> BMSCs osteogenic differentiation.
- The modification of the substrate mechanical properties did not modify the expression of the osteogenic markers *ALPL* and *RUNX2*.

The osteogenic differentiation potential of BMSCs was evaluated by quantifying ALPL activity, one of the most predictable markers for SSCs' osteogenic differentiation (Westhauser *et al.*, 2019). The first experiment (Figure 5.1) showed that unselected BMSCs exhibited higher ALPL staining in the presence of osteogenic supplements such as dexamethasone, ascorbic acid and  $\beta$ -glycerophosphate on TCP. Dexamethasone activates WNT/ $\beta$ -catenin signalling (crucial in osteogenic fate and depends on *RUNX2* expression), ascorbic acid promotes the formation of collagen chains and ECM secretion, and  $\beta$ -glycerophosphate regulates osteopontin and BMP2 expression (Langenbach *et al.*, 2013).

Selected Stro-1<sup>+</sup> BMSCs isolated from two samples showed more significant ALPL activity and DNA concentration in osteogenic than in basal conditions (Figure 5.2). Stro-1<sup>+</sup> was the first antibody used to select BMSCs, and it binds to a cell surface antigen found in less than 10% of the cell population. Therefore, Stro-1<sup>+</sup> BMSCs display many characteristics of multipotent stem cells (Fitter *et al.*, 2017). In the experiments, cells from different patients exhibited different ALPL staining on TCP, as ageing affects cells. For example, older patients show limited osteogenic differentiation potential and fracture repair (Lin *et al.*, 2019).

It has been established that cell morphology relates to BMSC differentiation. Round cells express higher adipogenesis markers, spread cells with dendrite-like processes show elevated neurogenesis markers, whereas SSCs with cuboidal and elongated forms, linear, stretched actin filaments exhibit high expression of osteogenic markers (Lee *et al.*, 2013; Zhao *et al.*, 2014). In the experiment, Stro-1<sup>+</sup> BMSCs displayed different morphologies on the substrates of different elastic modulus and media conditions; elongated cells on stiff hydrogels and TCP and spread or extended cells on soft PAAm hydrogels (Figure 5.4). These results correlate with previous reports from Matsuoka *et al.*, 2013 who defined fibroblastic shapes in basal media and flat and spread cells in osteogenic media and Su *et*

*al.*, 2018 who reported elongated cells on stiff hydrogels (48-53 kPa) and short cells with branches on softer matrices (13-16 kPa).

Previous studies highlighted that substrate mechanical properties influence BMSCs differentiation. Engler *et al.*, 2006, stated that SSCs differentiation is subject to changes in the ECM stiffness to differentiate to the specific cell type that matches the tissue stiffness. Indeed, 0.1-1 kPa hydrogels are neurogenic, 8-17 kPa are myogenic, and 25-40 kPa are osteogenic.

ALPL activity is a reliable indicator of the osteogenic potential in SSCs. Despite Mao *et al.*, 2016 and Sun *et al.*, 2018 reporting that stiff hydrogels promote an increase in cell proliferation and osteogenic differentiation, there was no significant difference in ALPL activity and DNA concentration between soft and stiff hydrogels (Figures 5.5 and 5.6). Due to the high seeding density, cells may have perceived the soft PAAm hydrogels as stiffer, which might influence their fate. Indeed, Venugopal *et al.*, 2018 reported that cell crowding increases the apparent stiffness due to cellular traction, which can reverse substrate stiffness effects on cellular morphology and functions. Additionally, cells from a younger patient exhibited a slight but not significant increase in ALPL activity and DNA concentration that can be explained as BMSCs losing their proliferative and multipotent capacity with the patient's age (Lin *et al.*, 2019).

The adipogenic differentiation capacity of BMSCs on PAAm hydrogels and TCP was also evaluated as multipotency is an essential characteristic to distinguish stem cells. On TCP, elongated cells were seen in basal media, disregarding the seeding density. In contrast, cuboidal cells with lipid accumulation were observed at the highest seeding density in adipogenic media on day 7 (Figure 5.7). However, no differences in seeding densities were encountered when quantifying oil red O absorbed by cells (Figure 5.8). This suggests cells differentiate into adipocytes on TCP regardless of the seeding density. This contradicts Khan *et al.* 2020 reports, stating that high but not low seeding promotes adipogenic differentiation on TCP.

On PAAm hydrogels, cell images in Figure 5.9 suggest that lipid and oil red O accumulation occurs regardless of hydrogel stiffness at low and high seeding densities. This agrees with Takata *et al.*, 2020, who reported that rigid matrices enhance the cell spreading of inguinal white adipose tissue pre-adipocytes. Nevertheless, the colourimetric quantification of the dye used here (Figures 5.10 and 5.12) might not be an appropriate method to detect any differences related to the substrate stiffness in the adipogenic differentiation potential of cells. This method uses isopropanol, which dries the hydrogels and might affect their structure and cell attachment and modify the oil red O quantification. In addition, the dye remains on the edges of the well plate. It can also be released and quantified, increasing the absorbance measurements and making it challenging to identify slight differences

related to the hydrogel stiffness. Thus, other methods, such as quantifying the percentage of stained area, might be more sensitive to detecting these differences.

Kim *et al.*, 2021, reported that BMSCs morphology changes during osteogenic differentiation and is highly associated with ALPL activity. They also emphasised how ECM stiffness, BMSCs morphology and cell fate are intimately related. Nevertheless, the results in this chapter showed that cell morphology changed depending on the substrate elastic modulus and media conditions (Figure 5.4) but not ALPL activity and DNA concentration (Figures 5.5 and 5.6). Therefore, other mechanical properties, such as thickness, might impact BMSCs differentiation.

Substrate thickness only influenced the ALPL activity of Stro-1<sup>+</sup> BMSCs isolated from sample M53 (Figure 5.14); no significant differences in the enzymatic activity were identified in cells isolated from samples from older patients (F67). This was also confirmed by different methods, colourimetric, fluorometric (Figure 5.18) and stained area (Figure 5.16) quantification, to discard any sensitivity problems. Besides ALPL activity, the expression of osteogenic genes (*ALPL* and *RUNX2*) is outstanding for evaluating the hydrogel mechanical properties' effect on osteogenic fate. The *ALPL* and *RUNX2* expression results (Figures 5.19-5.23) showed that the substrate elastic modulus and thickness did not significantly modify gene expression (regardless of the patient's age). Overall, results confirm that the changes in the substrate mechanical properties do not modify the phenotypic and genetic profiles associated with osteogenic fate. This might suggest that when cells are in close contact at high seeding densities, they exert forces between them, which modify how cells perceive the elasticity of the ECM or materials, promoting cell differentiation on soft and stiff matrices. It also must be considered that the hydrogel surface and the underlying matrix's proximity might influence stiffness sensing and cell differentiation. For instance, collagen type I might be differently distributed through the hydrogels and on their surface depending on the hydrogel thickness, which might modify cell attachment, crowding and differentiation.

Evaluating cell proliferation in SSCs is essential, as it is crucial in regenerative medicine. Leong *et al.*, 2010 reported that thick collagen hydrogels arrest the cell growth cycle as SSCs sense them as a very soft substrate. Although cell proliferation was not directly measured, the higher DNA content on soft, thin than soft, thick hydrogels might suggest that thin hydrogels increase cell proliferative activity. This might be explained as the effective substrate modulus being higher than the intrinsic elastic modulus due to the underlying matrix (Leong *et al.*, 2010).

According to Lin *et al.*, 2010, cells can sense the microenvironment in two ways: locally by sensing the intrinsic modulus of the substrate at the focal adhesion sites and laterally through the exerted traction forces that provide information to the cells about the substrate depth. Locally, cells transmit the forces generated by the actomyosin contraction to the

substrate and test their stiffness. Globally, the actin cytoskeleton acts as a large mechanosensor, acting as an elastic nematic gel and providing cues for cellular action. The actin cytoskeleton shows this nematic state when substrate stiffness increases and the actin filaments denser (Gupta *et al.*, 2016). Thus, cells can independently sense the intrinsic elastic modulus and thickness, affecting cell processes such as proliferation, as found here.

This variability in the ALPL activity and oil red O absorbance on the PAAm hydrogels might also be due to the intrinsic characteristics of the BMSC as SSCs might lose their proliferative and differentiation capacity *in vitro* after several cell divisions and proceed to a senescence phase (Kureel *et al.*, 2019). Also, the number of potential stem cells might vary within each population, passage number and patient. Other factors, such as cell crowding, might also impact cell differentiation through changes in cell traction forces.



## **Chapter 6 Cell traction forces and cell differentiation**

## 6.1 Introduction

Traction forces are exerted by the cells and applied to the hydrogel through the cell membrane or focal adhesions. They result from internal tension and allow the cells to feel the local and global mechanical properties of the ECM in a process known as cell mechanosensing (Evans-Gentleman, 2014; Lekka *et al.*, 2021) that occurs during contraction, spreading, crawling and migration (Butler *et al.*, 2001).

Cell mechanotransduction results from cell mechanosensing and defines how the produced strain is translated into biochemical signals (Evans and Gentleman, 2014). Mechanical forces applied to the hydrogels might cause cell changes through the focal adhesions on the attached cells. Strain leads to changes in the cell's actin cytoskeleton and nuclei disruption. These changes can result in the activation of ion channels and the consequent release of signalling molecules to neighbouring cells that direct different cellular processes (Ahearne, 2014).

Focal adhesions are crucial multi-protein structures that connect the ECM and the cell cytoskeleton during cell mechanosensing. They involve cell receptors such as integrins and proteoglycans and internal proteins such as paxilin, vinculin, actin and talin (Lekka *et al.*, 2021). Talin unfolds after traction forces reach a threshold and direct cell mechanotransduction during the cell-ECM interaction. Unfolded talin links to vinculin, promoting the adhesion and translocation of nuclear YAP, ECM modelling and gene expression. Hence, traction forces influence biochemical and biomechanical signals and dictate changes in cell phenotype (Lekka *et al.*, 2021).

Factors such as ECM stiffness and thickness significantly affect the tension applied by the cells and the resulting strain or deformation. The substrate intrinsic elastic modulus on thick substrates defines the effective substrate stiffness the cells perceive. However, this correlation between the intrinsic elastic modulus and the effective stiffness might not happen on thin substrates, which might also influence cell behaviour (Dembo and Wang, 1999). Boudou *et al.*, 2009 found that hydrogel thickness and nonlinear material properties impact the quantification of cellular forces on hydrogels  $\leq 60 \mu\text{m}$ .

Cells must apply greater forces to deform a stiff or soft, thin material which is attached to an underlying rigid material than a soft, thick substrate, where the resulting forces can be strong enough to generate high strains unimpeded by proximal rigid support (Butler *et al.*, 2001; Boudou *et al.*, 2009). A substrate comprising a PAAm attached to an underlying rigid material may not behave linearly when forces generated by the cells are large (Boudou *et al.*, 2009). Harris and collaborators started using a very elastic thin material on the surface of liquid silicone to analyse the forces exerted by the cells that were visible and semiquantitative (Dembo and Wang, 1999).

After a cell attaches to a soft substrate, it applies mechanical forces and generates a strain on the underlying hydrogel. The strain can be measured by tracking the displacements of fluorescent microbeads embedded in the substrate by traction force microscopy. The displacements of the fluorescent microbeads are used to compute the cell-induced forces, providing information about the applied cell forces that guide cell behaviour (Zancla *et al.*, 2022).

Reinhart-King *et al.*, 2008 showed that cells mechanically influence the behaviour of their neighbours by generating cellular traction stresses through the material/substrate. Similarly, mechanical communication in MG63 single cells and colonies through PAAm hydrogels was reported by Tusan *et al.*, 2018. Furthermore, the authors showed that cell colonies could sense the hydrogel thickness to a greater depth than single cells and propagate the forces far away from the colony periphery, which might influence their mechanical response.

These studies indicate that cell traction forces may influence how the neighbouring cells perceive the actual substrate mechanical properties, respond and influence critical processes such as differentiation.

Cell differentiation depends on the cell maturation state that, at the same time, might be influenced by the substrate stiffness; the maturation time decreases on stiff substrates by reducing the internal cell deformation (Mousavi and Doweidar, 2015). Traction forces might also influence cell differentiation by causing chromatin repositioning and modifications in the nuclei structure (Heo *et al.*, 2017). The actin cytoskeleton is rearranged during cell differentiation, influencing the cell's mechanical properties and traction forces (McAndrews *et al.*, 2015).

To sum up, quantifying the cell-induced deformations on PAAm hydrogels might provide information about the effect of ECM mechanical properties on cell traction forces and cell differentiation.

## 6.2 Aims

- To evaluate Stro-1<sup>+</sup> BMSCs stiffness sensing by quantifying the induced displacements on soft and stiff polyacrylamide hydrogels with different thicknesses at different time points using time-lapse displacement tracking microscopy.
- To evaluate if the increase in seeding density of Stro-1<sup>+</sup> BMSCs modifies their stiffness sensing on soft, thick polyacrylamide hydrogels in basal and osteogenic media for 1 day by quantifying hydrogel displacements by time-lapse displacement tracking microscopy.
- To evaluate if changes in seeding densities modify Stro-1<sup>+</sup> BMSCs mechanosensing on soft, thick polyacrylamide hydrogels in basal and osteogenic media on days 1, 7 and 14 by quantifying hydrogel's displacements.
- To test if the addition of osteogenic or adipogenic supplements influences stiffness sensing of Stro-1<sup>+</sup> BMSCs on soft and stiff PAAm hydrogels with different thicknesses on days 7 and 14 by quantifying the hydrogel deformations.

## 6.3 Results

### 6.3.1 Structure of soft and stiff PAAM hydrogels

Cells sense hydrogel stiffness by applying traction forces, which might cause a deformation that traction force microscopy studies can quantify. Cells are plated on PAAM hydrogels containing fluorescent microbeads, producing deformation and the displacements of the microbeads from the original position, which are quantified (Lekka *et al.*, 2021).

Figure 6.1 confirms the previous results in Chapter 3 (Figure 3.4), where fluorescent microbeads embedded in the PAAM hydrogels are accommodated in lines, forming different patterns on soft hydrogels regardless of their thickness. Contrastingly, fluorescent microbeads on stiff hydrogels are equally distributed all over the surface, where no wrinkles were observed.

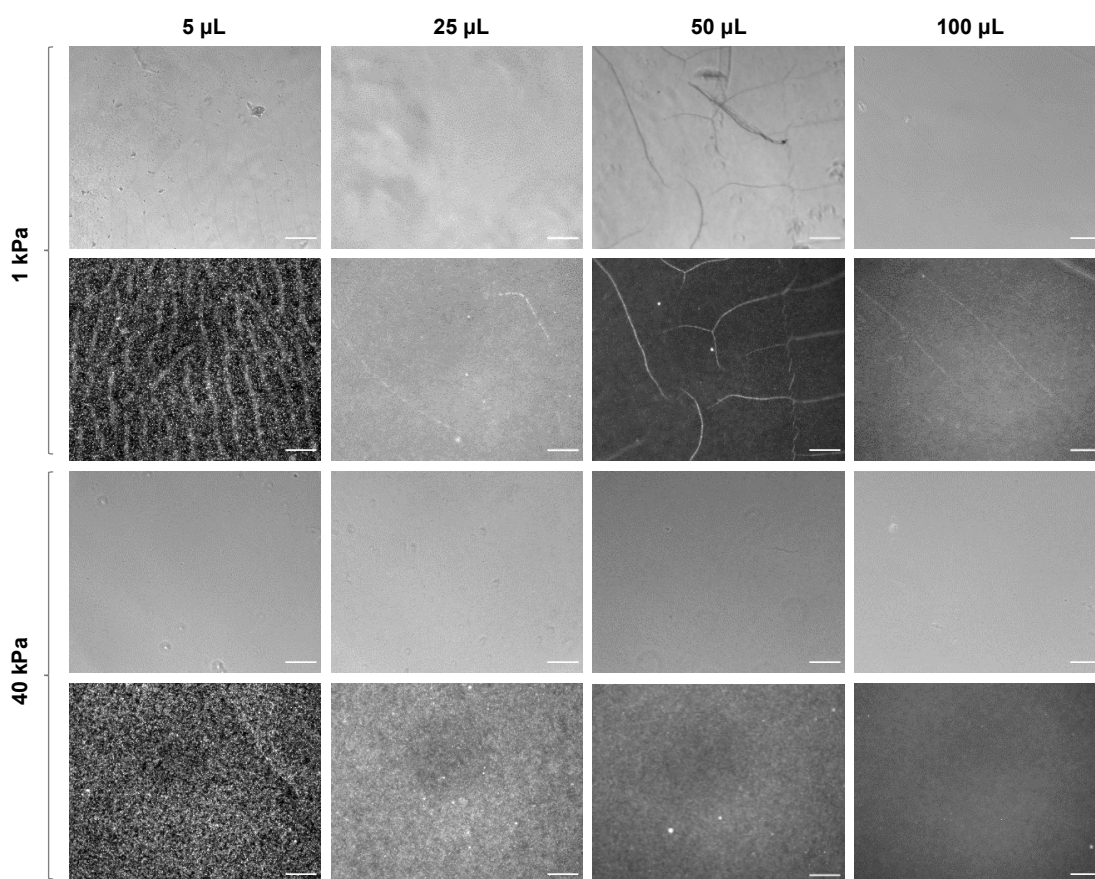


**Figure 6.1 Phase-contrast and fluorescent images of soft and stiff PAAM hydrogels with different thicknesses containing embedded fluorescent microbeads.** Microbeads were distributed within the stiff PAAM hydrogels, whereas they lined up about the wrinkles on the surface of soft hydrogels. Pictures were taken under a Nikon Eclipse Ti inverted microscope at 10X magnification. Scale bar: 100  $\mu\text{m}$ .

### 6.3.2 Soft and stiff hydrogel deformations by Stro-1<sup>+</sup> BMSCs during cell spreading

Time-lapse imaging was used for displacement microscopy studies to determine how cells perceive the rigidity of materials. Briefly, cells plated on soft and stiff PAAm hydrogels with different thicknesses were photographed every 5 minutes for a defined time using a Nikon Eclipse Ti inverted microscope. The phase-contrast and fluorescent images were extracted from the initial file in nd2 format and divided into folders corresponding to each location. The images corresponding to each hour were selected, renamed, and uploaded into a MATLAB algorithm. Firstly, a grid (10 x 8) was drawn, producing 99 nodes or locations for the analysis. The algorithm quantifies the displacements from the first image taken at 5 min (p01) to the following taken every hour (p02, p03, p24, etc.) at each node. The displacement data from the 99 nodes per hour in 3 hydrogel triplicates were used to calculate the 90<sup>th</sup> percentiles and standard deviation at each hour (see Section 2.2.10.2 in Chapter 2 for further details). These data were plotted in GraphPad Prism as XY graphs, and the average of the 90<sup>th</sup> percentiles corresponding to the stationary phase as grouped graphs.

The first interaction between the cells and the ECM occurs during cell spreading. Therefore, the first experiment aimed to evaluate hydrogel displacements generated by Stro-1<sup>+</sup> BMSCs during this process. Stro-1<sup>+</sup> BMSCs (F63, passage 4) were plated at 1,000 cells/cm<sup>2</sup> on soft and stiff PAAm (with different thicknesses: 5  $\mu$ L (thin) and 25  $\mu$ L (thick)), with embedded fluorescent microbeads and in  $\alpha$ -MEM medium + 1% BSA. After cell attachment, the well-plate was placed under the Nikon Eclipse Ti inverted microscope at 37°C and 5% CO<sub>2</sub>. Cells were located, and the time-lapse experiment was initiated 1 hour after seeding the cells and carried out for 24 hours. Hydrogel deformations are best observed by viewing the supplementary videos simultaneously; please refer to them for more information (list of accompanying material). Coloured vectors represent the direction and magnitude of the hydrogel displacement. Blue vectors represent small displacements, whereas orange and red vectors exhibit more significant displacements. Figure 6.2 shows the cells' representative phase-contrast and fluorescent images on soft, thick PAAm hydrogels every 6 hours. After 24 hours, Stro-1<sup>+</sup> BMSCs spread and modified their morphology on the soft, thick hydrogels ( $282.27 \pm 49.5 \mu\text{m}$ ) (Supplementary Video 1a), and additional wrinkles were seen in the fluorescent channel (Supplementary Video 1b), indicated with a white, thick arrow on the upper left and central section of the hydrogel. In contrast, Figure 6.3 shows that cells on the stiff, thick hydrogel ( $144.46 \pm 6.55 \mu\text{m}$ ) spread (Supplementary Video 2a) and no wrinkles were observed at the beginning and end of the experiment (Supplementary Video 2b).

Deformations caused by Stro-1<sup>+</sup> BMSCs depended on the substrate thickness (pictures not included). Cells on soft, thin hydrogels ( $64.3 \pm 11.3 \mu\text{m}$ ) spread and extend after 24 hours

in the phase contrast images (Supplementary Video 3a). No new wrinkles or patterns on the hydrogels can be observed in the fluorescent images (Supplementary Video 3b). Cells on stiff, thin hydrogels spread ( $27.15 \pm 6.54 \mu\text{m}$ ), but no deformations were appreciated on the fluorescent images (Supplementary Videos 4a, 4b).

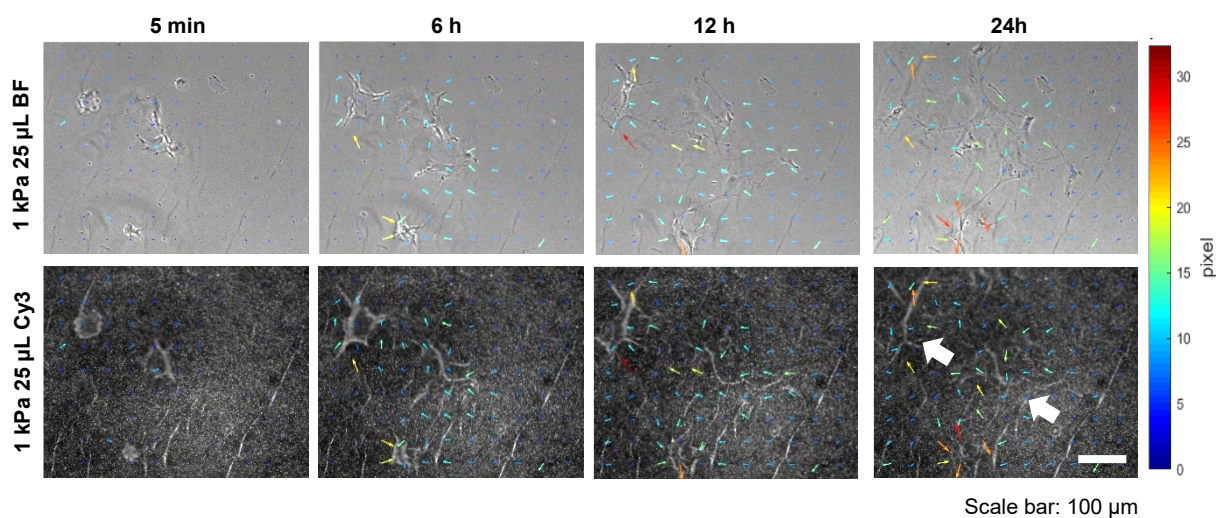


**Figure 6.6.2 Time-lapse imaging of the Stro-1<sup>+</sup> BMSCs on soft, thick PAAm hydrogels with embedded fluorescent microbeads.** Cell movements promote wrinkles formation over time which are indicated with white arrows, and hydrogel's deformations are indicated by coloured arrows. Phase-contrast (BF) and fluorescent (Cy3) images were obtained at 10X magnification under a Nikon Eclipse Ti inverted microscope.

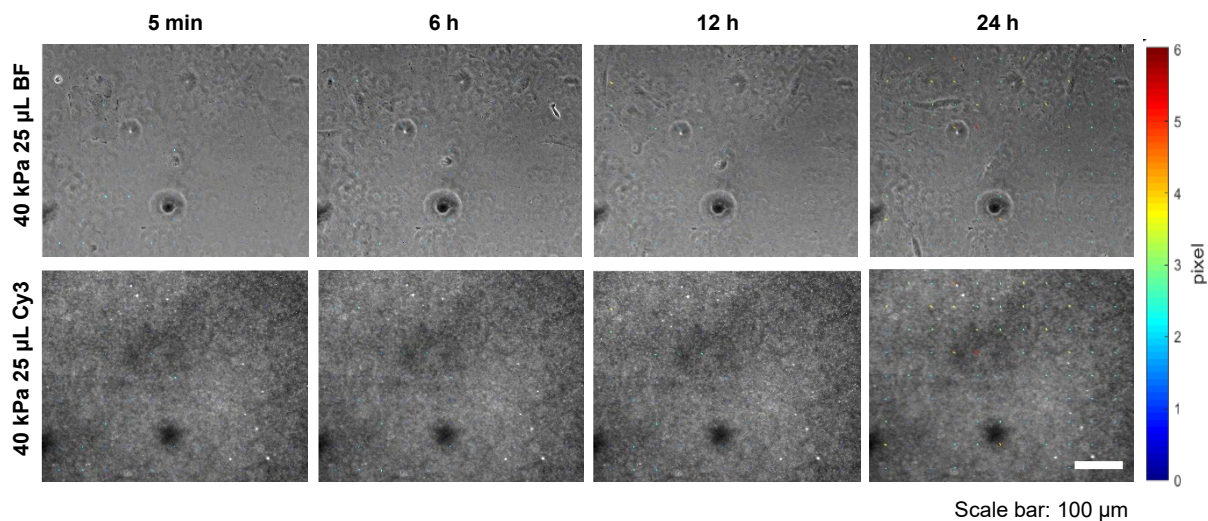


**Figure 6.3 Time-lapse imaging of the Stro-1<sup>+</sup> BMSCs on stiff, thick PAAm hydrogels with embedded fluorescent microbeads.** Cells hardly deform hydrogels, so no more wrinkles are formed despite cells moving around on the hydrogel's surface. Phase-contrast (BF) and fluorescent (Cy3) images were obtained at 10X magnification under a Nikon Eclipse Ti inverted microscope.

In summary, deformations on soft hydrogels (close to the cells) gradually increased, being more evident on soft, thick than soft, thin hydrogels at 24h. In contrast, fewer cells were observed on stiff hydrogels, and small deformations were seen. This confirms that cells can sense the stiffness and thickness of the PAAm hydrogels as they begin to spread.

The mean of the 90<sup>th</sup> percentiles of the hydrogel displacements at each hour (24) at the 99 nodes from the 3 hydrogel triplicates were plotted in Figure 6.4 (a). It shows that hydrogel deformations increased with time, greater on soft hydrogels than their counterparts. The mean of the 90th percentiles of the displacements at each hour during the stationary phase (from 9h to 24h) were plotted in Figure 6.4 (b). Soft, thick PAAm hydrogels exhibited more significant deformations ( $5.4 \pm 0.5 \mu\text{m}$ ) compared to soft, thin hydrogels ( $14.2 \pm 0.6 \mu\text{m}$ ). In contrast, stiff hydrogels were hardly deformed; stiff, thin hydrogels exhibited the lowest deformations ( $0.6 \pm 0.06 \mu\text{m}$ ) compared to stiff, thick hydrogels ( $1.6 \pm 0.4 \mu\text{m}$ ).

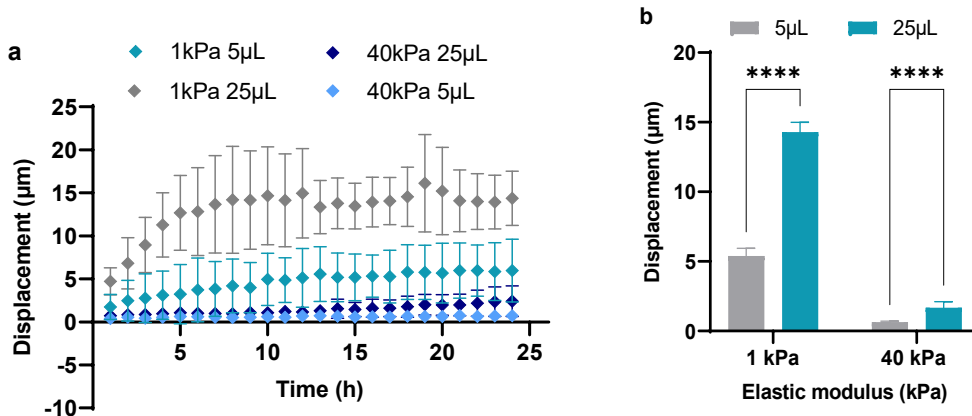


**Figure 6.4 Hydrogel displacements by Stro-1<sup>+</sup> BMSCs 1 h after seeding.** (a) Hydrogel displacements increased over time and were greater on soft hydrogels than on stiff matrices. Diamonds represent the mean and SD of the 90th percentiles of displacements at the 99 nodes ( $n = 3$  hydrogels). (b) Stro-1<sup>+</sup> BMSCs created more significant deformations on thick than thin PAAm hydrogels, regardless of the hydrogel rigidity. Statistical analysis was calculated by the Two-way ANOVA method; \*\*\*\*  $p < 0.0001$ .

The effect of hydrogel stiffness and thickness on cell spreading after 24 hours was evaluated in Chapter 4. Figure 6.4 confirmed that hydrogel displacements increased with time after 24 hours of incubation. However, crucial processes such as cell differentiation for bone regeneration require more time. For instance, the osteogenic commitment of BMSCs requires at least 7 days, while BMSCs' adipogenic differentiation needs 14 days. Hence, the following experiment aimed to evaluate and quantify the hydrogel deformations after 10 days and 7 weeks of incubation.

### 6.3.3 Effect of cell crowding on hydrogel deformations by Stro-1<sup>+</sup> BMSCs

Engler *et al.*, 2006 highlighted that stiff materials promote osteogenic differentiation, whereas soft matrices are neurogenic. Nonetheless, results presented in Chapter 5 showed that Stro-1<sup>+</sup> BMSCs differentiated into osteoblasts on stiff but also soft PAAm hydrogels. These results might suggest that the increase in cell density and/or cell crowding after 7-14 days of incubation might increase the apparent stiffness sensed by the cells, favouring BMSCs' osteogenic differentiation on soft hydrogels. If this were the case, soft hydrogels

would be more challenging to deform when cell crowding increases. This hypothesis was tested next by evaluating the hydrogel deformations by Stro-1<sup>+</sup> BMSCs on day 10.

Figure 6.5 compares representative fluorescent images of Stro-1<sup>+</sup> BMSCs on soft, stiff, thin, and thick PAAm hydrogels every 6 hours on day 10. Cell density appeared higher on soft, thick (Supplementary Video 5a) than soft, thin (Supplementary Video 5b) hydrogels. Coloured arrows represent the increase in hydrogel displacements, being more evident on soft, thick (Supplementary Video 6a) than soft, thin hydrogels (Supplementary Video 6b). In contrast, supplementary videos show that cells move on stiff, thick (Supplementary Video 7a) and soft, thin (Supplementary Video 7b) hydrogels but do not deform the material (Supplementary Videos 8a and 8b).

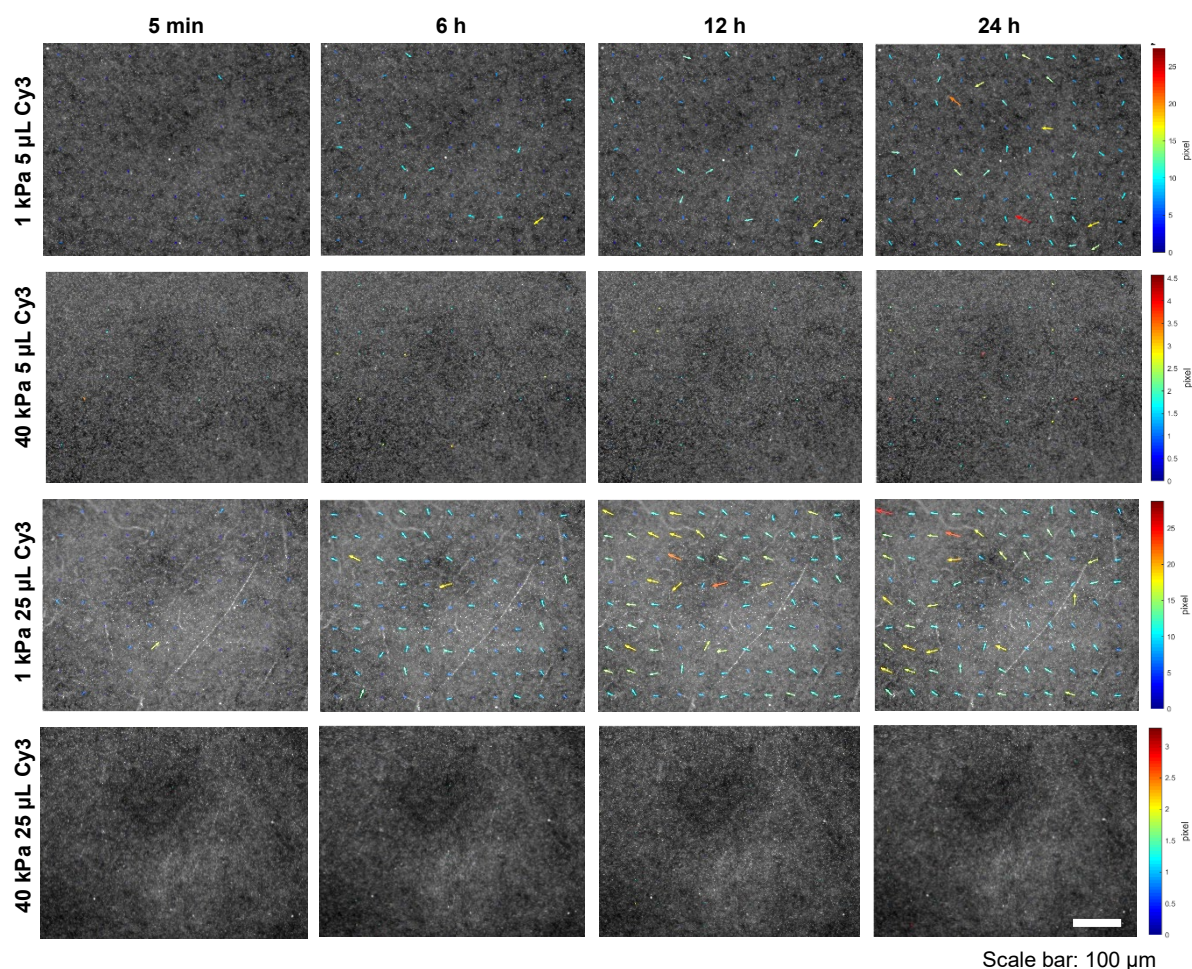


**Figure 6.5** Representative fluorescent images of Stro-1<sup>+</sup> BMSCs on soft, stiff, thin, and thick PAAm hydrogels with embedded fluorescent microbeads on day 10. The most significant deformations were presented on soft, thick PAAm hydrogels, followed by soft, thin matrices. No deformations were identified on stiff hydrogels.

Similarly to the previous experiment, hydrogel displacements were quantified in MATLAB, and 90<sup>th</sup> percentiles were plotted in Figure 6.6 (a). Hydrogel displacements gradually increased on soft matrices, being more significant on soft, thick hydrogels and remaining stable on stiff hydrogels regardless of their thickness. Newly, the 90<sup>th</sup> percentiles of the hydrogel displacements from 9 to 24 hours are plotted in Figure 6.6 (b). Hydrogel's

displacements were significantly greater on soft, thick ( $12.5 \pm 0.8 \mu\text{m}$ ) compared to soft, thin ( $6.6 \pm 0.6 \mu\text{m}$ ) matrices, whereas no significant difference was identified when modifying the thickness of stiff PAAm hydrogels (thick:  $0.8 \pm 0.05 \mu\text{m}$ ; thin:  $0.9 \pm 0.1 \mu\text{m}$ ).

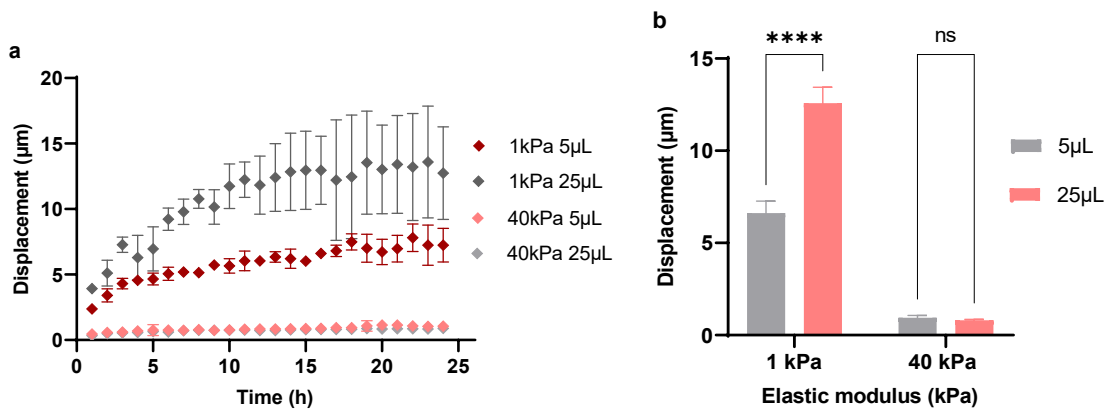


**Figure 6.6 Hydrogel displacements by Stro-1<sup>+</sup> BMSCs after 10 days of incubation.** (a) Hydrogel displacements gradually increased over time and were greater on soft hydrogels than on stiff matrices. Diamonds represent the mean and SD of the 90<sup>th</sup> percentiles of the displacements at the 99 nodes (n=3 hydrogels). (b) Soft hydrogels exhibited greater displacements than soft, thin matrices. In contrast, hydrogel thickness did not impact hydrogel displacements on stiff hydrogels. 2way ANOVA method was used to calculate significant differences between groups. \*\*\*\* p< 0.0001.

Stro-1<sup>+</sup> BMSCs were incubated for 7 weeks, hydrogel displacements were quantified, and 90<sup>th</sup> percentiles were calculated. Figure 6.7 compares phase-contrast and fluorescent images of Stro-1<sup>+</sup> BMSCs on soft, thick (Supplementary Video 9a) and soft, thin (Supplementary Video 9b) PAAm hydrogels. Cell density on week 7 increased on all hydrogels compared to day 10, hindering their spreading and influencing their morphology. The red arrows on soft, thick (Supplementary Video 10a) and soft, thin (Supplementary Video 10b) hydrogel indicate the areas where hydrogel deformations were encountered.

Figure 6.8 enumerates the 90<sup>th</sup> percentiles of the hydrogel displacements generated by Stro-1<sup>+</sup> BMSCs on PAAm hydrogels on week 7. Figure 6.8 (a) Hydrogel displacements remained similar over time regardless of the stiffness and thickness. However, Figure 6.8 (b) shows that hydrogel displacements were still more significant on soft, thick hydrogels ( $3.3 \pm 0.2 \mu\text{m}$ ) compared to soft, thin counterparts ( $2.1 \pm 0.1 \mu\text{m}$ ). At the same time, more significant displacements were quantified on stiff, thin ( $2.4 \pm 0.1 \mu\text{m}$ ) compared to thick hydrogels ( $0.4 \pm 0.05 \mu\text{m}$ ).

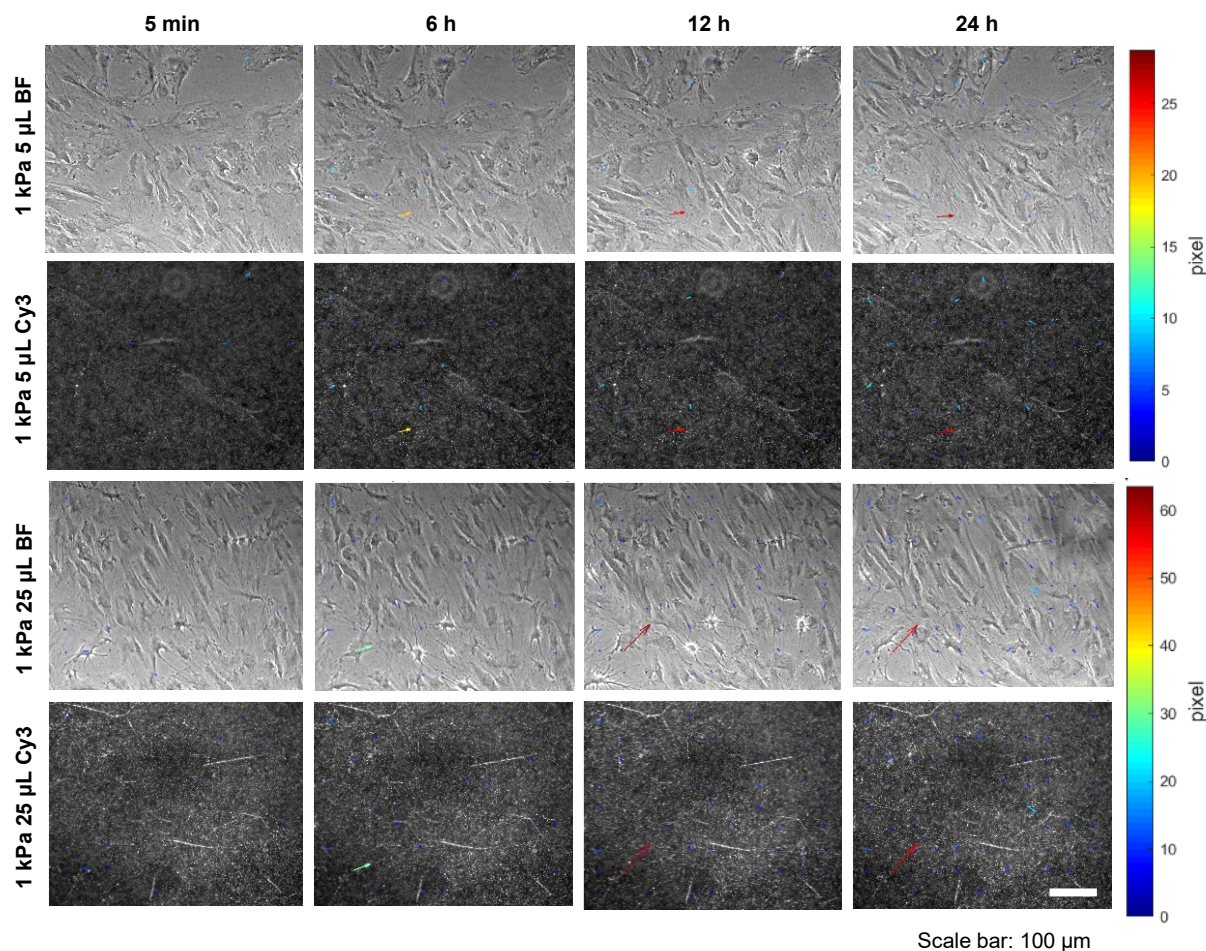


**Figure 6.7** Phase-contrast and fluorescent images of Stro-1<sup>+</sup> BMSCs on soft, thin and soft, thick PAAm hydrogels with embedded fluorescent microbeads in week 7 over 24 h. Cell crowding was evident on PAAm hydrogels regardless of their thickness, which impeded hydrogel deformations. Cell morphology is difficult to define due to high cell crowding. Red arrows indicate the area where soft hydrogels displayed higher deformations.

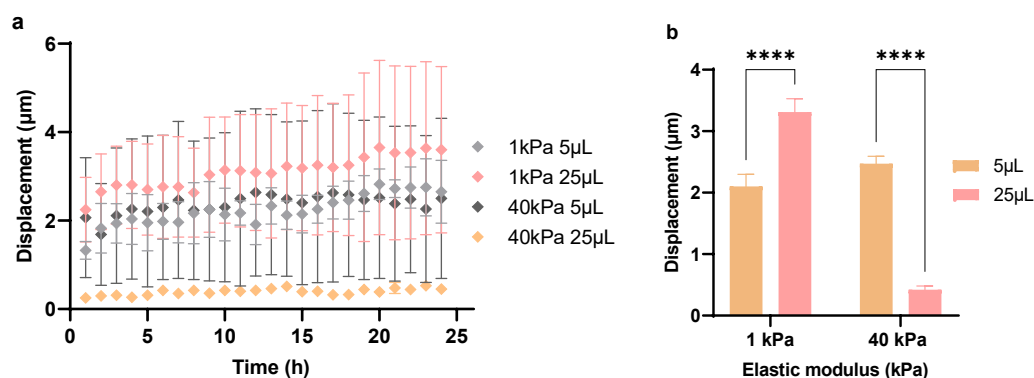


**Figure 6.8** Hydrogel deformations remained stable over 24 h on week 7, regardless of their mechanical properties. **(a)** Hydrogel deformations remained similar over time. Diamonds represent the mean and SD of the 90<sup>th</sup> percentile displacements at the 99 nodes ( $n=3$  hydrogels). **(b)** Compared to their counterparts, greater deformations were quantified on soft, thick hydrogels and stiff, thin matrices. \*\*\*\* =  $p < 0.0001$ .

Figure 6.9 shows that hydrogel displacements on soft, thick, and stiff, thick hydrogels decreased with cell crowding from day 1 to week 7. Therefore, the capacity of Stro-1<sup>+</sup>

BMSCs to differentiate on soft matrices might be highly related to the increase in the apparent hydrogel stiffness.

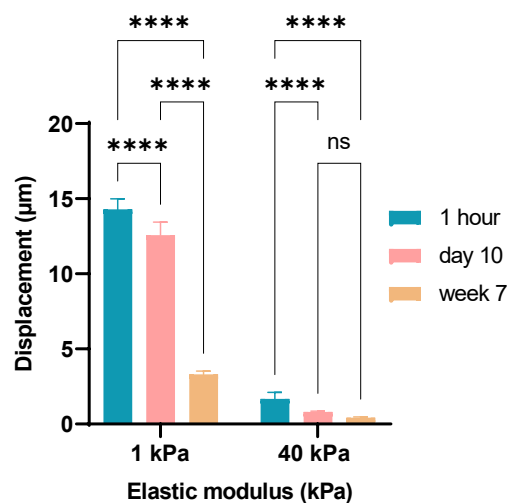


**Figure 6.9 Displacements on soft, thick, and stiff, thick PAAm hydrogel decreased from day 0 to week 7.** Mean displacements of the 90<sup>th</sup> Percentile at the 99 nodes in the 3 hydrogel triplicates per condition (n=3) were plotted, and significant differences were obtained by the 2way ANOVA method. 1kPa hydrogels: 1 hour (14.3 ± 0.6 µm) vs day 10 (12.6 ± 0.8 µm); 1 hour (14.3 ± 0.6 µm) vs week 7 (3.3 ± 0.2 µm); day 10 (12.6 ± 0.8 µm) vs week 7 (3.3 ± 0.2 µm). 40 kPa: 1 hour (1.7 ± 0.4 µm) vs day 10 (0.8 ± 0.05 µm); 1 hour (1.7 ± 0.4 µm) vs week 7 (0.4 ± 0.05 µm); day 10 (0.8 ± 0.05 µm) vs week 7 (0.4 ± 0.05 µm). \*\*\*\*= p<0.0001.

### 6.3.4 Effect of the seeding density on hydrogel deformations

Further experiments evaluated the effect of the initial seeding density on hydrogel displacements under basal and osteogenic conditions. Firstly, Stro-1<sup>+</sup> BMSCs (F67, passage 6) were plated on soft, thick (25 µL) PAAm hydrogels at 1,000, 5,000, 10,000 and 20,000 cells/cm<sup>2</sup> in basal (Supplementary Videos 11a-11d) and osteogenic (Supplementary Videos 12a-12d) medium for 24 h. Figure 6.10 illustrates that cell density increases with the seeding density in basal and osteogenic media. However, cell density seems more significant in the presence of osteogenic supplements at 5,000, 10,000 and 20,000 cells/cm<sup>2</sup>. More arrows indicate hydrogel deformations on hydrogels with cells at 1,000 and 5,000 cells/cm<sup>2</sup> compared to hydrogels with higher seeding densities regardless of media conditions.

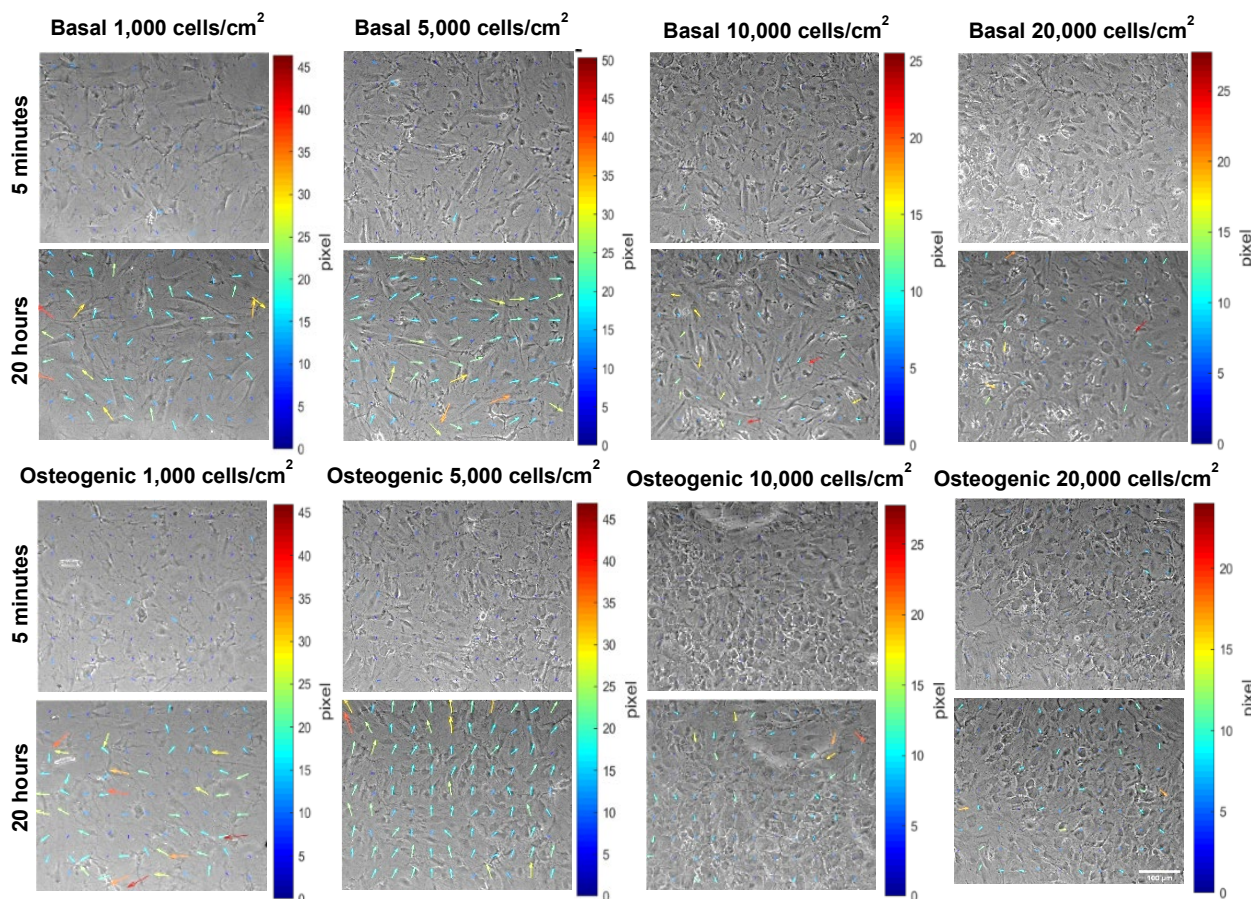


**Figure 6.10** Phase-contrast images of Stro-1<sup>+</sup> BMSCs at different seeding densities on soft, thick PAAm hydrogels in basal and osteogenic media at the beginning and end of the time-lapse experiment. The increase in cell seeding density and osteogenic supplements increase cell crowding and influence cell arrangement. Coloured arrows indicate more significant hydrogel displacements when plated at 1,000 and 5,000 cells/cm<sup>2</sup>. Images were obtained at 10X magnification with a Nikon Eclipse Ti inverted microscope.

90<sup>th</sup> percentiles of the hydrogel displacements were plotted in Figure 6.11. (a) They slightly increased for the first 9 hours and remained similar for the following hours; however, more significant deformations were generated with cells at 1,000 cells/cm<sup>2</sup>. (b) Hydrogels were more challenging to deform at higher seeding densities: 5,000 (basal:  $13.6 \pm 1.0 \mu\text{m}$ ; osteogenic:  $15.9 \pm 1.1 \mu\text{m}$ ), 10,000 (basal:  $11.7 \pm 0.9 \mu\text{m}$ ; osteogenic:  $7.4 \pm 1.0 \mu\text{m}$ ) and 20,000 cells/cm<sup>2</sup> (basal:  $6.3 \pm 0.4 \mu\text{m}$ ; osteogenic:  $8.8 \pm 0.4 \mu\text{m}$ ) compared to 1,000 cells/cm<sup>2</sup> (basal:  $21.8 \pm 1.1 \mu\text{m}$ ; osteogenic:  $16.7 \pm 0.6 \mu\text{m}$ ). Interestingly, cells at 5,000 and 20,000 cells/cm<sup>2</sup> created greater hydrogel deformations in osteogenic media, whereas cells at 1,000 and 10,000 cells/cm<sup>2</sup> easily deform the material in basal conditions.

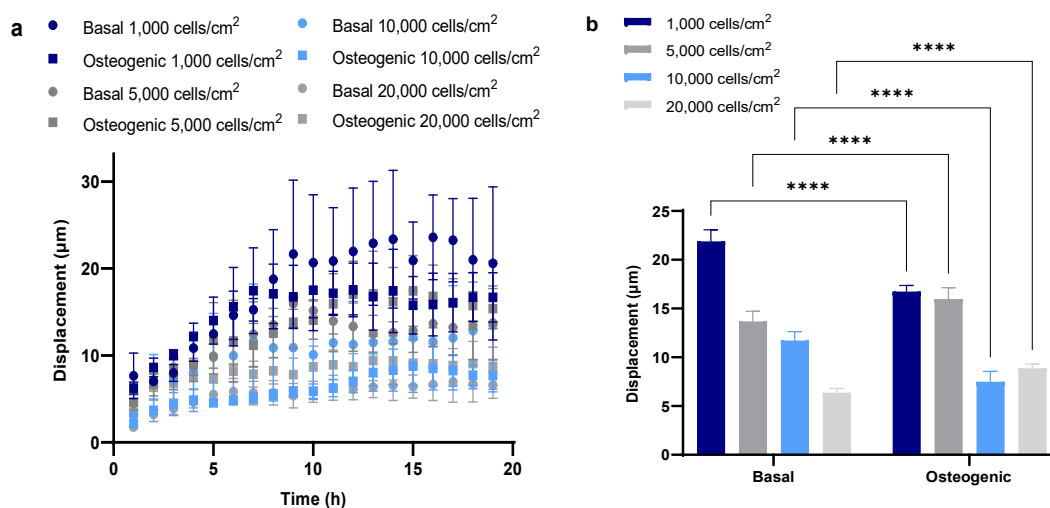
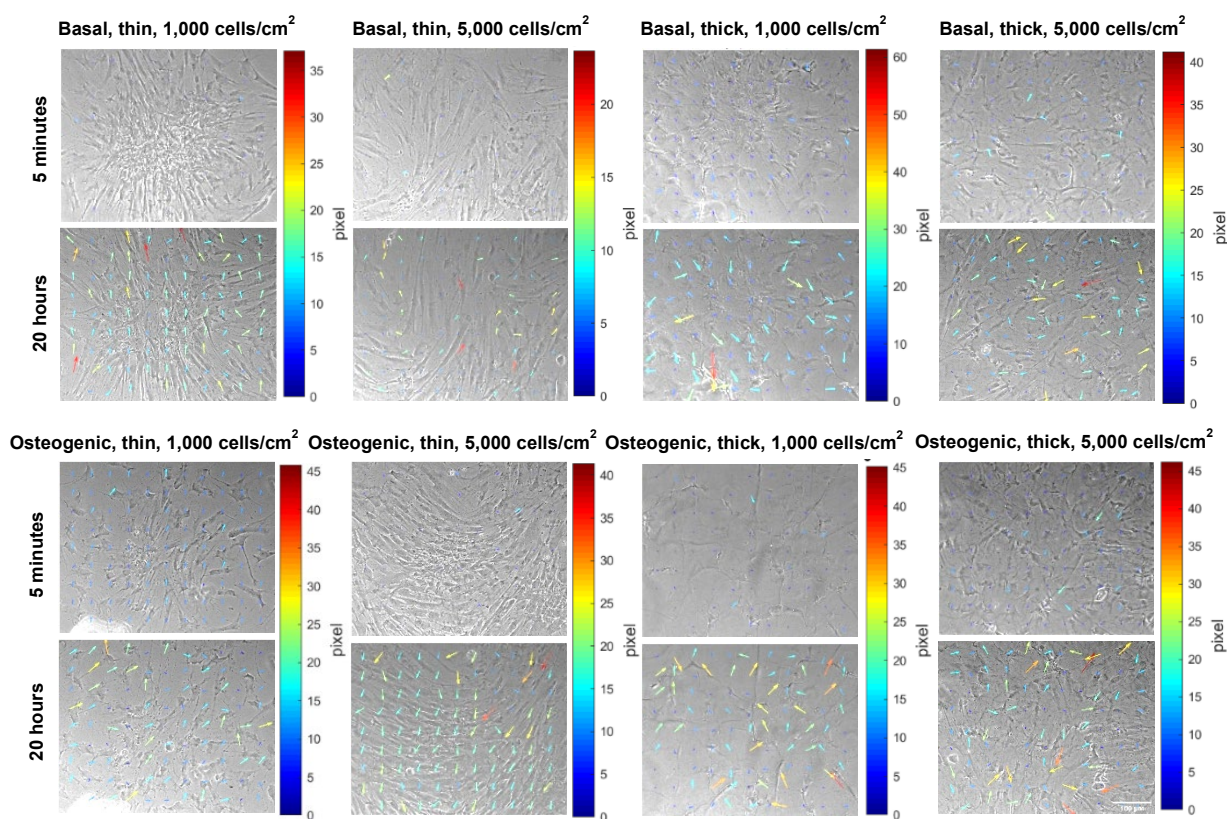


**Figure 6.11 Soft, thick hydrogel deformations decreased with the increase of the seeding density. (a)** Hydrogel deformations remained similar with the increase in time in the experiment's last hours. Diamonds represent the mean and SD of the 90<sup>th</sup> percentiles of displacements of the 99 nodes ( $n=3$  hydrogels). **(b)** Stro-1<sup>+</sup> BMSCs created greater hydrogel deformations at lower seeding densities. The presence of osteogenic supplements influenced them. Significant differences between groups were calculated by the 2-way ANOVA method. \*\*\*\* =  $p < 0.0001$ .

### 6.3.5 Hydrogel deformations by Stro-1<sup>+</sup> BMSCs at low seeding densities during osteogenic differentiation

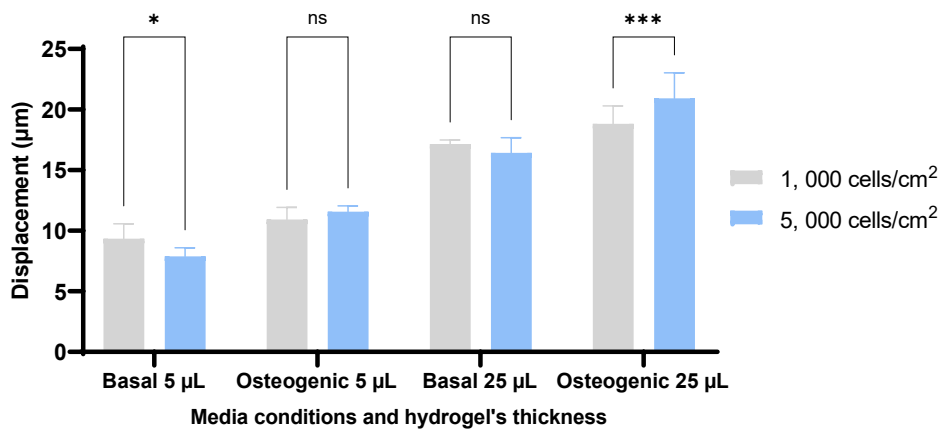
After confirming that seeding density and medium conditions influenced hydrogel deformations, the following experiments evaluated hydrogel deformations by Stro-1<sup>+</sup> BMSCs at low seeding densities in basal and osteogenic conditions on days 1, 7 and 14. For this, Stro-1<sup>+</sup> BMSCs (F67, P4) were plated at 1,000 and 5,000 cells/cm<sup>2</sup> on soft, thin (5  $\mu$ L) and thick (25  $\mu$ L) PAAm hydrogels in basal and osteogenic media for 14 days.

Figure 6.12 shows Stro-1<sup>+</sup> BMSCs on soft, thin, and thick PAAm hydrogels at different seeding densities in basal and osteogenic media on day 1. Fewer cells were observed at 1,000 cells/cm<sup>2</sup> on soft, thin hydrogels in basal (Supplementary Video 13a) compared to the osteogenic medium (Supplementary Video 13b). Elongated cells were appreciated at 5,000 cells/cm<sup>2</sup> on soft, thin hydrogels in basal media (Supplementary Video 14a) but compressed and crowded in osteogenic conditions (Supplementary Video 14b). Cells at 1,000 cells/cm<sup>2</sup> on soft, thick hydrogels appeared immersed in the hydrogels in basal media (Supplementary Video 15a), while they were difficult to distinguish in osteogenic media (Supplementary Video 15b). On soft, thick hydrogels, cells at 5,000 cells/cm<sup>2</sup> were elongated and widely distributed on the hydrogel surface in basal media (Supplementary Video 16a) but spread and crowded in osteogenic media (Supplementary Video 16b). More significant hydrogel deformations are indicated in coloured arrows.



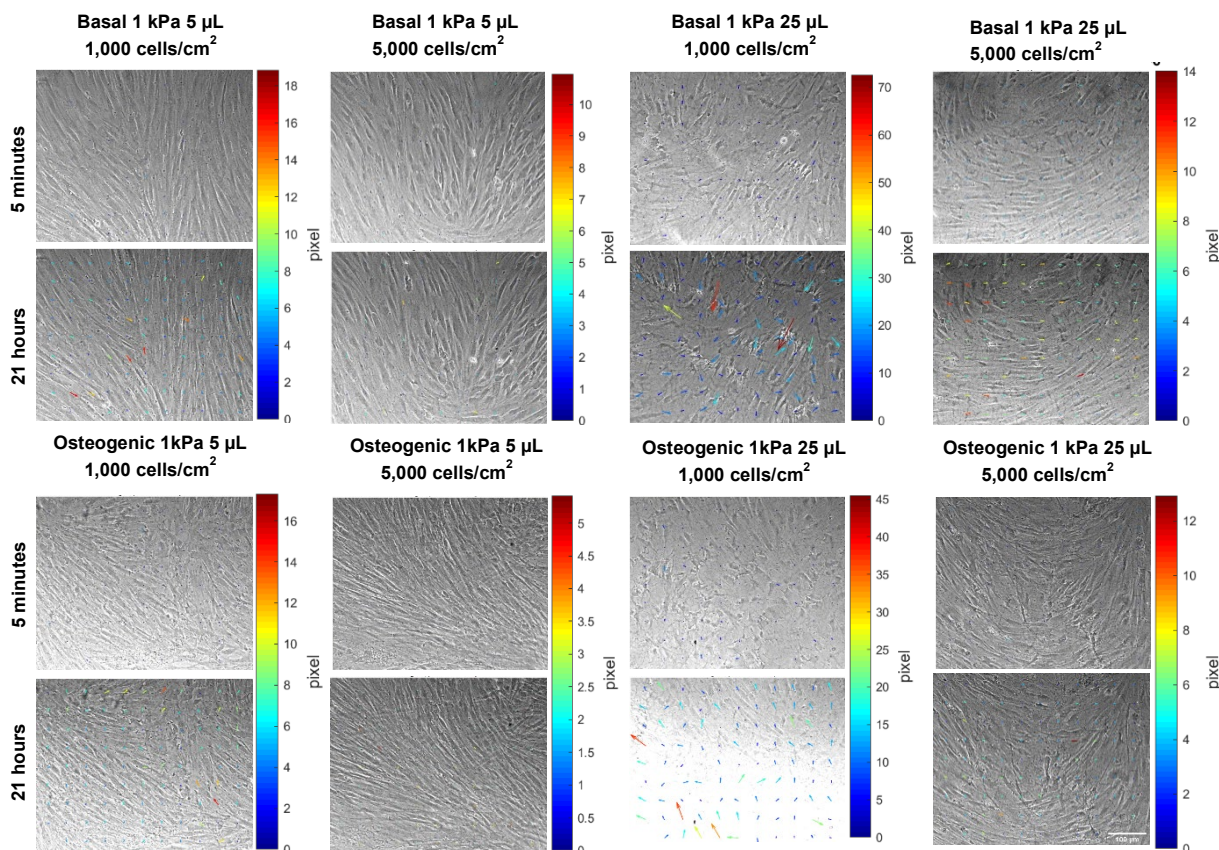
**Figure 6.12** Phase-contrast images of Stro-1<sup>+</sup> BMSCs on soft, thin, and thick PAAm hydrogels in basal and osteogenic media at low seeding densities at 5 minutes and 20 hours on day 1. Cell morphology and alignment varied with the increase in seeding density, the addition of osteogenic supplements and hydrogel thickness. Coloured arrows indicate more significant hydrogel displacements when plated at 1,000 and 5,000 cells/cm<sup>2</sup>. Images were obtained at 10X magnification with a Nikon Eclipse Ti inverted microscope.

Figure 6.13 compares the hydrogel displacements on soft and stiff PAAm hydrogels with different thicknesses by Stro-1<sup>+</sup> at 1,000 and 5,000 cells/cm<sup>2</sup> in basal and osteogenic medium. Cells generated more significant displacements in the presence of osteogenic supplements than in basal medium on soft, thin (left) (basal: 1,000 cells/cm<sup>2</sup>:  $9.3 \pm 1.2 \mu\text{m}$ ; 5,000 cells/cm<sup>2</sup>:  $7.8 \pm 0.7 \mu\text{m}$ ; osteogenic: 1,000 cells/cm<sup>2</sup>:  $10.9 \pm 1.0 \mu\text{m}$ ; 5,000 cells/cm<sup>2</sup>:  $11.5 \pm 0.4 \mu\text{m}$ ) and soft, thick (right) (basal: 1,000 cells/cm<sup>2</sup>:  $17.1 \pm 0.3 \mu\text{m}$ ; 5,000 cells/cm<sup>2</sup>:  $16.4 \pm 1.2 \mu\text{m}$ ; osteogenic: 1,000 cells/cm<sup>2</sup>:  $18.8 \pm 1.4 \mu\text{m}$ ; 5,000 cells/cm<sup>2</sup>:  $20.9 \pm 2.0 \mu\text{m}$ ) hydrogels. Displacements were greater on soft, thick hydrogels than on soft, thin hydrogels in basal and osteogenic mediums. Additionally, there were significant differences in hydrogel deformations when cells were plated at different seeding densities. Greater displacements were quantified at 1,000 cells/cm<sup>2</sup> than 5,000 cells/cm<sup>2</sup> on soft, thin hydrogels in basal medium and 5,000 cells/cm<sup>2</sup> compared to 1,000 cells/cm<sup>2</sup> on soft, thick hydrogels in osteogenic medium.



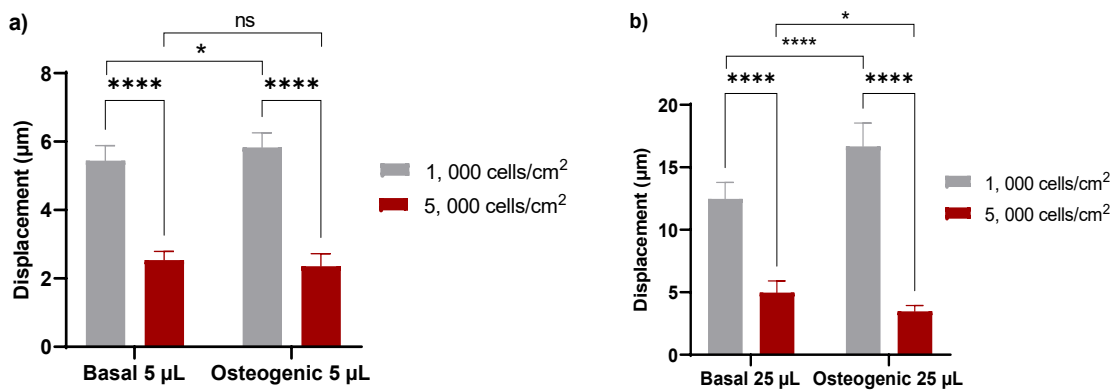
**Figure 6.13 Soft, thick hydrogels were highly deformed; displacements increased in osteogenic conditions and were influenced by seeding density on day 1.** Soft, thick hydrogels exhibited more deformations than their soft, thin counterparts. Stro-1<sup>+</sup> BMSCs generated greater displacements on soft, thin hydrogels in osteogenic medium than in basal medium. Cells caused more displacements at 1,000 cells/cm<sup>2</sup> than 5,000 cells/cm<sup>2</sup> on soft, thin hydrogels in basal media. Greater displacements were quantified on soft, thick hydrogels in osteogenic media. More significant displacements were quantified when cells were plated at 5,000 cells/cm<sup>2</sup> than 1,000 cells/cm<sup>2</sup>. Bars represent the mean and SD of the 90<sup>th</sup> percentiles in the 99 nodes (n=3 hydrogels) of the last 11 hours of the experiment. Significant differences between groups were calculated by the 2-way ANOVA method. \*\*\*\* = p < 0.0001.

The following experiment aimed to test the hypothesis that hydrogel displacements might decrease on day 7 after cell differentiation. Figure 6.14 illustrates that Stro-1<sup>+</sup> BMSCs at 1,000 cells/cm<sup>2</sup> appeared thin, elongated, and parallel on soft, thin hydrogels in basal media but disorganised in osteogenic media. Cells appeared thicker at 5,000 cells/cm<sup>2</sup> in basal media but thin in osteogenic media. In basal and osteogenic media, spread cells were seen on soft, thick hydrogels at 1,000 cells/cm<sup>2</sup>. Meanwhile, cells were organised but difficult to distinguish at 5,000 cells/cm<sup>2</sup> in basal media and disarranged in osteogenic media.



**Figure 6.14** Stro-1<sup>+</sup> BMSCs on soft, thin, and thick PAAm hydrogels at different seeding densities in basal and osteogenic conditions on day 7. Cell crowding increased, and alignment and morphology varied when modifying hydrogel mechanical properties, seeding density and media conditions. Coloured arrows indicate more significant displacements on soft, thick hydrogels under basal conditions. Images were obtained at 10X magnification with a Nikon Eclipse Ti inverted microscope.

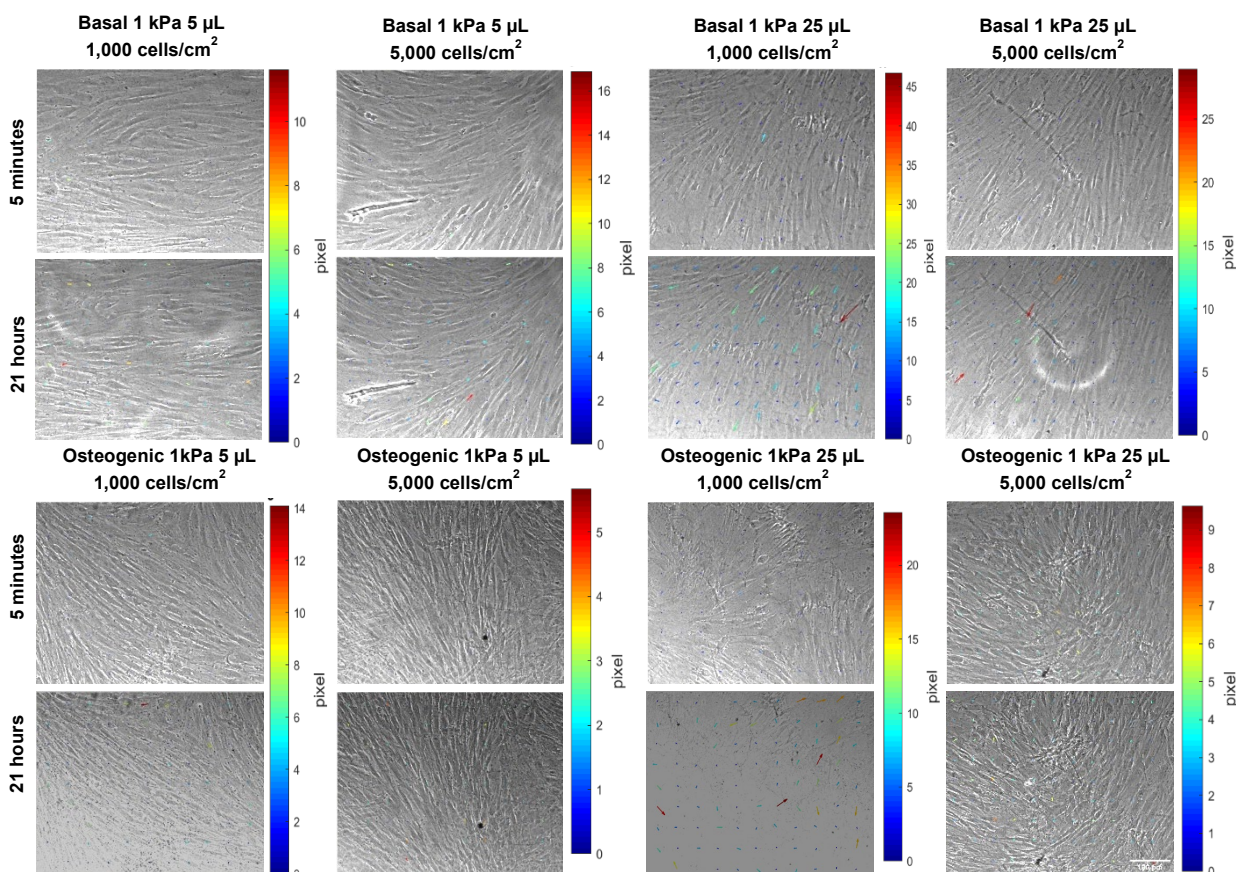
Figure 6.15 highlights that hydrogel deformations were more significant on soft, thick hydrogels (b) compared to soft, thin (a) counterparts on day 7. Nevertheless, displacements decreased from  $18.8 \pm 1.4 \mu\text{m}$  on day 1 to  $16.6 \pm 1.8 \mu\text{m}$  on day 7 in basal media. Cells created more significant displacements under osteogenic conditions on soft, thin hydrogels (basal:  $5.4 \pm 0.4 \mu\text{m}$ ; osteogenic:  $5.8 \pm 0.4 \mu\text{m}$ ) but more significant on soft, thick hydrogels (basal:  $12.4 \pm 1.3 \mu\text{m}$ ; osteogenic:  $16.6 \pm 1.8 \mu\text{m}$ ) at  $1,000 \text{ cells/cm}^2$ . Also, hydrogels exhibited greater displacements when cells were plated at lower seeding density regardless of hydrogel thickness and media conditions. For instance:  $1,000 \text{ cells/cm}^2$ :  $16.6 \pm 1.8 \mu\text{m}$ ;  $1,000 \text{ cells/cm}^2$ :  $3.4 \pm 0.4 \mu\text{m}$  on soft, thick hydrogels in osteogenic conditions.



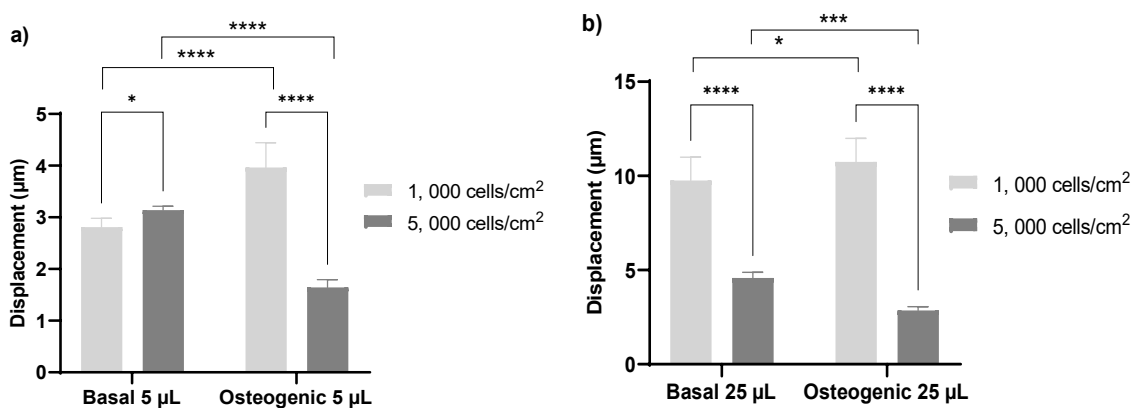
**Figure 6.15 Stro-1<sup>+</sup> BMSCs created greater deformations on soft, thick hydrogels at low seeding density and in osteogenic conditions on day 7.** Soft, thick hydrogels showed more displacements than soft, thin hydrogels, greater when cells were plated at lower seeding density. **(a)** Stro-1<sup>+</sup> BMSCs at 1,000 cells/cm<sup>2</sup> produced greater displacements in the presence of osteogenic supplements on soft, thin hydrogels. **(b)** More significant displacements were produced by cells at 1,000 cells/cm<sup>2</sup> on soft, thick hydrogels in the presence of osteogenic supplements. Bars represent the mean and SD of the 90<sup>th</sup> percentile of the displacements at the 99 nodes (n=3 hydrogels) at the last 12 hours of the experiment. Statistical analysis was done using the 2-way ANOVA method. \*\*\*\*=p<0.0001.

Figure 6.16 illustrates that after 14 days of incubation, cell crowding increased. Thick and organised cells were observed on soft, thin hydrogels in basal media at 1,000 and 5,000 cells/cm<sup>2</sup>, but thinner and disorganised cells appeared under osteogenic conditions. Spread cells were observed on soft, thick hydrogels in basal media (Supplementary Video 17a) regardless of the seeding density and in osteogenic media at 1,000 cells/cm<sup>2</sup> (Supplementary Video 17b). Still, they were very thin and disorganised in osteogenic media at 5,000 cells/cm<sup>2</sup>.

Figure 6.17 shows that soft, thick hydrogels (b) suffered greater deformations than soft, thin matrices (a). Displacements were greater in the osteogenic medium when plated at 1,000 cells/cm<sup>2</sup> (osteogenic: 3.9 ± 0.4 µm; basal: 2.8 ± 0.1 µm) and in basal media at 5,000 cells/cm<sup>2</sup> (basal: 3.1 ± 0.07 µm; osteogenic: 1.6 ± 0.1 µm) on soft, thin hydrogels. Displacements were greater on soft, thick hydrogels in osteogenic media at 1,000 cells/cm<sup>2</sup>. (osteogenic: 10.7 ± 1.2 µm; basal: 9.7 ± 1.2 µm) and in basal media at 5,000 cells/cm<sup>2</sup> (basal: 4.5 ± 0.2 µm; osteogenic: 2.8 ± 0.2 µm).



**Figure 6.16** Stro-1<sup>+</sup> BMSCs at 1,000 and 5,000 cells/cm<sup>2</sup> on 1kPa PAAm hydrogels with different thicknesses in basal and osteogenic media on day 14. Cell crowding was higher in osteogenic media than basal media, and cell arrangement varied with the changes in hydrogel thickness and media conditions. The presence of a few coloured arrows indicates that soft hydrogels suffered small displacements on day 14.

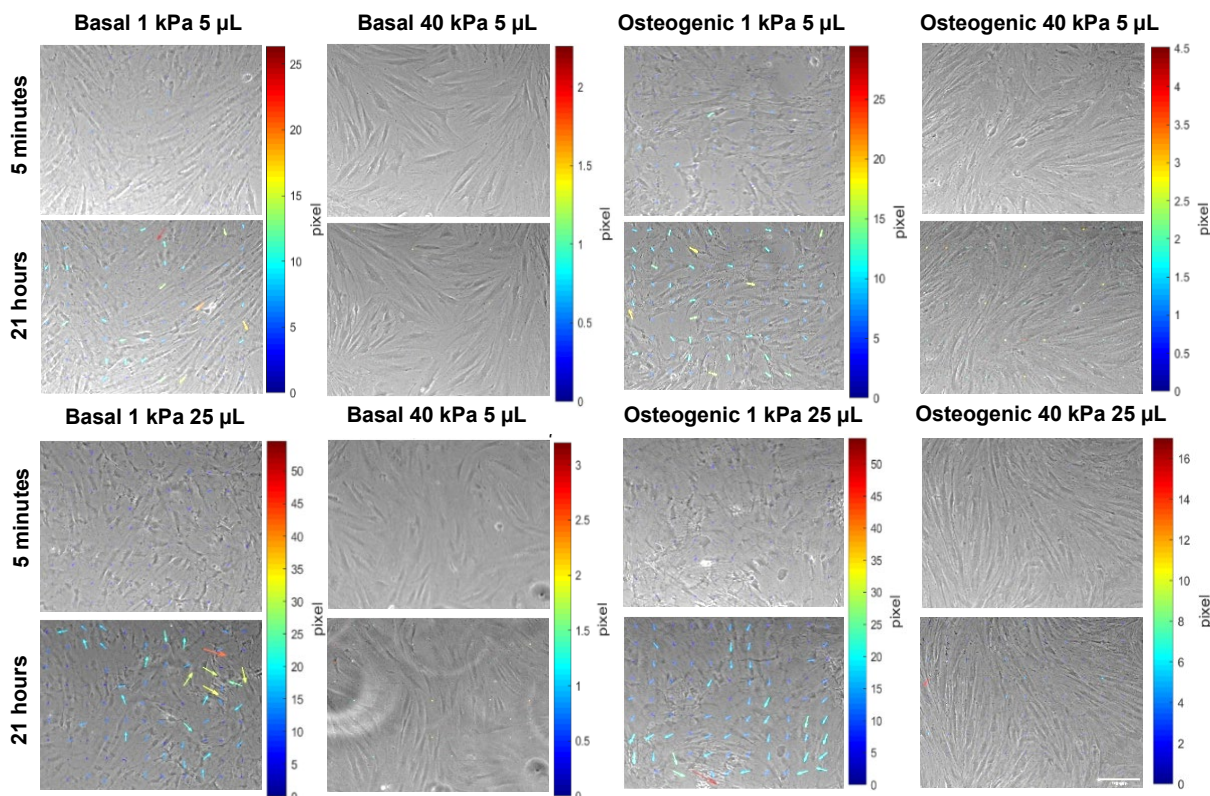


**Figure 6.17** Stro-1<sup>+</sup> BMSCs at lower seeding densities produced greater deformations on soft, thick hydrogels in osteogenic medium on day 14. Soft, thick hydrogels were more deformed than soft, thin hydrogels. **(a)** Cells at 1,000 cells/cm<sup>2</sup> caused greater displacements on soft, thin hydrogels in osteogenic medium than in the basal but more in basal conditions when plated at 5,000 cells/cm<sup>2</sup>. **(b)**. Greater displacements were produced on soft, thick hydrogels by cells at 1,000 cells/cm<sup>2</sup> in osteogenic media but in basal media at 5,000 cells/cm<sup>2</sup>. Bars represent the mean and SD of the 90<sup>th</sup> percentiles of the hydrogel displacements in the 99 nodes (n=3 hydrogels) in the last 11 h. Statistical differences between groups were calculated by the 2-way ANOVA method. \*\*\*\* = p < 0.0001.

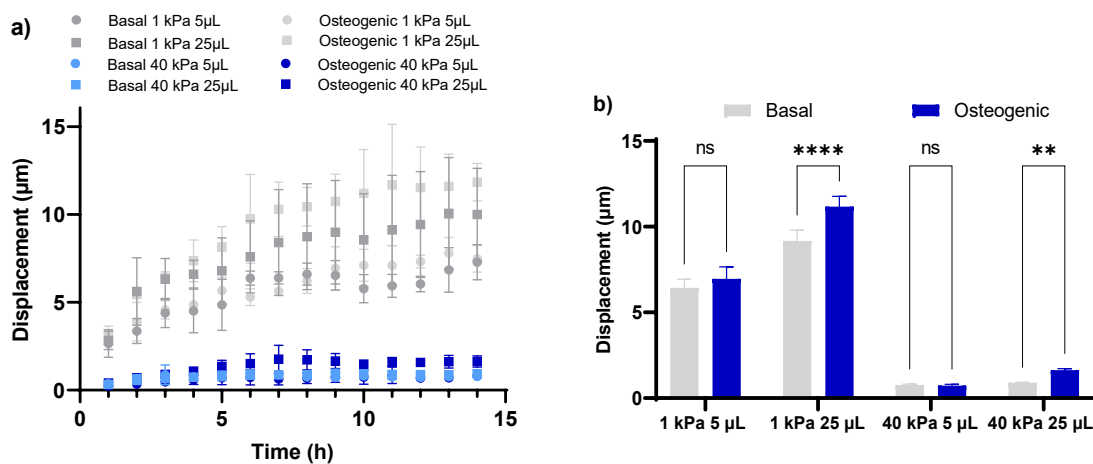
To summarise, hydrogel deformations decreased from day 1 to day 14 and were smaller when cells were plated at higher seeding densities (5,000 cells/cm<sup>2</sup>). Also, deformations were more significant on soft, thick hydrogels than on soft, thin hydrogels by cells plated at 1,000 cells/cm<sup>2</sup>. Thus, cell crowding might override the effect of substrate stiffness by hindering hydrogel deformations.

Hydrogel deformations by Stro-1<sup>+</sup> BMSCs from the same sample (F67) were evaluated in a second experiment using an earlier passage (P2). 5,000 cells/cm<sup>2</sup> were plated on soft and stiff PAAm hydrogels with different thicknesses (5 and 25  $\mu$ L), and time-lapse imaging was carried out on day 4 and day 7. Figure 6.18 illustrates thin cells in soft, thin hydrogels but cells immersed in soft, thick hydrogels. In contrast, extended cells were visible on stiff hydrogels regardless of the hydrogel thickness in basal media. In osteogenic media, irregular cells were observed on soft and thin hydrogels, difficult to distinguish on soft and thick hydrogels and huge and thin cells on stiff thin, and thick hydrogels.

Figure 6.19 indicates that displacements on soft hydrogels increased over time while the deformations on stiff matrices remained stable during the 14 hours of the experiment. The last 8h of the experiment were presented in the bar graph, showing that Stro-1<sup>+</sup> BMSCs exerted greater deformations on soft, thick hydrogels in osteogenic media ( $11.1 \pm 0.5 \mu\text{m}$ ) compared to basal media ( $9.1 \pm 0.6 \mu\text{m}$ ) and soft, thin hydrogels (basal:  $6.4 \pm 0.5 \mu\text{m}$ ;  $6.9 \pm 0.7 \mu\text{m}$ ). Stiff hydrogels were hardly deformed regardless of the hydrogel thickness (5  $\mu$ L: basal:  $0.7 \pm 0.04 \mu\text{m}$ ; osteogenic:  $0.7 \pm 0.07 \mu\text{m}$ ; 25  $\mu$ L: basal:  $9.1 \pm 0.6 \mu\text{m}$ ; osteogenic:  $11.1 \pm 0.5 \mu\text{m}$ ).

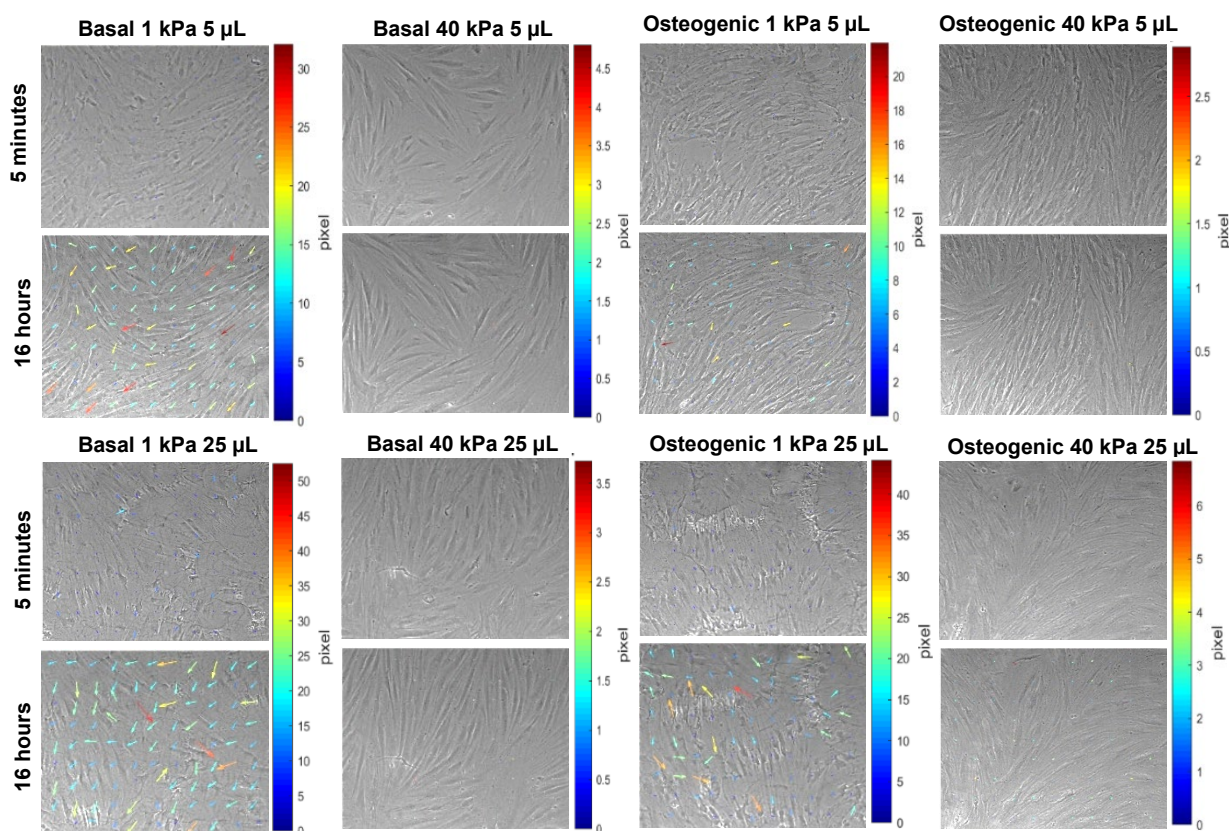


**Figure 6.18** Stro-1<sup>+</sup> BMSCs at 5,000 cells/cm<sup>2</sup> on soft, stiff, thin, and thick PAAm hydrogels in basal and osteogenic media on day 4. Cell morphology varied on soft hydrogels depending on the hydrogel thickness, and osteogenic media increased cell crowding. The presence of coloured arrows on soft, thin, and thick hydrogels in basal and osteogenic media indicates more significant displacements.



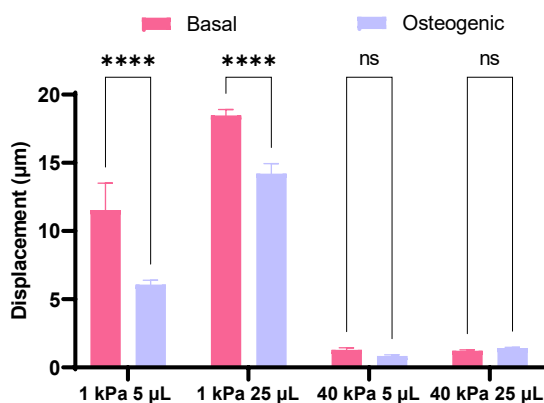
**Figure 6.19** Stro-1<sup>+</sup> BMSCs at 5,000 cells/cm<sup>2</sup> produced the greatest deformations on soft, thick hydrogels in osteogenic media on day 4. **(a)** Hydrogel deformations gradually increased over time on soft, thick hydrogels and remained stable on stiff hydrogels. Diamonds represent the mean and SD of the 90<sup>th</sup> percentile of displacements at the 99 nodes (n=3 hydrogels). **(b)** Stro-1<sup>+</sup> BMSCs created greater deformations on soft, thick hydrogels in osteogenic compared to basal media, and smaller deformations were quantified on stiff, thin and thick hydrogels. Statistical differences between groups were calculated by the 2-way ANOVA method. \*\*\*\* = p < 0.0001.

Figure 6.20 illustrates that cell morphology is similar between soft, thin, and thick hydrogels in basal medium but appears different in the presence of osteogenic supplements. Thinner cells were seen on soft, thin hydrogels and extended and formed networks on soft, thick counterparts. Cell crowding increased in basal medium compared to osteogenic conditions.



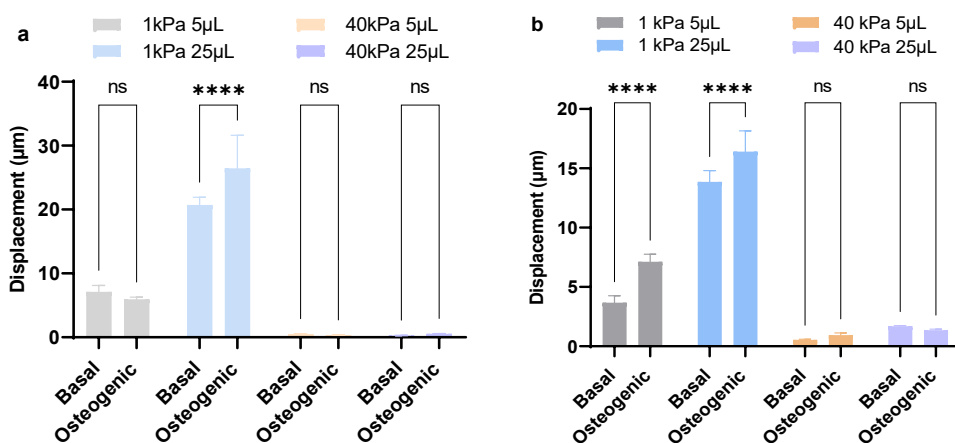
**Figure 6.20** Stro-1<sup>+</sup> BMSCs on soft, stiff, thin, and thick PAAm hydrogels in basal and osteogenic conditions on day 7. Cell morphology on soft hydrogels varied when modifying the hydrogel thickness and in the presence of osteogenic supplements. More significant displacements on soft, thin, and thick hydrogels in basal media and soft and thick in osteogenic conditions are indicated in coloured arrows.

Interestingly, after 7 days of incubation, Stro-1<sup>+</sup> BMSCs caused more hydrogel displacements on soft hydrogels in basal conditions (5 μL:  $11.5 \pm 1.9$  μm; 25 μL:  $18.4 \pm 0.4$  μm) compared to osteogenic media (5 μL:  $6.0 \pm 0.3$  μm; 25 μL:  $14.2 \pm 0.7$  μm); suggesting cells might grow faster in osteogenic compared to basal media. Meanwhile, stiff hydrogels were hardly deformed regardless of their thickness and the presence of osteogenic supplements (Figure 6.21).



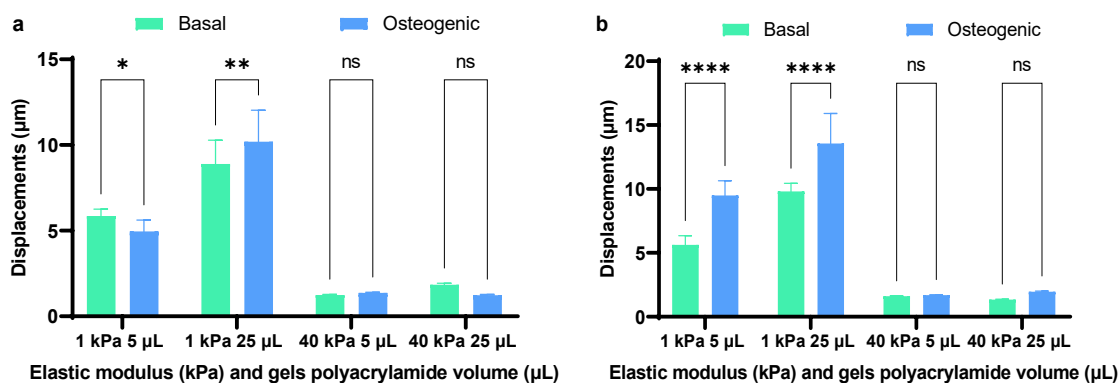
**Figure 6.21 Stro-1<sup>+</sup> BMSCs at 5,000 cells/cm<sup>2</sup> generated greater deformations in basal medium on soft PAAm hydrogels on day 7.** Stro-1<sup>+</sup> BMSCs created greater deformations on soft, thick hydrogels in basal compared to osteogenic medium and slight deformations on stiff hydrogels. Bars represent the mean and SD of the 90<sup>th</sup> percentiles of the displacements at the 99 nodes in the last 8h of the experiment (n=3 hydrogels). Statistical differences between groups were calculated by the 2-way ANOVA method. \*\*\*\* = p < 0.0001.

A similar experiment evaluated the cellular forces applied by Stro-1<sup>+</sup> BMSCs at 1,000 cells/cm<sup>2</sup> isolated from a different sample (F63, P6) on soft and stiff hydrogels during osteogenic differentiation for 7 days. Figure 6.22 enumerates that hydrogel deformations were more significant on soft, thick PAAm hydrogels in osteogenic media (26.4 ± 5.1 µm) compared to basal media (basal: 20.7 ± 1.2 µm) on day 1. Hydrogel displacements decreased on day 7; hydrogels were still more deformed in osteogenic media compared to basal media on soft, thin (7.1 ± 0.6 µm vs 3.6 ± 0.5 µm) and thick hydrogels (16.4 ± 1.7 µm vs 13.8 ± 0.9 µm).



**Figure 6.22 Hydrogel deformations by Stro-1<sup>+</sup> BMSCs at 1,000 cells/cm<sup>2</sup> during osteogenic differentiation on day 1 and day 7.** (a) Displacements on soft, thick hydrogels increased in the presence of osteogenic supplements on day 1. (b) Soft, thin, and thick hydrogels displayed greater deformations in osteogenic conditions on day 7. Bars represent the mean and SD of the 90<sup>th</sup> percentiles of the displacements at the 99 nodes in the last 7h of the experiment (n=3 hydrogels). Statistical analysis was done using the 2-way ANOVA method. \*\*\*\* = p < 0.0001.

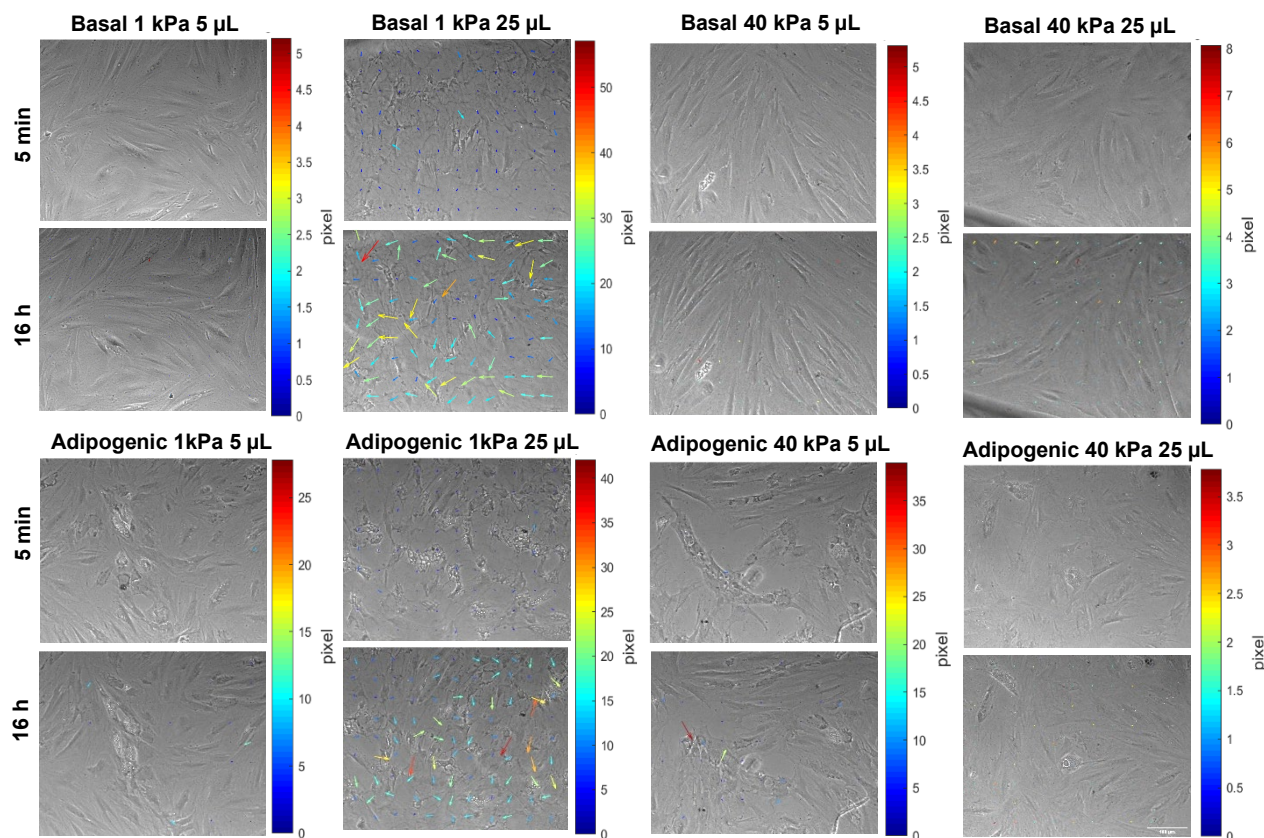
Stro-1<sup>+</sup> BMSCs at 1,000 cells/cm<sup>2</sup> from a different sample (M55, P5) exhibited similar behaviour. Figure 6.23 (a) shows that cells created greater hydrogels deformations on soft, thick gels (basal:  $8.8 \pm 1.3 \mu\text{m}$ ; osteogenic:  $10.1 \pm 1.8 \mu\text{m}$ ) than on soft, thin (basal:  $5.8 \pm 0.4 \mu\text{m}$ ; osteogenic:  $4.9 \pm 0.6 \mu\text{m}$ ) counterparts and increased in the presence of osteogenic supplements on day 1. Figure 6.23 (b) illustrates that the same trend remains after 7 days of incubation; soft, thick hydrogels in osteogenic media were more deformed compared to basal conditions ( $13.5 \pm 2.3 \mu\text{m}$  vs  $9.8 \pm 0.6 \mu\text{m}$ ).



**Figure 6.23 Hydrogel displacements by Stro-1<sup>+</sup> BMSCs at 1,000 cells/cm<sup>2</sup> increased in the presence of osteogenic supplements on day 1 and day 7. (a)** Displacements on soft, thick hydrogels increased in osteogenic conditions and were greater on soft, thin hydrogels in basal media on day 1. **(b).** Soft, thin, and thick hydrogels displayed greater deformations in osteogenic conditions on day 7. Bars represent the mean and SD of the 90<sup>th</sup> percentile of the displacements at the 99 nodes in the last 12 h of the experiment (n=3 hydrogels). Statistical differences were calculated using the 2-way ANOVA method. \*\*\*\* = p < 0.0001.

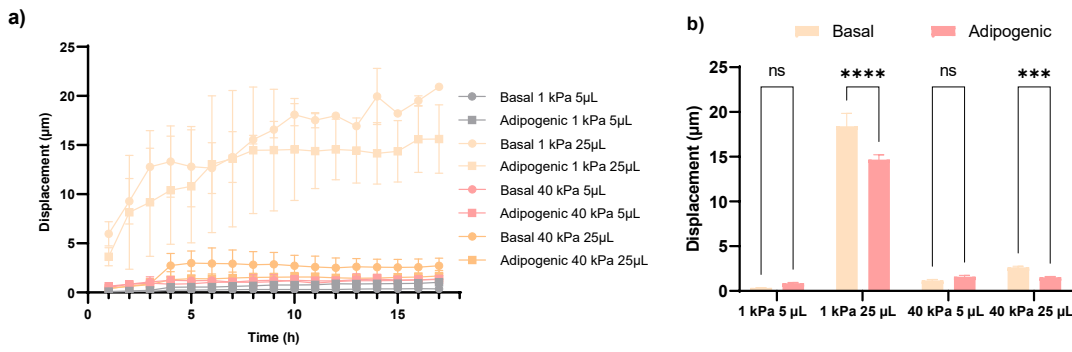
### 6.3.6 BMSCs adipogenic and osteogenic differentiation and hydrogel deformations

BMSCs have the potential to differentiate into osteoblasts but also adipocytes. Therefore, the following experiments aimed to evaluate the hydrogel deformations caused by cells in adipogenic conditions. Figure 6.24 compares the morphology of Stro-1<sup>+</sup> BMSCs (F67, P3) at 5,000 cells/cm<sup>2</sup> on soft and stiff PAAm matrices in basal and adipogenic media on day 7. Long and thin cells were observed on soft, thin hydrogels in basal conditions, whereas shorter and thicker cells accumulating lipids were seen in adipogenic conditions. Cells were difficult to distinguish on soft, thick PAAm hydrogels in basal media but acquired irregular forms in the presence of adipogenic supplements. Thin and long cells were also observed on stiff, thin, and thick hydrogels in basal media. In contrast, cells with varying sizes and forms were observed on stiff hydrogels in adipogenic media.



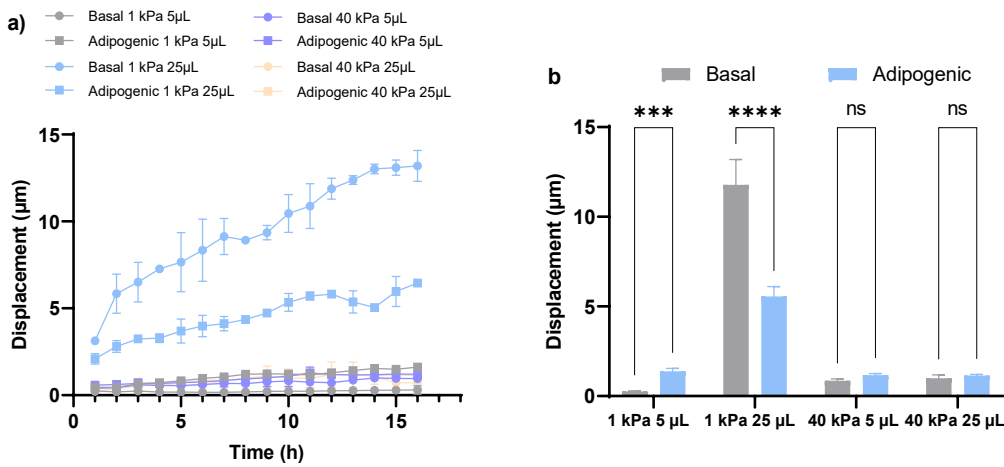
**Figure 6.24 Morphology of Stro-1<sup>+</sup> BMSCs on PAAm hydrogels of different elasticity and thickness during adipogenic differentiation on day 7.** Lipid accumulation was evident on soft, thin, and soft, thick PAAm hydrogels and shorter cells with lipids on stiff hydrogels. Coloured arrows on soft, thick hydrogels in adipogenic conditions indicate more significant hydrogel deformations. Pictures were taken with a Nikon Eclipse Ti inverted microscope at 10X.

Figure 6.25 (a) shows that displacements gradually increased over time on soft, thick hydrogels in basal and adipogenic conditions on day 7 and remained steady on soft, thin, and stiff hydrogels regardless of hydrogel thickness and the presence of adipogenic supplements. The average of the hydrogel deformations from the last 9h of the time-lapse experiment in Figure 6.25 (b) indicates that soft, thick hydrogels were easily deformed in basal media (basal:  $18.4 \pm 1.4 \mu\text{m}$ ; adipogenic:  $14.6 \pm 0.5 \mu\text{m}$ ) whereas more minor deformations were quantified on stiff, thick hydrogels in basal media (basal:  $2.6 \pm 0.1 \mu\text{m}$ ; adipogenic:  $1.5 \pm 0.06 \mu\text{m}$ ).



**Figure 6.25 Adding adipogenic supplements decreased hydrogel displacements by Stro-1<sup>+</sup> BMSCs on day 7. (a)** Soft, thick hydrogel displacements gradually increased over time. **(b)** Hydrogel deformations decrease on soft and stiff, thick hydrogels with adipogenic supplements. Bars represent the mean and SD of the 90<sup>th</sup> percentile of the displacements at the 99 nodes in the last 9h of the experiment (n=3 hydrogels). The 2-way ANOVA method was used to calculate any significant difference between groups. \*\*\*\* = p < 0.0001.

Figure 6.26 (a) outlines that after 14 days of incubation, displacements increased on soft, thick hydrogels but remained small on stiff (thin and thick) and soft, thin hydrogels regardless of the media conditions. Figure 6.26 (b) denotes that Stro-1<sup>+</sup> BMSCs generated minor hydrogel deformations in the presence of adipogenic supplements (5.5 ± 0.5 µm) compared to basal media (11.7 ± 1.4 µm) in the last 8h of the experiment.



**Figure 6.26 Stro-1<sup>+</sup> BMSCs generated small deformations on soft, thick matrices in adipogenic media on day 14. (a)** Soft hydrogel displacements gradually increased over time, being greater on thick materials, **(b)** Hydrogel deformations decrease on soft, thick hydrogels in adipogenic conditions. Bars represent the mean and SD of the 90<sup>th</sup> percentile of the displacements at the 99 nodes in the last 8h of the experiment (n=3 hydrogels). Statistical analysis was done using the 2-way ANOVA method. \*\*\*\* = p < 0.0001.

Another experiment assessed the deformations generated by Stro-1<sup>+</sup> BMSCs (F67, P4) on soft hydrogels. Cells were plated at 1,000 cells/cm<sup>2</sup> on soft, thin (5 µL), and thick (25 µL) PAAm hydrogels in basal, adipogenic and osteogenic media. Figure 6.27 (a) indicates that hydrogel displacements slightly increased over 18 hours. Figure 6.27 (b), with the mean of the 90<sup>th</sup> percentile of the last 10 hours of the experiment, enumerates that soft, thick

hydrogel (basal:  $8.5 \pm 0.3 \mu\text{m}$ ; osteogenic:  $9.0 \pm 0.7 \mu\text{m}$ ; adipogenic:  $7.9 \pm 0.9 \mu\text{m}$ ) suffered more significant deformations in comparison to their soft, thin counterparts (basal:  $5.9 \pm 0.2 \mu\text{m}$ ; osteogenic:  $6.3 \pm 0.4 \mu\text{m}$ ; adipogenic:  $3.7 \pm 0.4 \mu\text{m}$ ) on day 3. No significant differences were encountered when comparing displacements between basal and osteogenic conditions regardless of hydrogel thickness. However, significant differences were identified when comparing displacements on soft hydrogels in osteogenic and adipogenic media.

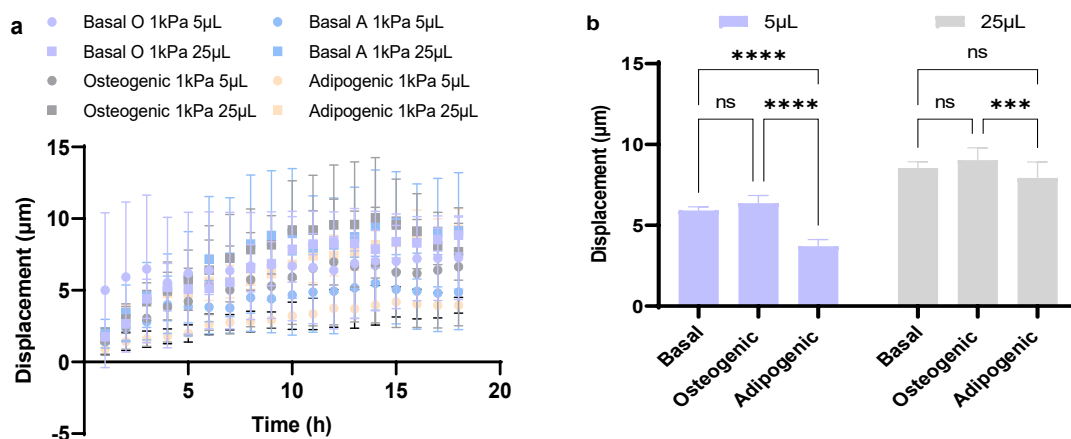


**Figure 6.27 Stro-1<sup>+</sup> BMSCs created smaller deformations on soft, thick matrices in adipogenic media on day 3.** (a) Hydrogel displacements gradually increased over 18 hours. (b) Hydrogel displacements were greater on soft, thick matrices and decreased with adipogenic supplements. Bars represent the mean and SD of the 90<sup>th</sup> percentile of the displacements at the 99 nodes in the last 10 h of the experiment (n=3 hydrogels). Statistical analysis was done by using the 2-way ANOVA method. \*\*\*\* = p < 0.0001.

Figure 6.28 highlights that after 12 days of incubation, soft, thick hydrogels (basal:  $13.9 \pm 1.6 \mu\text{m}$ ; osteogenic:  $13.4 \pm 1.2 \mu\text{m}$ ; adipogenic:  $6.1 \pm 1.0 \mu\text{m}$ ) were still more deformed in comparison to soft, thin hydrogels (basal:  $7.4 \pm 0.8 \mu\text{m}$ ; osteogenic:  $7.4 \pm 0.4 \mu\text{m}$ ; adipogenic:  $5.0 \pm 0.5 \mu\text{m}$ ) and decreased in the presence of adipogenic supplements.

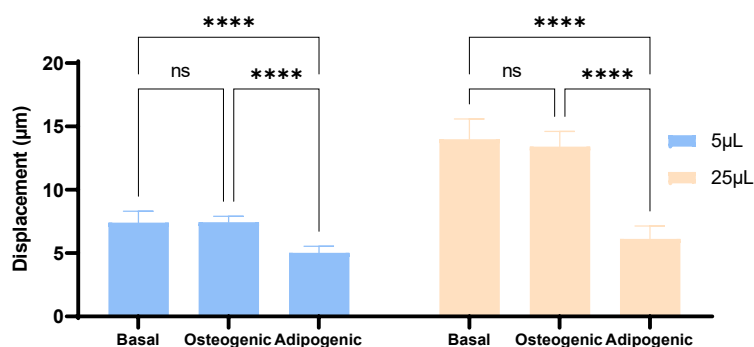


**Figure 6.28 Soft hydrogel displacements by Stro-1<sup>+</sup> BMSCs decreased in the presence of adipogenic supplements on day 12.** Soft, thick hydrogels suffered greater displacements than soft, thin hydrogels and decreased in adipogenic conditions. Bars represent the mean and SD of the 90<sup>th</sup> percentile of the displacements at the 99 nodes in the last 12 h of the experiment (n=3 hydrogels). Statistical differences were calculated by using the 2-way ANOVA method. \*\*\*\* = p < 0.0001.

To summarise, the mechanical forces applied by Stro-1<sup>+</sup> BMSCs are influenced by the hydrogel thickness, the addition of differentiation supplements and cell seeding. Cell differentiation is, in turn, dependent on mechanical forces. Hence, the increase in cell crowding might explain similar osteogenic or adipogenic differentiation rates on soft and stiff hydrogels seen in Chapter 5. This highlights that besides controlling hydrogel elasticity and thickness, controlling cell crowding would allow cells to perceive the actual material stiffness. Also, controlling colony size might be necessary as the contractile force that cells exert may be a function of the colony diameter and that as a result, the depth that cells in a colony can ‘feel’.

### 6.3.7 Cell micropatterning

A micropatterning technique was performed to delimit cell growth to specific areas on the collagen-coated PAAm hydrogels and evaluate the displacements generated by colonies on hydrogels with different elasticity and thickness. Firstly, PDMS stamps with patterns (circles, squares, and lines) were designed to create collagen islands on the soft and stiff PAAm hydrogels and flat stamps. Figure 6.29 illustrates the PDMS stamp designs and the measurements of the patterns on the 25 mm diameter stamps.

Once Dr Antonio DeGrazia fabricated the PDMS stamps at the Engineering department (University of Southampton), the collagen printing procedure was carried out (refer to Section 2.2.11 in Chapter 2 for detailed methodology). In brief, the collagen-PEG-acrylate solution was incubated for 4 hours on a roller, and then it was placed on top of the PDMS stamps and incubated for 2 hours at 37°C. Later, the excess collagen solution was removed, and the stamps were settled on the top of the treated slide to transfer the collagen patterns after incubating for 1 hour at 37°C. After incubating, the PDMS stamps were removed from the slide to obtain the collagen patterns. Last, the PAAm mixture was put on the collagen patterns and covered with the glass coverslip to polymerise the hydrogel.

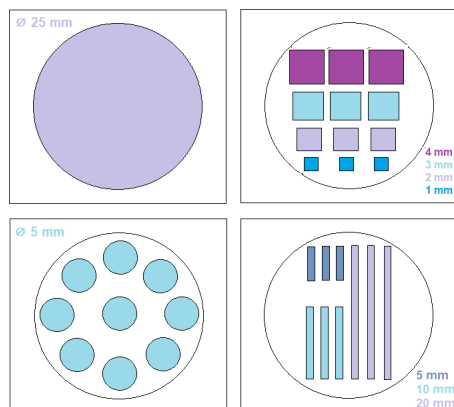


**Figure 6.29** Designs of the 3D printed PLA moulds to fabricate the PDMS stamps with and without patterns. Stamps of 25 mm diameter (flat, with 5 mm diameter circular islands, squares, and lines of different sizes) were fabricated in the Engineering department at the University of Southampton by Dr Antonio DeGrazia.

Once the patterned PAAm hydrogels were fabricated, the first aim was to confirm that cells could attach to the hydrogels only on the patterned areas using an initial collagen concentration of 0.1 mg/mL. MG63 cells were plated at 20,000 cells/cm<sup>2</sup> on stiff PAAm hydrogels and TCP in DMEM+0.1% BSA. After 24h, the media was removed, and the cells were rinsed with PBS, followed by the addition of DMEM+10% FBS and incubated for an additional 24h. Despite cells being plated at a high seeding density, cells did not fully cover the collagen patterns on the PAAm hydrogels (Figure 6.30). Thus, the collagen concentration on the islands was increased to 1 mg/mL, and Figure 6.31 illustrates MG63 cell morphology. MG63 cell attachment on the collagen islands was more efficient after FBS incubation.

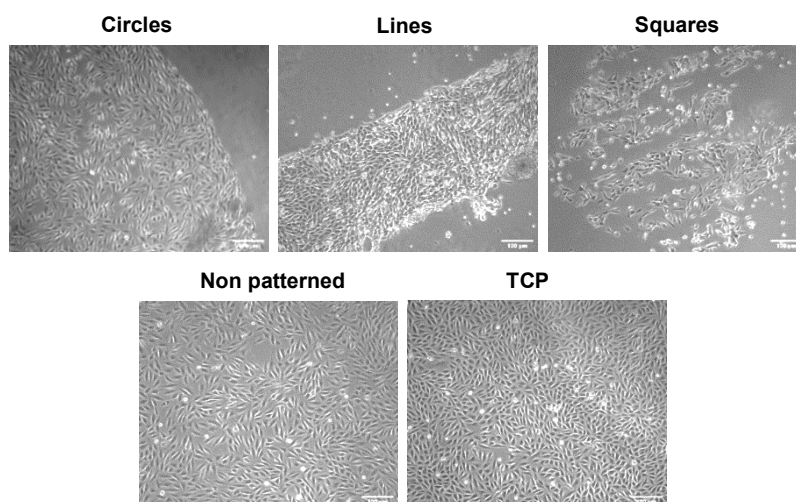


**Figure 6.30.** MG63 cells on stiff, flat, and patterned (collagen 0.1 mg/mL) PAAm hydrogels after 24h incubation in DMEM+10% FBS. Despite cell attachment being improved, some areas are still empty. Pictures were taken with a Nikon Eclipse Ti inverted microscope at 10X magnification.

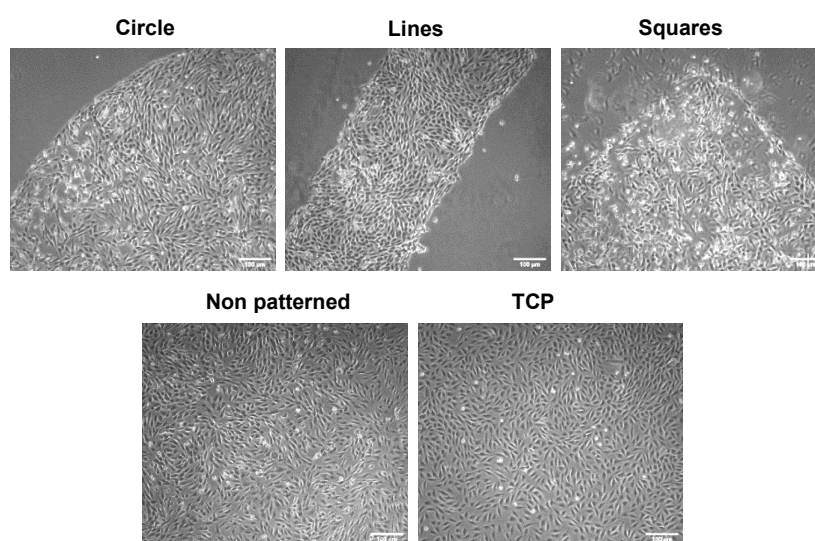


**Figure 6.31.** MG63 cells on stiff, flat, and patterned (collagen 1 mg/mL) PAAm hydrogels after 24h incubation in DMEM+10% FBS. Cell attachment was improved after incubating in DMEM + 10% FBS. Pictures were taken with a Nikon Eclipse Ti inverted microscope at 10X magnification.

Then, the same collagen concentration (1 mg/mL) was used on the 40 kPa PAAm hydrogels in a circular pattern. Stro-1<sup>+</sup> BMSCs were plated at 15,000 cells/cm<sup>2</sup> on those substrates to test if the cells could attach to the collagen islands at this collagen concentration and incubated first in DMEM+0.1% BSA and then in DMEM+10% FBS at 37°C on the hydrogels. Figure 6.32 illustrates the actin and nuclei staining of Stro-1<sup>+</sup> BMSCs on the patterned hydrogel (left) and the Sulfo-SANPAH crosslinked hydrogel (right) after 48h of incubation.

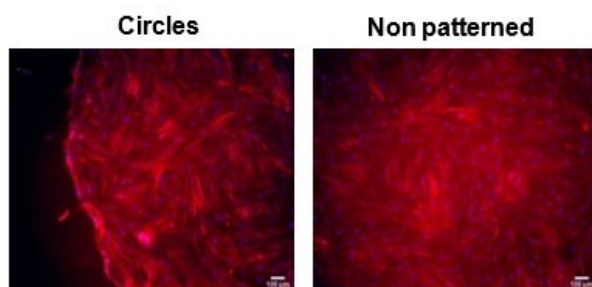


**Figure 6.32. Stro-1<sup>+</sup> BMSCs on the 5 mm collagen islands on the 40 kPa PAAm hydrogels.** Actin (red) and nuclei (blue) staining of Stro-1<sup>+</sup> BMSCs on stiff PAAm hydrogels after 48h incubation in DMEM + 10% FBS at 37°C. Cells were able to attach to the PAAm hydrogels through the collagen islands.

Because the aim was to evaluate the effect of substrate thickness on Stro-1<sup>+</sup> BMSCs differentiation, it was necessary to limit the lateral growth as the contractile forces exerted by the cells on the hydrogels might depend on hydrogel thickness. Then, new PDMS stamps with 1 mm circular patterns were fabricated and shown in Figure 6.33 to print smaller collagen islands on the PAAm hydrogels.

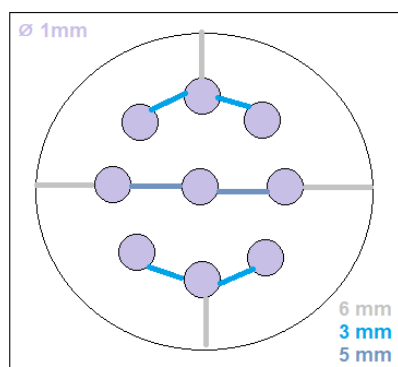


**Figure 6.33. Design of the 3D printed PLA mould to fabricate the PDMS stamps with 1 mm diameter circular patterns.** Moulds and stamps with circular islands of 1mm diameter, separated by 3 or 5 mm and 6 mm to the stamp's edge, were fabricated by Dr Antonio DeGrazia at the Engineering Department, University of Southampton.

New 1 mm collagen (3 mg/mL) patterns were printed on the treated slides to fabricate more patterned stiff but also soft PAAm hydrogels. Figure 6.34 shows better cell attachment after incubating with FBS; however, the cells occupied not all the islands.

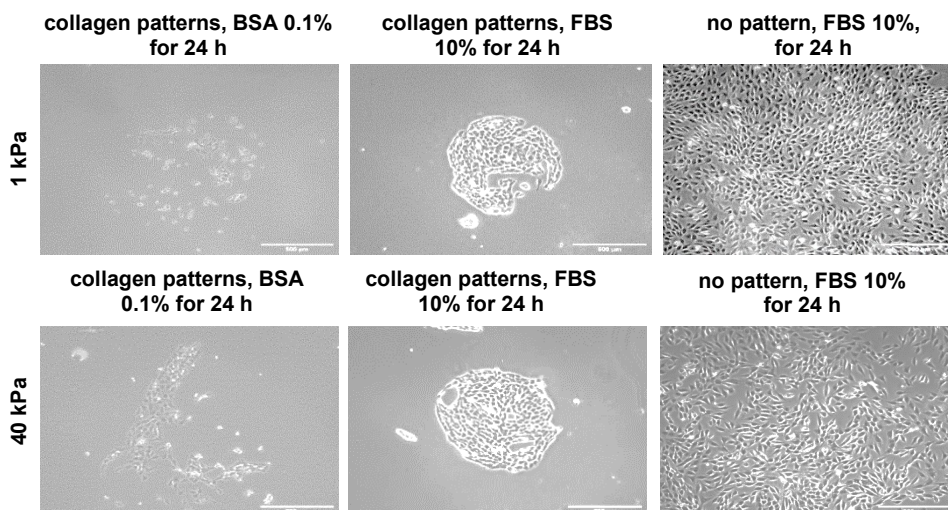


**Figure 6.34.** FBS increased cell attachment to the collagen islands after 24 h incubation in 0.1% BSA. MG63 cells were plated at 20,000 cells/cm<sup>2</sup> on soft and stiff PAAm hydrogels with and without collagen patterns at 3 mg/mL in BSA 0.1% for 24h and FBS 10%.

MG63 cells were incubated on the patterned hydrogels for more days to evaluate the effect of substrate elasticity and thickness on BMSCs differentiation in future experiments. Figure 6.35 shows MG63 cell growth on patterned PAAm hydrogels from day 1 in DMEM+0.1% BSA until day 7 in DMEM+10% FBS. Cells do not efficiently attach to the PAAm hydrogels on day 1 with BSA, regardless of the elasticity. However, cell attachment increased in the following days when incubated with FBS. Similarly, cell attachment on the 40kPa PAAm hydrogel was more efficient by incubating in DMEM+FBS. Nevertheless, cells did not occupy all the circular collagen patterns on the stiff hydrogel, although some circular islands were obtained in previous experiments. Also, when reviewing the 1 and 40 kPa triplicates that should have cells forming nine circular islands per hydrogel, only 1 or 2 isles per triplicate were observed, which indicates the method needed to be reproducible when using the stamps with a 1 mm diameter.

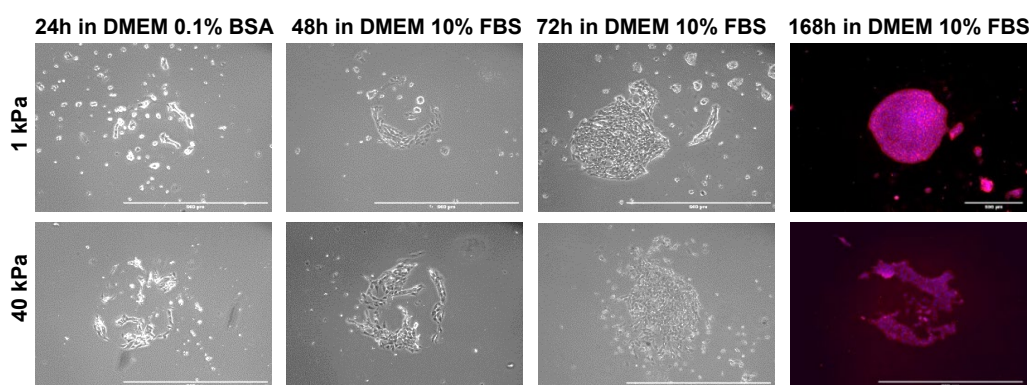


**Figure 6.35** FBS increased cell attachment to the collagen islands after 24 h incubation in 0.1% BSA. Phase-contrast images of MG63 cells plated at 20,000 cells/cm<sup>2</sup> on soft and stiff PAAm hydrogels with collagen

(3 mg/mL) patterns in DMEM 0.1% BSA at 24h and DMEM 10% FBS at 48h and 72h. Fluorescent images represent the actin (red) and nuclei (blue) staining of MG63 cells in DMEM 10% FBS on day 7.

In another experiment, 1  $\mu\text{L}$  of the collagen (3 mg/mL)-acrylate solution (previously incubated for 4h at 4°C to promote collagen-PEG acrylate binding) was placed on the treated slide instead of on the top of the PDMS stamps. Later, the slides were incubated for 1 hour at 37°C to dry the collagen solution. Once the collagen was printed on the glass slides, 50 or 100  $\mu\text{L}$  of the PAAm mixture was added to polymerise the soft and stiff hydrogels with different thicknesses.

Figure 6.36 illustrates MG63 cells at 20,000 cells/cm<sup>2</sup> on the PAAm hydrogels. In the first 24 incubation hours in DMEM+0.1% BSA, cells occupied the collagen island on soft, thick PAAm hydrogels, and some empty areas were observed on the non-patterned hydrogels. On the soft, thicker hydrogels, the cells grouped on the patterned hydrogel and around the collagen island but extended throughout the non-patterned hydrogel. After incubating in DMEM+10% FBS for 24h, cells appeared the same as on day 1 on the thick PAAm hydrogels, whereas groups of cells were more evident on both thicker hydrogels after incubating in FBS.

Cells covered the collagen island on stiff, thick hydrogels and occupied the non-patterned hydrogels on days 1 and 2. In contrast, on the patterned hydrogel, unspecific patterns were observed on the thicker hydrogels when incubating in DMEM+BSA on day 1. A circular pattern rounded by an empty area was seen after incubating in DMEM+FBS. That occurred because the hydrogel might have broken when detached from the treated slide. Cells on the thicker, no, patterned stiff hydrogel also covered the area.

This experiment showed that there are more suitable methods than directly adding the collagen-PEG acrylate solution to the treated slide to print the collagen islands. The hydrogel surface can be disrupted when detaching the PAAm hydrogel from the slides. Nevertheless, substrate thickness plays a vital role in cell morphology and behaviour as cells were grouped in colonies on the soft and thickest hydrogels. Thus, soft, thicker hydrogels ( $\geq 620\mu\text{m}$ ) should be used to identify the effect of substrate thickness on cell behaviour, as probably the 50  $\mu\text{L}$  hydrogels were too thin to affect cell morphology and differentiation.

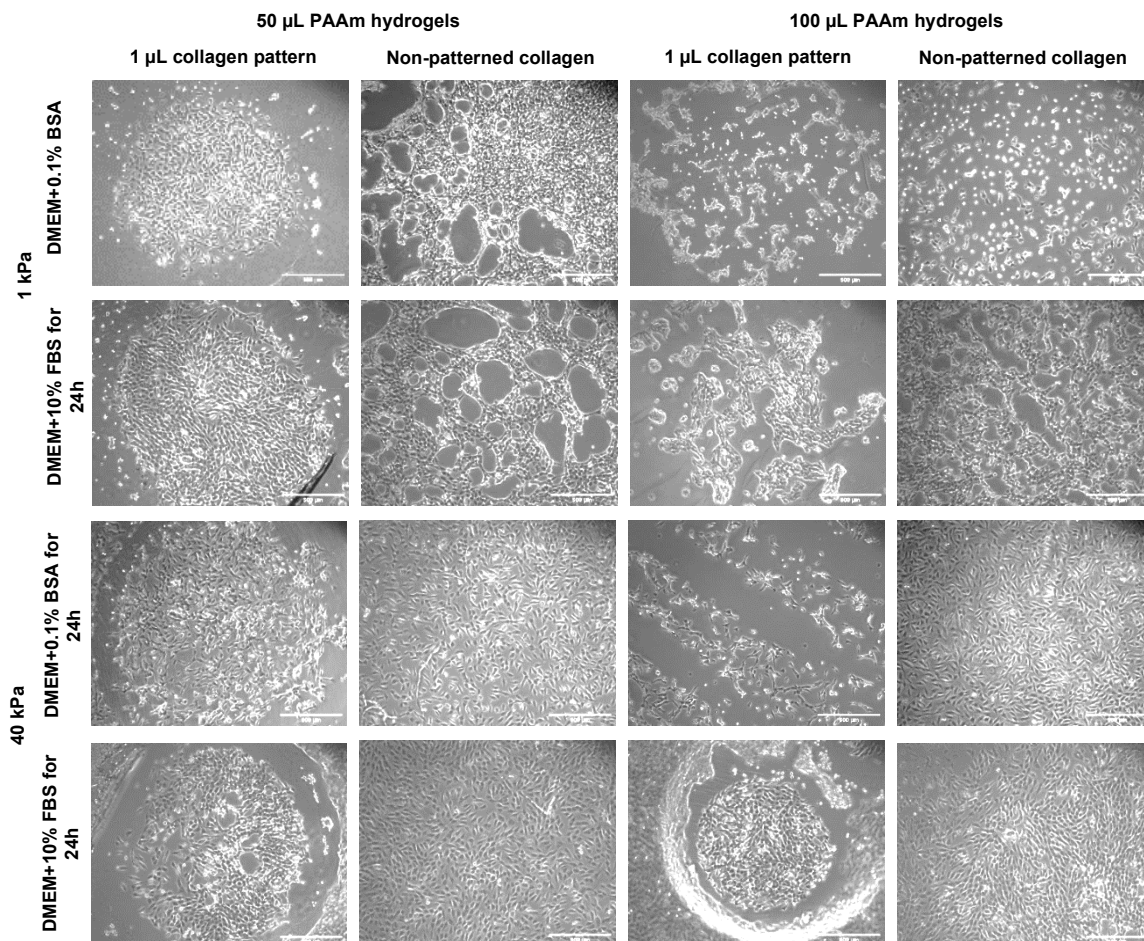
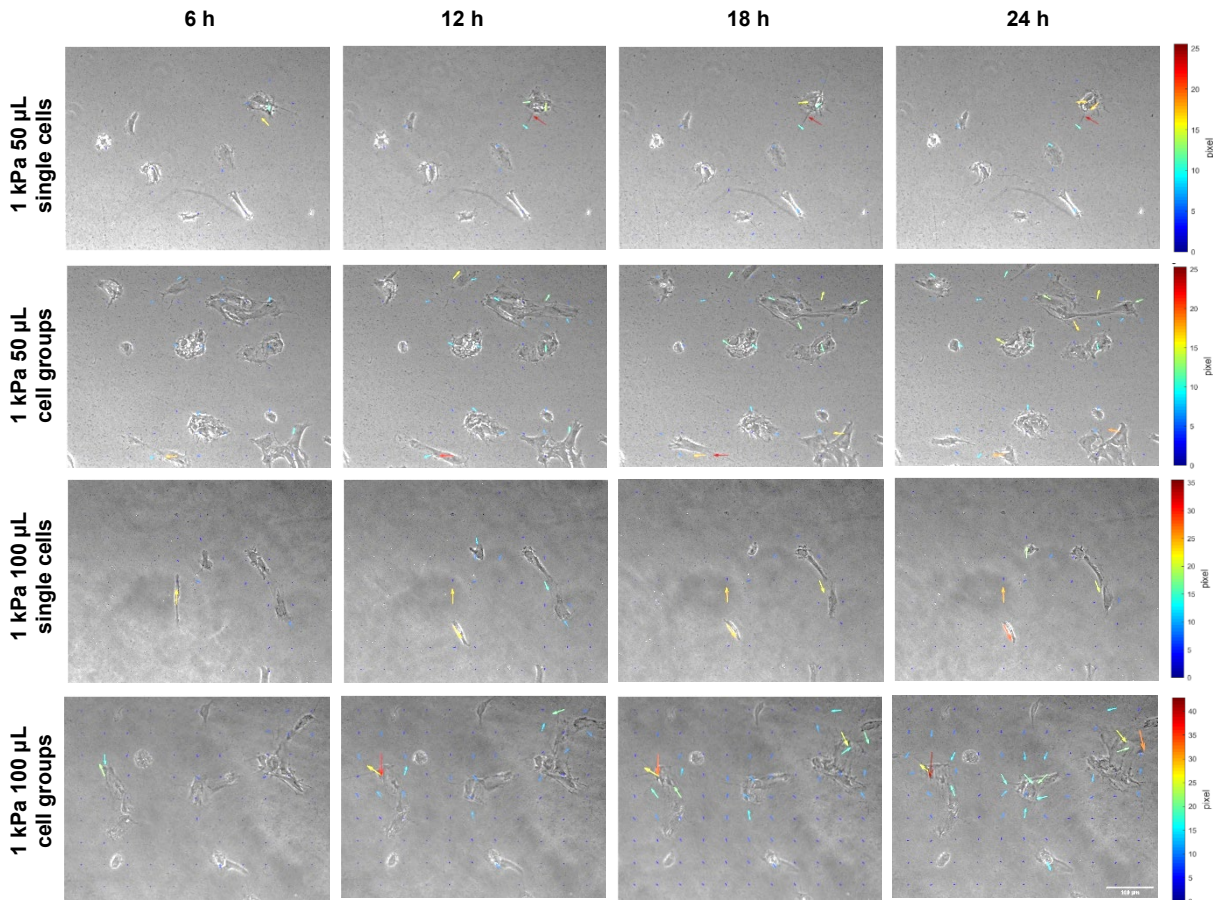


**Figure 6.36** The direct addition of the collagen-acrylate solution to the treated slide disrupts the hydrogel surface. MG63 cells are plated on soft, stiff, thick, and thicker PAAm hydrogels with and without collagen drops. Cells covered the collagen print on the soft, thick hydrogel, whereas some empty areas were appreciated on the non-patterned hydrogel. On a thicker, soft hydrogel, cells formed colonies on the collagen pattern and occupied the non-patterned counterpart. MG63 cells also covered the collagen section on the stiff, thick hydrogel and entirely occupied the non-patterned hydrogel. Cells accommodated in lines around the collagen on stiff, thicker hydrogels, whereas cells were highly confluent on non-patterned hydrogels.

### 6.3.8 Hydrogel deformations by single and groups of Stro-1<sup>+</sup> BMSCs

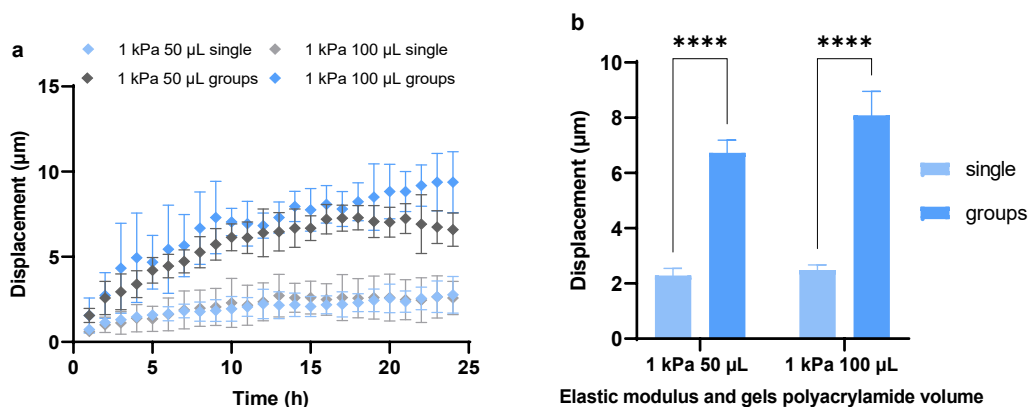
The deformations on soft hydrogels by Stro-1<sup>+</sup> BMSCs single cells and groups of cells were carried out by coating the hydrogels with the previous method. Namely, 1  $\mu\text{L}$  of collagen-PEG-Acrylate was placed on a glass slide and incubated for 1 hour to create collagen islands. Then, soft hydrogels were fabricated by adding 50  $\mu\text{L}$  or 100  $\mu\text{L}$  of PAAm mixture on the slide with the collagen island and sandwiched with a glass coverslip for 30 min to promote the hydrogel's polymerisation. Later, Stro-1<sup>+</sup> BMSCs were plated at 1,000 cells/cm<sup>2</sup> on soft, thick (50  $\mu\text{L}$ ) and soft, thicker (100  $\mu\text{L}$ ) PAAm hydrogels.

Coloured arrows in Figure 6.37 illustrate that hydrogel deformations were more significant by groups of cells than single cells, which are more evident in thicker hydrogels.



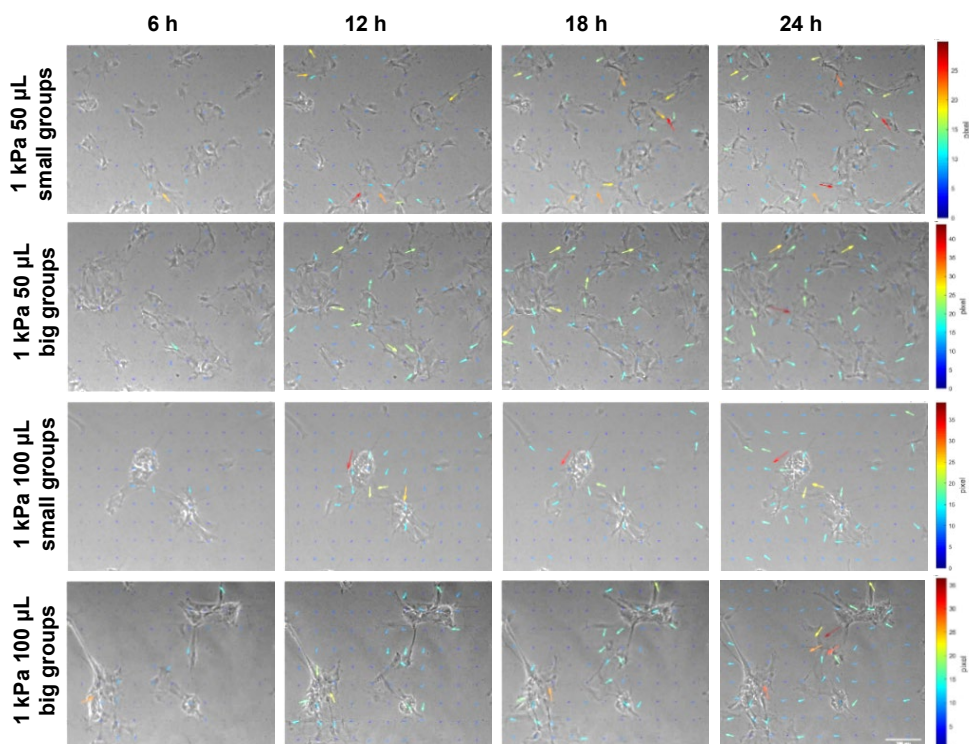
**Figure 6.37 Time-lapse imaging of Stro-1<sup>+</sup> BMSCs on soft hydrogels of different thicknesses for 24 hours.** Coloured arrows indicate more significant displacements on soft, thicker hydrogels by groups of cells than by single cells. Images were obtained under a Nikon Eclipse Ti inverted microscope.

Figure 6.38 (a) denotes those displacements on soft, thick hydrogels increased gradually over time (24 hours) by group (more than 3 cells grouped) of Stro-1<sup>+</sup> BMSCs compared to single cells where changes remained steady. Figure 6.38 (b) shows the mean displacements by Stro-1<sup>+</sup> BMSCs on soft hydrogels during the last 16 hours of the experiment. Cells, when arranged in groups (50 µL:  $6.7 \pm 0.4 \mu\text{m}$ ; 100 µL:  $8.0 \pm 0.8 \mu\text{m}$ ), created more significant deformations in comparison to the displacements caused by single cells (50 µL:  $2.2 \pm 0.2 \mu\text{m}$ ; 100 µL:  $2.4 \pm 0.1 \mu\text{m}$ ).



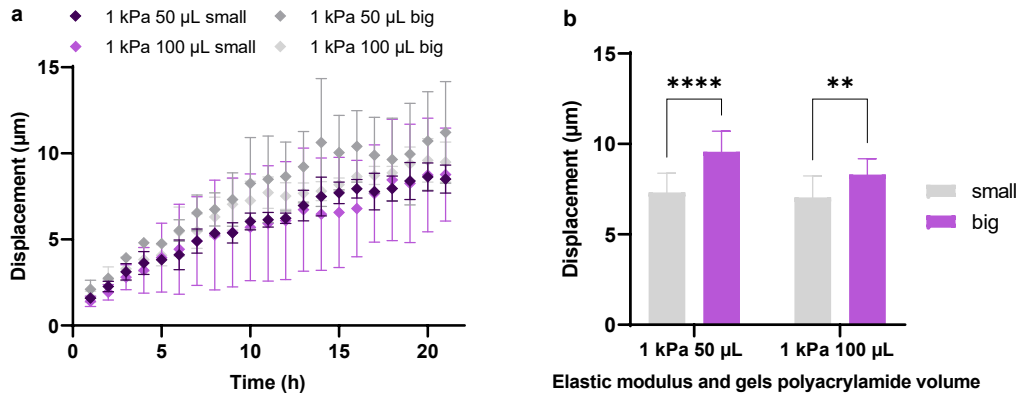
**Figure 6.38 Stro-1<sup>+</sup> BMSCs highly deformed soft hydrogels when arranged in groups (more than 3 cells) and not as single cells. (a)** Displacements gradually increased over 24 hours on soft, thick hydrogels by groups of Stro-1<sup>+</sup> BMSCs but not by single cells. Bars represent the mean and SD of the 90<sup>th</sup> percentiles of the displacements at the 99<sup>th</sup> nodes ( $n=3$  hydrogels). **(b)** Stro-1<sup>+</sup> BMSCs caused more deformations on soft hydrogels when arranged in groups. Statistical analysis was done by using the 2-way ANOVA method. \*\*\*\* =  $p < 0.0001$ .

After determining that the deformations caused by the Stro-1<sup>+</sup> BMSCs on soft PAAm hydrogels and, as a result, the applied mechanical forces were different by single cells and groups of cells. The following experiment aimed to evaluate how the changes in cell group size would modify applied cellular forces and, therefore, hydrogel deformations. Coloured arrows in Figure 6.39 illustrate that a big group (>5 cells) of Stro-1<sup>+</sup> BMSCs created more significant displacements than a small (2 or 3 cells) group of cells.



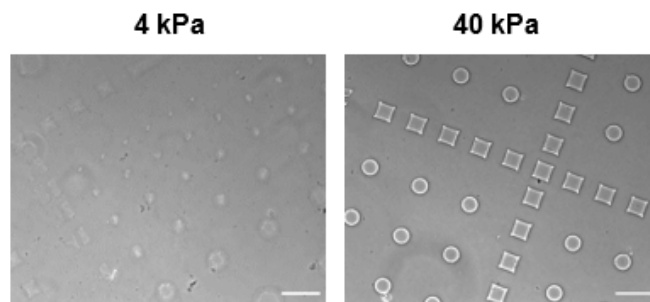
**Figure 6.39 Groups of Stro-1<sup>+</sup> BMSCs on soft hydrogels of different thicknesses for 24 hours.** Coloured arrows indicate more significant displacements on soft, thicker hydrogels by big groups of cells.

The 90<sup>th</sup> percentiles of hydrogel deformations were plotted in Figure 6.40. (a) hydrogel deformations by small and big groups of cells on soft hydrogels increased over time (21 hours). (b) The average displacements of the last 13 hours of the experiment show that big groups of cells (50  $\mu$ L:  $9.5 \pm 1.1 \mu$ m; 100  $\mu$ L:  $8.3 \pm 0.8 \mu$ m) created more significant deformations in comparison to small groups of cells (50  $\mu$ L:  $7.3 \pm 1.0 \mu$ m; 100  $\mu$ L:  $7.0 \pm 1.1 \mu$ m).



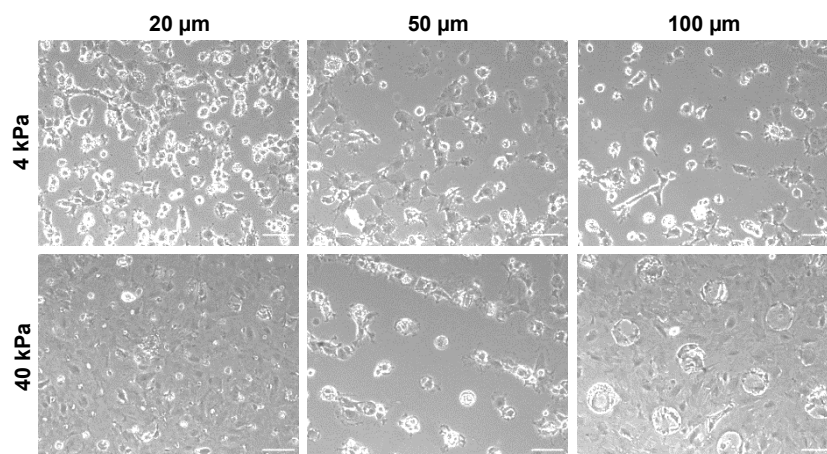
**Figure 6.40 Stro-1<sup>+</sup> BMSCs created greater displacements on soft hydrogels when arranged in big rather than small groups.** (a) Displacements gradually increased over 24 hours on soft, thick hydrogels by groups of Stro-1<sup>+</sup> BMSCs regardless of size. Bars represent the mean and SD of the 90<sup>th</sup> percentiles of the displacements at the 99 nodes (n=3 hydrogels). (b) Big groups (>5 cells) of Stro-1<sup>+</sup> BMSCs caused more deformations than small groups (2 or 3 cells) on soft hydrogels. Statistical analysis was done by using the 2-way ANOVA method. \*\*\*\* = p < 0.0001.

The previous experiment showed preliminary results regarding cell mechanosensing by single cells and cell groups of different sizes on soft, thick hydrogels. Nevertheless, this method for collagen coating is needed to produce precise collagen islands. Therefore, pre-fabricated 4 kPa, 40 kPa PAAm hydrogels with wells of different diameters were acquired from the company 4-D Cell (Montreuil, France) and used in an initial experiment to evaluate cell behaviour on them before evaluating hydrogel displacements. Figure 6.41 illustrates representative images of the soft and stiff hydrogels with wells. Wells on the hydrogel surface were seen on 40 kPa hydrogels but poorly defined on 4 kPa matrices.



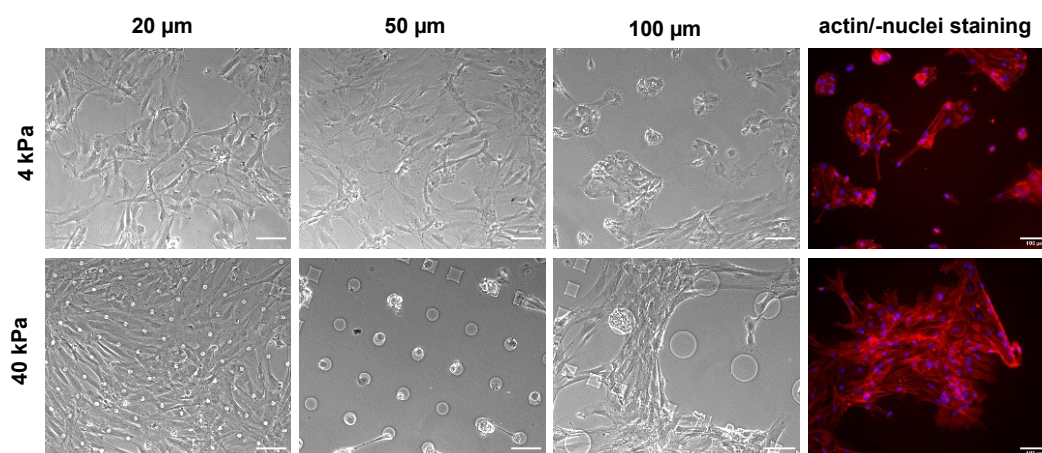
**Figure 6.41 4 kPa and 40 kPa hydrogels with wells of different sizes (10, 20  $\mu$ m).** Phase-contrast images of the soft and stiff hydrogels with squares or circular wells were taken under a Nikon Ti Eclipse microscope at 10X magnification.

MG63 were plated at 10,000 cells/cm<sup>2</sup> on the PAAm hydrogels. Figure 6.42 illustrates the attachment of cells on 4 kPa and 40 kPa hydrogels with wells of 20, 50 and 100  $\mu$ m diameter after 4 hours of incubation. Cell arrangement changed depending on the well size and hydrogel elasticity. Cellular clusters were observed on soft hydrogels, while cells were spread on stiff hydrogels with 20  $\mu$ m wells. At the same time, cells were inside 50  $\mu$ m wells and spread in and out of the wells on 100  $\mu$ m.



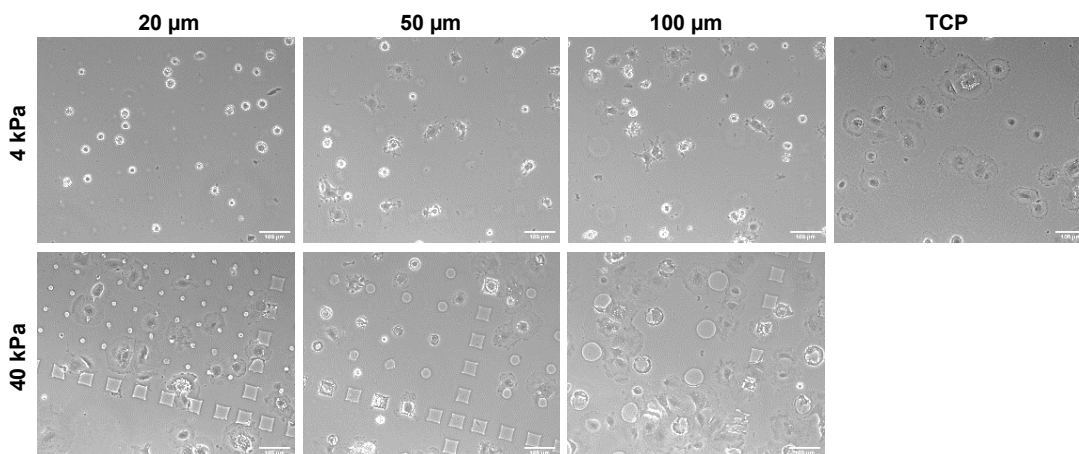
**Figure 6.42 MG63 cells within wells of different diameters: 20, 50 and 100  $\mu$ m on 4 kPa and 40 kPa hydrogels after 4 hours of incubation.** Cells were located within the 50 and 100  $\mu$ m wells on stiff hydrogels and clustered on soft hydrogels regardless of the well's size.

Figure 6.43 shows that cell crowding increased after 48 hours of incubation, and cells clustered in groups on 4 kPa hydrogels with 100  $\mu$ m wells. In contrast, cells were distributed around the surface of hydrogels at 20 and 50  $\mu$ m. Cell crowding appears greater on 40 kPa hydrogels than on 1 kPa hydrogels with 20  $\mu$ m diameter wells. However, more cells were seen on soft compared to stiff hydrogels with 50  $\mu$ m well, where cells were located. Interestingly, cells grouped on soft hydrogels with 100  $\mu$ m diameter well or located inside the cells but freely grew on the stiff counterparts.



**Figure 6.43 MG63 cells on 4 kPa and 40 kPa hydrogels with wells of different diameters: 20, 50 and 100  $\mu$ m after 48 hours of incubation.** Cells were distributed on soft and stiff hydrogels with 20  $\mu$ m wells and clustered on hydrogels with 100  $\mu$ m. Actin (red) and nuclei (blue) staining exhibited clear actin stress fibres on 4 and 40 kPa hydrogels.

A second test with a lower seeding density (1,000 cells/cm<sup>2</sup>) was used to avoid cell clustering and promote the location of cells within the wells. In Figure 6.44, round cells were identified on soft hydrogels with 20  $\mu$ m wells and spread cells on the hydrogels with 50 and 100  $\mu$ m. Spread cells were also seen on stiff hydrogels with 20  $\mu$ m, with few cells inside and outside the 50  $\mu$ m and 100  $\mu$ m wells. Supplementary Video 18a shows that cells do not remain within the hydrogels, moving around the hydrogel surface and not only within the wells. Therefore, this methodology was not advantageous for evaluating hydrogel deformations during cell differentiation with controlled cell-cell interaction in future experiments.



**Figure 6.44** MG63 cells at 1,000 cells/cm<sup>2</sup> on 4 kPa and 40 kPa hydrogels with wells of different diameters: 20, 50 and 100  $\mu$ m after 48 hours of incubation. Cells were located within the wells but on the surface of the hydrogels. Phase-contrast images were obtained with a Nikon Eclipse Ti inverted microscope at 10X magnification.

## 6.4 Discussion

Cell traction forces are produced by the actin cytoskeleton and transmitted to the ECM by integrins and focal adhesions, directing important cellular processes such as cell attachment, spreading and migration. Hence, evaluating cell traction forces might provide crucial information for understanding different biological processes (Plotnikov *et al.*, 2014).

This chapter aimed to study the effect of cell crowding and the presence of osteogenic and adipogenic supplements on cell-induced deformations by BMSCs on the ECM through traction force microscopy. TFM is the most used method for measuring cell traction forces by tracking the displacements of fluorescent fiducial markers embedded in hydrogels. The main findings were:

- Deformations created by Stro-1<sup>+</sup> BMSCs depended on the hydrogel elastic modulus and thickness. Soft, thick hydrogels exhibited more significant displacements than soft, thin, and stiff hydrogels.
- Hydrogel deformations decreased with the increase in cell crowding because of cell proliferation or seeding density.
- The addition of osteogenic or adipogenic supplements modifies cell mechanosensing, cell traction forces, and, therefore, hydrogel displacements which depend simultaneously on cell crowding.

The first results in this chapter highlighted that Stro-1<sup>+</sup> BMSCs created more significant displacements on soft compared to stiff hydrogels on day 0 (Figure 6.4) than on day 10 (Figure 6.6). This may be explained by the changes in cell area during cell attachment and spreading on day 0 that modify the cell traction forces that direct cell-hydrogel interaction (Kumar *et al.*, 2019). These forces might cause a deformation depending on the hydrogel elasticity. Soft substrates (Figure 6.2) suffered more significant deformations than stiff substrates (Figure 6.3). Then, fluorescent microbeads embedded within them displace greater distances on soft than stiff substrates (Knoll *et al.*, 2014). After 10 days of incubation, cells undoubtedly start interacting with each other (Figure 6.5), and therefore, the traction forces are transmitted to neighbouring cells and the hydrogel (Polacheck and Chen, 2016). This force transmission might explain the decrease in hydrogel displacements on day 10 (Figure 6.6) compared to day 0 (Figure 6.4) and the similar expression of osteogenic genes and ALPL activity in BMSCs on soft and stiff hydrogels (Figures 5.19-5.23) found in Chapter 5.

Chapter 4 confirmed that Stro-1<sup>+</sup> BMSCs sense changes in the hydrogel elastic modulus (Figure 4.2) and thickness (Figure 4.8) and slightly modified their cell spreading area in response. Stiff or soft, thin hydrogels are challenging to deform; therefore, cells accumulate tension within the cytoskeleton and spread. Meanwhile, the measurements of the hydrogel

Young's modulus detailed in Chapter 3 denoted those thin materials are stiffer than thick hydrogels (Figures 3.7 and 3.8). Accordingly, in this chapter, deformations generated by Stro-1<sup>+</sup> BMSCs rely on the hydrogel intrinsic elastic modulus and thickness; more significant displacements were quantified on soft, thick than soft, thin matrices (Figure 6.4). These results confirm that cells perceive the soft, thin hydrogel stiffer as the proximity of the underlying glass coverslip increases the effective stiffness that the cell senses, which hinders hydrogel deformation (refer to Section 1.2 in Chapter 1). The force required to deform a thin hydrogel is greater than the necessary force to deform a thick hydrogel, exceeding the cell's capacity, increasing cellular tension, promoting cell spreading and generating small deformations. In contrast, cells easily deform soft hydrogels, cannot strive for greater internal force, and remain round (Evans and Gentleman, 2014). As hydrogel deformations and displacements relate to cellular traction forces, these results highlight that the quantification of cellular forces depends on substrate intrinsic elastic modulus and thickness (Boudou *et al.*, 2009).

As previously mentioned, cells *in vivo* are actively in contact and do not remain just as single cells. For this reason, the cell traction forces exerted by Stro-1<sup>+</sup> BMSCs were evaluated by quantifying hydrogel displacements after several weeks of incubation. Results on week 7 showed (Figure 6.8) that the hydrogel displacements remained similar, and no significant difference was encountered when varying hydrogel thickness on soft PAAm hydrogels. However, hydrogel's displacements decreased at this time (week 7; Figure 6.8) compared to day 0 (Figure 6.4). In crowded cell cultures, cells form adhesions through cadherins, maintained by the cytoskeleton's traction forces that depend on the ECM stiffness. Indeed, the traction forces produced by a cell can be transmitted to their neighbours, inducing shear flows in opposite directions to each other (Gov, 2009). Hence, cells cannot apply forces to the substrate and cause deformation, which explains the small displacements registered on PAAm hydrogels after 7 weeks of incubation.

The grade of deformations on PAAm hydrogels by Stro-1<sup>+</sup> BMSCs depends on hydrogel elastic modulus, thickness, and incubation time. Further experiments highlighted that the deformations on soft, thick hydrogels decreased with the increase in cell seeding density on day 1 (Figure 6.11). Two ongoing situations might explain this; cells increase their cell traction forces during the cell cycle; however, at high seeding densities, cells continuously interact, create, and transmit traction forces between them (Vianay *et al.*, 2018), which hinder substrate deformations and consequent displacements.

Hydrogel displacements depended on the substrate's intrinsic elastic modulus, thickness, and cell crowding. Cells actively proliferated on the substrates after 10 days of incubation (Figure 6.5), which might favour cell-cell interaction and the consequent transmission of mechanical information between the cells (Venugopal *et al.*, 2018). The active pulling by

neighbouring cells (Evans and Gentleman, 2014) makes cells perceive the soft hydrogels stiffer, causing small deformations.

In the first experiments, cell crowding is explained by cell proliferation over time. Further experiments evaluated the effect of the initial seeding density on soft (thin and thick) hydrogel deformations over time (Figures 6.13, 6.15 and 6.17). Interestingly, it was seen that cells created more significant deformations on soft PAAm hydrogels in osteogenic media at 1 000 cells/cm<sup>2</sup> and in basal media at 5,000 cells/cm<sup>2</sup>. Further experiments using cell samples from different patients confirmed that hydrogel displacements on soft hydrogels change by adding osteogenic supplements. BMSCs undergoing osteogenic differentiation created more significant deformations than BMSCs (Figures 6.22 and 6.23).

Similarly, Sridharan *et al.*, 2019 reported that osteoblasts and adipocytes applied greater forces than SSCs due to their increase in the cell area. Nevertheless, these results cannot be thoroughly compared as they evaluated hydrogel deformations produced by cells previously incubated in basal, adipogenic and osteogenic media for 1-2 weeks on patterned hydrogels, which influence cell shape, traction forces and differentiation. Evaluating traction forces on patterned hydrogels helps to control cell-cell contact, spreading and shape, which regulate cell fate.

BMSCs differentiated into adipocytes on PAAm hydrogels regardless of their elastic modulus (Chapter 5, Figure 5.12); hence, additional experiments aimed to evaluate hydrogel deformations by BMSCs during adipogenic differentiation to detect differences in cell-applied forces depending on the differentiation state and the substrate mechanical properties. BMSCs created greater deformations in basal media than in adipogenic media (Figures 6.25 and 6.26). This might be explained as cell shape changes during differentiation. Adipocytes store lipids which might change the area of contact between the cells and the ECM, the formation of FAs and the resultant activation of the actin cytoskeleton to generate forces, hindering hydrogel displacements.

Overall, the quantification of hydrogel displacements during osteogenic or adipogenic differentiation suggested that the changes in cell density and the presence of osteogenic or adipogenic supplements modify the cell traction forces exerted by the cells.

Previous reports evaluated cell traction forces when combining adipogenic and osteogenic supplements. For instance, McAndrews *et al.*, 2015 used multiple particle tracking microrheology (MPTM) and traction force microscopy to study the mechanical properties and traction forces of cells during SSCs differentiation on soft (2 kPa) and stiff (8 kPa) materials in adipogenic, osteogenic media and mixed media. They highlighted that the substrate rigidity directed cell differentiation in mixed media but did not alter the bulk rheological properties. The presence of adipogenic media produced the same

displacements on soft and stiff substrates. In contrast, they decreased in the presence of osteogenic supplements (McAndrews *et al.*, 2015). This contradicts the findings here, where BMSCs in osteogenic media create greater deformations than cells in basal or adipogenic media (Figures 6.27 and 6.28). Nevertheless, factors such as cell density and shape need not be considered.

Cell-cell interactions and collective behaviour are important in cell mechanosensing, tissue homeostasis and regeneration. A micropatterning technique was developed to control colony size and evaluate hydrogel displacements by BMSCs during cell differentiation. However, it was not reproducible as the protein was not completely attached to the PAAm hydrogels (Figure 6.35). Despite the methodology not being successfully applied, a modification of the technique limited BMSCs' attachment to some areas of the PAAm hydrogel. The direct addition of collagen before the hydrogel's polymerisation supported the evaluation of hydrogel displacements by single cells and groups of cells (Figures 6.37 and 6.38). As reported by Tusan *et al.*, 2018 for MG63 cells, groups of BMSCs created greater deformations than single cells, and displacements were more significant with the increase in group size. Despite these preliminary data suggesting differences in cell traction forces, further standardisation is required to delimit the colony area and to evaluate any differences during cell differentiation.

All the above results highlight that cell mechanosensing is a complex process involving different variables such as ECM modulus and thickness, cell density and shape and the presence of supplements, determining cell traction forces and cell performance.

## **Chapter 7 Discussion and future work**

## 7.1 Discussion

### 7.1.1 Achievements of the study

The main aim of this project was to determine how the changes in ECM thickness would influence the behaviour of mesenchymal stem cells for bone regeneration. However, this was a complex system to work with as different variables besides hydrogel thickness influenced SSCs differentiation, such as hydrogel stiffness and geometry, differentiation supplements and cell crowding. Considering all these variables, collagen-coated PAAm hydrogels were used to test the hypothesis that soft, thin substrates might promote the osteogenic differentiation of BMSCs, which is crucial for bone repair.

This thesis achieved the aims mentioned above by:

- The fabrication and characterisation of soft and stiff PAAm hydrogels with different thicknesses with or without embedded fluorescent microbeads.
- The demonstration that BMSCs sense changes in substrate elastic modulus and thickness.
- The demonstration that changes in hydrogel thickness, but not elastic modulus, influenced the osteogenic differentiation of BMSCs.
- The demonstration that cell differentiation and traction forces are interrelated and depend on the hydrogel elastic modulus, thickness, and cell crowding.

Finding that:

- The measured elasticity of the PAAm hydrogels with the same acrylamide/bisacrylamide ratio increased with reduced hydrogel thickness, which was not modified by adding fluorescent microbeads.
- Changes in hydrogel thickness and elasticity slightly impact single-cell spreading area and morphology, while thickness influences the arrangement of actin stress fibres and focal adhesions.
- ALPL activity and expression of *ALPL* and *RUNX2* were not significantly different between BMSCs on soft and stiff matrices.
- BMSCs exerted significantly larger deformations on soft, thick than soft, thin matrices, and the magnitude of deformations depends on cell crowding and the differentiation state. Small deformations were quantified on hydrogels with greater cell crowding, and the undifferentiated cells exerted greater deformations.
- Displacements on soft hydrogels by BMSCs depended on the cell arrangements; cell groups create more significant deformations than single cells, greater when comparing big and small groups of cells.

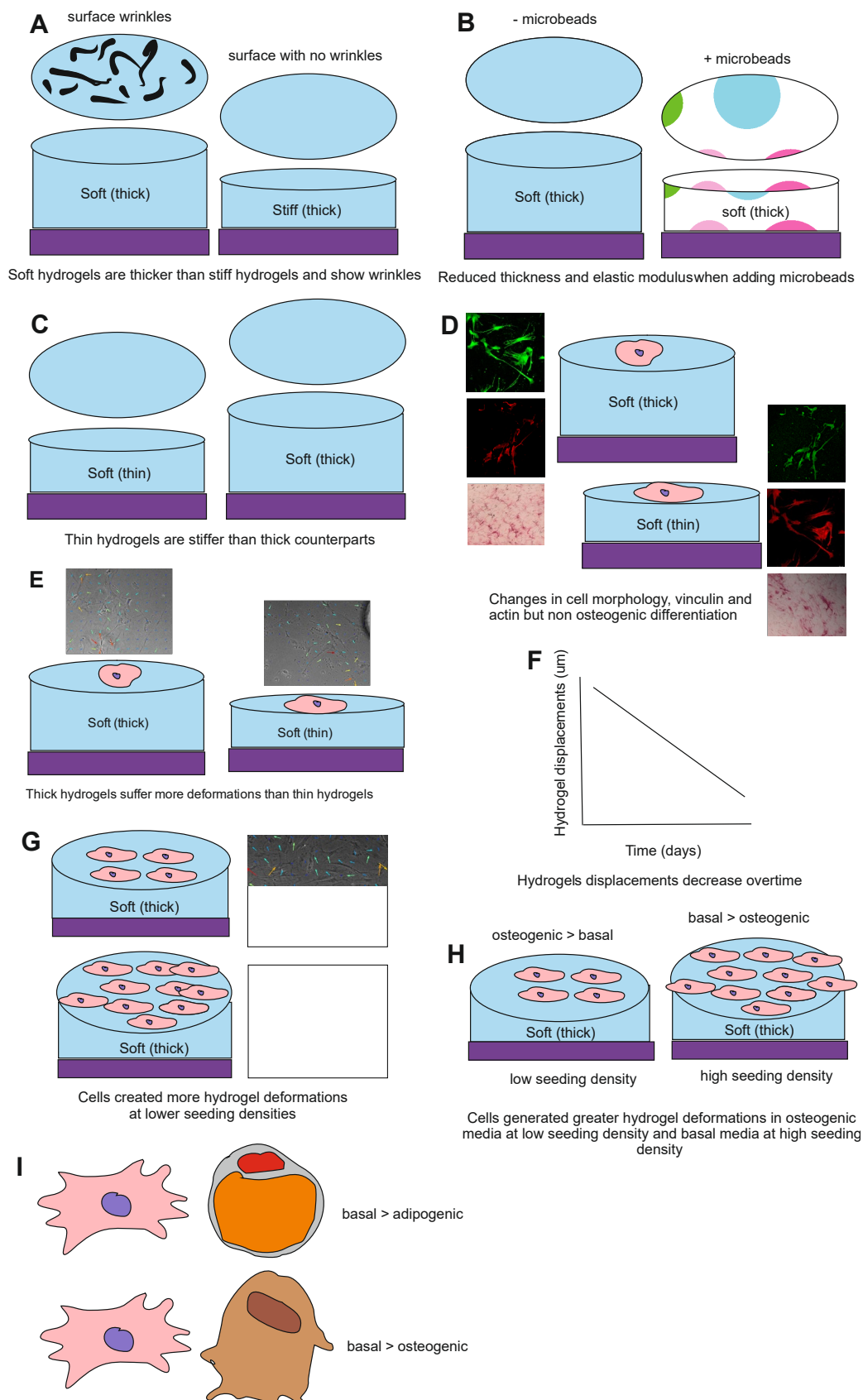


**Figure 7.1. Summary of the main findings.** (a) Surface characterisation and thickness of soft and stiff polyacrylamide hydrogels. (b) The effect of the addition of fluorescent microbeads into soft, thick hydrogels. (c) The effect of hydrogel thickness on the elastic modulus of soft hydrogels. (d) The influence of hydrogel thickness in cell behaviour. (e) Cell-induced deformations by BMSCs on soft hydrogels of different thicknesses. (f) Cell-induced deformations by BMSCs over time. (g) The effect of cell crowding on cell-induced deformations on soft, thick hydrogels. (h) Soft, thick hydrogel deformations by BMSCs in basal and osteogenic media (i) The effect of cell differentiation on hydrogel deformations.

Collagen-coated polyacrylamide hydrogels can mimic the ECM as their mechanical properties can be easily modified to imitate their physical properties. For this, Chapter 3 aimed to evaluate the stiffness, thickness, and structure of the PAAm hydrogels. Firstly, it was found that soft hydrogels are thicker than their stiff counterparts, and the increase in hydrogel thickness is achieved by increasing the volume of the PAAm mixture. Also, it was found that soft but not stiff hydrogels presented wrinkles on the surface, which changed with hydrogel thickness. Fluorescent microbeads were embedded in the hydrogels for traction force microscopy studies. Hence, this chapter also aimed to evaluate the effect of adding fluorescent microbeads on the hydrogel elasticity, thickness, and structure. It was found that hydrogel thickness was not modified by microbead addition, and the microbeads aligned within the wrinkles on the surface of soft PAAm hydrogels. Interestingly, the nanoindentation results indicated that the stiffness increased on thinner PAAm matrices. These findings highlight that the changes in the acrylamide/bisacrylamide ratio, hydrogel thickness and structure are highly interconnected, which might impact cell behaviour.

After studying the mechanical properties of the PAAm hydrogels, Chapter 4 aimed to evaluate the effect of the changes in substrate elastic modulus and thickness on the single-cell spreading area, morphology, focal adhesions, and actin fibres of Stro-1<sup>+</sup> BMSCs. The single-cell spreading area slightly increased when substrate effective stiffness increased by decreasing hydrogel thickness or increasing the intrinsic elastic modulus of the hydrogel. Also, the results demonstrated that the increase in seeding density (at low numbers) did not impact stiffness sensing and the cell spreading area. Cell morphology slightly varied on hydrogels with different mechanical properties. However, crucial structures in cell mechanosensing, such as actin stress fibres and focal adhesions, depended on the thickness and elasticity of the PAAm hydrogels. Actin stress fibres and focal adhesions were clearly defined on soft, thin and stiff hydrogels. These results show that Stro-1<sup>+</sup> BMSCs mechanosense the hydrogel stiffness and thickness changes and respond by slightly modifying their spreading area, morphology actin fibres and focal adhesions, which also relates to cell differentiation.

After measuring the cell-spreading area and confirming that Stro-1<sup>+</sup> BMSCs sense changes in substrate elastic modulus and thickness. Chapter 5 aimed to evaluate the effect of hydrogel thickness and stiffness changes on BMSCs' adipogenic and osteogenic differentiation. Firstly, Stro-1<sup>+</sup> BMSCs differentiated into osteoblasts and adipocytes on TCP and PAAm hydrogels, regardless of their elastic modulus. Indeed, no differences in ALPL activity, red Oil O absorption, and the expression of osteogenic markers (*ALPL* and *RUNX2*) were encountered when modifying substrate elastic modulus. Nevertheless, the ALPL activity of BMSCs varied when modifying the thickness of soft PAAm hydrogels. These results are crucial as most of the literature highlighted that substrate stiffness is crucial in differentiating SSCs. Previous reports found that MSCs differentiate into osteoblasts on stiff

substrates, but the results here confirmed that Stro-1<sup>+</sup> BMSCs differentiated even on soft PAAm hydrogels. This opened the question of how other factors, such as thickness and cell crowding, influence the interaction between the cells and ECM and might affect Stro-1<sup>+</sup> BMSCs' osteogenic and adipogenic differentiation.

Cell traction forces dictate different processes such as spreading, migration and differentiation; simultaneously, they depend on the characteristics of the ECM microenvironment. Hence, the relationship between cell traction forces and mechanosensing, cell crowding and BMSCs differentiation was evaluated. This was done by quantifying the displacements of the fluorescent microbeads produced by the cells on PAAm hydrogels of different elastic modulus and thicknesses. Firstly, hydrogel displacements gradually increased over time during cell spreading and attachment on the PAAm hydrogels regardless of their mechanical properties. Nonetheless, soft PAAm hydrogels exhibited more significant displacements than their stiff counterparts, and thicker matrices were easier to deform.

Additionally, it was found that BMSCs still produced different grades of hydrogel displacement on day 10 but not on week 7, as stiff, thin hydrogels suffer greater deformations than their stiff, thick counterparts. These findings highlight that the increase in cell crowding makes it difficult for the cells to deform soft hydrogels. This might have explained why BMSCs differentiated into osteoblasts on stiff and soft PAAm hydrogels in Chapter 5. Cell traction forces generated during osteogenic and adipogenic differentiation were evaluated to find this out. Interestingly, hydrogel displacements by Stro-1<sup>+</sup> BMSCs at low seeding density increased in the presence of osteogenic supplements but decreased at higher seeding density. Additionally, adding adipogenic supplements decreased hydrogel deformations by Stro-1<sup>+</sup> BMSCs, which might be explained by the changes in cell morphology and the interaction between the cells and the ECM. It was also found that soft hydrogel displacements increased when cells clumped together, and these clumps were more significant, highlighting the importance of cell crowding and cell traction forces.

### **7.1.2 Discussion of the main findings and their context**

This project contributes to the mechanobiology field by highlighting that the ECM's mechanical properties, such as elastic modulus and thickness, cell crowding and differentiation supplements, play an important role in cell mechanosensing and behaviour.

The study of the biochemical and mechanical signals is outstanding in understanding tissue development and homeostasis, tissue regeneration and disease progression. Cells must sense their physical microenvironment and respond to maintain tissue structure and functionality. This requires the development of different mechanisms between cells and the

extracellular matrix and cell-cell junctions, such as the folding and unfolding of nucleic acids and proteins and the regulation of the interactions between filamins, integrins and talins (Shivashankar *et al.*, 2015).

### 7.1.2.1 Embryonic and tissue development

ECM stiffness is vital in organ development. For instance, the cardiac matrix becomes stiffer during the heart's maturation due to the expression of myosin and collagen I by cardiac fibroblasts (Gaetani *et al.*, 2020). Besides stiffness, depth sensing is also outstanding in morphogenesis. The cells from the gastrula suffer positional changes that promote the interaction between groups of cells and tissues that, lead to cell fate changes and the subsequent transformation into a multi-layered embryo (Dzamba *et al.*, 2018). During this process, the changes in the adhesion between cells and cells-ECM should be precisely coordinated to allow the reorganisation while maintaining the necessary adhesion to maintain the structure of the embryo and tissue stiffness (Shawky and Davidson, 2015; Dzamba *et al.*, 2018).

Cell-cell, cell-ECM interaction and traction forces explain tissue homeostasis, development, and functionality. The traction forces generated in the actin cytoskeleton and the microtubules of one single cell are transmitted to neighbouring cells by adhesion molecules. Strong cell-matrix and weak cell-cell adhesions are essential for the epithelium's expansion, folding and maintenance (Wang *et al.*, 2021). This led to the remodelling and differentiation of specialised cell types that support tissue homeostasis and organ functioning (Shawky and Davidson, 2015; Kindberg *et al.*, 2020). For the enlargement of cell monolayers, cells on the front apply the most significant traction forces; then, the mechanical stress is greater on the edges of the monolayer towards the bulk of the tissue (Chen *et al.*, 2018). However, the transmission of traction forces can be exerted onward or inward on neighbouring cells, which causes cell extension (fibroblasts) or contraction (epithelial and neuronal progenitor cells), respectively (Chen *et al.*, 2018). This implies that the cells communicate on one plane and within different levels, highlighting the importance of depth mechanosensing in tissue homeostasis. Indeed, the movement of cellular monolayers causes large movements that can be extended over 10-15 cells. The coordinated movement of cells in a monolayer depends on cell-cell junctions but also cell division and crowding; the increase in cell crowding decreases the movement of the monolayers due to the friction between the cells but promotes cells' migration inwards within several cell layers (Chen *et al.*, 2018). Here, groups of cells comprised of a few or thousand move co-ordinately driven by traction forces on the ECM or intercellular forces transmitted through the adhesion complex (Serra-Picamal *et al.*, 2015). When cells are in an aligned region, the forces tend to be balanced, and the arrangement is stable. Otherwise, large-scale motion defects can be generated (Chen *et al.*, 2018).

The findings presented in this thesis, such as the differences in hydrogel deformations depending on the material's thickness and cell crowding, indicate that tissue geometry and cell density are fundamentally important in how cells and groups of cells mechanosense the elasticity of tissues. This may impact cell movement and tissue patterning during development and differentiation, as determined in Chapter 5, where cell crowding might impact stiffness sensing and osteogenic differentiation. Also, cell traction forces determine how the cells interact within them and migrate for tissue patterning and maintenance.

### **7.1.2.2 Tissue homeostasis and disease development**

After development, ECM stiffness homeostasis is still essential to avoid disease development. For instance, interstitial arterial cells maintain ECM stiffness to support functionality. In contrast, the increased stiffness of the myocardial ECM network leads to inflammatory, fibrotic, and hypertrophic responses, leading to diastolic or systolic unfunctionally (Humphrey *et al.*, 2014; Frangogiannis, 2017; Frangogiannis 2019). Heart functionality also relies on detecting stretch signals close to the plasma membrane that opens ion channels, releasing  $\text{Ca}^+$  from the sarcoplasmic reticulum, which, together with the actin cytoskeleton, acts as mechanotransducers, producing biochemical signals that regulate heart functionality (Gaetani *et al.*, 2020). ECM thickness is also crucial for heart functionality. Collagen crosslinking or fibronectin deposition increases ECM stiffness and thickness, leading to heart ageing (Angelini *et al.*, 2020). Besides the ECM mechanical properties, traction forces also direct heart function. Traction forces generated by myofibroblasts are important for ECM remodelling and modulating the activities of the neighbouring cells. Then, any alteration might result in the loss of the homeostasis of the aortic wall. For instance, smooth muscle cells in the media layer lose their contractile capacity, leading to apoptosis and weakening the aortic wall in an aneurysm (Petit *et al.*, 2021).

It was found here in this thesis that substrate deformations by the cells depend on their mechanical properties, such as thickness. In this way, the ECM thickness might influence mechanical cell responses by modifying stiffness sensing and dictating cell-cell and cell-ECM, which might define cell positioning and tissue homeostasis, influencing heart functionality. Also, the methods used in this thesis to quantify and analyse cell-induced traction forces of skeletal stem cells might be used to evaluate and improve the contractile capacity of cardiac cells after a stroke by modifying the ECM mechanical properties and cell contact.

### **7.1.2.3 Tissue regeneration**

The acellular dermal matrix is used in prosthetic breast reconstruction as a scaffold for cell growth and revascularisation of the autologous cells. Still, patients with thicker matrices

require a more extended period for engraftment (Hur and Han, 2021). Indeed, this highlights the importance of studying the effect of substrate thickness on cell behaviour so the cells can adapt to the microenvironment, proliferate, and restore the tissue.

In dentistry, the thickness of the soft tissue is critical during bone remodelling after implant installation; if thinner, the bone is reabsorbed, whereas thicker tissues extend the duration of the implant (Suárez-López *et al.*, 2016).

The success in regenerating bone fractures also depends on the mechanical forces and how the new cells interact and adapt to the new microenvironment. After implantation, the mechanobiology of the surrounding bone might be altered, changing the mechanical responses; low stress induces bone loss, whereas high stress enhances bone formation (García-Aznar *et al.*, 2021). Hence, it is important to evaluate how the cells interact with the material and generate changes, as evaluated in this thesis.

#### **7.1.2.4 Cancer development**

The ECM microenvironment is also crucial in cancer development. Firstly, ECM stiffness plays a vital role in cancer progression as stiffer ECM promote the conversion from normal to cancer cells. Cancer cells modify the composition and cross-linkage of the ECM, which alters the biochemical and biophysical properties of the tumour stroma, such as stiffness. ECM stiffening increases cell traction forces, disrupting tissue morphogenesis, promoting the formation of new capillaries, cell migration and metastasis, leading to poor outcomes (Najafi *et al.*, 2019; Eble and Niland, 2019). For instance, increased ECM deposition, crosslinking and decreased ECM degradation increase ECM stiffness in colorectal and breast cancer and promote tumour invasion, metastasis, and drug resistance (Najafi *et al.*, 2019; Liu *et al.*, 2020). Then, controlling the ECM stiffness might improve the efficacy of cancer treatments. Indeed, the decrease in ECM stiffness with recombinant collagenase and/or inhibitors of different mechanosignal transducers such as YAP/TAZ, Hsp47 or piezol work as cancer therapeutics such as pirfenidone, which inhibits Hsp47 and collagen expression, stopping fibrosis formation (Jiang *et al.*, 2022).

The transformation from healthy to malignant cells also relies on the rupture of cell-cell adhesions due to the loss of E-cadherins, transitioning from epithelial cells to mesenchymal cells. This phenotypic profile promotes the extravasation and survival of single cancer cells in distant organs (Niit *et al.*, 2015). However, tumour cells also migrate collectively from the main mass to different tissues with a “swarm-like behaviour”. Here cells lead and cooperate actively in a polarised movement, led by cell traction forces simultaneously dictated by cell shape and ECM mechanical properties (Spatarelu *et al.*, 2019).

In addition, cell-cell communication through exosome secretion containing lipids, nucleic acids, and proteins is crucial as it promotes angiogenesis, invasion, and immunologic remodelling (Maia *et al.*, 2018). Given the importance of cell-cell interactions in cancer development, immune suppressors target critical molecules such as integrins, siglecs (surface proteins that bind sialic acid) and selectins (Murai *et al.*, 2020).

Previous studies highlighted that quantifying cell traction forces are also important in cancer development, and it is used as a metastatic and malignancy biomarker. For instance, MCF7 breast cancer cells exert greater traction forces than MCF10A breast epithelial cells (Li *et al.*, 2017).

To sum up, cell traction forces, and cell-cell contact, drive collective cell migration, which is crucial for the metastasis of tumour cells. Highlighting that collective mechanosensing is an essential biological process in tissue regeneration and the development of different diseases.

## **7.2 Limitations of the study and suggestions for future work**

Although this thesis achieved its primary aim of testing the effect of substrate thickness and cell crowding on BMSCs differentiation, several experimental weaknesses could be improved to clarify unresolved questions, such as the substrate deformations by groups of cells during differentiation.

PAAm hydrogels were used to mimic the mechanical properties of the ECM. Despite this material being widely used, the attachment and viability are outstanding for any mechanobiology study. The limitation was that different numbers of cells were attached to the hydrogel surface when modifying the mechanical properties of the hydrogels, even though collagen concentration was not modified, which inherently impacts cell behaviour. This opens the question of further characterising these materials in future experiments by evaluating the rate and grade of hydrogel degradation (intrinsic and by cells), cell viability, and possibly the associated immunological response.

Mechanobiology has many implications for tissue development and regeneration. Here, Stro-1<sup>+</sup> BMSCs were used for bone regeneration; however, stem cells from different sources might be used too. For instance, umbilical cord mesenchymal stem cells could be used in future experiments, given their greater pluripotential capacity and wide use in transplantations due to their lower risk of patient rejection and high cell proliferation (Xie *et al.*, 2020). In this sense, evaluating their mechanosensitive capacity would be outstanding in their adaptation, proliferation, and differentiation to the new tissue microenvironment and treating different diseases. Indeed, the effect of substrate stiffness (Xu *et al.*, 2017; Sun *et al.*, 2020) but not thickness on their differentiation has been investigated. Expanding stem

cell sources might provide more comprehensive information about the effect of ECM geometry on differentiation.

Cell spreading is crucial as it dictates many cell functions, such as migration and differentiation. Although it was possible to measure the single-cell spreading area of Stro-1<sup>+</sup> BMSCs on PAAm hydrogels with different stiffness and thickness by manually limiting cell perimeter, this was a drawback as being was time-consuming. Also, Stro-1<sup>+</sup> BMSCs acquired different morphologies, which makes it difficult to establish an automated method for area quantification. Because cell spreading area did not significantly vary on hydrogels with different mechanical properties, it would be interesting to evaluate in future experiments the changes in the cell area, morphology, traction forces and migration during cell attachment in a time-lapse experiment when modifying substrate stiffness and thickness to track all the changes as the initial changes might be clearer.

Osteogenic and adipogenic differentiation was vital in evaluating the pluripotential capacity of Stro-1<sup>+</sup> BMSCs; however, different issues were faced during their evaluation. Firstly, Stro-1<sup>+</sup> BMSCs cells are a specific population of MSCs that might contain a certain proportion of stem cells (Murphy *et al.*, 2013). Therefore, the osteogenic and adipogenic differentiation capacity of the selected BMSCs might depend on the proportion of stem cells found in the population isolated from a specific sample and the capacity of these cells to maintain stemness through different generations. These factors represent a challenge because cells isolated from one specific sample might be able to differentiate into osteoblasts or adipocytes. However, others would not be able to do it.

Besides the intrinsic characteristics of the samples, some problems were encountered when quantifying ALPL activity and Oil Red O absorbance. Staining the Stro-1<sup>+</sup> BMSCs cells for evaluating ALPL activity and lipid storage formation showed that cells differentiated on TCP. However, the quantification did not significantly differ on the PAAm hydrogels with different mechanical properties. Indeed, during the staining with Oil Red O, the TCP around the PAAm hydrogel retained a proportion of the dye that, after releasing it, might have increased the absorbance dataset and overtaken the actual proportion of Oil Red O delivered by the cells on the hydrogels as TCP around the hydrogel was coloured. Regarding the quantification of the ALPL activity, two separate approaches should be carried out (ALPL staining and quantification), which implies using a higher number of cells, complicating the experiments. Osteogenic differentiation might be evaluated by quantifying bone matrix collagenous and non-collagenous proteins by immunofluorescence staining and bone mineralisation to detect calcium deposition by alizarin red staining (Meesuk *et al.*, 2022).

Despite the abovementioned issues, quantifying the ALPL activity by three methods confirmed substrate stiffness does not influence BMSCs' osteogenic differentiation. This agrees with the low expression of the osteogenic markers *ALPL* and *RUNX2*. However,

more osteogenic genes, such as *OPN* and *OCN*, could be included in future experiments, together with *PPAR*, to evaluate adipogenic differentiation and the chondrogenic potential as these genes were not included in the current project and might provide more information about the effect of the material's mechanical properties on osteogenic and adipogenic differentiation.

Factors influencing cell differentiation, such as cell-cell contact, traction forces and mechanosensing, are challenging to separate (Trappmann *et al.*, 2012). Indeed, cell differentiation might not occur if cells are maintained as single cells (Mathieu and Lobo, 2012), which also might not resemble the *in vivo* microenvironment as cells continuously migrate and interact collectively within tissues. Evaluating the effect of the ECM thickness on MSCs behaviour would probably be more accurate when using a 3D model (Lee *et al.*, 2016), which would be interesting to test in future investigations.

To quantify cell traction forces, it was essential to determine the impact of factors such as grid size, guide node, max move and the maximum number of pictures that could be analysed. Here, selecting the guide node was the most challenging element as this required an area with no movement, and high cell crowding sometimes obstructed this selection. It was also essential to include a correction that removed the "background noise" generated by the movement of the microscope. Even though this methodology produces valuable information, it requires many previous steps, from extracting the files and selecting and renaming them for the analysis. Despite this, many improvements were made to the code, directly allowing for a more precise calculation of hydrogel displacements between images and the obtention of the 90<sup>th</sup> percentiles and standard deviation. This facilitated information about the traction forces exerted by the cells during cell differentiation when cells are actively interacting between them. Indeed, previous reports have evaluated the traction forces of isolated cells during cell migration or cell cycle. However, this project studied the cell traction forces generated in crowded populations during cell differentiation.

A micropatterning method to create collagen islands on the surface of the hydrogel was used to evaluate BMSC osteogenic differentiation on thin hydrogels by controlling cell-cell contact and colony size. This was so challenging for different reasons. Firstly, even though cell attachment was improved by increasing the collagen concentration. Still, cells did not entirely cover the collagen islands, as the PDMS stamps did not fully transfer the collagen prints to the slides. Secondly, the lines within the patterns on the PDMS stamps and the diameter and height of the pillars for printing the small collagen islands could have been more problematic. It was impossible to press the stamps on the slides to improve the collagen printing as they were bending, which printed undesired patterns together with the excess collagen from the PDMS stamps. In this sense, collagen could have been labelled to be detected before sandwiching the PAAm mixture for the hydrogel fabrication. Tang *et*

*al.*, 2012 managed to use this micropatterning technique to culture fibroblasts on patterned PAAm hydrogels. They carried out the exact methodology, except they used fibronectin and laminin besides collagen. The PDMS also had a greater point of contact with the glass slide (long lines), and weights were placed on them to enhance the protein transfer. Increasing the pattern size greatly enhances protein and cell attachment; however, this project did not desire large patterns. Then, the challenge was transferring tiny collagen islands due to the small contact area between the PDMS stamp and the slide.

The issues cited above lead to different alternatives. The direct addition and incubation of the collagen I-PEG-acrylate solution to the slides before sandwiching the solution might produce the islands. Despite this methodology helping to evaluate hydrogel displacements by groups of cells and single cells, the size of the groups and the number of cells within the group differed.

Given the abovementioned challenges, another alternative was to control colony size for evaluating traction forces during cell differentiation. Pre-fabricated PAAm hydrogels with wells of different diameters were acquired despite their standard mechanical properties (5 kPa and 35 kPa and defined thickness) and lack of embedded fluorescent microbeads. They were tested at initial experiments to check their usage, finding different issues. Firstly, cells were attached to the hydrogels within and outside the wells. Secondly, cell arrangements and maintenance within the wells depended on cell crowding, the size of the wells and the cell size. Thirdly, even though the hydrogels might have worked, modifying hydrogel thickness and adding fluorescent microbeads was expensive. Then, further standardisation is required to control colony size. Methods such as lift-off protein patterning could be considered. Here the glass coverslips are coated with an S1818 photoresist by photolithography; the UV light photo mask promotes the photo-resist development. Then the coverslips are incubated with a bio-passive copolymer that binds to the empty spaces, enabling protein attachment after lifting off; the PAAm hydrogels are fabricated by sandwiching the mixture between the silanised slide and the patterned coverslip (Moeller *et al.*, 2018).

### 7.3 Conclusions

This project confirmed that Stro-1<sup>+</sup> BMSCs sense changes in substrate stiffness and thickness, highlighting that substrate thickness but not stiffness influences osteogenic differentiation. Traction forces exerted by the cells are intimately related to cell fate and depend on the cell-cell interaction and substrate mechanical properties. These findings set a precedent for investigating the mechanisms driving cell differentiation based on cell traction forces.

## Appendix A MATLAB Functions

### A.1 rrlmageTrackGUI.m

```

function varargout = rrlmageTrackGUI(varargin)
% RRIMAGETRACKGUI M-file for rrlmageTrackGUI.fig
%   RRIMAGETRACKGUI, by itself, creates a new RRIMAGETRACKGUI or raises the existing
%   singleton*.
%
%   H = RRIMAGETRACKGUI returns the handle to a new RRIMAGETRACKGUI or the handle to
%   the existing singleton*.
%
%   RRIMAGETRACKGUI('CALLBACK',hObject,eventData,handles,...) calls the local
%   function named CALLBACK in RRIMAGETRACKGUI.M with the given input arguments.
%
%   RRIMAGETRACKGUI('Property','Value',...) creates a new RRIMAGETRACKGUI or raises the
%   existing singleton*. Starting from the left, property value pairs are
%   applied to the GUI before rrlmageTrackGUI_OpeningFcn gets called. An
%   unrecognized property name or invalid value makes property application
%   stop. All inputs are passed to rrlmageTrackGUI_OpeningFcn via varargin.
%
%   *See GUI Options on GUIDE's Tools menu. Choose "GUI allows only one
%   instance to run (singleton)".
%
% See also: GUIDE, GUIDATA, GUIHANDLES

% Edit the1 above text to modify the response to help rrlmageTrackGUI

% Last Modified by GUIDE v2.5 08-Jul-2010 15:02:52

% Begin initialization code - DO NOT EDIT
gui_Singleton = 1;
gui_State = struct('gui_Name',    mfilename, ...
                  'gui_Singleton', gui_Singleton, ...
                  'gui_OpeningFcn', @rrlmageTrackGUI_OpeningFcn, ...
                  'gui_OutputFcn', @rrlmageTrackGUI_OutputFcn, ...
                  'gui_LayoutFcn', [] , ...
                  'gui_Callback', []);
if nargin && ischar(varargin{1})
    gui_State.gui_Callback = str2func(varargin{1});
end

if nargout
    [varargout{1:nargout}] = gui_mainfcn(gui_State, varargin{:});
else
    gui_mainfcn(gui_State, varargin{:});
end
% End initialization code - DO NOT EDIT

% -----
% ----- GUI Opening Func -----
% -----

% --- Executes just before rrlmageTrackGUI is made visible.
function rrlmageTrackGUI_OpeningFcn(hObject, eventdata, handles, varargin)
% This function has no output args, see OutputFcn.
% hObject    handle to figure
% eventdata  reserved - to be defined in a future version of MATLAB
% handles    structure with handles and user data (see GUIDATA)
% varargin   command line arguments to rrlmageTrackGUI (see VARARGIN)

% Choose default command line output for rrlmageTrackGUI
handles.output = hObject;
handles.checkboxStatus=0;

visibleArray = zeros(1,8);

```

```

visibleArray(1)=1;
handles.visibleArray= visibleArray;

set(hObject,'toolbar','figure');

set(handles.axesImage,'Visible','off');

set(handles.axes_p01,'Visible','off');
set(handles.axes_p02,'Visible','off');
set(handles.axes_Corr,'Visible','off');

set(handles.uipanel_Controls,'Visible','on');

set(handles.pushbutton_AcceptCorr,'Visible','off');
set(handles.pushbutton_CancelCorr,'Visible','off');

guidata(hObject, handles);

setVisibility(hObject, eventdata, handles);
% set(handles.uipanel_MeshOption,'Visible','off');
% set(handles.uipanel_TrackParam,'Visible','off');
% set(handles.pushbutton_Guide,'Visible','off');
% set(handles.pushbutton_RunGuide,'Visible','off');
% set(handles.pushbutton_Animate,'Visible','off');
% set(handles.pushbutton_Track,'Visible','off');

% Update handles structure

% UIWAIT makes rrlmageTrackGUI wait for user response (see UIRESUME)
% uiwait(handles.figure1);

% -----
% ----- GUI Output Func -----
% -----

% --- Outputs from this function are returned to the command line.
function varargout = rrlmageTrackGUI_OutputFcn(hObject, eventdata, handles)
% varargout cell array for returning output args (see VARARGOUT);
% hObject handle to figure
% eventdata reserved - to be defined in a future version of MATLAB
% handles structure with handles and user data (see GUIDATA)

% Get default command line output from handles structure
varargout{1} = handles.output;

% -----
% ----- Load Image (button) -----
% -----

% --- Executes on button press in pushbutton_LoadImage.
function pushbutton_LoadImage_Callback(hObject, eventdata, handles)
% hObject handle to pushbutton_LoadImage (see GCBO)
% eventdata reserved - to be defined in a future version of MATLAB
% handles structure with handles and user data (see GUIDATA)

global imp01 imp02

numFiles=1; % initialize

[FileName,PathName] = uigetfile('p01.tif','Select the p01.tif image');

```

```

if FileName ~= 0

    dlg_title= 'How many files?          ';
    prompt= 'Enter the number (greater than 1) of images to track';
    answer= inputdlg(prompt,dlg_title);
    if size(answer,1) == 1

        [val status] = str2num(answer{1}); % Use curly bracket for subscript
        if ~status
            % Handle empty value returned for unsuccessful conversion
            disp('Error with number of files!');
        else
            numFiles=val;
        end

        % val is a scalar or matrix converted from the first input
        p01=sprintf('%sp%02d.tif',PathName,1);
        imp01=imread(p01);
        imshow(imp01,'Parent',handles.axesImage);
        axis equal;

        p02=sprintf('%sp%02d.tif',PathName,2);
        imp02=imread(p02);

        % handles.imp01= imp01;
        % handles.imp02= imp02;

        handles.visibleArray(2:8)=0;

        if numFiles > 1
            % set(handles.uipanel_MeshOption,'Visible','on');
            % else
            % set(handles.uipanel_MeshOption,'Visible','off');
            handles.visibleArray(2)=1;
        end

        setVisibility(hObject, eventdata, handles);

        % set(handles.uipanel_TrackParam,'Visible','off');
        % set(handles.pushbutton_Guide,'Visible','off');
        % set(handles.pushbutton_RunGuide,'Visible','off');
        % set(handles.pushbutton_Animate,'Visible','off');
        % set(handles.pushbutton_Track,'Visible','off');

    end

    handles.numFiles = numFiles;
    handles.PathName = PathName;

end

guidata(hObject,handles);

% -----
% ----- Mesh Apply (button) -----
% -----

% --- Executes on button press in pushbutton_Mesh.
function pushbutton_Mesh_Callback(hObject, eventdata, handles)
% hObject handle to pushbutton_Mesh (see GCBO)
% eventdata reserved - to be defined in a future version of MATLAB
% handles structure with handles and user data (see GUIDATA)

global meshOption xy minxy maxxxy elements imp01

% imp01=handles.imp01;

if meshOption == 1

```

```

% Make a grid mesh from user input of the corners

[imrows imcols]= size(imp01);

imshow(imp01,'Parent',handles.axesImage);

[xsel1 ysel1]=ginput(1);
xsel1=round(xsel1);
ysel1=round(ysel1);

if ( (xsel1 < 1) || (xsel1> imcols) || (ysel1 < 1) || (ysel1> imrows) )
    disp('Point out of mesh bounding box! Not accepted');
else
    str=sprintf('You chose (%d, %d) for top-left corner ',xsel1,ysel1);
    disp(str);

    hold on;
    plot(handles.axesImage, xsel1,ysel1,'r*');

[xsel2 ysel2] =ginput(1);
xsel2=round(xsel2);
ysel2=round(ysel2);

if ( (xsel2 < xsel1) || (xsel2 > imcols) || (ysel2 < ysel1) || (ysel2 > imrows) )
    disp('Point not allowed. Choose two points for bounding box. Do both again!');
else
    str=sprintf('You chose (%d, %d) for bottom-right corner ', xsel2, ysel2);
    disp(str);
    plot(handles.axesImage,xsel2,ysel2,'r*');
    hold off;

    dlg_title= 'X-Size';
    prompt= 'Enter number of divisions along x';
    answer= inputdlg(prompt,dlg_title);

    if size(answer,1) == 1

        [val status] = str2num(answer{1}); % Use curly bracket for subscript
        if ~status
            % Handle empty value returned for unsuccessful conversion
            disp('Error with x spacing');
        else
            xdiv=val;
            xsize= (xsel2-xsel1)/double(xdiv);

            dlg_title= 'Y-Size';
            num_lines=1;

            prompt= sprintf('Enter number of divisions along y. \nSuggested number is shown');
            ydiv= round((ysel2-ysel1)/xsize);

            def=sprintf('%d',ydiv);
            def={def};
            answer= inputdlg(prompt,dlg_title,num_lines,def);
            if size(answer,1) == 1

                [val status] = str2num(answer{1}); % Use curly bracket for subscript
                if ~status
                    % Handle empty value returned for unsuccessful conversion
                    disp('Error with x spacing');
                else
                    ydiv=val;

                    makeGridMesh(xsel1,ysel1,xsel2,ysel2,xdiv,ydiv);
                    Mesh_Update(hObject, eventdata, handles);

            end
        end
    end

```

```

        end % if size(answer)

        end % if ~status

        end % if size(answer)

        end % if second point is in limits

    end % if 1st point is in limits

else

    % Mesh option is 2

    % Read the nodes and elements from current directory

    % put node x y in array mesh
    xy=load('GUInodes.dat');
    xy(:,2)= -xy(:,2); % convert from cartesian to image coord sys

    % put element id and contour value in array elements
    elements=load('GULElements.dat');

    Mesh_Update(hObject, eventdata, handles);

end

handles.visibleArray(5:8)=0;
handles.visibleArray(3:4)=[1 1];
setVisibility(hObject, eventdata, handles);

% set(handles.uipanel_TrackParam,'Visible','on');
% set(handles.pushbutton_Guide,'Visible','on');
%
% set(handles.pushbutton_RunGuide,'Visible','off');
% set(handles.pushbutton_Animate,'Visible','off');
% set(handles.pushbutton_Track,'Visible','off');
guidata(hObject,handles);

% -----
% ----- Make grid mesh (function) -----
% -----

% --- Executes on button press in pushbutton_Mesh.
function makeGridMesh(xsel1,ySEL1,xsel2,ySEL2,xdiv,ydiv)

global xy elements

xvec=linspace(xsel1,xsel2,xdiv+1);
yvec=linspace(ySEL1,ySEL2,ydiv+1);

[gridx, gridy]= meshgrid(xvec,yvec);

xnodes=gridx';
ynodes=gridy';
xy=[xnodes(:) ynodes(:)];
tmpele=zeros(xdiv*ydiv,4);

for j= 1:ydiv

    for i=1:xdiv
        tmpele((j-1)*xdiv + i,:)= [(i+(j-1)*(xdiv+1)) (1+i+(j-1)*(xdiv+1)) ...
            (xdiv+2+i+(j-1)*(xdiv+1)) (xdiv+1+i+(j-1)*(xdiv+1))];
    end
end

elements=tmpele;

```

```

% -----
% ----- Mesh Update (function) -----
% -----

% --- Executes on button press in pushbutton_Mesh.
function Mesh_Update(hObject, eventdata, handles)

global xy elements imp01

% imp01=handles.imp01;

imshow(imp01,'Parent',handles.axesImage);
hold(handles.axesImage,'on');
patch('faces',elements(:,1:4),'vertices',[xy(:,1), xy(:,2)],'EdgeColor','red','FaceColor','none', ...
    'Parent',handles.axesImage);
hold(handles.axesImage,'off');

guidata(hObject,handles);

% -----
% ----- Specify guide point (button) -----
% -----

% --- Executes on button press in pushbutton_Guide.
function pushbutton_Guide_Callback(hObject, eventdata, handles)
% hObject    handle to pushbutton_Guide (see GCBO)
% eventdata  reserved - to be defined in a future version of MATLAB
% handles    structure with handles and user data (see GUIDATA)

global xy elements minxy maxxy

[xsel ysel]=ginput(1);
xsel=round(xsel);
ysel=round(ysel);

minxy=min(xy);
maxxy=max(xy);

if ( (xsel < minxy(1)) || (xsel> maxxy(1)) || (ysel < minxy(2)) || (ysel> maxxy(2)) )
    disp('Point out of mesh bounding box! Not accepted');

    handles.visibleArray(5:8) = 0;

    % set(handles.pushbutton_RunGuide,'Visible','off');
else
    str=sprintf('You chose (%d, %d) for guide point ',xsel,ysel);
    disp(str);
    Mesh_Update(hObject, eventdata, handles);
    hold(handles.axesImage,'on');
    plot(handles.axesImage,xsel,ysel,'oy');
    hold(handles.axesImage,'off');

    handles.xGuide=xsel;
    handles.yGuide=ysel;

    handles.visibleArray(5:8) = [1 0 0 0];
%     set(handles.pushbutton_RunGuide,'Visible','on');
%     set(handles.uipanel_TrackParam,'Visible','on');
%     set(handles.pushbutton_Guide,'Visible','on');
%
%
%     set(handles.pushbutton_Animate,'Visible','off');
%     set(handles.pushbutton_Track,'Visible','off');
end

```

```

setVisibility(hObject, eventdata, handles);

guidata(hObject,handles);

% -----
% ----- Perform tracking (button) -----
% -----

% --- Executes on button press in pushbutton_Track.
function pushbutton_Track_Callback(hObject, eventdata, handles)
% hObject    handle to pushbutton_Track (see GCBO)
% eventdata  reserved - to be defined in a future version of MATLAB
% handles    structure with handles and user data (see GUIDATA)

global xy elements imp01 minxy maxxy

numFiles= handles.numFiles;
PathName= handles.PathName;

staticNode= handles.staticNode;
staticX= handles.staticX;
staticY= handles.staticY;

kernelSize= (handles.M)*2 +1;
subpixM= handles.subpixM;
maxMove= handles.maxMove;
smoothing= handles.smoothing;
smoothGridSize= handles.smoothGridSize;

% write out the nodes and elements to files which will be read by tracking

fid=fopen('GUInodes_out.dat','w');
tmpxy=[xy(:,1) -xy(:,2)]; % flip to convert from image coord to Cartesian
fprintf(fid,'%12.4f %12.4f \n',tmpxy);
fclose(fid);

fid=fopen('GUElements_out.dat','w');
fprintf(fid,'%d %d %d %d \n',elements');
fclose(fid);

% Get bounding box for smoothing. Better estimate= faster run time

% Avoid spending time in smoothing on grid points outside of mesh
% If this gives trouble then use the full image size for smoothing

bx1=floor(minxy(1)-100);
if bx1<1
    bx1=1;
end

bx2=ceil(maxxy(1)+100);
if bx2 > size(imp01,2)
    bx2=size(imp01,2);
end

by1=floor(minxy(2)-100);
if by1<1
    by1=1;
end

by2=ceil(maxxy(2)+100);
if by2 > size(imp01,1)
    by2=size(imp01,1);
end

disp('-----');

s=sprintf('%s(%d,"%s",...','rrMultiImageTrack_simple',numFiles-1,PathName);
disp(s);
s=sprintf(' "%s","%s",...','
    'GUInodes_out.dat','GUElements_out.dat');

```

```

disp(s);
s=sprintf('      %d,%d,%d,%d,%d,%d,%d,...',...
    staticNode,staticX,staticY,bx1,by1,bx2,by2);
disp(s);
s=sprintf('      %d,%d,%d,%d,%d)',...
    smoothing,kernelSize,maxMove,subpixmap,smoothGridSize);
disp(s);

rrMultImageTrack_simple(numFiles-1,PathName,'GUInodes_out.dat','GUIelements_out.dat',...
    staticNode,staticX,staticY,bx1,by1,bx2,by2,...
    smoothing,kernelSize,maxMove,subpixmap,smoothGridSize,handles); % Added handles as an argument 6-10-
14

disp('-----');
disp('Finished tracking all steps! Ready to animate');

handles.visibleArray(7:8) = [1 1];
setVisibility(hObject, eventdata, handles);
% set(handles.pushbutton_Animate,'Visible','on');

% -----
% ----- Animate (button) -----
% -----

% --- Executes on button press in pushbutton_Animate.
function pushbutton_Animate_Callback(hObject, eventdata, handles)
% hObject    handle to pushbutton_Animate (see GCBO)
% eventdata  reserved - to be defined in a future version of MATLAB
% handles    structure with handles and user data (see GUIDATA)

global xy elements imp01

numFiles=handles.numFiles;
PathName=handles.PathName;

% imp01=handles.imp01;
tmpxy=xy;

gifString="";

for i= 1:numFiles

    s=sprintf('%sp%02d.tif',PathName,i);
    im=imread(s);

    imshow(im,'Parent',handles.axesImage);
    hold(handles.axesImage,'on');

    if i ~=1
        s=sprintf('disp%02d.dat',i-1);
        dispU=load(s);
        dispU(:,2)= -dispU(:,2);
        tmpxy = tmpxy + dispU;
    end

    plot(handles.axesImage,tmpxy(:,1),tmpxy(:,2),'.r');
    hold(handles.axesImage,'off');

    animFrame=getframe(handles.axesImage);
    [theImage, map]=frame2im(animFrame);
    s=sprintf('caps%02d.tif',i);
    imwrite(theImage,s,'tif');
    gifString=sprintf('%s %s',gifString,s); % concatenate file names
    pause(1);
end

gifString=sprintf('convert -delay 15 %s -loop 0 animation.gif',gifString);
disp(gifString);

```

```

% execute the ImageMagick command
[status, result]=system(gifString)

if (status ==0)
    disp('Wrote animation.gif');
else
    disp('Could not make animation.gif');
end

guidata(hObject,handles);

% -----
% ----- Parameter KernelSize (callback) -----
% -----

function edit_KernelSize_Callback(hObject, eventdata, handles)
% hObject   handle to edit_KernelSize (see GCBO)
% eventdata reserved - to be defined in a future version of MATLAB
% handles   structure with handles and user data (see GUIDATA)

% Hints: get(hObject,'String') returns contents of edit_KernelSize as text
%        str2double(get(hObject,'String')) returns contents of edit_KernelSize as a double

kernelSize = str2num(get(handles.edit_KernelSize,'String'));

M=fix(kernelSize/2); % integer part of kernelSize/2

handles.M=M;

s=sprintf('M is %d',M);
disp(s);
guidata(hObject,handles);

% -----
% ----- Parameter KernelSize (create) -----
% -----

% --- Executes during object creation, after setting all properties.
function edit_KernelSize_CreateFcn(hObject, eventdata, handles)
% hObject   handle to edit_KernelSize (see GCBO)
% eventdata reserved - to be defined in a future version of MATLAB
% handles   empty - handles not created until after all CreateFcns called

% Hint: edit controls usually have a white background on Windows.
%       See ISPC and COMPUTER.
if ispc && isequal(get(hObject,'BackgroundColor'), get(0,'defaultUicontrolBackgroundColor'))
    set(hObject,'BackgroundColor','white');
end

handles.M= 15; % default value
disp('M is 15');
guidata(hObject,handles);

% -----
% ----- Parameter Subpix (callback) -----
% -----

function edit_Subpix_Callback(hObject, eventdata, handles)
% hObject   handle to edit_Subpix (see GCBO)
% eventdata reserved - to be defined in a future version of MATLAB
% handles   structure with handles and user data (see GUIDATA)

% Hints: get(hObject,'String') returns contents of edit_Subpix as text
%        str2double(get(hObject,'String')) returns contents of edit_Subpix as a double

subpixM = str2num(get(handles.edit_Subpix,'String'));
handles.subpixM=subpixM;

```

```

s=sprintf('subpixM is %d',subpixM);
disp(s);
guidata(hObject,handles);

% -----
% ----- Parameter Subpix (create) -----
% -----

% --- Executes during object creation, after setting all properties.
function edit_Subpix_CreateFcn(hObject, eventdata, handles)
% hObject   handle to edit_Subpix (see GCBO)
% eventdata reserved - to be defined in a future version of MATLAB
% handles   empty - handles not created until after all CreateFcns called

% Hint: edit controls usually have a white background on Windows.
%       See ISPC and COMPUTER.
if ispc && isequal(get(hObject,'BackgroundColor'), get(0,'defaultUicontrolBackgroundColor'))
    set(hObject,'BackgroundColor','white');
end

handles.subpixM= 9; % default value
disp('subpixM is 9');
guidata(hObject,handles);

% -----
% ----- Parameter Smooth (callback) -----
% -----

function edit_Smooth_Callback(hObject, eventdata, handles)
% hObject   handle to edit_Smooth (see GCBO)
% eventdata reserved - to be defined in a future version of MATLAB
% handles   structure with handles and user data (see GUIDATA)

% Hints: get(hObject,'String') returns contents of edit_Smooth as text
%       str2double(get(hObject,'String')) returns contents of edit_Smooth as a double

smoothing = str2num(get(handles.edit_Smooth,'String'));
handles.smoothing=smoothing;

s=sprintf('smoothing is %d',smoothing);
disp(s);
guidata(hObject,handles);

% -----
% ----- Parameter Smooth (create) -----
% -----

% --- Executes during object creation, after setting all properties.
function edit_Smooth_CreateFcn(hObject, eventdata, handles)
% hObject   handle to edit_Smooth (see GCBO)
% eventdata reserved - to be defined in a future version of MATLAB
% handles   empty - handles not created until after all CreateFcns called

% Hint: edit controls usually have a white background on Windows.
%       See ISPC and COMPUTER.
if ispc && isequal(get(hObject,'BackgroundColor'), get(0,'defaultUicontrolBackgroundColor'))
    set(hObject,'BackgroundColor','white');
end

smoothing=5;
handles.smoothing=smoothing;

disp('smoothing is 5');

guidata(hObject,handles);

% -----

```

```

% ----- Parameter maxMove (callback) -----
% -----

function edit_MaxMove_Callback(hObject, eventdata, handles)
% hObject handle to edit_MaxMove (see GCBO)
% eventdata reserved - to be defined in a future version of MATLAB
% handles structure with handles and user data (see GUIDATA)

% Hints: get(hObject,'String') returns contents of edit_MaxMove as text
% str2double(get(hObject,'String')) returns contents of edit_MaxMove as a double

maxMove = str2num(get(handles.edit_MaxMove,'String'));
handles.maxMove=maxMove;

s=sprintf('maxMove is %d',maxMove);
disp(s);
guidata(hObject,handles);

% -----
% ----- Parameter maxMove (create) -----
% -----

% --- Executes during object creation, after setting all properties.
function edit_MaxMove_CreateFcn(hObject, eventdata, handles)
% hObject handle to edit_MaxMove (see GCBO)
% eventdata reserved - to be defined in a future version of MATLAB
% handles empty - handles not created until after all CreateFcns called

% Hint: edit controls usually have a white background on Windows.
% See ISPC and COMPUTER.
if ispc && isequal(get(hObject,'BackgroundColor'), get(0,'defaultUicontrolBackgroundColor'))
    set(hObject,'BackgroundColor','white');
end

maxMove = 15;
handles.maxMove=maxMove;

s=sprintf('maxMove is %d',maxMove);
disp(s);
guidata(hObject,handles);

% -----
% ----- Parameter smoothGridSize (callback) -----
% -----

function edit_smoothGridSize_Callback(hObject, eventdata, handles)
% hObject handle to edit_smoothGridSize (see GCBO)
% eventdata reserved - to be defined in a future version of MATLAB
% handles structure with handles and user data (see GUIDATA)

% Hints: get(hObject,'String') returns contents of edit_smoothGridSize as text
% str2double(get(hObject,'String')) returns contents of edit_smoothGridSize as a double

smoothGridSize = str2num(get(handles.edit_smoothGridSize,'String'));
handles.smoothGridSize=smoothGridSize;

s=sprintf('smoothGridSize is %d',smoothGridSize);
disp(s);
guidata(hObject,handles);

% -----
% ----- Parameter smoothGridSize (create) -----
% -----

% --- Executes during object creation, after setting all properties.
function edit_smoothGridSize_CreateFcn(hObject, eventdata, handles)
% hObject handle to edit_smoothGridSize (see GCBO)
% eventdata reserved - to be defined in a future version of MATLAB
% handles empty - handles not created until after all CreateFcns called

```

```

% Hint: edit controls usually have a white background on Windows.
% See ISPC and COMPUTER.
if ispc && isequal(get(hObject,'BackgroundColor'), get(0,'defaultUicontrolBackgroundColor'))
    set(hObject,'BackgroundColor','white');
end

smoothGridSize = 25;
handles.smoothGridSize=smoothGridSize;

s=sprintf('smoothGridSize is %d',smoothGridSize);
disp(s);
guidata(hObject,handles);

% -----
% ----- MeshOption (param select) -----
% -----

% --- Executes when selected object is changed in uipanel_MeshOption.
function uipanel_MeshOption_SelectionChangeFcn(hObject, eventdata, handles)
% hObject handle to the selected object in uipanel_MeshOption
% eventdata structure with the following fields (see UIBUTTONGROUP)
% EventName: string 'SelectionChanged' (read only)
% OldValue: handle of the previously selected object or empty if none was selected
% NewValue: handle of the currently selected object
% handles structure with handles and user data (see GUIDATA)

global meshOption

switch get(eventdata.NewValue,'Tag') % Get Tag of selected object.
case 'radiobutton_CreateGrid'
    % Code for when Create Grid is selected.
    meshOption=1;
    disp('You selected Create grid');
case 'radiobutton_ReadMesh'
    % Code for when Read Mesh is selected.
    meshOption=2;
    disp('You selected Read mesh');
otherwise
    % Code for when there is no match.
end

% --- Executes during object creation, after setting all properties.
function uipanel_MeshOption_CreateFcn(hObject, eventdata, handles)
% hObject handle to uipanel_MeshOption (see GCBO)
% eventdata reserved - to be defined in a future version of MATLAB
% handles empty - handles not created until after all CreateFcns called

global meshOption

meshOption =2;

% -----
% ----- Correlation Accept -----
% -----

% --- Executes on button press in pushbutton_AcceptCorr.
function pushbutton_AcceptCorr_Callback(hObject, eventdata, handles)
% hObject handle to pushbutton_AcceptCorr (see GCBO)
% eventdata reserved - to be defined in a future version of MATLAB
% handles structure with handles and user data (see GUIDATA)

global xy elements

cla(handles.axes_p01,'reset');
set(handles.axes_p01,'Visible','off');

```

```

cla(handles.axes_p02,'reset');
set(handles.axes_p02,'Visible','off');

cla(handles.axes_Corr,'reset');
set(handles.axes_Corr,'Visible','off');

set(handles.axesImage,'Visible','on');

set(handles.pushbutton_AcceptCorr,'Visible','off');
set(handles.pushbutton_CancelCorr,'Visible','off');
set(handles.text_Corr,'Visible','off');
set(handles.text_p01,'Visible','off');
set(handles.text_p02,'Visible','off');

set(handles.uipanel_Controls,'Visible','on');

handles.visibleArray(6:8)= [1 0 0];
setVisibility(hObject, eventdata, handles);

% set(handles.pushbutton_Track,'Visible','on');
% set(handles.pushbutton_Animate,'Visible','off');

Mesh_Update(hObject, eventdata, handles);
hold(handles.axesImage,'on');
plot(handles.axesImage,handles.xGuide,handles.yGuide,'oy');
hold(handles.axesImage,'off');

% compute the staticNode which is the node closest to the guide point
xGuide= handles.xGuide;
yGuide= handles.yGuide;

tmpxy= xy;
tmpxy(:,1)= tmpxy(:,1)-xGuide;
tmpxy(:,2)= tmpxy(:,2)-yGuide;
dist= tmpxy(:,1).*tmpxy(:,1) + tmpxy(:,2).*tmpxy(:,2);
[minDist, minIndex]=min(dist);
s=sprintf('Closest static node is #%d at (%10.3f,%10.3f)',minIndex,xy(minIndex,1),xy(minIndex,2));
disp(s);
handles.staticNode=minIndex;

guidata(hObject,handles);

% -----
% ----- Correlation Cancel -----
% -----

% --- Executes on button press in pushbutton_CancelCorr.
function pushbutton_CancelCorr_Callback(hObject, eventdata, handles)
% hObject handle to pushbutton_CancelCorr (see GCBO)
% eventdata reserved - to be defined in a future version of MATLAB
% handles structure with handles and user data (see GUIDATA)

cla(handles.axes_p01,'reset');
set(handles.axes_p01,'Visible','off');

cla(handles.axes_p02,'reset');
set(handles.axes_p02,'Visible','off');

cla(handles.axes_Corr,'reset');
set(handles.axes_Corr,'Visible','off');

set(handles.axesImage,'Visible','on');

set(handles.pushbutton_AcceptCorr,'Visible','off');
set(handles.pushbutton_CancelCorr,'Visible','off');
set(handles.text_Corr,'Visible','off');
set(handles.text_p01,'Visible','off');
set(handles.text_p02,'Visible','off');

```

```

set(handles.uipanel_Controls,'Visible','on');

handles.visibleArray(6:8)=0;
% set(handles.pushbutton_Track,'Visible','off');
% set(handles.pushbutton_Animate,'Visible','off');

Mesh_Update(hObject, eventdata, handles);
setVisibility(hObject, eventdata, handles);

hold(handles.axesImage,'on');
plot(handles.axesImage,handles.xGuide,handles.yGuide,'oy');
hold(handles.axesImage,'off');

guidata(hObject,handles);

% -----
% ----- Run and Check Guide -----
% -----

% --- Executes on button press in pushbutton_RunGuide.
function pushbutton_RunGuide_Callback(hObject, eventdata, handles)
% hObject    handle to pushbutton_RunGuide (see GCBO)
% eventdata  reserved - to be defined in a future version of MATLAB
% handles    structure with handles and user data (see GUIDATA)

global imp01 imp02

cla(handles.axesImage,'reset');
cla(handles.axes_p01,'reset');
cla(handles.axes_p02,'reset');
cla(handles.axes_Corr,'reset');

set(handles.axesImage,'Visible','off');
set(handles.pushbutton_AcceptCorr,'Visible','on');
set(handles.pushbutton_CancelCorr,'Visible','on');
set(handles.text_Corr,'Visible','on');
set(handles.text_p01,'Visible','on');
set(handles.text_p02,'Visible','on');

% set(handles.uipanel_Corr,'Visible','on');
set(handles.uipanel_Controls,'Visible','off');

M=handles.M;

% imp01=handles.imp01;
% imp02=handles.imp02;
% imp01=imread('p01.tif');
% imp02=imread('p02.tif');

xGuide= handles.xGuide;
yGuide= handles.yGuide;

cut0=imcrop(imp01,[(xGuide-M) (yGuide-M) (2*M) (2*M)]);
cut1=imcrop(imp02,[(xGuide-2*M) (yGuide-2*M) (4*M) (4*M)]);

% Want to display the kernel inside the axes of size 124,124.

xleft= xGuide-64;
if xleft < 0
    xleft = 1;
    xright= xleft+124
else
    xright=xleft+124;
end

yleft= yGuide-64;
if yleft < 0

```

```

yleft = 1;
yright= yleft+124
else
yright=yleft+124;
end

if xright > size(imp01,2)
xright=size(imp01,2);
end
if yright > size(imp01,1)
yright=size(imp01,1);
end

dcut1= imcrop(imp01,[yleft yleft (xright-xleft) (yright-yleft)]);
dcut2= imcrop(imp02,[yleft yleft (xright-xleft) (yright-yleft)]);

xbox1= [ (xGuide-xleft+1-M) ; (xGuide-xleft+1+M) ; (xGuide-xleft+1+M) ; (xGuide-xleft+1-M) ; (xGuide-xleft+1-M)
];
ybox1= [ (yGuide-yleft+1-M) ; (yGuide-yleft+1-M) ; (yGuide-yleft+1+M) ; (yGuide-yleft+1+M) ; (yGuide-yleft+1-M)
];

h_p01=handles.axes_p01;
h_p02=handles.axes_p02;
h_corr= handles.axes_Corr;

axes(h_p01);
imshow(dcut1,'Parent',h_p01);

hold(h_p01);
plot(h_p01,xGuide-xleft+1, yGuide-yleft+1,'.y');
plot(h_p01,xbox1',ybox1','-y');
hold(h_p01);

% cut0=handles.imCropp01; % size (2M+1, 2M+1)
% cut1=handles.imCropp02; % size (4M+1, 4M+1)
% M=(handles.kernelSize-1)/2;

[czncc]=normxcorr2(cut0,cut1); % size (6M+1, 6M+1)

czncc2=czncc( (1+M):(1+5*M) , (1+M):(1+5*M) ); % size is (4M+1, 4M+1)

% offset found by correlation
[max_c, imax] = max(abs(czncc(:)));
[ypeak, xpeak] = ind2sub(size(czncc),imax(1));

% Find offset of peak from the center
center_offset = [(xpeak-3*M-1) (ypeak-3*M-1)]

%%%%%%%%%%%%%%%%%%%%%%%%%%%%%%%%%%%%%%%%%%%%%%%%%%%%%%%%%%%%%%%%%%%%%%%% Modified by E.A.S. on 11/26/13 to remove offset %%%%%%%%%%%%%%
% In the future add button to GUI so that subsequent users are aware %%
center_offset = [0 0];
%%%%%%%%%%%%%%%%%%%%%%%%%%%%%%%%%%%%%%%%%%%%%%%%%%%%%%%%%%%%%%%%%%%%%%%%
%%%%%%%%%%%%%%%%%%%%%%%%%%%%%%%%%%%%%%%%%%%%%%%%%%%%%%%%%%%%%%%%%%%%%%%%
axes(h_p02);
imshow(dcut2,'Parent',h_p02);
hold(h_p02);
plot(h_p02,xGuide-xleft+1, yGuide-yleft+1,'.y');
plot(h_p02,xGuide-xleft+1+center_offset(1), yGuide-yleft+1+center_offset(2),'c');
plot(h_p02,xbox1'+center_offset(1),ybox1'+center_offset(2),'-c');

hold(h_p02);

[xx,yy]=meshgrid([-3*M:3*M],[-3*M:3*M]);
axes(h_corr);
surf(h_corr,xx,yy,czncc);
xlabel(h_corr,'x');

```

```

ylabel(h_corr,'y');

shading(h_corr,'flat');

handles.staticX=center_offset(1);
handles.staticY=center_offset(2);

% Matlab doesn't let us use more than 1 colormap in a figure (includes
% subfigures). So we use freezeColors external code as a workaround
colormap(h_corr,'jet');
freezeColors(h_corr);
colormap('gray');

% set(handles.axes_Corr,'Toolbar','figure');

guidata(hObject,handles);

% -----
% ----- Write the Strains for Tecplot -----
% -----

% --- Executes on button press in pushbutton_writeStrains.
function pushbutton_writeStrains_Callback(hObject, eventdata, handles)
% hObject    handle to pushbutton_writeStrains (see GCBO)
% eventdata  reserved - to be defined in a future version of MATLAB
% handles    structure with handles and user data (see GUIDATA)

global xy elements

numFiles=handles.numFiles;

[writeStrainFile, writeStrainPath] = uigetfile({'writeStrainRR_simple',...
'C++ executable (writeStrainRR_simple)', 'Where is the writeStrainRR_simple file?');

if writeStrainFile == 0
    % Handle empty value returned for unsuccessful conversion
    disp('Error with location of writeStrainRR_simple');
else
    dispString=sprintf('%swriteStrainRR_simple      %d      %d      %d',writeStrainPath,numFiles-
1,size(xy,1),size(elements,1))

    [status, result] = system(dispString)

    % if (status ==0)
    %     disp('Finished writing');
    % else
    %     disp('Problem with tecplot strains');
    % end
end

guidata(hObject, handles);

% -----
% ----- Checkbox for Visibility -----
% -----

% --- Executes on button press in checkbox_Visible.
function checkbox_Visible_Callback(hObject, eventdata, handles)
% hObject    handle to checkbox_Visible (see GCBO)
% eventdata  reserved - to be defined in a future version of MATLAB
% handles    structure with handles and user data (see GUIDATA)

% Hint: get(hObject,'Value') returns toggle state of checkbox_Visible

%checkboxStatus = 0, if the box is unchecked,
%checkboxStatus = 1, if the box is checked

```

```

checkboxStatus = get(hObject,'Value');
handles.checkboxStatus = checkboxStatus;

%if box is unchecked, only buttons that are relevant are visible

setVisibility(hObject, eventdata, handles);

guidata(hObject, handles);

% -----
% ----- Set Visibility of Windows -----
% -----

function setVisibility(hObject, eventdata, handles)

visibleArray = handles.visibleArray;
checkboxStatus = handles.checkboxStatus;

handlesArray = {
    handles.pushbutton_LoadImage, ...
    handles.uipanel_MeshOption, ...
    handles.uipanel_TrackParam, ...
    handles.pushbutton_Guide, ...
    handles.pushbutton_RunGuide, ...
    handles.pushbutton_Track, ...
    handles.pushbutton_Animate, ...
    handles.pushbutton_writeStrains};

for i= 1:size(handlesArray,2)

    if (checkboxStatus == 1) || (visibleArray(i) == 1)
        set(handlesArray{i}, 'Visible', 'on');
    else
        set(handlesArray{i}, 'Visible', 'off');
    end
end

guidata(hObject, handles);

```



```

figure(1)
clf;
% load and display original reference image
im=imread([imnamebrightfield,'01.tif']);
if adjcontrast, im=imadjust(im,stretchlim(im,0),[0,1]); end% adjust contrast
imshow(im);
hold on

% load positon grid points (nodes)
xyraw=load('GUInodes_out.dat');
xy0=xyraw;
xy0(:,2)=-xy0(:,2); % y-axis images is mirrored vertically

% plot original reference grid
plot(xy0(:,1),xy0(:,2),'*g');
if refnode && correctshift==1, plot(xy0(refnode,1),xy0(refnode,2),'og'); end% plot circle around reference node
when correcting for image movement, check rotation as well
nnodes = length(xy0(:,1)); % number of grid points
if plotnumbers, for i=1:nnodes, text(xy0(i,1),xy0(i,2),num2str(i),'Color',[0 1 0]); end, end % plot numbers

% --- Load data for the incremental displacement between each image and the next

% disp01.dat is the displacement between image 01 and image 02
% disp02.dat is the displacement between image 02 and image 03
% etc

% --- initialise variables
Uabs=zeros(nnodes,numFiles-1); % initialise array with absolute displacements with respect to the original
reference image for each image
Umean=zeros(1,numFiles-1); %mean
Ustd=zeros(1,numFiles-1); %std
Uperc95=zeros(1,numFiles-1); %95th percentile
Uperc90=zeros(1,numFiles-1); %90th percentile
Uavtop=zeros(1,numFiles-1);
dispUtoti=zeros(nnodes,2,numFiles-1); % initialise array with total displacement for each time point
dispTranstot=zeros(2,numFiles-1); % total translation image with respect to reference image for each time point
dispRefnodetot=zeros(2,numFiles-1); % total translation reference point with respect to reference image for
each time point

imref=imread([imnamefluor,num2str(1,'%02d'),'tif']); % load first fluorescent image
imref=imadjust(imref,stretchlim(imref,0),[0,1]);
% --- start loop over image pairs:
dispUtot=zeros(nnodes,2); % initialise array with total displacement
tmpxy_old=xy0;
for i=1:numFiles-1

    if correctshift==2
        % calculate image translation -> now do this with respect to reference image instead to avoid cumulative
rounding errors?
        imnew=imread([imnamefluor,num2str(i+1,'%02d'),'tif']); % load fluorescent image
        imnew=imadjust(imnew,stretchlim(imnew,0),[0,1]);
        tformEstimate = imregcorr(imnew,imref,'translation');
        xshift=tformEstimate.T(3,1);
        yshift=tformEstimate.T(3,2);
        dispTranstot(:,i)=[-xshift;-yshift];
    end

    % get displacements with respect to the previous image and add to total displacement with respect to
reference image
    s=[ 'disp',num2str(i,'%02d'),'dat'];
    dispU=load(s);
    dispU(:,2)= -dispU(:,2); % image coordinates upside down, verify this
    dispUtot = dispUtot+dispU; % add incremental displacement to total displacement
    dispUtoti(:,i) = dispUtot; % store displacement for this time point

    if refnode, dispRefnodetot(:,i)=dispUtoti(refnode,:,i); end % get total displacement for reference node

    dispUtotcorr(:,i)=dispUtoti(:,i);
    if refnode && correctshift==1 % correct displacements for image shift using either a reference node or image
registration

```

## Appendix A

```
dispUtotcorr(:,1)=dispUtoti(:,1,i) - dispRefnodetot(1,i);
dispUtotcorr(:,2)=dispUtoti(:,2,i) - dispRefnodetot(2,i);
elseif correctshift==2
dispUtotcorr(:,1)=dispUtoti(:,1,i) - dispTranstot(1,i);
dispUtotcorr(:,2)=dispUtoti(:,2,i) - dispTranstot(2,i);
end

Uabs(:,i)= sqrt(dispUtotcorr(:,1).^2 + dispUtotcorr(:,2).^2); % absolute corrected displacement gridpoints with
respect to reference image

Umean(i)=mean(Uabs(:,i));
Ustd(i)=std(Uabs(:,i));
Uperc90(i) = prctile(Uabs(:,i),90); % 90th percentile
Uperc95(i) = prctile(Uabs(:,i),95); % 95th percentile

% calculate average top displacement,
ind=find(Uabs(:,i)>=bgthresh); % find points with displacements greater than the background noise
Ufg = Uabs(ind,i); % get displacements for these nodes
k=ceil(length(Ufg)*topfrac/100); % calculate number of points that make up the highest 'topfrac' percentage.
This will be rounded up. Note for small grids this is less meaningful.
Utop = maxk(Ufg,k); % displacements for the highest 'topfrac' percentage
Uavtop(i)=mean(Utop);

% plot new positions in original image
tmpxy_new = xy0 + dispUtotcorr(:,i); % new node positions
plot(tmpxy_new(:,1),tmpxy_new(:,2),'*r');
for j = 1:nnodes
plot([tmpxy_old(j,1), tmpxy_new(j,1)], [tmpxy_old(j,2), tmpxy_new(j,2)], 'b') % blue line to connect old and new
node positions
end
tmpxy_old = tmpxy_new; % store node positions for next step
end
if refnode && correctshift==1
title(['Nodal positions over time shown in reference image. Displacements node ',num2str(refnode),'
subtracted'])
elseif correctshift==2
title(['Nodal positions over time shown in reference image. Displacements due to image shifts corrected using
image registration'])
elseif correctshift==0
title(['Nodal positions over time shown in reference image. Displacements not corrected for image shifts'])
end
% Example:
% type Uabs(:,1) to access the displacement of image 2 with respect to image 1
% type Uabs(:,2) to access the displacement of image 3 with respect to image 1
% type Uabs(:,5) to access the displacement of image 6 with respect to image 1

% -----
% plot images with displacement arrows (use scale factor to magnify if needed)
jetcol; % script with colours from jet colourmap, stored in jetcols;
maxdispexp=max(max(Uabs));
if custmaxdisp
maxdisp=custmaxdisp;% CAN USE A CUSTOM VALUE INSTEAD BASED ON THE MAXIMUM
DISPLACEMENT ACROSS MULTIPLE EXPERIMENTS TO GET A CONSISTENT COLOUR SCALING
else
maxdisp=maxdispexp;
end

for ivid=1:2
switch ivid
case 1
imnamemovarrow=imnamebrightfield;
case 2
imnamemovarrow=imnamefluor;
end

if makemov
vidobj1=VideoWriter(['cellmov_arrow_',imnamemovarrow]); % make sure movie is closed in media player if
overwriting
```

```

set(vidobj1,'FrameRate',Frameratemov);
open(vidobj1);
end
% --- start loop over image pairs:
for i=1:numFiles-1
    figure(3+ivid)
    clf;
    im=imread([imnamemovarrow,num2str(i+1,'%02d'),'tif']); % load image
    if adjcontrast, im=imadjust(im,stretchlim(im,0),[0,1]); end % adjust contrast
    imshow(im);
    hold on;
    % plot arrows from original position shifted with the reference node so it
    % matches the current image
    xy0plot=xy0;
    dispUtotcorr(:,:)=dispUtoti(:,i);
    if refnode && correctshift==1 % correct plot positions and displacements for image shifts
        xy0plot(:,1)=xy0(:,1) + dispRefnodetot(1,i);
        xy0plot(:,2)=xy0(:,2) + dispRefnodetot(2,i);
        dispUtotcorr(:,1)=dispUtoti(:,1,i) - dispRefnodetot(1,i);
        dispUtotcorr(:,2)=dispUtoti(:,2,i) - dispRefnodetot(2,i);
    elseif correctshift==2
        xy0plot(:,1)=xy0(:,1) + dispTranstot(1,i);
        xy0plot(:,2)=xy0(:,2) + dispTranstot(2,i);
        dispUtotcorr(:,1)=dispUtoti(:,1,i) - dispTranstot(1,i);
        dispUtotcorr(:,2)=dispUtoti(:,2,i) - dispTranstot(2,i);
    end
    %quiver(xy0plot(:,1),xy0plot(:,2),dispUtot(:,1),dispUtot(:,2),Scalefactor,'color',[0 1 0]); %Scalefactor = 0; %
    set to zero for no automatic scaling of displacement arrows in movie and final image
    % --- Plot coloured arrows instead ---
    for j=1:nnodes
        dispi=Uabs(j,i);
        colind=1+round((dispi/maxdisp)*63);

h2=quiver(xy0plot(j,1),xy0plot(j,2),ScalefactorNEW*dispUtotcorr(j,1),ScalefactorNEW*dispUtotcorr(j,2),0,'color',
,jetcols(colind,:));
        set(h2,'LineWidth',1.5);
        set(h2,'Maxheadsize',5);
    end
    % ---
    if refnode && correctshift==1
        title(['Displacement vectors shown in image ',num2str(i+1),' positions and displacements corrected for
node ',num2str(refnode)])
    elseif correctshift==2
        title(['Displacement vectors shown in image ',num2str(i+1),' positions and displacements corrected
using image registration'])
    elseif correctshift==0
        title(['Displacement vectors shown in image ',num2str(i+1),' positions and displacements not corrected
for image shifts'])
    end
    saveas(gcf,[imnamemovarrow,num2str(i+1,'%02d'),'arrows'],'tif');

    if makemov
        frame=getframe(gcf);
        writeVideo(vidobj1,frame); % add image to movie
    end
end

if makemov, close(vidobj1); end % close movie file

end

figure
colormap(jetcols)
caxis([0, maxdisp])
h=colorbar;
h.Label.String='pixel';
h.Label.FontSize=12;
axis off;
title(['Colourscale used in vector plots, max displacement = ',num2str(maxdisp)])
saveas(h,['arrow_colourscale'],'tif');
% -----

```

## Appendix A

```
% Make movie - does not use reference node, positions identified plotted in the corresponding images
if makemov
    vidobj=VideoWriter(['cellmovie_',imnameflour]); % make sure movie is closed in mediaplayer if overwriting
    set(vidobj,'FrameRate',Frameratemov);
    open(vidobj);

    figure(3)
    clf;
    im=imread([imnameflour,'01.tif']); %
    if adjcontrast, im=imadjust(im,stretchlim(im,0),[0,1]); end% adjust contrast
    imshow(im);
    hold on
    % axis off;
    % set(gcf,'color','w');
    % set(gca,'color','w');
    % set(gcf,'InvertHardCopy','off');
    % drawnow
    frame=getframe(gcf);
    writeVideo(vidobj,frame); % add image to movie

    dispUtot2=zeros(nnodes,2); % initialise array with total displacement
    % --- start loop over image pairs:
    for i=1:numFiles-1
        % get displacements with respect to the previous image and add to total displacement with respect to
reference image
        % could have used previously loaded data, but this keeps it modular
        s=['disp',num2str(i,'%02d'),' .dat'];
        dispU=load(s);
        dispU(:,2)=-dispU(:,2); % verify this
        dispUtot2 = dispUtot2 + dispU; % add incremental displacement to total displacement

        figure(3)
        clf
        im=imread([imnameflour,num2str(i+1,'%02d'),' .tif']); % load brightfield image
        if adjcontrast, im=imadjust(im,stretchlim(im,0),[0,1]); end% adjust contrast
        imshow(im);
        hold on;
        % plot new positions in current image
        tmpxy_new = xy0 + dispUtot2; % new node positions
        h=plot(tmpxy_new(:,1),tmpxy_new(:,2),'r'); % comment out if you don't want a 'r' plotted
        set(h,'MarkerSize',12);
        for j = 1:nnodes
            plot([xy0(j,1), tmpxy_new(j,1)],[xy0(j,2),tmpxy_new(j,2)],'c') % cyan line to connect reference and
current node positions
        end

        frame=getframe(gcf);
        writeVideo(vidobj,frame); % add image to movie
    end

    close(vidobj) % close movie file
end
if plotnumbers, for i=1:nnodes, text(xy0(i,1),xy0(i,2),num2str(i),'Color',[0 1 0]); end, end % plot numbers
plot(xy0(:,1),xy0(:,2),'g'); % comment out if you don't want a 'g' plotted
title(['Image ',num2str(numFiles),', original (green) and last position (red) uncorrected for image movement'])

save('workspace_vars')
```

## List of References

- Adamopoulos C, Gargalionis AN, Piperi C, Papavassiliou AG. (2017). Recent Advances in Mechanobiology of Osteosarcoma. *J Cell Biochem.* 118(2):232-236. doi: 10.1002/jcb.25660.
- Ahearne M. (2014). Introduction to cell-hydrogel mechanosensing. *Interface Focus.* 4(2):20130038. doi: 10.1098/rsfs.2013.0038.
- Ahmed EM. (2015). Hydrogel: Preparation, characterization, and applications: A review. *J Adv Res.* 6(2):105-21. doi: 10.1016/j.jare.2013.07.006.
- Angelini A, Trial J, Ortiz-Urbina J, Cieslik KA. (2020). Mechanosensing dysregulation in the fibroblast: A hallmark of the ageing heart. *Ageing Res Rev.* 63:101150. doi: 10.1016/j.arr.2020.101150.
- Bao, M., Xie, J., Katoele, N., Hu, X., Wang, B., Piruska, A., & Huck, W. (2019). Cellular Volume and Matrix Stiffness Direct Stem Cell Behavior in a 3D Microniche. *ACS applied materials & interfaces*, 11(2), 1754–1759. doi:10.1021/acsami.8b19396
- Barreca MM, Cancemi P, Geraci F. (2020). Mesenchymal and Induced Pluripotent Stem Cells-Derived Extracellular Vesicles: The New Frontier for Regenerative Medicine? *9(5):1163.* doi: 10.3390/cells9051163.
- Basu S, Sutradhar S, Paul R. (2018). Substrate stiffness and mechanical stress due to intercellular cooperativity guides tissue structure. *J Theor Biol.* 457:124-136. doi: 10.1016/j.jtbi.2018.08.001
- Bellas E., Chen C. (2014) Forms, forces, and stem cell fate. *ScienceDirect Current Opinion in Cell Biology.* 31:92–97. doi:10.1016/j.ceb.2014.09.006.
- Benayahu D, Wiesenfeld Y, Sapir-Koren R. (2019). How is mechanobiology involved in mesenchymal stem cell differentiation toward the osteoblastic or adipogenic fate? *J Cell Physiol.* 234(8):12133-12141. doi: 10.1002/jcp.28099.
- Bianco P, Riminucci M, Gronthos S, Robey PG. (2001). Bone marrow stromal stem cells: nature, biology, and potential applications. *Stem Cells.* 19(3):180-92. doi: 10.1634/stemcells.19-3-180.
- Bianco P, Robey PG, Simmons PJ. (2008). Mesenchymal stem cells: revisiting history, concepts, and assays. *Cell Stem Cell.* 2(4):313-319. doi:10.1016/j.stem.2008.03.002
- Bianco, P., & Gehron Robey, P. (2000). Marrow stromal stem cells. *The Journal of clinical investigation*, 105(12), 1663–1668. doi:10.1172/JCI10413.
- Bianco P, Robey PG. (2015). Skeletal stem cells. *Development.* 142(6):1023-7. doi: 10.1242/dev.102210.

## List of References

- Bonnans C, Chou J., Werb Z. (2014). Remodelling the extracellular matrix in development and disease. *Nat Rev Mol Cell Biol.* 15(12): 786–801. doi:10.1038/nrm3904.
- Boudou T, Ohayon J, Picart C, Pettigrew RI, Tracqui P. (2009). Nonlinear elastic properties of polyacrylamide gels: implications for quantification of cellular forces. *Biorheology.* 46(3):191-205. doi:10.3233/BIR-2009-0540.
- Burdick J., Mauck R., Gerecht S. (2016). To serve and protect Hydrogels from improving stem cell-based therapies. *Cell Stem Cell* 18. doi: 10.1016/j.stem.2015.12.004.
- Butler JP, Tolić-Nørrelykke IM, Fabry B, Fredberg JJ. (2002). Traction fields, moments, and strain energy that cells exert on their surroundings. *Am J Physiol Cell Physiol.* 282(3): C595-C605. doi:10.1152/ajpcell.00270.2001
- Buxboim A, Rajagopal K, Brown AE, Discher DE. (2010). How deeply cells feel: methods for thin gels. *J Phys Condens Matter.* 22(19):194116. doi: 10.1088/0953-8984/22/19/194116.
- Carter DR, Wong M. (1988). The role of mechanical loading histories in the development of diarthrodial joints. *J Orthop Res* 6:804–816.
- Caliarì S, Burdick JA. (2016). A Practical Guide to Hydrogels for Cell Culture. *Nat Methods.* 13(5): 405–414. doi:10.1038/nmeth.3839.
- Carvalho MS, Cabral JMS, da Silva CL, Vashishth D. (2021). Bone Matrix Non-Collagenous Proteins in Tissue Engineering: Creating New Bone by Mimicking the Extracellular Matrix. *Polymers (Basel).* 13(7):1095. doi: 10.3390/polym13071095.
- Chaudhuri O, Cooper-White J, Janmey PA, Mooney DJ, Shenoy VB. (2020). Effects of extracellular matrix viscoelasticity on cellular behaviour. *Nature.* 584(7822):535-546. doi: 10.1038/s41586-020-2612-2.
- Chen FM, Liu X. Advancing biomaterials of human origin for tissue engineering. (2016). *Prog Polym Sci.* 53:86-168. doi: 10.1016/j.progpolymsci.2015.02.004.
- Chen ML, Ruberti JW, Nguyen TD. (2018). Increased stiffness of collagen fibrils following cyclic tensile loading. *J Mech Behav Biomed Mater.* 82:345-354. doi: 10.1016/j.jmbbm.
- Chen T, Saw TB, Mège RM, Ladoux B. (2018). Mechanical forces in cell monolayers. *J Cell Sci.* 131(24):jcs218156. doi: 10.1242/jcs.218156.
- Christensen L., Camitz L., Illigen K., Hansen M., Sarvaa R., Conaghan P.G. (2016). Synovial incorporation of polyacrylamide hydrogel after injection into normal and osteoarthritic animal joints. *Osteoarthritis and Cartilage* 24: 1999-2002. doi: 10.1016/j.joca.2016.07.007.
- Dembo M, Wang YL. (1999). Stresses at the cell-to-substrate interface during locomotion of fibroblasts. *Biophys J.* 76(4):2307-16. doi: 10.1016/S0006-3495(99)77386-8.

- Deng Z, Jia Y, Liu H, He M, Yang Y, Xiao W, Li Y. (2019). RhoA/ROCK pathway: implication in osteoarthritis and therapeutic targets. *Am J Transl Res.* 11(9):5324-5331.
- Discher DE, Janmey P, Wang YL. (2005). Tissue cells feel and respond to the stiffness of their substrate. *Science.* 310(5751):1139-43. doi: 10.1126/science.1116995.
- Doyle A., Yamada K. (2016). Mechanosensing via cell-matrix adhesions in 3D microenvironments. *Experimental Cell Research.* 343(2016):60–66. doi: 10.1016/j.yexcr.2015.10.033.
- Dulak J, Szade K, Szade A, Nowak W, Józkwicz. (2015). A. Adult stem cells: hopes and hypes of regenerative medicine. *Acta Biochim Pol.* 62(3):329-337. doi:10.18388/abp.2015\_1023.
- Dzamba BJ, DeSimone DW. (2018). Extracellular Matrix (ECM) and the Sculpting of Embryonic Tissues. *Curr Top Dev Biol.* 245-274. doi: 10.1016/bs.ctdb.2018.03.006.
- Eble JA, Niland S. (2019) The extracellular matrix in tumour progression and metastasis. *Clin Exp Metastasis.* 36(3):171-198. doi: 10.1007/s10585-019-09966-1.
- El-Rashidy AA, El Moshly S, Radwan IA, Rady D, Abbass MMS, Dörfer CE, Fawzy El-Sayed KM. (2021). Effect of Polymeric Matrix Stiffness on Osteogenic Differentiation of Mesenchymal Stem/Progenitor Cells: Concise Review. *Polymers (Basel).* 13(17):2950. doi: 10.3390/polym13172950.
- Engler AJ, Sen S, Sweeney HL, Discher DE. (2006). Matrix elasticity directs stem cell lineage specification. *Cell.* 126(4):677-89. doi:10.1016/j.cell.2006.06.044.
- Evans ND, Gentleman E. (2014). The role of material structure and mechanical properties in cell-matrix interactions. *J. Mater. Chem. B.* doi: 10.1039/c3tb21604g.
- Evans ND, Minelli C, Gentleman E, LaPointe V, Patankar SN, Kallivretaki M, Chen X, Roberts CJ, Stevens MM. (2009). Substrate stiffness affects early differentiation events in embryonic stem cells. *Eur Cell Mater.* 18:1-13. doi: 10.22203/ecm.v018a01.
- Feng CH, Cheng YC, Chao PH. (2013). The influence and interactions of substrate thickness, organization and dimensionality on cell morphology and migration. *Acta Biomater.* 9(3):5502-10. doi: 10.1016/j.actbio.2012.11.024.
- Fitter S, Gronthos S, Ooi SS, Zannettino AC. (2017). The Mesenchymal Precursor Cell Marker Antibody Stro-1 Binds to Cell Surface Heat Shock Cognate 70. *Stem Cells.* 2017 Apr;35(4):940-951. doi: 10.1002/stem.2560.
- Fitzsimmons REB, Mazurek MS, Soos A, Simmons CA. (2018). Mesenchymal Stromal/Stem Cells in Regenerative Medicine and Tissue Engineering. *Stem Cells Int.* 8031718. doi: 10.1155/2018/8031718.
- Frangogiannis NG. (2017). The extracellular matrix in myocardial injury, repair, and remodelling. *J Clin Invest.* 127(5):1600-1612. doi: 10.1172/JCI87491.

## List of References

- Frantz C, Stewart KM, Weaver VM. (2010). The extracellular matrix at a glance. *J Cell Sci.* 123(Pt 24):4195-200. doi: 10.1242/jcs.023820.
- Fu X, Liu G, Halim A, Ju Y, Luo Q, Song AG. (2019). Mesenchymal Stem Cell Migration and Tissue Repair. *Cells.* 8(8):784. doi: 10.3390/cells8080784.
- Fusco, S., Panzetta, V. & Netti, P.A. (2017). Mechanosensing of substrate stiffness regulates focal adhesions dynamics in the cell. *Meccanica* 52, 3389–3398. doi:10.1007/s11012-017-0676-3.
- Gaetani R, Zizzi EA, Deriu MA, Morbiducci U, Pesce M, Messina E. (2020). When Stiffness Matters: Mechanosensing in Heart Development and Disease. *Front Cell Dev Biol.* 2020 8:334. doi: 10.3389/fcell.2020.00334.
- García-Aznar JM, Nasello G, Hervas-Raluy S, Pérez MÁ, Gómez-Benito MJ. (2021). Multiscale modeling of bone tissue mechanobiology. *Bone.* 151:116032. doi: 10.1016/j.bone.2021.116032.
- Gov NS. (2009). Traction forces during collective cell motion. *HFSP J.* 3(4):223-7. doi: 10.2976/1.3185785.
- Guimarães, C.F., Gasperini, L., Marques, A.P. et al. (2020). The stiffness of living tissues and its implications for tissue engineering. *Nat Rev Mater* 5, 351–370. doi: 10.1038/s41578-019.
- Gupta M, Doss B, Lim CT, Voituriez R, Ladoux B. (2016). Single-cell rigidity sensing: A complex relationship between focal adhesion dynamics and large-scale actin cytoskeleton remodelling. *Cell Adh Migr.* 10(5):554-567. doi:10.1080/19336918.2016.1173800.
- Handorf AM, Zhou Y, Halanski MA, Li WJ.. (2015). Tissue stiffness dictates development, homeostasis, and disease progression. *Organogenesis.* 11(1):1-15. doi: 10.1080/15476278.2015.1019687.
- Hao J, Zhang Y, Jing D, Shen Y, Tang G, Huang S, Zhao Z. (2015). Mechanobiology of mesenchymal stem cells: Perspective into mechanical induction of MSC fate. *Acta Biomater.* 20:1-9. doi: 10.1016/j.actbio.2015.04.008.
- Heller E, Fuchs E. (2015). Tissue patterning and cellular mechanics. *J Cell Biol.* 211(2):219-31. doi: 10.1083/jcb.201506106.
- Heo SJ, Cosgrove BD, Dai EN, Mauck RL. (2018). Mechano-adaptation of the stem cell nucleus. *Nucleus.*9(1):9-19. doi: 10.1080/19491034.2017.1371398.
- Ho-Shui-Ling A, Bolander J, Rustom LE, Johnson AW, Luyten FP, Picart C. (2018). Bone regeneration strategies: Engineered scaffolds, bioactive molecules and stem cells current stage and future perspectives. *Biomaterials.* 180:143-162. doi: 10.1016/j.biomaterials.2018.07.017.

- Humphrey JD, Dufresne ER, Schwartz MA. (2014). Mechanotransduction and extracellular matrix homeostasis. *Nat Rev Mol Cell Biol.* 15(12):802-12. doi: 10.1038/nrm3896.
- Hunt JA, Chen R, van Veen T, Bryan N. (2014). Hydrogels for tissue engineering and regenerative medicine. *J Mater Chem B.* 2(33):5319-5338. doi: 10.1039/c4tb00775a.
- Hur J, Han HH. (2021). Outcome Assessment According to the Thickness and Direction of the Acellular Dermal Matrix after Implant-Based Breast Reconstruction. *Biomed Res Int.* 2021:8101009. doi: 10.1155/2021/8101009.
- Iolascon G, Resmini G, Tarantino U. (2013). Mechanobiology of bone. *Aging Clin Exp Res.* 25 Suppl 1: S3-7. doi: 10.1007/s40520-013-0101-2.
- Janeczek AA, Tare RS, Scarpa E, Moreno-Jimenez I, Rowland CA, Jenner D, Newman TA, Oreffo RO, Evans ND. (2016). Transient Canonical Wnt Stimulation Enriches Human Bone Marrow Mononuclear Cell Isolates for Osteoprogenitors. *Stem Cells.* 34(2):418-30. doi: 10.1002/stem.2241.
- Janson I., Putnam A. (2015). Extracellular matrix elasticity and topography: material-based cues that affect cell function via conserved mechanisms. *J Biomed Mater Res A.* 103(3): 1246–1258. doi:10.1002/jbm.a.35254.
- Jiang Y, Zhang H, Wang J, Liu Y, Luo T, Hua H. (2022). Targeting extracellular matrix stiffness and mechanotransducers to improve cancer therapy. *J Hematol Oncol.* 15(1):34. doi: 10.1186/s13045-022-01252-0.
- Khan AU, Qu R, Fan T, Ouyang J, Dai J. (2020). A glance on the role of actin in osteogenic and adipogenic differentiation of mesenchymal stem cells. *Stem Cell Res Ther.* 11(1):283. doi: 10.1186/s13287-020-01789-2.
- Kim S, Uroz M, Bays JL, Chen CS. (2021). Harnessing Mechanobiology for Tissue Engineering. *Dev Cell.* 56(2):180-191. doi: 10.1016/j.devcel.2020.12.017.
- Kim YH, Yoon DS, Kim HO, Lee JW. (2012). Characterization of different subpopulations from bone marrow-derived mesenchymal stromal cells by alkaline phosphatase expression. *Stem Cells Dev.* 21(16):2958-68. doi: 10.1089/scd.2011.0349.
- Kim Y, Ko H, Kwon IK, Shin K. (2016). Extracellular Matrix Revisited: Roles in Tissue Engineering. *Int Neurourol J.* Erratum in: *Int Neurourol J.* 20(2):168. Kwon, Ik Keun [corrected to Kwon, Il Keun]. doi: 10.5213/inj.1632600.318. Epub 2016 May 26.
- Kindberg A, Hu JK, Bush JO. (2020). Forced to communicate: Integration of mechanical and biochemical signalling in morphogenesis. *Curr Opin Cell Biol.* 66:59-68. doi: 10.1016/j.ceb.2020.05.004.
- Knoll SG, Ali MY, Saif MT. (2014). A novel method for localizing reporter fluorescent beads near the cell culture surface for traction force microscopy. *J Vis Exp.* (91):51873. doi: 10.3791/51873.

## List of References

- Kolios G, Moodley Y. (2013). Introduction to stem cells and regenerative medicine. *Respiration*. 85(1):3-10. doi:10.1159/000345615.
- Kular JK, Basu S, RI Sharma. (2014). The extracellular matrix: Structure, composition, age-related differences, tools for analysis and applications for tissue engineering. *Journal of Tissue Engineering*. 5: 1–17. doi: 10.1177/2041731414557112.
- Kumar R, Saha S, Sinha B. (2019). Cell spread area and traction forces determine myosin-II-based cortex thickness regulation. *Biochim Biophys Acta Mol Cell Res*. 1866(12):118516. doi: 10.1016/j.bbamcr.2019.07.011.
- Kuo CH, Xian J, Brenton JD, Franze K, Sivaniah E. (2012). Complex stiffness gradient substrates for studying mechanotactic cell migration. *Adv Mater*. 24(45):6059-6064. doi:10.1002/adma.201202520.
- Kureel SK, Mogha P, Khadpekar A, Kumar V, Joshi R, Das S, Bellare J, Majumder A. (2019). Soft substrate maintains proliferative and adipogenic differentiation potential of human mesenchymal stem cells on long-term expansion by delaying senescence. *Biol Open*. 8(4):bio039453. doi: 10.1242/bio.039453.
- Lamandé SR, Bateman JF. (2020). Genetic Disorders of the Extracellular Matrix. *Anat Rec (Hoboken)*. 303(6):1527-1542. doi: 10.1002/ar.24086.
- Lange JR, Fabry B. (2013). Cell and tissue mechanics in cell migration. *Exp Cell Res*. 319(16):2418-23. doi: 10.1016/j.yexcr.2013.04.023.
- Langenbach F, Handschel J. (2013). Effects of dexamethasone, ascorbic acid and  $\beta$ -glycerophosphate on the osteogenic differentiation of stem cells in vitro. *Stem Cell Res Ther*. 4(5):117. doi: 10.1186/scrt328.
- Lee J, Abdeen AA, Tang X, Saif TA, Kilian KA. (2015). Geometric guidance of integrin mediated traction stress during stem cell differentiation. *Biomaterials*. 69:174-83. doi: 10.1016/j.biomaterials.2015.08.005.
- Lee J, Abdeen AA, Zhang D, Kilian KA. (2013). Directing stem cell fate on hydrogel substrates by controlling cell geometry, matrix mechanics and adhesion ligand composition. *Biomaterials*. 34(33):8140-8. doi: 10.1016/j.biomaterials.2013.07.074.
- Lee JP, Kassianidou E, MacDonald JI, Francis MB, Kumar S. (2016). N-terminal specific conjugation of extracellular matrix proteins to 2-pyridinecarboxaldehyde functionalized polyacrylamide hydrogels. *Biomaterials*. 102:268-76. doi: 10.1016/j.biomaterials.2016.06.022.
- Lee, D., Zhang, H., Ryu, S. (2019). Elastic Modulus Measurement of Hydrogels. In: Mondal, M. (eds) *Cellulose-Based Superabsorbent Hydrogels*. *Polymers and Polymeric Composites: A Reference Series*. Springer, Cham. [https://doi.org/10.1007/978-3-319-77830-3\\_60](https://doi.org/10.1007/978-3-319-77830-3_60).

- Lekka M, Gnanachandran K, Kubiak A, Zieliński T, Zemła J. (2021). Traction force microscopy - Measuring the forces exerted by cells. *Micron*. 150:103138. doi: 10.1016/j.micron.2021.103138.
- Leong WS, Tay CY, Yu H, Li A, Wu SC, Duc DH, Lim CT, Tan LP. (2010). Thickness sensing of hMSCs on collagen gel directs stem cell fate. *Biochem Biophys Res Commun*. 401(2):287-92. doi: 10.1016/j.bbrc.2010.09.052.
- Leong WS, Tay CY, Yu H, Li A, Wu SC, Duc DH, Lim CT, Tan LP. (2010). Thickness sensing of hMSCs on collagen gel directs stem cell fate. *Biochem Biophys Res Commun*. 401(2):287-92. doi: 10.1016/j.bbrc.2010.09.052.
- Li J, Han D, Zhao YP. (2014). Kinetic behaviour of the cells touching substrate: the interfacial stiffness guides cell spreading. *Scientific Reports*. 4: 3910. doi: 10.1038/srep03910.
- Li L, Eyckmans J, Chen CS. (2017). Designer biomaterials for mechanobiology. *Nat Mater*. 16(12):1164-1168. doi:10.1038/nmat5049.
- Lin et al., (2010). Mechanosensing of substrate thickness. *Physical Review*. doi: 10.1103/PhysRevE.82.041918.
- Lin H, Sohn J, Shen H, Langhans MT, Tuan RS. (2019). Bone marrow mesenchymal stem cells: Aging and tissue engineering applications to enhance bone healing. *Biomaterials*. 203:96-110. doi: 10.1016/j.biomaterials.2018.06.026.
- Liu C, Pei H, Tan F. (2020). Matrix Stiffness and Colorectal Cancer. *Onco Targets Ther*. 13:2747-2755. doi: 10.2147/OTT.S231010.
- Liu J., Yang C., Yin T., Wang Z., Qu S., Suo Z. (2019). Polyacrylamide hydrogels. II. elastic dissipater. *Journal of the Mechanics and Physics of Solids*. Volume 133. doi: 10.1016/j.jmps.2019.103737.
- Liu N, Zhou M, Zhang Q, Yong L, Zhang T, Tian T, Ma Q, Lin S, Zhu B, Cai X. (2018). Effect of substrate stiffness on proliferation and differentiation of periodontal ligament stem cells. *Cell Prolif*. 51(5):e12478. doi: 10.1111/cpr.12478.
- Livak KJ, Schmittgen TD. (2001). Analysis of relative gene expression data using real-time quantitative PCR and the 2(-Delta Delta C(T)) Method. *Methods*. 25(4):402-8. doi: 10.1006/meth.2001.1262.
- Luby AO, Ranganathan K, Lynn JV, Nelson NS, Donneys A, Buchman SR. (2019). Stem Cells for Bone Regeneration: Current State and Future Directions. *J Craniofac Surg*. (3):730-735. doi: 10.1097/SCS.00000000000005250.
- Lukomska B, Stanaszek L, Zuba-Surma E, Legosz P, Sarzynska S, Drela K. (2019). Challenges and Controversies in Human Mesenchymal Stem Cell Therapy. *Stem Cells Int*. 2019:9628536. doi: 10.1155/2019/9628536.

## List of References

- Maia J, Caja S, Strano Moraes MC, Couto N, Costa-Silva B. (2018). Exosome-Based Cell-Cell Communication in the Tumor Microenvironment. *Front Cell Dev Biol.* 6:18. doi: 10.3389/fcell.2018.00018.
- Maloney JM, Walton EB, Bruce CM, Van Vliet KJ. (2008). Influence of finite thickness and stiffness on cellular adhesion-induced deformation of compliant substrate. *Phys Rev E Stat Nonlin Soft Matter Phys.* 78(4 Pt 1):041923. doi:10.1103/PhysRevE.78.041923.
- Mann, C., Leckband, D. (2010). Measuring Traction Forces in Long-Term Cell Cultures. *Cel. Mol. Bioeng.* 3, 40–49. doi:10.1007/s12195-010-0108-0
- Mao AS, Shin JW, Mooney DJ. (2016). Effects of substrate stiffness and cell-cell contact on mesenchymal stem cell differentiation. *Biomaterials.* 98:184-91. doi: 10.1016/j.biomaterials.2016.05.004.
- Martino F, Perestrelo AR, Vinarský V, Pagliari S, Forte G. Cellular (2018). Mechanotransduction: From Tension to Function. *Front Physiol.* 5; 9:824. doi: 10.3389/fphys.2018.00824.
- Mathieu PS, Lobo EG. (2012). Cytoskeletal and focal adhesion influences on mesenchymal stem cell shape, mechanical properties, and differentiation down osteogenic, adipogenic, and chondrogenic pathways. *Tissue Eng Part B. Rev.* 18(6):436-444. doi:10.1089/ten.TEB.2012.0014.
- Matsuoka F, Takeuchi I, Agata H, Kagami H, Shiono H, Kiyota Y, Honda H, Kato R. (2013). Morphology-based prediction of osteogenic differentiation potential of human mesenchymal stem cells. *PLoS One.*8(2):e55082. doi: 10.1371/journal.pone.0055082.
- McAndrews KM, McGrail DJ, Quach ND, Dawson MR. (2014). Spatially coordinated changes in intracellular rheology and extracellular force exertion during mesenchymal stem cell differentiation. *Phys Biol.* 11(5):056004. doi: 10.1088/1478-3975/11/5/056004.
- McBeath R, Pirone DM, Nelson CM, Bhadriraju K, Chen CS. (2004). Cell shape, cytoskeletal tension, and RhoA regulate stem cell lineage commitment. *Dev Cell.* 6(4):483-95. doi: 10.1016/s1534-5807(04)00075-9.
- McDaniel DP, Shaw GA, Elliott JT, Bhadriraju K, Meuse C, Chung KH, Plant AL. (2007). The stiffness of collagen fibrils influences vascular smooth muscle cell phenotype. *Biophys J.* 92(5):1759-69. doi: 10.1529/biophysj.
- Meesuk L, Suwanprateeb J, Thammarakcharoen F, Tantrawatpan C, Kheolamai P, Palang I, Tantikanlayaporn D, Manochantr S. (2022). Osteogenic differentiation and proliferation potentials of human bone marrow and umbilical cord-derived mesenchymal stem cells on the 3D-printed hydroxyapatite scaffolds. *Sci Rep.* 12(1):19509. doi: 10.1038/s41598-022-24160-2.

- Moeller J, Denisin AK, Sim JY, Wilson RE, Ribeiro AJS, Pruitt BL. (2018). Controlling cell shape on hydrogels using lift-off protein patterning. *PLoS One*. 13(1):e0189901. doi: 10.1371/journal.pone.0189901.
- Mousavi SJ, Doweidar MH. (2015). Role of Mechanical Cues in Cell Differentiation and Proliferation: A 3D Numerical Model. *PLoS One*. 10(5):e0124529. doi: 10.1371/journal.pone.0124529.
- Mullen C., Vaughan T., Billiar K., McNamara L. (2015). The effect of substrate stiffness, thickness and cross-linking density on osteogenic behaviour. *Biophysical Journal V*. 108: 1604–1612. doi: 10.1016/j.bpj.2015.02.022.
- Mullen CA, Haugh MG, Schaffler MB, Majeska RJ, McNamara LM. (2013). Osteocyte differentiation is regulated by extracellular matrix stiffness and intercellular separation. *J Mech Behav Biomed Mater*. 183-94. doi: 10.1016/j.jmbbm.2013.06.013.
- Murai T, Kawashima H, Naor D. Editorial: (2020). Cell-Cell and Cell-Matrix Adhesion in Immunobiology and Cancer. *Front Immunol*. 10:3126. doi: 10.3389/fimmu.2019.03126.
- Muresan CG. (2019). Collective cell behaviour in long-range mechanosensing of extracellular matrix dimensions. University of Southampton, Faculty of Medicine, PhD Thesis, page 76.
- Murphy MB, Moncivais K, Caplan AI. (2013). Mesenchymal stem cells: environmentally responsive therapeutics for regenerative medicine. *Exp Mol Med*. 45(11):e54. Nov 15. doi:10.1038/emm.2013.94.
- Najafi M, Farhood B, Mortezaee K. (2019). Extracellular matrix (ECM) stiffness and degradation as cancer drivers. *J Cell Biochem*. 120(3):2782-2790. doi: 10.1002/jcb.27681.
- Nakamura A, Osonoi T, Terauchi Y. (2010). Relationship between urinary sodium excretion and pioglitazone-induced edema. *J Diabetes Investig*. 1(5):208-11. doi: 10.1111/j.2040-1124.2010.00046.
- Naqvi SM, McNamara LM. (2020). Stem Cell Mechanobiology and the Role of Biomaterials in Governing Mechanotransduction and Matrix Production for Tissue Regeneration. *Front Bioeng Biotechnol*. 8:597661. Doi: 10.3389/fbioe.2020.597661.
- Nehls S, Nöding H, Karsch S, Ries F, Janshoff A. (2019). Stiffness of MDCK II Cells Depends on Confluency and Cell Size. *Biophys J*. 116(11):2204-2211. doi: 10.1016/j.bpj.2019.04.028.
- Niit M, Hoskin V, Carefoot E, Geletu M, Arulanandam R, Elliott B, Raptis L. (2015). Cell-cell and cell-matrix adhesion in survival and metastasis: Stat3 versus Akt. *Biomol Concepts*. 6(5-6):383-99. doi: 10.1515/bmc-2015-0022.
- Novoseletskaia E, Grigorieva O, Nimiritsky P, Basalova N, Eremichev R, Milovskaya I, Kulebyakin K, Kulebyakina M, Rodionov S, Omelyanenko N, Efimenko A. Mesenchymal Stromal Cell-Produced Components of Extracellular Matrix Potentiate Multipotent Stem

## List of References

- Cell Response to Differentiation Stimuli. *Front Cell Dev Biol.* 2020 Sep 22; 8:555378. doi: 10.3389/fcell.2020.555378.
- Oakes P., Banerjee S., Marchetti C., and Gardel M. (2014). Geometry Regulates Traction Stresses in Adherent Cells. *Biophysical Journal* Volume 107: 825–833. doi:10.1016/j.bpj.2014.06.045.
  - Ohashi K, Fujiwara S, Mizuno K. (2017). Roles of the cytoskeleton, cell adhesion and rho signalling in mechanosensing and mechanotransduction. *J Biochem.*161(3):245-254. doi: 10.1093/jb/mvw082.
  - Olson EN, Nordheim A. (2010). Linking actin dynamics and gene transcription to drive cellular motile functions. *Nat Rev Mol Cell Biol.* 11(5):353-65. doi: 10.1038/nrm2890.
  - Parekh SH, Chatterjee K, Lin-Gibson S, Moore NM, Cicerone MT, Young MF, Simon CG Jr. (2011). Modulus-driven differentiation of marrow stromal cells in 3D scaffolds that is independent of myosin-based cytoskeletal tension. *Biomaterials.* 32(9):2256-64. doi: 10.1016/j.biomaterials.2010.11.065.
  - Pauwels F. (1980). Biomechanics of the locomotor apparatus. Contributions on the functional anatomy of the locomotor apparatus. Berlin: Springer-Verlag. p 520.
  - Pawar SN, Edgar KJ. (2012). Alginate derivatization: a review of chemistry, properties, and applications. *Biomaterials.*33(11):3279-305. doi: 10.1016/j.biomaterials.2012.01.007.
  - Pelham RJ Jr, Wang YI. (1997). Cell locomotion and focal adhesions are regulated by substrate flexibility. *Proc Natl Acad Sci USA.* 94(25):13661-5. doi: 10.1073/pnas.94.25.13661.
  - Pérez-Calixto, D., Amat-Shapiro, S., Zamarrón-Hernández, D., Vázquez-Victorio, G., Puech, P. H., & Hautefeuille, M. (2021). Determination by Relaxation Tests of the Mechanical Properties of Soft Polyacrylamide Gels Made for Mechanobiology Studies. *Polymers*, 13(4), 629. doi: 10.3390/polym13040629
  - Petit C, Karkhaneh Yousefi AA, Ben Moussa O, Michel JB, Guignandon A, Avril S. (2021). Regulation of SMC traction forces in human aortic thoracic aneurysms. *Biomech Model Mechanobiol.* 20(2):717-731. doi: 10.1007/s10237-020-01412-6.
  - Plotnikov SV, Sabass B, Schwarz US, Waterman CM. (2014). High-resolution traction force microscopy. *Methods Cell Biol.* 123:367-94. doi: 10.1016/B978-0-12-420138-5.00020-3.
  - Polacheck WJ, Chen CS. (2016). Measuring cell-generated forces: a guide to the available tools. *Nat Methods.* 13(5):415-23. doi: 10.1038/nmeth.3834.
  - Protick FK, Amit SK, Amar K, Nath SD, Akand R, Davis VA, Nilufar S, Chowdhury F. (2022). Additive Manufacturing of Viscoelastic Polyacrylamide Substrates for Mechanosensing Studies. *ACS Omega.* 7(28):24384-24395. doi: 10.1021/acsomega.2c01817.

- Quan FS, Kim KS. (2016). Medical applications of the intrinsic mechanical properties of single cells. *Acta Biochim Biophys Sin (Shanghai)*. 48(10):865-871. doi: 10.1093/abbs.
- Reinhart-King CA, Dembo M, Hammer DA. (2008). Cell-cell mechanical communication through compliant substrates. *Biophys J*. 95(12):6044-51. doi: 10.1529/biophysj.107.127662.
- Ringer P, Colo G, Fässler R, Grashoff C. (2017). Sensing the mechano-chemical properties of the extracellular matrix. *Matrix Biol*. 64:6-16. doi: 10.1016/j.matbio.2017.03.004.
- Rouillard AD, Berglund CM, Lee JY, Polacheck WJ, Tsui Y, Bonassar LJ, Kirby BJ. (2011). Methods for photocrosslinking alginate hydrogel scaffolds with high cell viability. *Tissue Eng Part C Methods*. 17(2):173-9. doi: 10.1089/ten.TEC.2009.0582.
- Rustad KC, Wong VW, Gurtner GC. (2013). The role of focal adhesion complexes in fibroblast mechanotransduction during scar formation. *Differentiation*. 86(3):87-91. doi: 10.1016/j.diff.2013.02.003.
- Saha K, Kim J, Irwin E, Yoon J, Momin F, Trujillo V, Schaffer DV, Healy KE, Hayward RC. (2010). Surface creasing instability of soft polyacrylamide cell culture substrates. *Biophys J*. 99(12):L94-6. doi: 10.1016/j.bpj.2010.09.045.
- Salvi AM, DeMali KA. (2018). Mechanisms linking mechanotransduction and cell metabolism. *Curr Opin Cell Biol*. 54:114-120. doi: 10.1016/j.ceb.2018.05.004.
- Schwarz US, Soiné JR. (2015). Traction force microscopy on soft elastic substrates: A guide to recent computational advances. *Biochim Biophys Acta*. 1853(11 Pt B):3095-104. doi: 10.1016/j.bbamcr.2015.05.028.
- Sen S, Engler AJ, Discher DE. (2009). Matrix strains induced by cells: Computing how far cells can feel. *Cell Mol Bioeng*. 2(1):39-48. doi:10.1007/s12195-009-0052-z.
- Serra-Picamal X, Conte V, Sunyer R, Muñoz JJ, Trepas X. (2015). Mapping forces and kinematics during collective cell migration. *Methods Cell Biol*. 309-30. doi: 10.1016/bs.mcb.2014.11.003.
- Shawky JH, Davidson LA. (2015). Tissue mechanics and adhesion during embryo development. *Dev Biol*. 401(1):152-64. doi: 10.1016/j.ydbio.2014.12.005.
- Shin JW, Swift J, Ivanovska I, Spinler KR, Buxboim A, Discher DE. (2013). Mechanobiology of bone marrow stem cells: from myosin-II forces to compliance of matrix and nucleus in cell forms and fates. *Differentiation*. 86(3):77-86. doi: 10.1016/j.diff.2013.05.001.
- Shivashankar GV, Sheetz M, Matsudaira P. *Mechanobiology*. (2015). *Integr Biol (Camb)*. 7(10):1091-2. doi: 10.1039/c5ib90040a.
- Spatarelu CP, Zhang H, Trung Nguyen D, Han X, Liu R, Guo Q, Notbohm J, Fan J, Liu L, Chen Z. (2019). Biomechanics of Collective Cell Migration in Cancer Progression:

## List of References

- Experimental and Computational Methods. *ACS Biomater Sci Eng.* 5(8):3766-3787. doi: 10.1021/acsbomaterials.8b01428.
- Sridharan Weaver S, Li Y, Foucard L, Majeed H, Bhaduri B, Levine AJ, Kilian KA, Popescu G. (2019). Simultaneous cell traction and growth measurements using light. *J Biophotonics.* 12(3):e201800182. doi: 10.1002/jbio.201800182.
  - Štefková K, Procházková J, Pacherník J. (2015). Alkaline phosphatase in stem cells. *Stem Cells Int.* 2015:628368. doi: 10.1155/2015/628368.
  - Steward AJ, Kelly DJ. (2015). Mechanical regulation of mesenchymal stem cell differentiation. *J Anat.* 227(6):717-731. doi:10.1111/joa.12243.
  - Suárez-López Del Amo F, Lin GH, Monje A, Galindo-Moreno P, Wang HL. (2016). Influence of Soft Tissue Thickness on Peri-Implant Marginal Bone Loss: A Systematic Review and Meta-Analysis. *J Periodontol.* 87(6):690-9. doi: 10.1902/jop.2016.150571. Epub 2016 Jan 16. PMID: 26777766.
  - Subramani, Ramesh & Izquierdo-Alvarez, Alicia & Bhattacharya, Pinaki & Meerts, Mathieu & Moldenaers, Paula & Ramon, Herman & Oosterwyck, Hans. (2020). The Influence of Swelling on Elastic Properties of Polyacrylamide Hydrogels. *Frontiers in Materials.* 7. 212. doi: 10.3389/fmats.2020.00212.
  - Sun M, Chi G, Li P, Lv S, Xu J, Xu Z, Xia Y, Tan Y, Xu J, Li L, Li Y. (2018). Effects of Matrix Stiffness on the Morphology, Adhesion, Proliferation and Osteogenic Differentiation of Mesenchymal Stem Cells. *Int J Med Sci.* 15(3):257-268. doi: 10.7150/ijms.21620.
  - Svitkina TM. (2018). Ultrastructure of the actin cytoskeleton. *Curr Opin Cell Biol.* 54:1-8. doi: 10.1016/j.ceb.2018.02.007.
  - Syed S, Karadaghy A, Zustiak S. (2015). Simple polyacrylamide-based multiwell stiffness assay for the study of stiffness-dependent cell responses. *J Vis Exp.* 25;(97). doi: 10.3791/52643
  - Takata K, Goto T, Kuroda M, Kimura Y, Harada I, Ueda K, Kawada T, Kioka N. (2020). Stiffness of the extracellular matrix regulates differentiation into beige adipocytes. *Biochem Biophys Res Commun.* 532(2):205-210. doi: 10.1016/j.bbrc.2020.08.032.
  - Tang X, Ali MY, Saif MT. (2012). A Novel Technique for Micro-patterning Proteins and Cells on Polyacrylamide Gels. *Soft Matter.* 8(27):7197-7206. doi: 10.1039/C2SM25533B.
  - Tapial Martínez P, López Navajas P, Lietha D. (2020). FAK Structure and Regulation by Membrane Interactions and Force in Focal Adhesions. *Biomolecules.* 10(2):179. doi: 10.3390/biom10020179.
  - Tee SY, Fu J, Chen CS, Janmey PA. (2011). Cell shape and substrate rigidity both regulate cell stiffness. *Biophys J.* 100(5): L25-7. doi: 10.1016/j.bj.2010.

- Turing AM. (1953). The chemical basis of morphogenesis. *Bull Math Biol.* 1990;52(1-2):153-97. doi: 10.1007/BF02459572.
- Trappmann B, Gautrot JE, Connelly JT, Strange DG, Li Y, Oyen ML, Cohen Stuart MA, Boehm H, Li B, Vogel V, Spatz JP, Watt FM, Huck WT. (2012). Extracellular-matrix tethering regulates stem-cell fate. *Nat Mater.* 11(7):642-9. doi: 10.1038/nmat3339.
- Tusan CG, Hin Y, Zarkoob H, Johnston D, Andriotis OG, Thurner PJ, Yang S, Sander EA, Gentleman E, Sengers BG, Evans ND. (2018). Collective Cell Behavior in Mechanosensing of Substrate Thickness. *Biophysical Journal* 114, 2743–2755. 10.1016/j.bpj.2018.03.037.
- Venugopal B., Mogha P , Dhawan J, Majumder A . (2018). Cell density overrides the effect of substrate stiffness on human mesenchymal stem cells' morphology and proliferation. *Biomater Sci.* 6(5):1109-1119. doi: 10.1039/c7bm00853h.
- Vianay B, Senger F, Alamos S, Anjur-Dietrich M, Bearce E, Cheeseman B, Lee L, Théry M. (2018). Variation in traction forces during cell cycle progression. *Biol Cell.* 110(4):91-96. doi: 10.1111/boc.201800006.
- Vining KH, Mooney DJ. (2017). Mechanical forces direct stem cell behaviour in development and regeneration. *Nat Rev Mol Cell Biol.* (12):728-742. doi: 10.1038/nrm.2017.108.
- Wall M, Butler D, El Haj A, Bodle JC, Lobo EG, Banes AJ. (2018). Key developments that impacted the field of mechanobiology and mechanotransduction. *J Orthop Res.* 36(2):605-619. doi: 10.1002/jor.23707.
- Wang B, Qinglai T, Yang Q, Li M, Zeng S, Yang X, Xiao Z, Tong X, Lei L, Li S. (2022). Functional acellular matrix for tissue repair. *Mater Today Bio.* 18:100530. doi: 10.1016/j.mtbio.2022.100530.
- Wang JH, Thampatty BP. (2008). Mechanobiology of adult and stem cells. *Int Rev Cell Mol Biol.* 271:301-46. doi: 10.1016/S1937-6448(08)01207-0.
- Wang S, Matsumoto K, Lish SR, Cartagena-Rivera AX, Yamada KM. (2021). Budding epithelial morphogenesis is driven by cell-matrix versus cell-cell adhesion. *184(14):3702-3716.e30.* doi: 10.1016/j.cell.2021.05.015.
- Wang, J.H.C., Thampatty, B.P. (2006). An Introductory Review of Cell Mechanobiology. *Biomech Model Mechanobiol* 5, 1–16 (2006). doi: 10.1007/s10237-005-0012-z
- Wells RG. (2008). The role of matrix stiffness in regulating cell behaviour. *Hepatology.* 47(4):1394-400. doi: 10.1002/hep.22193.
- Wells RG. (2013). Tissue mechanics and fibrosis. *Biochim Biophys Acta.* 1832(7):884-90. doi: 10.1016/j.bbadis.
- Westhauser F, Karadjian M, Essers C, Senger AS, Hagmann S, Schmidmaier G, Moghaddam A. (2019). Osteogenic differentiation of mesenchymal stem cells is enhanced in a 45S5-supplemented  $\beta$ -TCP composite scaffold: an in-vitro comparison

## List of References

- of Vitoss and Vitoss BA. PLoS One. 14(2): e0212799. doi: 10.1371/journal.pone.0212799.
- Wickström SA, Niessen CM. (2018). Cell adhesion and mechanics as drivers of tissue organization and differentiation: local cues for large scale organization. *Curr Opin Cell Biol.* 54:89-97. doi: 10.1016/j.ceb.2018.05.003.
  - Xie Q, Liu R, Jiang J, Peng J, Yang C, Zhang W, Wang S, Song J. (2020). What is the impact of human umbilical cord mesenchymal stem cell transplantation on clinical treatment? *Stem Cell Res Ther.* 11(1):519. doi: 10.1186/s13287-020-02011-z.
  - Xu D., Hernandez-Miranda M.L., Evans N., Sengers B., Browne M., Cook R. Depth profiling via nanoindentation for characterisation of the elastic modulus and hydraulic properties of thin hydrogel layers. *Acta biomaterialia*. Submitted on 23rd September 2022.
  - Xu J, Sun M, Tan Y, Wang H, Wang H, Li P, Xu Z, Xia Y, Li L, Li Y. (2017). Effect of matrix stiffness on the proliferation and differentiation of umbilical cord mesenchymal stem cells. *Differentiation.* 96:30-39. doi: 10.1016/j.diff.2017.07.001.
  - Xue R, Li JY, Yeh Y, Yang L, Chien S. (2013). Effects of matrix elasticity and cell density on human mesenchymal stem cells differentiation. *J Orthop Res.* (9):1360-5. doi: 10.1002/jor.22374.
  - Yang C, Yin T, Suo Z. (2019) Polyacrylamide hydrogels. I. Network imperfection, *Journal of the Mechanics and Physics of Solids*, Volume 131, Pages 43-55. doi: 10.1016/j.jmps.2019.06.018.
  - Ye K, Cao L, Li S, Yu L, Ding J. (2015). Interplay of Matrix Stiffness and Cell-Cell Contact in Regulating Differentiation of Stem Cells. *ACS Appl Mater Interfaces.* 8(34):21903-13. doi: 10.1021/acsami.5b09746.
  - Yen MH, Chen YH, Liu YS, Lee OK. (2020). Alteration of Young's modulus in mesenchymal Stromal cells during osteogenesis measured by atomic force microscopy. *Biochem Biophys Res Commun.* 526(3):827-832. doi: 10.1016/j.bbrc.2020.03.146
  - Zakrzewski W, Dobrzyński M, Szymonowicz M, Rybak Z. (2019). Stem cells: past, present, and future. *Stem Cell Res Ther.* 10(1):68. doi: 10.1186/s13287-019-1165-5.
  - Zanca A, Mozetic P, Orsini M, Forte G, Rainer A. (2022). A primer to traction force microscopy. *J Biol Chem.* 298(5):101867. doi: 10.1016/j.jbc.2022.101867.
  - Zhao L, Fan F, Wang P, Jiang X. (2013). Culture medium optimization of a new bacterial extracellular polysaccharide with excellent moisture retention activity. *Appl Microbiol Biotechnol.* 97(7):2841-50. doi: 10.1007/s00253-012-4515-0.
  - Zhao W, Li X, Liu X, Zhang N, Wen X. (2014). Effects of substrate stiffness on adipogenic and osteogenic differentiation of human mesenchymal stem cells. *Mater Sci Eng C Mater Biol Appl.* 2014. 40:316-23. doi: 10.1016/j.msec.2014.03.048.

- Zheng C, Chen J, Liu S, Jin Y. (2019). Stem cell-based bone and dental regeneration: a view of microenvironmental modulation. *Int J Oral Sci.* 11(3):23. doi: 10.1038/s41368-019-0060-3.
- Zhou, D. W., Lee, T. T., Weng, S., Fu, J., & García, A. J. (2017). Effects of substrate stiffness and actomyosin contractility on the coupling between force transmission and vinculin-paxillin recruitment at single focal adhesions. *Molecular biology of the cell*, 28(14), 1901–1911. doi:10.1091/mbc.E17-02-0116.
- Zhou HY, Cao Y, Wu J, Zhang WS. (2017). Role of corneal collagen fibrils in corneal disorders and related pathological conditions. *Int J Ophthalmol.* 10(5):803-811. doi: 10.18240/ijo.
- Zhou Y, Jin L. (2020). Hydrolysis-induced large swelling of polyacrylamide hydrogels. *Soft Matter.* 16, 5740. DOI: 10.1039/d0sm00663g.